Program and Abstract Volume

LPI Contribution No. 1820

LUNAR AND PLANETARY INSTITUTE

USRA

Annual Meeting of the Lunar Exploration Analysis Group

October 22–24, 2014 • Laurel, Maryland

INSTITUTIONAL SUPPORT

NASA Lunar Exploration Analysis Group
The Johns Hopkins University/Applied Physics Laboratory
Universities Space Research Association (USRA)
Lunar and Planetary Institute
National Aeronautics and Space Administration

CONVENERS

Samuel Lawrence
Arizona State University
Stephen Mackwell
Lunar and Planetary Institute
Clive Neal
University of Notre Dame
Jeffrey Plescia
The Johns Hopkins University/Applied Physics Laboratory

SCIENCE ORGANIZING COMMITTEE

Samuel Lawrence
Arizona State University
Clive Neal
University of Notre Dame
Noah Petro
NASA Goddard Space Flight Center
Jeffrey Plescia
The Johns Hopkins University/Applied Physics Laboratory
Charles Shearer
University of New Mexico
Stephen Mackwell
Lunar and Planetary Institute
James Carpenter
European Space Agency-ESTEC
Jasper Halekas
University of Iowa
Greg Schmidt
NASA Ames Research Center

Lunar and Planetary Institute 3600 Bay Area Boulevard Houston TX 77058-1113

LPI Contribution No. 1820

Compiled in 2014 by

Meeting and Publication Services
Lunar and Planetary Institute
USRA Houston
3600 Bay Area Boulevard, Houston TX 77058-1113

This material is based upon work supported by NASA under Award No. NNX08AC28A. Any opinions, findings, and conclusions or recommendations expressed in this volume are those of the author(s) and do not necessarily reflect the views of the National Aeronautics and Space Administration.

The Lunar and Planetary Institute is operated by the Universities Space Research Association under a cooperative agreement with the Science Mission Directorate of the National Aeronautics and Space Administration.

Abstracts in this volume may be cited as

Author A. B. (2014) Title of abstract. In *Annual Meeting of the Lunar Exploration Analysis Group,* p. XX. LPI Contribution No. 1820, Lunar and Planetary Institute, Houston.

ISSN No. 0161-5297

Preface

This volume contains abstracts that have been accepted for presentation at the Annual Meeting of the Lunar Exploration Analysis Group, October 22–24, 2014, Laurel, Maryland.

Administration and publications support for this meeting were provided by the staff of the Meeting and Publication Services Department at the Lunar and Planetary Institute.

Technical Guide to Sessions

Wednesday, October 22, 2014

8:30 a.m.	Bldg. 200, Room 100	Lunar Programmatic Issues - NASA/LEAG
1:30 p.m.	Bldg. 200, Room 100	Lunar Volatiles: Current Understanding I
5:30 p.m.	Bldg. 200, Lobby	Poster Session

Thursday, October 23, 2014

8:30 a.m.	Bldg. 200, Room 100	Lunar Volatiles: Current Understanding II
1:30 p.m.	Bldg. 200, Room 100	Lunar Volatiles: Current Understanding III

Friday, October 24, 2014

8:30 a.m.	Bldg. 200, Room 100	Future Exploration: Instruments, Missions, and Techniques
1:30 p.m.	Bldg. 200, Room 100	Future Exploration: Strategies and Opportunities

Contents

Program

Wednesday, October 22, 2014
LUNAR PROGRAMMATIC ISSUES - NASA/LEAG
8:30 a.m. Bldg. 200, Room 100

Chairs: **Jeffrey Plescia**
Clive Neal

8:30 a.m. Plescia J. *
LEAG Update

8:40 a.m. Crusan J. *
HEOMD/ASE Update

9:00 a.m. Green J. *
PSD Update

9:20 a.m. Chabot N. *
SBAG Update

9:35 a.m. Guidi J. *
Global Exploration Roadmap

9:50 a.m. Derleth, J.†*
NASA Technology†Programs

10:05 a.m. Lucey P. *
Lunar Polar Volatile Strategic Action Team Report

10:20 a.m. Gruener J. E. * Suzuki N. H.
International Strategy for the Exploration of Lunar Polar Volatiles **[#3061]**
The International Space Exploration Coordination Group (ISECG) has begun an effort to develop a strategy to investigate lunar polar volatiles in a cooperative approach that is technically feasible, yet programmatically implementable.

10:35 a.m. Neal C. R. * Schmidt G. Crawford I. A. Ehrenfreund P. Carpenter J.
Developing the Global Exploration Roadmap **[#3050]**
The GER can be developed by mapping existing international and detailed documents to it.

10:50 a.m. Carpenter J. D. * Houdou B. Fisackerly F. De Rosa D. Patti B. Schiemann J. Hufenbach B. Foing B.
Lunar Exploration in ESA **[#3019]**
We report on current ESA plans and activities in the area of lunar exploration.

11:05 a.m. Keller J., Petro N. *
LRO Mission Update - Extended Mission

11:20 a.m. Dankanich J. *
CubeSat Studies - MSFC

11:35 a.m. Colaprete A. *
Resource Prospector Mission

11:50 a.m. Archinal B. A. Kirk R. L. Gaddis L. R. Hagerty J. Skinner J. Titus T. N. Keszthelyi L. P. Hare T. Lawrence S. J. * Beyer R. Nefian A. Fong T. Duxbury T.
The Need for Lunar and Planetary Cartography Planning **[#3029]**
A lack of planning in planetary cartography has had and will have serious consequences for planetary missions. Here we highlight the current lack of formal cartographic planning for the U.S. space program and recommend a community-driven solution.

Wednesday, October 22, 2014
LUNAR VOLATILES: CURRENT UNDERSTANDING I
1:30 p.m. Bldg. 200, Room 100

Chairs: **Samuel Lawrence**
Paul Hayne

1:30 p.m. Elphic R. *
LADEE and Volatiles

1:50 p.m. Hurley D. M. * Benna M. Mahaffy P. Elphic R. Goldstein D.
Water Interactions with Lunar Regolith from LADEE Observations **[#3044]**
Water in lunar polar regions may arise in part from migration of water through the exosphere. We study important parameters in that migration using LADEE NMS data from engine burn experiments.

2:10 p.m. Paige D. *
Lunar Thermal Environment

2:30 p.m. McClanahan T. P. * Mitrofanov I. G. Boynton W. V. Chin G. Evans L. G. Starr R. D. Livengood T. Sagdeev R. Parsons A. M. Su J. J. Murray J. Sanin A. Litvak M. Harshman K. Hamara D. Bodnarik J.
Epithermal Neutrons, Illumination, Spatial Scale and Topography: A Correlative Analysis of Factors Influencing the Detection of Slope Hydration Using LRO's Lunar Exploration Neutron Detector **[#3039]**
This research correlates the Moon's south polar epithermal neutron flux, topography and a visible illumination model and shows that there is a widespread hydration of polward-facing (PF) slopes that is occurring at a continuum of spatial scales.

2:50 p.m. Livengood T. A. * Chin G. Sagdeev R. Z. Mitrofanov I. G. Boynton W. V. Evans L. G. Litvak M. L. McClanahan T. P. Sanin A. B. Starr R. D. Su J. J.
Diurnally Variable Hydrogen-Bearing Volatiles at the Moon's Equator: Evidence, Concentration, Transport, Implications **[#3058]**
Neutron remote-sensing demonstrates significant quantities of volatiles in the equatorial region that cycle in and out of subsurface sequestration diurnally. Solar wind and micrometeoroids supply insufficient hydrogen to support equilibrium.

3:10 p.m. Teodoro L. F. A. * Lawrence D. J. Elphic R. C. Eke V. R. Feldman W. C. Maurice S.
The Search for a Diurnal Effect in Lunar Hydrogen Abundance **[#3023]**
We studied the LP data exhibit diurnal variations of the same magnitude as those reported by Livengood et al 2014, however the LPNS variations are systemically anti-correlated with instrument temperature.

3:30 p.m. Lawrence D. J. * Peplowski P. N. Plescia J. B. Greenhagen B. T. Maurice S. Prettyman T. H.
Lunar Highlands Bulk Hydrogen Concentrations **[#3038]**
A map of bulk hydrogen concentration across the lunar highlands is presented. These concentrations are measured with data from the Lunar Prospector Neutron Spectrometer.

3:50 p.m. BREAK

4:05 p.m. Smith D *
LOLA Observations - Lunar Volatiles

4:25 p.m. Robinson M *
LROC Observations of Permanently Shadowed Regions

4:45 p.m. Patterson G. W. * Bussey D. B. J. Stickle A. M. Cahill J. T. S. Spudis P. Mini-RF Team
Mini-RF Bistatic Observations of Cabeus Crater **[#3049]**
Observations of the south polar crater Cabeus indicate anomalous scattering behavior associated with crater floor materials (behavior not observed with monostatic data). We interpret this behavior as consistent with the presence of water ice.

5:05 p.m. DISCUSSION

Wednesday, October 22, 2014
POSTER SESSION: POSTER SESSION
5:30 p.m. Bldg. 200, Lobby

Kring D. A.
Production of Volatiles at Lunar Pyroclastic Volcanic Vents **[#3056]**
Significant masses of CO, CO_2, and H_2O can be released by pyroclastic eruptions.

Fink H.
Lunar Surface Models **[#3010]**
Lunar surface models in raised relief give the user a tactile impression of the terrain shown on the map.

Robinson M. S. Lawrence S. J. Speyerer E. J. Stopar J. D.
Intrepid: Lunar Roving Prospector — Providing Ground Truth and Enabling Future Exporation **[#3026]**
We propose a long range lunar roving prospector, Intrepid, to collect essential measurements to address key questions and demonstrate technologies required for future robotic and human exploration of the Moon, Mars, and other terrestrial bodies.

Guven U. G. Velidi G. V. Datta L. D.
Space Mission to the Moon with a Low Cost Moon Probe Nanosatellite: University Project Feasibility Analysis and Design Concepts **[#3005]**
This paper discusses the possibility of launching a 10 kg nanosatellite moon probe with a joint university effort along with industrial partners for a low cost mission to the moon. It will allow for vital experiments to take place.

Guven U. G.
Why Do We Need the Moon: Next Steps Forward for Moon Exploration **[#3036]**
This paper outlines the various possibilities for the future of the moon and it details how it can be beneficial for future space technology endeavors and discusses alternatives of Nanosatellite Moon missions as well as private sector missions.

Knicely J. Rickman D.
Inversion Algorithms to Determine Likely 3D Solids from a Population of Particles **[#3027]**
The 3D shape of particles affects many aspects of science and engineering. Two inversion algorithms were developed to determine sets of 3D solids that approximate the 2D measures of a population of particles of lunar regolith and lunar simulant.

Leiter R. M. Himwich Z. Natarajan A. Rosenthall J. Clark P. E.
Small Payloads and Advanced Concepts for Exploration (SPACE) Early Mission Design Tool **[#3009]**
This tool allows scientists and engineers in early phases of mission development to select a compact instrument for a science application and find initial estimates mass, power, volume, and bandwidth for a specific nanosatellite mission.

Lawrence S. J. Robinson M. S. Stopar J. D. Speyerer E. J. Jolliff B. L.
Lunar Surface Traverse and Exploration Planning: Farside Locations **[#3069]**
We describe morphometric properties of farside exploration destinations.

Huber S. A. Hendrickson D. B. Jones H. L. Thornton J. P. Whittaker W. L. Wong U. Y.
Astrobotic Technology: Planetary Pits and Caves for Science and Exploration **[#3065]**
This paper describes lunar pits and caves as a potential destination for future science and exploration missions and crewed lunar outposts.

Clark P. E. Didion J. Cox R.
An ALSEP-Like Lunar Surface Science Package in a Cubesat Form Factor? **[#3008]**
How scalable is the thermal design developed for the ALSEP-like LEMS (without RTGs or RHUs) concept for Project Constellation to a cubesat form factor package?

Wilson J. K. Schwadron N. Spence H. E. Case A. W. Golightly M. J. Jordan A. P. Kasper J. Looper M. D. Mazur J. E. Petro N. E. Robinson M. S. Stubbs T. J. Zeitlin C. Blake J. B. Smith S. S. Townsend L. W.
Lunar Proton Albedo Anomalies: Soil, Surveyors, and Statistics **[#3006]**
We see several regional features in the map of lunar albedo protons. We consider several natural sources for the features, as well as man-made anomalies and statistical artifacts.

Stickle A. M. Patterson G. W. Bussey D. B. J. Cahill J. T. S. Mini-RF Team
Mini-RF Observations of Mare Ejecta Emplacement Diversity **[#3064]**
Significant diversity is seen in the radar scattering characteristics of mare crater ejecta. Here, signatures of subsurface layering emplaced on the lunar surface following impact events are observed using Mini-RF radar data.

Barker M. K. Mazarico E. Neumann G. A. Smith D. E. Zuber M. T.
Coregistration of Elevation Data from the Lunar Orbiter Laser Altimeter and the SELENE Terrain Camera **[#3034]**
Our goal is to produce the most complete, accurate, and precise global terrain model of the lunar surface by coregistering and merging the digital elevation models from LOLA and the SELENE terrain camera.

Chi P. J.
Investigation of Ionized Volatiles and Interior Structure of the Moon: Implications from Restored Apollo Magnetic Field Data **[#3020]**
The restored Apollo magnetic field data have revealed ion cyclotron waves that suggest the presence of ionized volatiles from the Moon. Further restoration of the Apollo-era data can help probe the electrical conductivity of the lunar interior.

Mazarico E. Nicholas J. B. McClanahan T. P. Neumann G. A.
Lunar Polar Illumination Modeling to Support Data Analysis **[#3022]**
We show that illumination modeling at the lunar poles can be useful to support calibration and analysis of lunar datasets such as the neutron data, in particular when studying time-variable effects and correlation with time of day.

Murray J. Su J. J. Sagdeev R. Chin G. McClanahan T. P. Livengood T. Starr R. D. Evans L. G.
Cross Calibration of Omnidirectional Orbital Neutron Detectors LPNS of Lunar Prospector and SETN/LEND of Lunar Reconnaissance Orbiter **[#3045]**
In this research we cross calibrate the omnidirectional neutron detectors from Lunar Prospector mission and Lunar Reconnaissance Orbiter mission by Monte Carlo simulations.

Swain R. K.
Lunar Gene Bank for Endangered Species **[#3004]**
The concept of a gene bank in the lunar polar craters provides a permanent solution to the menace of endangered species and the failure of the prevailing strategies to protect them. This is one vital, technologically viable yet cost effective option.

Mahanti P. Robinson M. S. Lawrence S. J. Stelling R. Boyd A.
Communication and Illumination Conditions at Ina-D — An Information Fusion Approach for Lunar Exploration Planning **[#3055]**
Knowledge of line-of-sight and solar illumination conditions (LoSSIC) drive lunar surface exploration planning. LoSSIC information derived from LROC NAC DTMs is used to greatly enhance communication and traverse planning on the lunar surface.

Petro N. E. Keller J. W.
Five Years at the Moon with the Lunar Reconnaissance Orbiter (LRO): New Views of the Lunar Surface and Environment **[#3059]**
The Lunar Reconnaissance Orbiter (LRO) has been orbiting the Moon for over five years. During that time, data from the seven instruments onboard the spacecraft have made significant advances in our understanding of the Moon and its environment.

Lucey P. G. Abshire J. B. Sun X. Neumann G. A. Mazarico E. M.
A Laser Spectrometer for Global Mapping of the Abundance, Distribution and Variability of Water on the Moon **[#3035]**
A multispectral laser spectrometer under development at Goddard Space Flight Center can definitively detect and map surface ice from orbit, and also quantify the abundance and variation of global bound water at the 10–100 ppm level.

Thursday, October 23, 2014
LUNAR VOLATILES: CURRENT UNDERSTANDING II
8:30 a.m. Bldg. 200, Room 100

Chairs: **Noah Petro**
David Lawrence

8:30 a.m. Retherford K. *
LAMP Observations of Lunar Volatiles

8:50 a.m. Hayne P. O. * Hendrix A. Sefton-Nash E. Lucey P. G. Retherford K. D. Williams J.-P. Siegler M. A. Greenhagen B. T. Paige D. A.
Evidence for Exposed Water Frost in the Moon's South Polar Regions from LRO Ultraviolet Albedo and Temperature Measurements **[#3013]**
We use data from LRO Diviner and LAMP to show that the distribution of surface water frost appears to follow the coldest temperatures within the lunar polar cold traps.

9:10 a.m. Lucey P. G. * Neumann G. A. Smith D. E. Zuber M. T. Bussey D. B. Cahill J. T. Mazarico E. M. Paige D. A.
Lunar Polar Surface Frost: The View from LOLA **[#3015]**
LOLA shows that permanently shadowed regions are systematically more reflective than illuminated areas. Several percent water ice and increased porosity can account for the reflectance anomalies at 1064 and 122 nm.

9:30 a.m. Smith D. *
LOLA Observations of Lunar Volatiles

9:50 a.m. Siegler M. A. * Lucey P. Neumann G. Hayne P. O. Paige D. A. Greenhagen B. G.
Evidence for Surface Volatiles on the Moon and Mercury: A Planetary Comparison **[#3011]**
The Moon and Mercury both have shadowed regions featuring temperatures low enough to preserve water and other volatiles. We compare LRO and MESSENGER laser altimeter data sets to look for evidence of polar volatiles on these two solar system bodies.

10:10 a.m. Halekas J. S. * ARTEMIS Team
ARTEMIS Observations of the Space Environment Around the Moon and its Interaction with the Atmosphere and Surface **[#3016]**
ARTEMIS observations reveal both the effects of the plasma environment on the lunar surface and atmosphere, and the perturbations to the plasma environment caused by the presence of the Moon.

10:25 a.m. Jordan A. *
Deep Dielectric Charging of Regolith Within Permanently Shadowed Regions

10:40 a.m. Oliversen R. J. * Mierkiewicz E. J. Kuruppuaratchi D. C. P. Derr N. J. Gardner D. D. Lupie O. L. Roesler F. L.
High-Spectral Resolution, May 2013 Ground-Based Observations of the Lunar Sodium and Potassium Exosphere **[#3024]**
Fabry-Perot spectroscopy line profiles measurements of lunar exospheric Na D2 (5889.951 A) and K D1 (7698.965 A) emissions were obtained from the National Solar Observatory McMath-Pierce telescope during the May 2013 first to third quarter periods.

11:00 a.m. Farrell W. M. * Hurley D. M. Zimmerman M. I.
Solar Wind Implantation into Lunar Regolith: Hydrogen Retention in a Surface with Defects **[#3021]**
Hydrogen implantation and subsequent retention is found to highly dependent on both temperature and activation energy at the H-implantation/defect site. We specifically explore the latter variable herein using a statistical approach.

11:20 a.m. Zimmerman M. I. * Bussey D. B. J. Hurley D. M.
Can Solar Wind Volatiles Survive the Day Inside a Lunar Pit? **[#3012]**
We use a new three-dimensional illumination and heat diffusion code to characterize the daily heating cycle inside a lunar pit. This allows a detailed assessment of volatile stability in adjacent shadowed regions such as prospective lava tubes.

11:40 a.m. Stopar J. D. * Robinson M. S. Asphaug E. Jolliff B. L. Speyerer E. J. Christensen P. R.
In Search of Impact-Induced H_2O-Alteration Signatures: Initial Thermal Constraints **[#3030]**
Initial heat-transfer calculations suggest that polar ice can be melted and vaporized via impact-generated heating in the near-surface surrounding a crater. Water (liquid + gas) trapped in pore-spaces is available to form chemical alteration products.

12:00 p.m. DISCUSSION

Thursday, October 23, 2014
LUNAR VOLATILES: CURRENT UNDERSTANDING III
1:30 p.m. Bldg. 200, Room 100

Chairs: **William Farrell**
Timothy Glotch

1:30 p.m. Schwadron N. *
CRATER

1:50 p.m. Chin G. * Sagdeev R. Millikh G. M. Usikov D. Su J. J. Boynton W. Golovin D. Harshman K. Litvak M. Mitrofanov I. G. McClanahan T. Livengood T. A. Evans L. Starr R.
Determining the Magnitude of Neutron and Galactic Cosmic Ray (GCR) Fluxes at the Moon Using the Lunar Exploration Neutron Detector (LEND) During the Historic Space-Age Era of High GCR Flux **[#3001]**
The Lunar Reconnaissance Orbiter was launched during an era of minimum solar activity that also gave rise to historically high Galactic Cosmic Ray flux. Simultaneous LEND observations determine the scale of emergent lunar neutron flux unambiguously.

2:10 p.m. McCubbin F. M. * Shearer C. K.
Volatiles (H, C, N, F, S, Cl) in the Lunar Mantle, Crust, and Regolith: What Questions Remain and Where do We go Next? **[#3052]**
This paper presents a summary of data pertaining to the "magmatic volatile" elements H, C, N, F, S, Cl in and on the Moon. The progress made thus far is presented and future avenues of research are highlighted.

2:30 p.m. Robinson K. L. * Taylor G. J.
Variable Abundance and Isotopic Composition of Hydrogen Inside the Moon **[#3028]**
Measurements of H abundance and isotopes in lunar samples show that H is distributed heterogeneously in the lunar interior.

2:50 p.m. Pieters C. M. * Milliken R. E.
Important SKGs for Lunar Water Resources: Time/Space Variations of Surficial OH/H_2O **[#3051]**
The pervasive nature of surficial OH/H_2O across the Moon may make it the most valuable resource. Although our knowledge of its origin, abundance, and properties is currently very limited, this is easy to correct with new orbital spectroscopic data.

3:05 p.m. Kring D. A. * Kramer G. Y. Bussey D. B. J. Hurley D. M.
Prominent Volcanic Source of Volatiles in the South Polar Region of the Moon **[#3057]**
Volatiles produced by an immense pyroclastic vent in Schrodinger basin may be a good target for future missions that test models of volatile production, transport, and deposition.

3:25 p.m. BREAK

3:40 p.m. Allen C. C. *
Taurus Littrow Pyroclastic Deposit — An Optimum Feedstock for Lunar Oxygen **[#3046]**
A lunar resources demonstration mission to Taurus Littrow will encounter a >10 m thick pyroclastic deposit with few landing hazards, a uniform composition, and a predicted oxygen yield of approximately 3 wt. %, among the highest values on the Moon.

4:00 p.m. Petro N. E. *
Association Between Small Thorium Enhancements, Silicic Volcanism, and Enhanced OH/H_2O as Measured by the Moon Mineralogy Mapper **[#3053]**
The association between the 3 μm absorption feature measured by M^3 and locations of silicic volcanism is evaluated. There are a number of small-scale features on the Moon that appear to contain abundance endogenic hydroxyls at the lunar surface.

4:20 p.m. Glotch T. D. * Bandfield J. L. Lucey P. G. Hayne P. O. Greenhagen B. T. Arnold J. A. Ghent R. R. Paige D. A.
Spectral and Thermophysical Properties of Lunar Swirls from the Diviner Lunar Radiometer **[#3017]**
Diviner Lunar Radiometer observations support the solar wind standoff model for lunar swirl formation. Spectral and thermophysical data are consistent with retarded or abnormal space weathering at the swirls.

4:40 p.m. Clegg R. N. * Jolliff B. L. Boyd A. K. Stopar J. D. Sato H. Robinson M. S. Hapke B. W.
LROC NAC Photometry as a Tool for Studying Physical and Compositional Properties of the Lunar Surface **[#3032]**
LROC NAC photometry has been used to study the effects of rocket exhaust on lunar soil properties, and here we apply the same photometric methods to place compositional constraints on regions of silicic volcanism and pure anorthosite on the Moon.

5:00 p.m. DISCUSSION

Friday, October 24, 2014
FUTURE EXPLORATION: INSTRUMENTS, MISSIONS, AND TECHNIQUES
8:30 a.m. Bldg. 200, Room 100

Chairs: **Barbara Cohen**
Mark Robinson

8:30 a.m. Garry W. B. * Hughes S. S. Kobs Nawotniak S. E. Neish C. D. Haberle C. W. Heldmann J. L. Lim D. S. S. FINESSE Team
The Geology of Inferno Chasm, Idaho: A Terrestrial Analog for Lunar Rilles? **[#3047]**
We compare field observations at a rille-like channel (Inferno Chasm) at Craters of the Moon in Idaho to a rille in Marius Hills on the Moon.

8:45 a.m. Lawrence D. J. * Miller R. S. Peplowski P. N. Ozimek M. Scott C.
Lunar PLANE: Lunar Polar Low-Altitude Neutron Experiment for High-Spatial Resolution Hydrogen Concentration and Depth Measurements **[#3042]**
This presentation describes a low-cost, low-resource orbital mission that can obtain high-spatial resolution (<10 km) measurements of the hydrogen spatial and depth distributions for the lunar poles.

9:00 a.m. Cohen B. A. * Hayne P. O. Paige D. A. Greenhagen B. T.
Lunar Flashlight: Mapping Lunar Surface Volatiles Using a Cubesat **[#3031]**
The Lunar Flashlight mission will measure surface ice within the permanently shadowed regions of the lunar south pole in support of NASA's Strategic Knowledge Gap to understand water and other volatiles in lunar cold traps.

9:15 a.m. Zacny K. * Paulsen G. Chu P. Kleinhenz J. Smith J. Trautwein J. Quinn J.
Lunar Prospecting Drill **[#3048]**
We report on development and testing of a drill designed to capture volatile rich samples on the Moon from up to 1 meter depth. The drill was recently tested in lunar chamber at NASA GRC.

9:30 a.m. Clark P. E. * MacDowall R. Reuter D. Mauk R. Didion J. Patel D. Farrell W. Cox R.
Deep Space Cubesat Orbiter and Compact Broadband IR Instrument to Determine the Systematics of Lunar Water **[#3007]**
We have applied the CubeSat Paradigm to science requirements-driven deep space exploration mission, referred to as a LunarCube, and are developing a compact 'workhorse' instrument for a high priority science application.

9:45 a.m. Woerner D. F. *
Radioisotope Thermoelectric Generators (RTGs) for Lunar Exploration **[#3002]**
A Multi-Mission RTG (MMRTG) is powering the Curiosity rover and was designed as a compact, rugged power source capable of landing on other bodies. NASA is considering development of an enhanced MMRTG and Advanced RTG. More info presented here.

10:00 a.m. Nagihara S. * Zacny K. Hedlund M. Taylor P. T.
Modular Heat Flow Probe for Small Lunar Landers **[#3037]**
We report the latest on our effort for developing a modular lunar heat flow probe that can be accommodated on small landers.

10:15 a.m. BREAK

10:30 a.m. Carpenter J. D. * Barber S. Cerroni P. Fisackerly R. Fumagalli A. Houdou B. Howe C. Magnani P. G. Morse A. Monchieri E. Reiss P. Richter L. Rizzi F. Sheridan S. Waugh L. Wright I. P.
Accessing and Assessing Lunar Resources with PROSPECT **[#3018]**
PROSPECT is a package in development by ESA to assess the in-situ resource potential of lunar regolith. PROSPECT will: obtain sub-surface regolith samples, extract volatiles, identify chemical species, quantify abundances, and characterize isotopes.

10:45 a.m. Speyerer E. J. * Lawrence S. J. Stopar J. D. Robinson M. S. Jolliff B. L.
Optimized Traverse Planning for Future Lunar Polar Prospectors **[#3066]**
Ground-truth measurements are required to fully understand the resource potential of lunar volatiles. A mobile polar prospector that leverages persistently illuminated areas would address many outstanding questions by sampling multiple nearby PSRs.

11:00 a.m. Robinson M. S. * Thanga J. Wagner R. V. Hernandez V. A.
Arne — Sublunarean Explorer **[#3025]**
We propose a simple and cost effective reconnaissance of the Mare Tranquillitatis Pit with Arne, a small lander (<130 kg) that carries three flying microbots (or pit-bots) each with mass of 3 kg. Objectives serve key science and exploration needs.

11:15 a.m. Dhingra D. * Pieters C. M. Head J. W.
Copernicus Crater: Compelling Science Exploration Target Waiting for Future Missions **[#3054]**
Copernicus crater has several scientifically interesting locations that provide a strong motivation for its exploration. We provide a summary of new scientific insights, exploration objectives and potential targets.

11:30 a.m. Young K. E. * Bleacher J. E. Evans C. A. Arzoumanian Z. Gendreau K. Hodges K. V.
The Integration of Handheld Technologies into Planetary Surface Exploration **[#3043]**
Developing a suite of in situ geochemical instruments to assist in sample collection and high-grading is crucial in enhancing the efficiency and effectiveness of astronaut surface activities. We highlight several of these instruments here.

11:45 a.m. Bleacher J. E. * Eppler D. B. Tewksbury B. J. Helper M. A.
Astronaut Geology Training **[#3033]**
We discuss the current status of astronaut training.

Friday, October 24, 2014
FUTURE EXPLORATION: STRATEGIES AND OPPORTUNITIES
1:30 p.m. Bldg. 200, Room 100

Chairs: **Clive Neal**
Benjamin Greenhagen

1:30 p.m. Klaus K. *
The Space Launch System and the Proving Ground: Pathways to Mars **[#3014]**
The SLS provides a critical heavy-lift launch capability enabling diverse deep space missions including human exploration, planetary science, astrophysics, heliophysics, planetary defense, and commercial space exploration.

1:45 p.m. Huber S. A. Thornton J. P. * Hendrickson D. H.
Astrobotic Technology: Commercial Lunar Payload Delivery Service **[#3063]**
This paper describes Astrobotic Technology's financial and technical model for delivery of commercial lunar landing capabilities through government partnership.

2:00 p.m. Greenhagen B. T. * Donaldson Hanna K. L. Thomas I. R. Bowles N. E. Allen C. C. Pieters C. M. Paige D. A.
The Benefits of Sample Return: Connecting Apollo Soils and Diviner Lunar Radiometer Remote Sensing Data **[#3067]**
Here we present a comprehensive study to reproduce an accurate simulated lunar environment, evaluate the most appropriate sample and measurement conditions, collect thermal infrared spectra of Apollo soils, and correlate them with Diviner observations.

2:15 p.m. Shearer C. K. * Lawrence S. Jolliff B. L.
Robotic Sample Return I. Advancing our understanding of Planetary Differentiation **[#3041]**
We examine the role of lunar SR for advancing our knowledge of the early differentiation of the Moon and other planetary bodies.

2:45 p.m. Lawrence S. J. * Jolliff B. L. Shearer C. Robinson M. S. Stopar J. D. Braden S. E. Speyerer E. J. Hagerty J. T. Denevi B. W. Neal C. R. Draper D. S.
Robotic Sample Return II: Addressing Fundamental Exploration Themes **[#3062]**
A campaign of automated sample return to specific locations identified by recent mission results as a critical aspect of an integrated exploration strategy is discussed; specific ROIs are identified to inform future hardware choices.

3:05 p.m. Shearer C. K. * Neal C. R. Jolliff B. L. Wieczorek M. A. Mackwell S.
A New Moon. An Initiative to Integrate new Lunar Information into our Fundamental Understanding of the Moon and the next Stages of Lunar Exploration **[#3040]**
We propose a new initiative that will integrate recent mission observations into producing a richer understanding of the Moon, revealing new clues about the history of the solar system, and providing new information for renewed lunar exploration.

3:35 p.m. DISCUSSION

TAURUS LITTROW PYROCLASTIC DEPOSIT – AN OPTIMUM FEEDSTOCK FOR LUNAR OXYGEN.

Carlton C. Allen, NASA Johnson Space Center, Houston, TX USA (carlton.c.allen@nasa.gov).

Introduction: Future human habitation of the Moon will likely require the use of locally derived materials because of the high cost of transportation from Earth. Oxygen, extracted from oxides and silicates, is a potentially abundant lunar resource vital for life support and spacecraft propulsion. The anticipated costs of supplying all oxygen needs for a lunar base from Earth are high enough to warrant serious study of oxygen production from local resources.

Lunar Oxygen Production: Over 20 different processes have been proposed for oxygen production on the Moon [1]. Among the simplest and best studied of these processes is the reduction of oxides in lunar minerals and glass using hydrogen gas.

Oxygen can be extracted from lunar soils and pyroclastic glass beads by exposing the samples to flowing hydrogen at subsolidus temperatures (~1050°C). Total oxygen yield is directly correlated to the sample's abundance of FeO, but is not correlated to the abundance of any other oxide [2]. Oxygen is extracted predominantly from FeO, with lesser contributions from TiO_2 and SiO_2. Oxygen yield is independent of soil maturity. All major FeO-bearing phases contribute oxygen, with extraction from ilmenite and glass significantly more efficient than from olivine and pyroxene.

Lunar Pyroclastic Deposits: Pyroclastic glass may be an optimum feedstock for lunar oxygen production using the hydrogen reduction process, based on oxygen yield. Telescopic observations and orbital images of the Moon reveal at least 75 lunar pyroclastic deposits, interpreted as the products of explosive volcanic eruptions [3]. The deposits are understood to be composed primarily of sub-millimeter beads of basaltic composition, ranging from glassy to partially-crystallized [4]. Delano [5] documented 25 distinct pyroclastic bead compositions in lunar soil samples, with a range of FeO abundances from 16.5 - 24.7 wt%. The FeO-rich species, represented by the isochemical orange and black glasses collected by the Apollo 17 astronauts, promise particularly high yields. In hydrogen reduction experiments, samples of this material yielded 3.7 wt. % oxygen, the highest percentage of oxygen of any Apollo rock or soil [2]. These samples are uniformly fine grained, offering a feedstock which reacts rapidly and can be used with little or no processing prior to oxygen extraction.

Taurus Littrow: The Taurus Littrow regional pyroclastic deposit, located in eastern Mare Serenitatis (Fig. 1), extends across the Apollo 17 landing site. The Shorty crater orange and black glass beads, with an average diameter of 44 μm [6], are understood to be samples of this deposit. The orange and black glasses are identical in major elemental composition, with the color indicating the degree of ilmenite and olivine crystallization following eruption [7]. These glasses have FeO abundances of 22.7 wt%, among the highest abundances of any pyroclastic glass.

A future mission to demonstrate oxygen production on the lunar surface could yield maximum results if targeted to an FeO-rich pyroclastic deposit. Analyses by the Diviner Lunar Radiometer Experiment (Diviner) on the Lunar Reconnaissance Orbiter (LRO) spacecraft, coupled with high-resolution images of the Taurus Littrow deposit from the Apollo Metric Mapping Camera and the Lunar Reconnaissance Orbiter Narrow Angle Camera (LROC NAC), provide new information to support landing site selection.

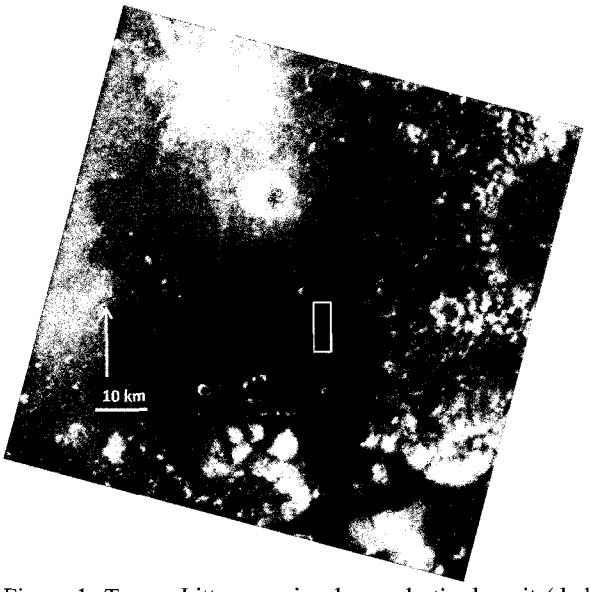

Figure 1. Taurus Littrow regional pyroclastic deposit (dark area), with region of interest outlined (Apollo metric mapping camera image AS15-M-0972)

Diviner Lunar Radiometer Experiment: Diviner is a near- and thermal-infrared mapping radiometer on LRO, with a 320 m (in track) by 160 m (cross track) detector field of view at an altitude of 50 km [8]. Three channels centered near 8 μm are used to calculate the emissivity maximum known as the Christiansen feature (CF) [9]. Diviner CF wavelength values, taken from

data obtained near local noon, were reduced using the recent corrections of Greenhagen *et al.* [10]. These corrected CF values are particularly sensitive to silica polymerization in minerals including plagioclase, pyroxene and olivine. Given the restricted mineralogy of most lunar samples, CF values are closely correlated to major element abundances, particularly FeO. The CF and FeO values correlate across the full range of Apollo soil and pyroclastic glass compositions. The published correlation [11] between FeO abundance (wt. %) and CF (μm) is:

$$FeO = 74.24 \times CF - 599.9; \; r^2 = 0.90$$

Region of Interest: A region of interest with an area of ~ 20 km^2 (Fig. 1), bounded by 20.93 to 21.15° N and 30.02 to 30.10° E, was selected for detailed examination, based on consistently high Diviner CF values. This area, in the eastern portion of Taurus Littrow, is within the darkest area of the deposit. The combination of albedo and CF data indicate that the region of interest encompasses one of the least-contaminated sections of the deposit, and that the material is uniform in composition.

Within the region of interest, LROC NAC images show the surface to be extremely smooth, with uniform albedo. Very few craters or other landing hazards are visible at the sub-10 m scale (Figs. 2,3).

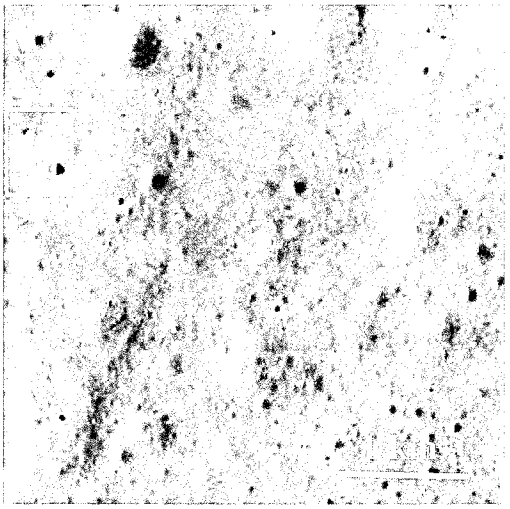

Figure 2. 15 km^2 area of the eastern Taurus Littrow pyroclastic deposit, within region of interest (LROC NAC image; area of Figure 3 outlined)

Figure 3 also provides an estimate of the thickness of the pyroclastic deposit. The ~100 m diameter crater ejected distinct rays of dark material, indicating that the crater did not penetrate to higher-albedo material beneath the deposit. This observation indicates that the

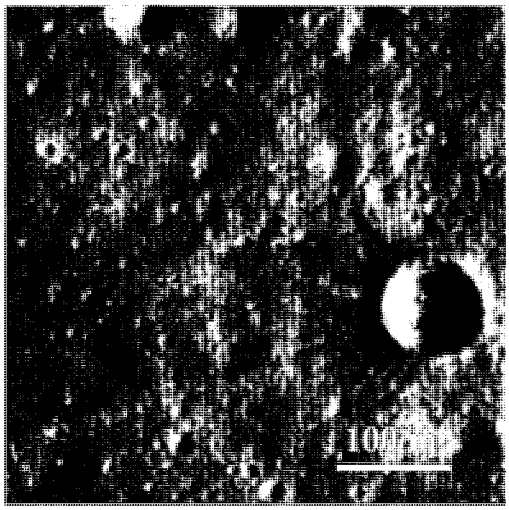

Figure 3. Area of eastern Taurus Littrow pyroclastic deposit, inset in Figure 2 (LROC NAC image)

deposit has a minimum thickness of ~10 m at this location, in accord with the estimated thicknesses of pyroclastic deposits in Mare Orientale [12].

The averaged CF value in the region of interest is 8.37 μm, corresponding to an FeO abundance of 21.5 wt. %. The standard deviation of these values is 0.03 μm, corresponding to an uncertainty in FeO abundance of 2.2 wt. % [13]. These values predict an oxygen yield from hydrogen reduction of ~3.0 wt. % [2].

Implications for Lunar Oxygen Production: This study demonstrates that the optimum location for a lunar resources demonstration mission can be identified, and that the oxygen yield can be predicted, using a combination of high-resolution imaging and thermal-infrared data. A mission to Taurus Littrow will encounter a deposit at least 10 m in depth with few landing hazards, a uniform composition, and a predicted oxygen yield of approximately 3 wt. %, among the highest values on the Moon.

References: [1] Taylor L. A. and Carrier W. D. III (1992) *Engineering, Construction and Operations In Space III,* Am. Soc. Of Civ. Eng., 752-762. [2] Allen, C. C. et al. (1996) *JGR*, 101, 26,085. [3] Gaddis, L. R. et al. (2003) *Icarus, 161,* 262. [4] Pieters, C.M. et al. (1974) *Science, 183,* 1191. [5] Delano, J. (1986), *Proc. LPSC, 16th,* D201-D213. [6] Heiken, G. et al. (1974) *GCA, 38,* 1703. [7] Weitz, C.M. et al. (1999) *Meteorit. Planet. Sci., 34,* 527. [8] Paige, D.A. *et al.* (2009) *Space Sci. Revs.*, DOI 10.1007/s11214-009-9529-2. [9] Greenhagen, B.T. et al. (2010) *Science, 329,* 1507-1509. [10] Greenhagen, B.T. et al. (2011) *LPS XLII,* Abstract # 2679. [11] Allen C. C. *et al.* (2012) *JGR, 117,* E00H28, doi:10.1029/2011JE003982. [12] Gaither T. A. et al. (2014) *LPS XLV,* Abstract # 1933. [13] Allen C. C. et al. (2014) *LPS XLV,* Abstract # 2447.

THE NEED FOR LUNAR AND PLANETARY CARTOGRAPHY PLANNING. B. A. Archinal[1], R. L. Kirk[1], L. R. Gaddis[1], J. Hagerty[1], J. Skinner[1], T. N. Titus[1], L. P. Keszthelyi[1], T. Hare[1], S. J. Lawrence[2], R. Beyer[3,4], A. Nefian[4], T. Fong[4], and T. Duxbury[5]. [1]U. S. Geological Survey, Astrogeology Science Center (2255 N. Gemini Drive, Flagstaff, AZ 86001, barchinal@usgs.gov), [2]School of Earth and Space Exploration, Arizona State University (Tempe, AZ 85287-3603), [3]Carl Sagan Center, SETI Institute (Mountain View, CA, 94043), [4]NASA Ames Research Center (Moffett Field, CA, 94035), [5]George Mason University (Fairfax, VA, 22030).

Introduction: Cartography is the science and art of placing information in a community-recognized spatial framework. Cartography involves geodetic control, geographic standards, geospatial registration, and data processing. Cartography is essential for comparing or combining data taken at different times or by different instruments. As such, cartography is the foundation for lunar and planetary science and exploration, especially when addressing important questions by looking for subtle variations (e.g., spectral, photometric, and temporal) between different observations.

A lack of planning in planetary cartography has had and will have serious consequences for the operation of and scientific return from planetary missions. Here we highlight the current, unprecedented lack of formal cartographic planning for the U.S. space program and recommend a community-driven solution.

Background: While the USGS has been heavily involved in planetary cartography for over 50 years, this work has always been part of a broad community effort. During the late 1960s and 1970s multiple organizations helped plan and carry out this work, including NASA JSC, the National Geodetic Survey, the Defense Mapping Agency, RAND, and various universities. The table below lists the various groups chartered to coordinate these efforts, effectively disseminate information to the broader community, and/or advise NASA leadership on cartographic matters [1].

Start Date	Name
1974	Lunar Photography and Cartography Committee
1977	Lunar and Planetary Photography and Cartography Committee
1979	Planetary Cartography Working Group
1994	Planetary Cartography & Geologic Mapping Working Group (PCGMWG)

The last of these, the PCGMWG, includes the chair of the NASA Geologic Mapping Subcommittee (GEMS). Other groups have been active in making recommendations on cartographic standards (e.g., IAU WGCCRE, 1976-present; MGCWG, mid-'90's-present; LGCWG, 2007~2009) but not in general cartography planning [2-4].

From 1994-2012, the PCGMWG made cartography recommendations to NASA, including submitting a white paper on the importance of planetary cartography [5] to the NRC Decadal Survey. The PCGMWG ceased making cartography recommendations in 2012. The group continues its other responsibilities.

The Need for Lunar Cartography Planning: In the absence of an official plan, many important questions related to cartographic and mapping support to missions and research are unanswered. *Below are examples of practical issues for lunar researchers:*

- LRO LOLA data are archived in the Planetary Data System (PDS) in two different coordinate systems – how can users convert these cartographic data for their use? Should they need to?
- Kaguya, Chandrayaan-1 (C-1), and Chang'E data have been released in different reference frames than LRO data. Who is going to register them to one coordinate frame so they can be used together at known accuracy levels?
- Clementine and Lunar Orbiter datasets currently have displacements of up to several km relative to LRO data. Clementine multispectral data are still unique in some bandpasses and so are still needed for applications such as resource determination and optical maturity measurements. Who will register them to LRO to enable coanalysis with the more recent datasets at acceptable cartographic accuracy levels?
- How will the multitude of lunar topography datasets be merged and who will do it? Current sources are LRO LOLA, LROC WAC stereo, and LROC NAC stereo; Kaguya LALT and TC stereo; C-1 TMC stereo; and Apollo Metric and Panoramic stereo. A merged global set is essential for the best projection of all types of data, in order to compare such data at accuracy levels that approach their resolution.
- What is the absolute positional accuracy of the LROC WAC data? Do these data need to be controlled to the LOLA reference frame?
- Will the usability of all the LROC NAC stereo pairs be checked to see if they can be used to generate DTMs in the future?
- Who is going to perform high-resolution lunar topographic mapping once LRO funding runs out?
- Is a new mission needed in order to characterize lunar topography and landing sites with sufficient accuracy and coverage for future exploration mission operations

(landing, resource location and extraction, surface activities, etc.) and science (registration of datasets)?
• What requirements should be placed on future lunar missions to gather the most valuable data and to ensure that their data can be integrated at high precision? For example, should there be uniform requirements for instrument calibration and cartographic processing?

More general issues:
• Who is responsible for establishing lunar cartographic standards and how can compliance be assured?
• What new techniques need to be developed or perfected to support cartographic data processing and the analysis of existing and future data? How will such techniques be tested to quantify their accuracy?
• How will resources for research and analysis of data be prioritized to address these issues? How will the reorganization of NASA-funded research, with cartographic processing concentrated in the PDART program [6], affect prioritization?

The most salient of these issues are discussed below in greater detail.

Need for geodetic control. Controlling datasets with photo- or radar-grammetric, or altimetric solutions is the only way to register data in a common frame at known levels of accuracy to meet data fusion needs. Such knowledge is critically important for science (e.g., analysis of body orientation variations, photometric correction for spectral/mineral studies, geologic mapping, change detection, and multi-instrument comparisons) and mission operations (e.g., landing site selection, targeting images from orbit, and landed surface operations), making control one of the most fundamental cartographic activities. Though some analyses can tolerate uncontrolled data, we underscore the fact that spatial accuracy can only be quantified through the control process. Recognizing the importance of controlled datasets for science and exploration purposes, in 2007 *the NASA Advisory Council recommended that* ***all lunar datasets*** *be geodetically controlled* [7].

Cartographic Standards. Controlling each data set to a different cartographic standard only minimally improves the scientific value of the data. In a spacecraft operational environment, confusion regarding coordinate systems could have catastrophic consequences. The effect is comparable to that of not standardizing measurement units. While the development of standards may seem an arcane subject, the pragmatic goal is universal acceptance of a single standard – even when there is no one clear choice based on technical considerations.

As such, a current and recurring concern is to find the most effective inducements to obtain the widest acceptance of planetary cartographic standards, especially by active missions. NASA has the opportunity to lead by example; however such leadership cannot occur without a plan developed by key stakeholders.

Prioritizing tool development. The need for improved techniques is driven both by the increasing volume of data and the increasing complexity of instruments. Examples of new capabilities that are needed include (1) faster, more robust, automatic feature matching between disparate data types, enabling new types of data fusion; (2) ability to simultaneously adjust data from different platforms (e.g., flyby, orbital, descent, lander, and rover) and data types (e.g., images, spectra, radar, and altimetry); (3) new tools to combine different methods for generating topographic information, especially combining LIDAR and image-based and new techniques, including those based on photoclinometry.

Multi-mission data analysis. Individual instrument teams usually understand and address their mapping needs, but without broader guidance, multi-mission cartography can be neglected. Such concerns are relevant to exploration and mapping of the entire Solar System. For the Moon, petabytes of data have been collected by multiple nations, missions, and instruments, posing both challenges and opportunities for co-analysis [8]. The coordination of national efforts both to develop tools for data processing and to process lunar datasets, in particular to process such datasets jointly in order to ensure their consistency, would be of tremendous benefit to all spacefaring nations.

Recommendation: In principle, re-instituting a program of cartography planning should be straightforward – a new working group should be chartered to resume this essential work. This issue cuts across all disciplines of planetary science. So ***we recommend that the present planetary Advisory Groups (including LEAG) issue a "finding" that a new cartographic planning group should be chartered, to consider lunar and general planetary mapping needs.***

References: [1] PCWG, 1993, "Planetary Cartography 1993-2003." [2] Archinal, B. et al., 2011, *Cel. Mech. Dyn. Ast.* 109, 101. [3] Duxbury, T. et al., 2002, http://astrogeology.usgs.gov/search/details/Research/ISPRS/Duxbury/pdf. [4] Archinal, B. et al., 2009, *LPS XL*, #2095. [5] Johnson, J. et al., 2010, http://www.lpi.usra.edu/decadal/sbag/topical_wp/JeffreyRJohnson.pdf. [6] NASA, 2014, Research Opportunities in Space and Earth Sciences - 2014, C.7, Planetary Data Archiving, Restoration, and Tools. [7] NAC, 2007, Tracking Number: S-07-C-1, http://bit.ly/x0HnnM. [8] Archinal, A. et al., 2012, *LPS XLIII*, #2394; Kirk, R. et al., 2012, "Lunar Cartography...", *ISPRS Comm. IV.*

COREGISTRATION OF ELEVATION DATA FROM THE LUNAR ORBITER LASER ALTIMETER AND THE SELENE TERRAIN CAMERA. M. K. Barker[1], E. Mazarico[2], G. A. Neumann[2], D. E. Smith[2,3] and M. T. Zuber[3] [1]Sigma Space Corp., 4600 Forbes Blvd. Lanham, MD 20706 michael.k.barker@nasa.gov, [2]Solar System Exploration Division, NASA Goddard Space Flight Center 8800 Greenbelt Rd. Greenbelt, MD 20771, [3]Dept. of Earth, Atmospheric and Planetary Sciences, MIT, 77 Massachusetts Ave. Cambridge, MA 02139.

Introduction: The Lunar Orbiter Laser Altimeter (LOLA) aboard the Lunar Reconnaissance Orbiter (LRO) has collected over 6.3 billion measurements of surface height with a vertical precision of ~10 cm and an accuracy of ~1 m. The ability of LOLA to obtain measurements under uniform illumination conditions and in shadowed regions globally provides an advantage over passive stereoscopic imaging, particularly at high latitudes (> 60°) where imaging is hindered by low solar incidence angles. This has allowed LOLA to produce the highest resolution and most accurate polar terrain models to date. However, due to LRO's polar orbit, a few gaps in the LOLA coverage as wide as ~4 km still persist near the equator.

Here we present preliminary results of efforts to fill in gaps in LOLA coverage by incorporating an independently-derived terrain model into the data post-processing. Recently, the Terrain Camera (TC) aboard the SELENE (Kaguya) spacecraft produced a global digital elevation model (DEM) from stereo imaging with 10 m spatial posting [1]. The TC DEM is a highly complementary dataset with which to augment the LOLA topography. We show here that the TC DEM can be registered to the LOLA geodetic framework with 3-4 m root-mean-square (RMS) elevation residuals. The goal of this work is to produce the most complete global terrain model of the lunar surface by merging both high-resolution datasets while preserving the geodetic accuracy of the LOLA data.

TC-to-LOLA Registration: The global TC DEM dataset (SLDEM2013) is divided into separate 1°x1° tiles (available from the SELENE Data Archive [2]) that are mosaics of the TC's 1°-wide ground swaths. We obtained the 43,200 tiles covering latitudes within ±60° and down-sampled them from the original resolution of 3600 pix/deg to 512 pix/deg (60 m/pix at the equator), which we found to be closer to the effective resolution of the dataset. The LOLA data coverage is sufficiently dense for most purposes at latitudes outside this range.

Errors in the TC DEMs result from imperfect knowledge of the SELENE orbit, as well as camera pointing, flat-field, and distortion. Offsets in the LOLA profiles are due largely to orbit uncertainties and errors in the laser boresight model. To isolate these error sources, we follow a two-step approach when registering the TC DEMs to the LOLA data: (1) We derive a 5-parameter coordinate transformation between every TC DEM tile and the full resolution (unbinned) LOLA data in that tile. This tile-averaged transformation includes a 3-dimensional (3-D) translational offset (lon,lat,vertical) and two vertical planar tilts in the horizontal directions. We employ a downhill simplex minimization algorithm with multiple random starting locations. The best fit minimizes the root-mean-square (RMS) vertical residual after removal and down-weighting of outlier points. Each LOLA profile in a tile is further weighted inversely proportional to its number of points so that profiles with more points do not adversely dominate the fit. In step (2), to account for LOLA geolocation errors, we fit a 3-D offset to each LOLA profile in the transformed TC DEM.

Results: Figure 1 shows the distribution of weighted RMS vertical residuals of all tiles before (blue) and after (red) applying the best-fit transformations in step (1). The initial/final median RMS is ~4.5/3.5 m and the median absolute deviation (MAD) is 0.9/0.3 m. The 90th percentile is decreased from ~10 m to ~4 m. The median absolute tile-averaged translational offsets were at the sub-pixel level: ~10 m horizontal and ~1 m vertical, with MADs of ~10 m and ~1 m, respectively. The individual LOLA profile 3-D off-

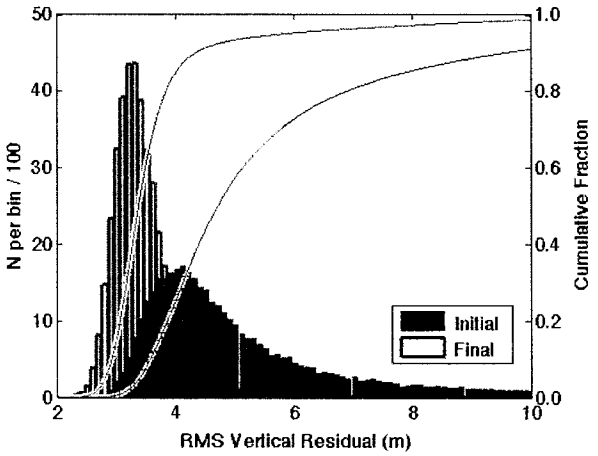

Figure 1 - Distribution of weighted RMS vertical residuals between unbinned LOLA data and 43,200 1°x1° TC DEMs at 512 ppd resolution within ±60° latitude before (blue) and after (red) best-fit transformations for each DEM.

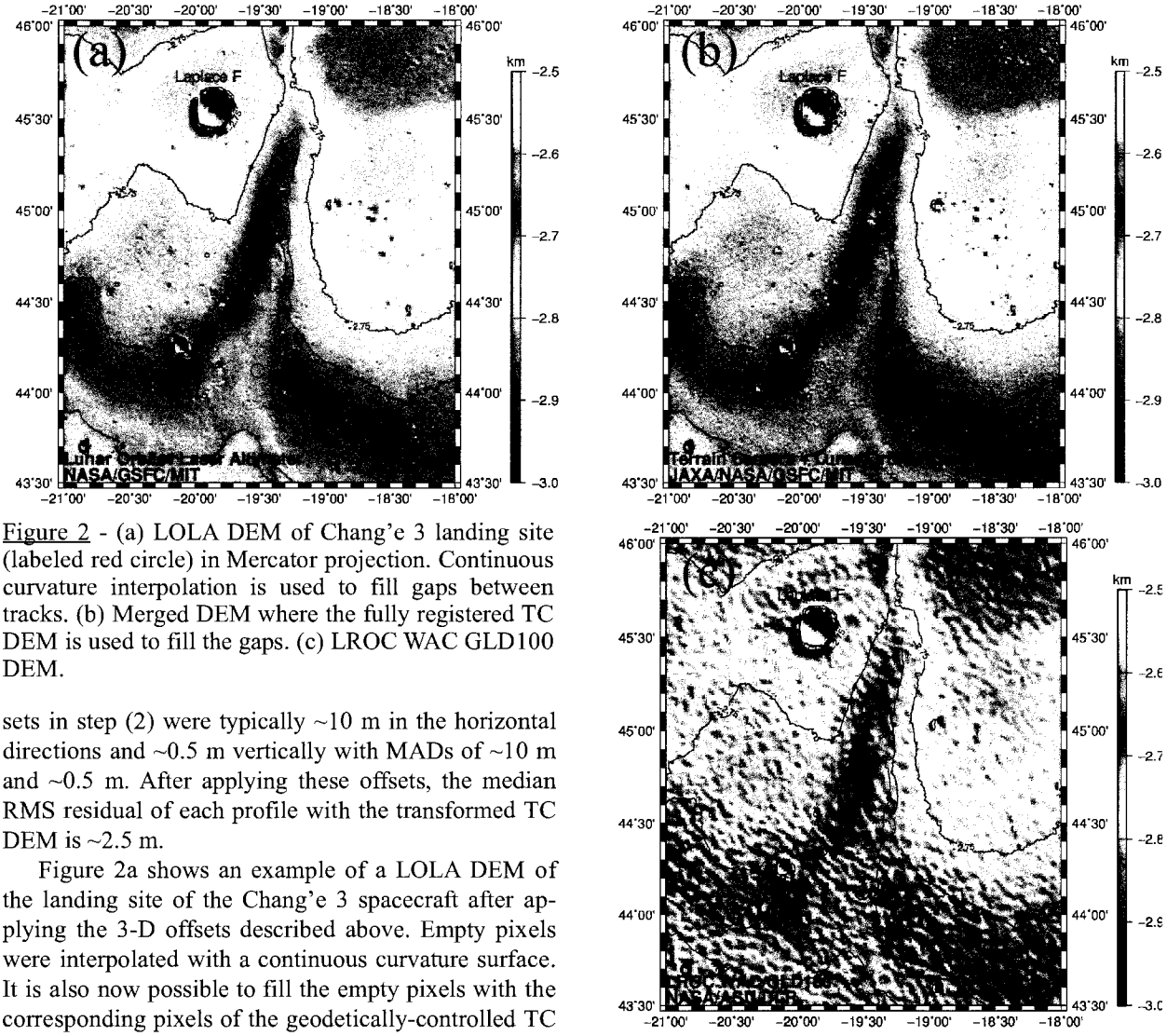

Figure 2 - (a) LOLA DEM of Chang'e 3 landing site (labeled red circle) in Mercator projection. Continuous curvature interpolation is used to fill gaps between tracks. (b) Merged DEM where the fully registered TC DEM is used to fill the gaps. (c) LROC WAC GLD100 DEM.

sets in step (2) were typically ~10 m in the horizontal directions and ~0.5 m vertically with MADs of ~10 m and ~0.5 m. After applying these offsets, the median RMS residual of each profile with the transformed TC DEM is ~2.5 m.

Figure 2a shows an example of a LOLA DEM of the landing site of the Chang'e 3 spacecraft after applying the 3-D offsets described above. Empty pixels were interpolated with a continuous curvature surface. It is also now possible to fill the empty pixels with the corresponding pixels of the geodetically-controlled TC DEM. The resulting merged DEM (Figure 2b) reveals surface detail that would otherwise be absent or heavily smoothed in the LOLA-only interpolated DEM (e.g., crater at [45° N, -19.5° E]). The merged DEM gives an elevation of -2630 m for the Chang'e 3 site, using the location (44.1214° N, -19.5116° E) derived in [3] from Lunar Reconnaissance Orbiter Camera (LROC) Narrow Angle Camera images. This is 10 m higher than the value [3] derived using the Wide Angle Camera (WAC) GLD100 DEM (Figure 2c), but within the ~20 m vertical uncertainties of the GLD100 [4].

The merged TC/LOLA dataset has many applications. Studies requiring the high geodetic accuracy of the LOLA data (~20 m horizontal and ~1 m vertical) and the good coverage of the TC data will especially benefit. In addition, the individual profile 3-D offsets form "pseudo-crossovers" which will help characterize LOLA orbital errors, the LOLA boresight, and lunar tidal deformations [5]. In the future, the coregistration accuracy could be improved by using the individual 1°-wide TC ground swaths instead of the 1°x1° tiles because the boundaries of the former do not generally align with those of the latter.

Acknowledgments: We gratefully acknowledge J. Haruyama, the entire TC team, and the SELENE Data Archive for kindly providing the TC data. SELENE is a Japanese mission developed and operated by JAXA.

References: [1] Haruyama, J. et al. (2012) LPSC 43, #1200. [2] SELENE Data Archive site, http://l2db.selene.darts.isas.jaxa.jp/archive/index.html.en. [3] Robinson, M. et al., (2013) Dec. 30, http://lroc.sese.asu.edu/news/index.php. [4] Scholten, F. et al. (2012) *JGR Plan.*, *117*, E12. [5] Mazarico, E. et al. (2014) *GRL*, *41*, 2282-2288.

ASTRONAUT GEOLOGY TRAINING. J. E. Bleacher[1], D. B. Eppler[2], B. J. Tewksbury[3], M. A. Helper[4]
[1]NASA Goddard Space Flight Center, Planetary Geodynamics Laboratory, Greenbelt, MD, 20771 (jacob.e.bleacher@nasa.gov)
[2]NASA Johnson Space Center, Exploration Science Office, Houston, TX, [3]Department of Geosciences, Hamilton College, Clinton, NY, [4]Jackson School of Geosciences, The University of Texas at Austin, Austin, TX.

Introduction: The scientific success of the Apollo Missions is a testament to the scientists, engineers and managers who developed the exploration architecture that accomplished their goals. There will be numerous differences between the Apollo Program and HEOMD approaches to surface science during future human exploration of the Solar System. However, many similarities will likely exist. The Apollo Program approach to preparation for science operations included extensive geology training, including over 1000 hours per crew member during the J-Missions [1]. Fielding well trained crew members, particularly for those who do not possess a science background, was considered a major influence on the science success of those missions [1-4]. Although the Apollo geologic training program was discontinued in 1972, Space Shuttle crewmembers received 40-50 hours of limited training in Earth observations prior to their flights [5]. In 2008, it was decided to revamp the geologic training curriculum to include more thorough classroom work and geologic mapping to improve the astronaut's observations skills and understanding of basic geological concepts. The two most recent astronaut candidate classes (2009 and 2013) received this improved geology training, and the Astronaut Office has also involved senior members in short field geology mapping courses and field assistant programs. Here we discuss the current status of astronaut geology training.

Background: Between 2008 and 2010 LEAG and CAPTEM jointly conducted the Lunar Sample Acquisition and Curation Review (LSACR) [6] to assess sample identification, documentation, collection and curation during the Apollo Missions as a basis for recommendations to ensure successful science exploration of the Moon in the future. Among many recommendations the LSACR suggested the development of a geology training program for future human exploration beyond low Earth orbit.

Geology training for the Apollo Program was conducted in an atmosphere of known targets and defined science objectives. The current environment within NASA involves development of hardware to carry humans to a series of possible destinations, with a long range vision of humans at Mars. As such, geology training at this time is primarily focused on basic geologic concepts as a means of enhancing observations and science that might be conducted from the ISS. The goal is not to train astronauts in lunar science or Mars geology, but to begin training the mindset that all astronauts should know the scientific value of, and routinely consider the observations they can make from their unique vantage point. We hope to help develop a Crew Office within which consideration for science operations is the norm for all decision making steps during the development of the human exploration architecture.

Geology Training: Geology training for the astronauts can be generally dividied among three main approaches, including: 1) class room teaching and field exercises, 2) a field assistant program, and 3) integrated analog field tests. Classroom and field exercises incorporate an "outcrop to orbit" perspective; whether it be structural geology or volcanology, all topical training integrates orbital observations. The field component of geology training is also integrated with a Crew Office requirement to routinely provide expeditionary training and team building experiences.

***Classroom & Field Exercises*:** Classroom training and field exercises are the primary mechanism for training during astronaut candidacy. The curriculum, as it has evolved between the 2009 and 2013 includes input from > 30 geologists both within and outside of NASA. Classroom training is focused on basic field geology concepts and for the 2013 class involved three weeks of class room activies. Discussion of target specific science was limited and generally presented in a historical context with respect to lunar science associated with the Apollo Program.

The approach to classroom training involves a daily focus on a single geologic discipline. Typically the crew were presented with a perspective of what they can expect to see from ISS, essentially a regional to global perspective from orbit. Lectures and activies become more focused on details within each discipline. The details are not presented as material that is expected to be memorized and retained but in a manner that enables the crew to understand why the observations they can make from ISS are important to scientists on the ground. For example, the crew are trained not to necessarily interpret that a volcano is rhyolitic but to explain that they see a volcano with steep flanks and a dark colored plume that extends nearly 3 volcano diameters to the north. The goal is to train scientific observational skills and an understanding of the value of those observations.

During classroom training each crew memberconstructs a preliminary geologic map of the field exercise area, a volcanic region of about 140 km^2,

from remote sensing data . Most days are concluded with a new look at their map based on the geologic discipline of the day. In other words, each day ends by revisiting and revising the map on the basis of the geologic lessons that day. The end result is a well constructed remote sensing map from which they develop field-testable hypotheses and plan their field activities.

Shortly after completion of classroom training the crew are taken into the field. Although the primary objectives are geological, living and working outdoors also provides opportunities for expeditionary training. With preselected field targets and their prelimary maps in hand, crew member pairs and a field geologist conduct geologic mapping, sample characterization and collection, and data collection with a range of geologic instruments. A geologic map and cross section that integrate both remote sensing and field observations are the final team products of these efforts. Results are later compared with published interpretation(s) for the site. Upon requests from the Crew Office, a similar approach has been adopted for senior members who joined the Astronaut Corp prior to the 2009 class. Field training exercises for this purpose have been conducted several times in the last few years with the intent of providing a baseline level of geologic training and experience for the entire Crew Office.

***Field Assistants*:** Classroom training and field exercises provide a large group with a basic level of geologic knowledge. However, basic field exercises can lack a sense of "doing new science". To address this the field assistant program was developed. In this program geology trainers inform the Crew Office of opportunites for astronauts to take part in current research projects. As field assistants the crew members are given an opportunity to experience the reality of testing multiple working hypotheses and dealing with the real-life difficulties of doing so. The participants are exposed to situations where field geologists disagree while discussing their observations in the field. This provides the field assistants with a realistic view of how geologists communicate and present their observations and testable hypotheses. The emphasis complements the goals of the classroom/field activities in which training observational capabilities is the goal.

We consistently find the field assistant program to benefit the geologists as well. Astronauts often approach field science from well outside the geologist's "box" of thinking. By challenge the team's conventional thinking the assistants help push the research in new directions. Because many of these projects are related to planetary analogs, the astronauts who participate are also given a chance to gain relevant planetary science knowledge, which they typically present to the Crew Office through briefings. Perhaps the best testament to the quality of the students in the training is the recognition that astronauts have often made observations that the professionals have missed.

***Integrated Analog Field Tests*:** NASA and ESA conduct a range of integrated analog field tests such as the *NASA Extreme Environment Mission Operations* (NEEMO) or ESA's *Cooperative Adventure for Valuing and Exercising human behaviour and performance Skills* (CAVES), among many others. These field tests provide opportunites to assess various aspects of human exploration including hardware, operations, environments, duration, and science. The Crew Office often provides personnel to support these tests, which opens opportunities for the science community to provide scientific content and training to the participants. For instance, when active, NASA's *Desert Research And Technology Studies* (Desert RATS) focuses on conducting basic geology as influenced by current NASA hardware and operations concepts. Thus, crew members are routinely provided with basic field geology backgrounds to enable them to evaluate how the hardware and operations hindered or enhanced their ability to provide geologic observations.

Conclusions: Field geology training was a fundamental aspect of the success of the Apollo Program. Astroanauts of the Shuttle Program era received roughly one week of training related to orbital observations of the Earth. LEAG and CAPTEM recently recommended an increase in this training and the development of a official geology training program to ensure the science success of future human exploration programs. Geology training that was developed and implemented within NASA for the 2009 and 2013 astronaut classes, included NASA personnel, US and State Geological Surveys and participants from academia. This effort builds upon the Apollo geology training, is reestablishing the links between NASA and professional geologists ouside of NASA, and has exposed several early career participants to the institutional Apollo knowledge base that is now retired or might be retired over the next decade. The goals of the training program are to develop a Crew Office with a healthy understanding of how science fits within human exploration of the Solar System and to put in place and provide experience for the next generation of astronaut geology trainers.

References: [1] Lofgren, Horz, Eppler (2011) GSA SP483, 33-48. [2] Schmitt et al., (2011) GSA SP483, 1-16.. [3] Hodges, K. & Schmitt, H. (2011) GSA SP483, 17-32. [4] El-Baz, (2011) GSA SP483, 49-66. [5] Evans, Wilkinson, Stefanov, Willis, (2011) GSA SP483, 67-74. [6] Shearer et al. (2010) LEAG-CAPTEM Analysis Document, http://www.lpi.usra.edu/leag/reports/LEAG_CAPTEMCurationReview.pdf.

ACCESSING AND ASSESSING LUNAR RESOURCES WITH PROSPECT. J. D. Carpenter[1], S. Barber[2], P. Cerroni[3], R. Fisackerly[1], A. Fumagalli[4], B. Houdou[1], C. Howe[5], P.G. Magnani[4] A. Morse[2], E. Monchieri[6], P. Reiss[7], L. Richter[8], F. Rizzi[4], S. Sheridan[2], L. Waugh[6], I.P. Wright[2], [1]ESA ESTEC, Keplerlaan 1, 2201AZ, Noordwijk, The Netherlands (james.carpenter@esa.int), [2]The Open University, UK, [3]INAF, Italy, [4]Selex-ES, Italy, [5]RAL Space, UK,[6]Airbus SD, UK, [7]Technische Universitaet Muenchen, Germany, [8]Kayser-Threde, Germany.

Introduction: A Package for Resource Observation and in-Situ Prospecting for Exploration, Commercial exploitation and Transportation (PROSPECT) is in development by ESA for application at the lunar surface as part of international lunar exploration missions in the coming decade, including the Russian Luna-27 mission planned for 2019.

Establishing the utilization potential of resources found in-situ on the Moon may be key to enabling sustainable exploration in the future. The purpose of PROSPECT is to support the identification of potential resources, to assess the utilization potential of those resources at a given location and to provide information to help establish the broader distribution. PROSPECT will also perform investigations into resource extraction methodologies that maybe applied at larger scales in the future and provide data with important implications for fundamental scientific investigations on the Moon.

Objectives: PROSPECT aims to assess the in-situ resource potential of lunar regolith at any given location on the Moon. In order to achieve this PROSPECT is required to:

- Extract samples from depths of up to 2m.
- Extract water, oxygen and other chemicals of interest in the context of resources.
- Identify the chemical species extracted.
- Quantify the abundances of these species.
- Characterize isotopes such that the origins and emplacement processes can be established.

In the lunar polar regions PROSPECT is able to target water ice. At all locations on the Moon PROSPECT is able to extract solar wind implanted volatiles from the regolith through heating and aims to extract oxygen and other chemicals of interest as resources from minerals by a variety of techniques.

System Functions:

Drilling and sampling: PROSPECT includes a drill that is required to access the subsurface to depths of up to 2m. Once at the required depth a sampling tool removes small (~3 cm^3) samples, whilst preserving sample temperature. Samples must then be extracted and handled whilst minimizing alteration of the samples.

The drill is derived from that being developed for EXOMARS [1] (shown in Figure 1) and the Rosetta drill [2], currently in-situ at comet 67P/Churyumov-Gerasimenko. Modifications are considered to account for unique lunar mission requirements and material properties.

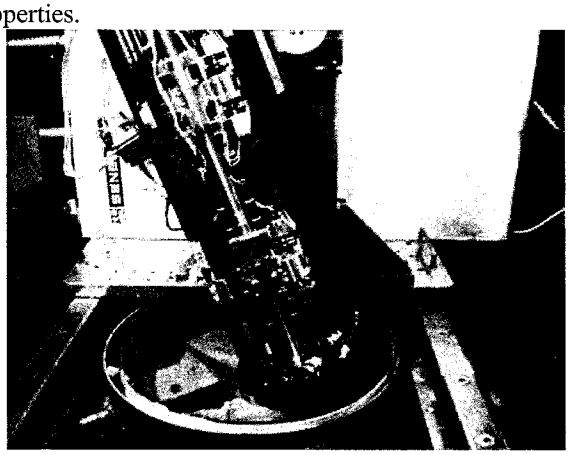

Figure 1. Breadboard of the Exomars drill from which the PROSPECT drill is derived.

Assessment of sample mineralogy and volatile content. Infrared spectra of samples are recorded, using an instrument derived from MAMISS [3] on EXOMARS, in order to provide an assessment of the mineralogy of the bulk sample and to investigate water content, prior to heating. A goal here is to extend the bandpass of the instrument from 2.2μm as for MAMISS up to 3.3μm.

Sample heating and chemical extraction: Samples are sealed in ovens, derived with heritage from those developed for EXOMARS [4], Rosetta and activities performed through the German LUISE programme. Samples can then be heated to temperatures as high at 1000°C. Heating in vacuum extracts ices and solar wind implanted volatiles and pyrolyses some volatiles from minerals. Reacting gasses may also be introduced to the ovens to extract additional chemistry of interest. A number of techniques are under investigation, based on a combination of flight heritage and laboratory investigations. These include combustion with oxygen [5], oxidation using fluorine [6] and reduction using hydrogen and methane [7].

Gas compositional analysis: Evolved gasses can be analyzed using an ion trap mass spectrometer [5]. This gives a qualitative measure of the composition. Additional separation of gas composition could be achieved through the addition of a MEMS GC, which is currently in development, but is not envisaged at this time.

Gas chemical processing: Target gasses are prepared for isotopic analysis through refinement or con-

version to other chemicals [5]. Such conversion can prepare chemicals which are better suited than the original compounds to analysis using a mass spectrometer and can rremove isobaric interferences.

Gas isotopic analysis: Isotopes of the elements of interest are measured using a magnetic sector mass spectrometer, along with measurements of reference standards [5]. Using this technique accurate analysis is achieved, allowing comparison with laboratory measurements on Earth. The expected performance of isotopic analysis is shown in table 1.

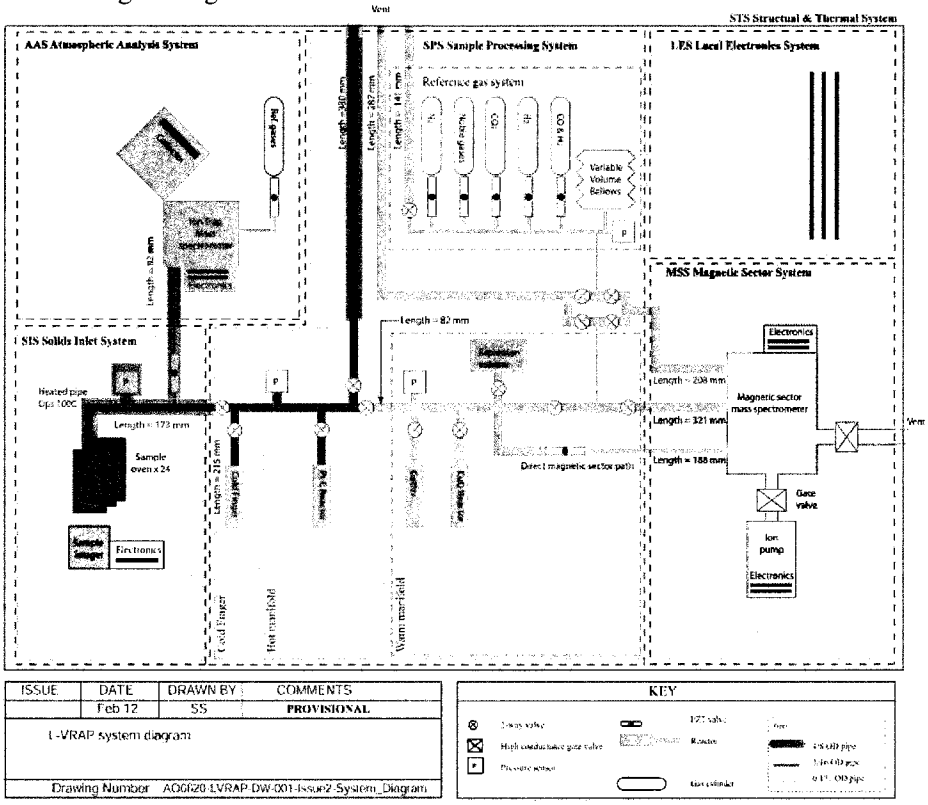

Figure 2. Schematic diagram of the PROSPECT processing and analysis system as defined during the ESA L-VRAP [5] study. In the current project phase additional functionality is being investigated to enhance the resource extraction demonstration capabilties of the system.

	H2, H_2O, -OH, hydrocarbons	10‰
	CO, CO_2, hydrocarbons	0.1-1‰
	N_2, NH_3, nitrogen oxides	0.1-1‰
	H_2O, CO and CO_2	0.1‰

Table. Predicted isotopic performance of the PROSPECT analytical package, based on experience with existing flight and laboratory hardware.

Conclusions: PROSPECT is a package for the investigation of lunar volatiles and other potential resources with potential applications for both exploration and fundamental science. The package builds on extensive flight heritage and a unique set of capabilities, developed over decades by a number of groups across Europe.

PROSPECT is targeting flight readiness by 2019 and will be available as part of international missions in this time frame.

References: [1] Magnani P. et al. (2010) *Proceeding of i-SAIRAS*. [2] Marchesi M. et al. (2001), *Proceedings of the 9th European Space Mechanisms and Tribology Symposium*, 91 - 96. [3] Coradini A. et al. (2011) EPSC-DPS EPSC-DPS Joint Meeting 2011 abstract. [4] Schulte W. et al. (2010), *Proceeding of i-SAIRAS*. [5] Wright I.P. et al. (2012) *Planetary and space science*, 74, 1, 254-263. [6] Sebolt W. et al, (1993) in Resources of Near Earth Space, The University of Arizona Press, 129. [7] Schwandt et al., (2012) *Planetary and space science*, 74, 1, 49-56.

Acknowlegement: We would like to acknowledge the important contributions of our colleague Colin Pillinger, who sadly died ealier this year.

LUNAR EXPLORATION IN ESA. J. D. Carpenter, B. Houdou, R. Fisackerly, D. De Rosa, B. Patti, J. Schiemann, B. Hufenbach, B. Foing, ESA ESTEC, Keplerlaan 1, 2201AZ, Noordwijk, The Netherlands (james.carpenter@esa.int).

Introduction: The multiple orbital missions of the last decade coupled with present activities and future plans of various agencies and actors to target the lunar surface, indicate the emergence of a renaissance in lunar exploration. Through participation in this new era of lunar exploration ESA seeks to provide Europe with access to the lunar surface.

This is best achieved through an exploration programme which combines the strengths and capabilities of both robotic and human explorers. Preparations include a combination of human and robotic activities, the development of cooperation with international partners and the development of core capabilities and exploration products.

Exploration Products: Building on more than a decade of technology investments, ESA is deriving core exploration products, which can be provided to the missions of partners for flight before the end of the decade.

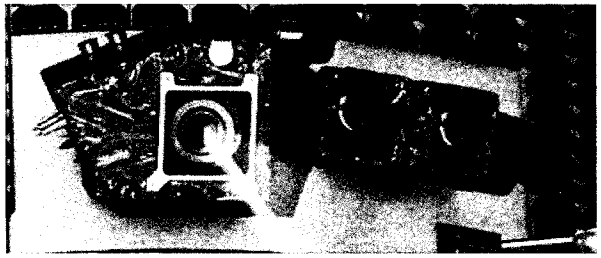

Figure 1. PILOT uses image based navigation techniques and hazard detection using LIDAR to enable precise and safe access to landing sites.

PILOT (Precise and Intelligent Landing Using On-board technologies): PILOT provides a navigation and guidance solution to allow safe and precise access to any given location on the lunar surface. PILOT uses a combination of relative and absolute navigation techniques using images for navigation. Hazard identification is performed using LIDAR. Such a system allows access to sites of high interest for science and exploration, for which special extent is highly limited, but also allows coordinated surface access for multi element missions.

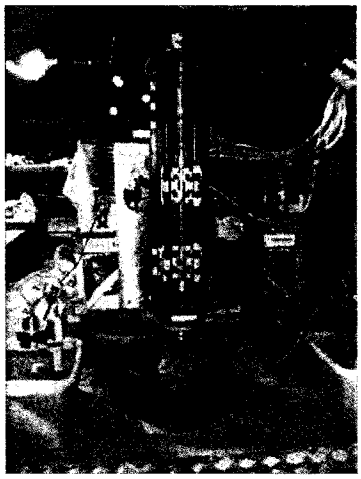

Figure 2. Breadboard of the Exomars drill from which the PROSPECT drill is derived.

PROSPECT (Package for Resource Observation, in-Situ analysis and Prospecting for Exploration Commercial exploitation and Transportation): PROSPECT provides access to and comprehensive analysis of potential resources anywhere on the Moon, including the lunar poles. It uses a drill, derived from Exomars and Rosetta heritage, to access the subsurface to depths of up to 2m. Samples from this depth are then extracted and passed to a chemical processing and analytical suite. Drilling and sampling activities are performed with a view to enabling analysis of volatiles at very low temperatures. Following optical imaging and IR spectral analysis samples are heated to extract volatiles gasses by pyrolysis and processed chemically through combustion, oxidation and reduction reactions to extract chemicals of interest from minerals. Qualitative compositional analysis then compliments accurate and precise isotopic analysis, comparable with that achieved in terrestrial laboratories. The analytical systems are derived from flight hardware on Rosetta, Beagle 2 and Exomars.

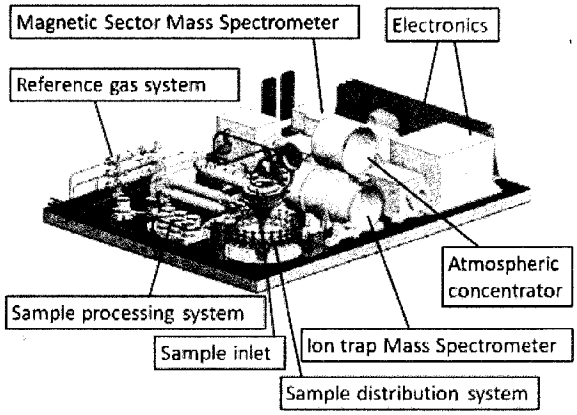

Figure 3. CAD representation of the chemical processing and gas analysis subsystem of PROSPECT package, which is derived from the PTOLEMY on Rosetta and GAP on Beagle 2.

SPECTRUM (Space Exploration Communications Technology for Robustness and Usability between Missions): SPECTRUM provides a communications link between a lander or other exploration asset on another celestial body, and an orbiting platform. The system is suitable for application on missions performed by space agencies and private entities alike.

The system includes a complete UHF Orbiter-Lander subsystem and the associated communications link, including all the equipment on-board both the orbiter and the lander.

The transponder is a key component of such a UHF communications subsystem. The SPECTRUM transponder is derived from heritage from the European unit for the surface elements of the ExoMars mission.

Human Exploration Activities: ESA's multiple activities on the ISS (including teleoperation of surface assets) and contribution of the service model of the US led Multi-Purpose Crew Vehicle, which is planned for a first unmanned lunar flight in 2017, are also important steps towards achieving access to the Moon. All of these activities are performed with a view to generating the technologies, capabilities, knowledge and heritage that will make Europe an indispensible partner in the exploration missions of the future.

Investigations are also underway into the utilization of human tended infrastructure in cis-lunar space in support of robotic lunar surface missions, including surface mobility and sample return.

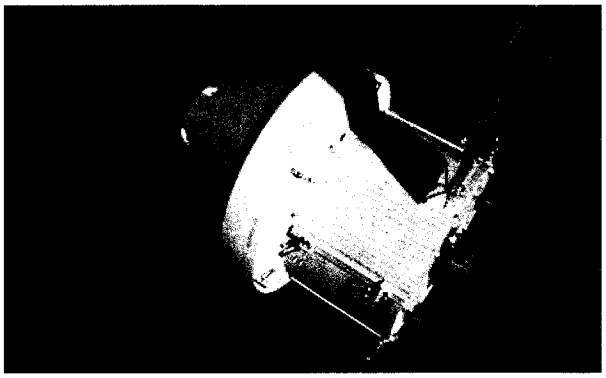

Figure 4. Orion-MPCV, including the ESA provided service module, in orbit at the Moon.

International partnerships: Future exploration of the Moon by ESA will only be possible through international partnerships. ESA's approach is to build those partnerships and establish roles for the future.

In the area of human exploration a partnership has been established with NASA on the MPCV service module.

In robotic exploration ESA is planning to contribute to the Russian led robotic missions, Luna-Glob, Luna-Resurs orbiter and Luna-Resurs lander. Contributions to these early missions should be followed by contributions at the level of mission elements to a joint Lunar Polar Sample Return mission.

This partnership with Russia will provide access for European investigators to the opportunities offered by the Russian led instruments on the missions, as well as providing Europe with a unique opportunity to characterize and utilize polar volatile populations and advance important technologies and capabiltities for exploration. A longer term goal is to ensure that samples of high scientific value, from as of yet unexplored and unsampled locations, shall be made available to the scientific community.

Ultimately these robotic activities are being performed with a view to enabling a future more comprehensive programme in which robotic and human activities are integrated to provide the maximum benefits from lunar surface access.

Conclusions: The surface of the Moon is an important exploration destination for ESA, which is working to secure roles in future exploration missions with international partners.

Core ESA competencies exist in precision landing, communications and the search for future resources, as well as key areas relating to human transportation, habitation and operations.

INVESTIGATION OF IONIZED VOLATILES AND INTERIOR STRUCTURE OF THE MOON: IMPLICATIONS FROM RESTORED APOLLO MAGNETIC FIELD DATA. P. J. Chi[1], [1]UCLA, EPSS and IGPP, 3845 Slichter Hall, 603 Charles Young Drive, Los Angeles CA 90095-1567, USA, pchi@igpp.ucla.edu.

Introduction: Magnetic field fluctuations may reveal the state of ambient plasma or the interior of solar system bodies. As the Moon is surrounded by plasma in the solar wind, the Earth's magnetosheath, or the magnetotail, characteristics of magnetic fluctuations or waves may infer the presence of ionized lunar volatiles. On the other hand, if saline ice exists inside the Moon, it induces magnetic variations on and above the lunar surface, which can be used to infer the electrical conductivity of the lunar interior.

Restoration of Apollo Magnetic Field Data: Among the series of lunar missions that carried magnetometers since the 1960s, the Apollo missions made earliest yet unique contributions to the measurements of the lunar magnetic field. After the conclusion of the Apollo Program, the format in which the Apollo magnetic field data were stored gradually became obsolete, and for several decades the data could not easily be understood. In 2008, an effort began to restore the Apollo magnetic field data with the help by NSSDC and support from the NASA LASER Program. The digital data include the 0.3-s samples from Apollo 12, 15 and 16 Lunar Surface Magnetometers (LSM) and the 24-s samples from Apollo 15 and 16 Sub-satellite Biaxial Magnetometers (SBM). After a lengthy process of identifying legitimate data structures in the binary data stream [1], all the SBM data archived at NSSDC have now been restored. The restoration of the LSM data has been slower due to the irregular pattern of time words, but the data during April-July 1972 when both Apollo 15 and 16 LSMs were operational have been recovered.

Ionized Volatiles near the Moon: An unexpected discovery in the restored Apollo LSM data is the ion cyclotron waves on the lunar surface [2]. A class of narrowband waves with frequencies ranging from 0.04 to 0.17 Hz were found only when the Moon was in the terrestrial magnetotail, including regions in and near the current sheet as implied from magnetic field directions. The wave properties are consistent with those of ion cyclotron waves: A wave frequency at or slightly lower than the local proton gyrofrequency, a dominant transverse component, and left-hand polarization. When the plasma convection is present and perpendicular to the ambient magnetic field, the pickup ions originating from the lunar exosphere can travel along cycloid trajectories resulting in a ring distribution in the velocity space (see Figure). This is how ion cyclotron waves are generated near comets, Venus, and Mars, in the Io torus, or in the Saturn E-ring. Because the lunar exosphere is tenuous, pickup ions from the Moon may not constitute a significant amount of particles in the solar wind plasma where a typical density is 5 cm^{-3}. When the Moon is in the terrestrial magnetotail, however, the ambient plasma density is at the order of 0.1 cm^{-3} or less, and pickup ions can be much more noticeable and form an unstable ring-type distribution.

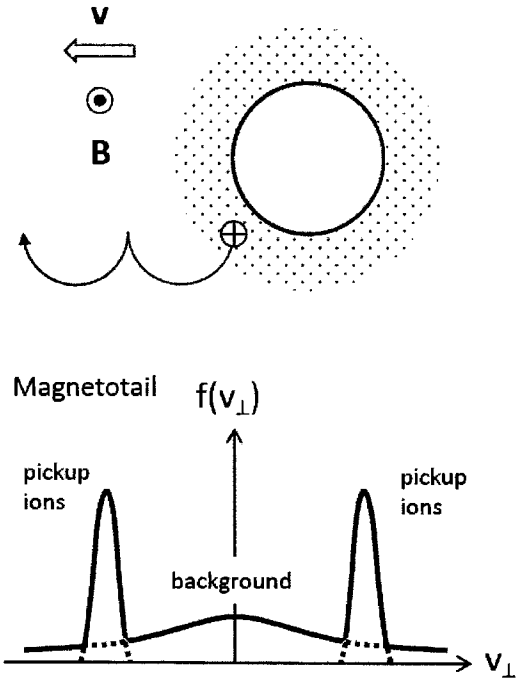

More studies are needed to confirm the generation mechanism of ion cyclotron waves at the Moon and where these waves are present. An ongoing study using the Apollo Suprathermal Ion Detector Experiment (SIDE) data suggests that many events of ion cyclotron waves were seen in the tail lobes rather than in the plasma sheet [3], favoring the generation by pickup ions associated with lunar volatiles.

Magnetic Sounding of Lunar Interior: One of the important uses of the lunar magnetic field measurements is detecting the electrical conductvitiy and the metallic core in the lunar interior. During the Apollo era, the electrical conductivity of the Moon has been inferred from examining the transfer function between external and surface magnetic field fluctuations [4], the decay of magnetic impulses on the lunar surface [5], and the deflection of the magnetic field above the lunar

surface when the Moon was in the magnetotail tail lobes [6]. Most magnetic sounding studies using surface magnetic field measurements are based on the Apollo 12 LSM data, but the Apollo 15, 16 LSM data with larger quantity and higher quality have not been fully explored. We have examined the transfer function using the restored Apollo 15 LSM data and Explorer 35 magnetometer and found that the responses in both radial and transverse components at high frequencies ($f > 10^{-4}$ Hz) are consistent with modeled results. For the data during the short interval when these two datasets overlap, the statistical uncertainty for frequencies below 10^{-4} Hz is too large to resolve the size of the conducting core. We will report the ongoing effort in recovering the orbit data of Apollo sub-satellites and the SBM data in the full three components in order to improve the precision of magnetic sounding analysis with Apollo magnetic field data.

References:

[1] Chi P. J. et al. (2011) *42nd LPSC*, 2444. [2] Chi P. J. et al. (2013) *PSS, 89*, 21-28. [3] Collier M. and Newheart A. (2014), personal communications. [4] Hood L. L. et al. (1982) *JGR, 26*, 2327-2330. [5] Dyal, P. and Parkin C. W. (1973) Phys. Earth & Planet. Int., 7, 251-265. [6] Russell, C. T. et al. (1981) Proc. Lunar Planet. Sci., 12B, 831-836.

Determining the Magnitude of Neutron and Galactic Cosmic Ray (GCR) Fluxes at the Moon using the Lunar Exploration Neutron Detector (LEND) during the Historic Space-Age Era of High GCR Flux

G. Chin[2], R. Sagdeev[1], G.M. Milikh[1], D. Usikov[1], J.J. Su[1], W. Boynton[3], D. Golovin[4], K. Harshman[3], M. Litvak[4], I.G. Mitrofanov[4], T. McClanahan[2], T. Livengood[5], L.G. Evans[6], A. Sanin[4], and R. Starr[7]

[1] Department of Physics, University of Maryland, College Park, Maryland, USA(rsagdeev@gmail.com), [2] NASA Goddard Space Flight Center, Greenbelt, Maryland, USA, [3]University of Arizona, Tucson, Arizona, USA, [4]Institute for Space Research (IKI), Moscow, Russia, [5] CRESST/UMD/GSFC, Greenbelt, Maryland, USA, [6] Computer Science Corporation, Lanham-Seabrook, Maryland, USA, [7] Catholic University of America, Washington, DC, USA.

Historic Space-Age Era of High Galactic Cosmic Ray Flux: The Lunar Reconnaissance Orbiter (LRO) was launched June 18, 2009 during an historic space-age era of minimum solar activity [1]. The lack of solar sunspot activity signaled a complex set of heliospheric phenomena [2,3,4] that also gave rise to a period of unprecedentedly high Galactic Cosmic Ray (GCR) flux [5]. These events coincided with the primary mission of the Lunar Exploration Neutron Detector (LEND, [6]), onboard LRO in a nominal 50-km circular orbit of the Moon [7].

LEND measures the leakage flux of thermal, epithermal, and fast neutrons [6] that escape from the lunar surface. Neutrons are produced within the top 1-2 meters of the regolith by spallation from the GCR flux. The energy spectrum and flux of the emergent neutron population is highly dependent on the incident flux of the GCR due to its influence on the depth of neutron production and total number of neutron-producing events.

Methods to calculate the emergent neutron albedo population using Monte Carlo techniques [8] rely on an estimate of the GCR flux and spectra calibrated at differing periods of solar activity [9,10,11]. Estimating the actual GCR flux at the Moon during the LEND's initial period of operation requires a correction using a model-dependent heliospheric transport modulation parameter [12] to adjust the GCR flux appropriate to this unique solar cycle. These corrections have inherent uncertainties depending on model details [13]. Precisely determining the absolute neutron and GCR fluxes is especially important in understanding the emergent lunar neutrons measured by LEND and subsequently in estimating the hydrogen/water content in the lunar regolith [6].

Simultaneous measurements of the LEND detectors determine the absolute GCR and neutron flux levels: LEND is constructed with a set of neutron detectors to meet differing purposes [6]. Specifically there are two sets of detector systems that measure the flux of epithermal neutrons: a) the uncollimated Sensor for Epi-Thermal Neutrons (SETN) and b) the Collimated Sensor for Epi-Thermal Neutrons (CSETN).

LEND SETN and CSETN observations form a complementary set of simultaneous measurements that determine the absolute scale of emergent lunar neutron flux in an unambiguous fashion and without the need for correcting to differing solar-cycle conditions. LEND measurements are combined with a detailed understanding of the sources of instrumental background, and the performance of CSETN and SETN. This comparison allows us to calculate a constant scale factor that determines the absolute flux of neutrons at the Moon and then subsequently to deduce the proper scale of the GCR flux model without correction by use of the heliospheric modulation potential for this unique solar cycle minimum.

References:

[1] H. S. Ahluwakia and R. C. Ygbuhay (2010) *Twelfth International Solar Wind Conference,* 699-702. [2] F. B. McDonald et al. (2010) *JRL, 37,* L18101. [3] H. Moraal and P. H. Stoker (2010) *JGR, 115,* 12109-12118. [4] R. Kataoka et al. (2012) *Space Weather, 10,* 11001-11007. [4] C-L. Huang et al. (2009), *JRL, 37,* L09109-L09104. [5] R. A. Mewaldt et al. (2010) *Ap. J Lett., 723,* L1-L6. [6] I. G. Mitrofanov et al. (2010) *Space Science Rev., 150,* 283-207. [7] C. R. Tooley et al. (2010) *Space Science Rev., 150,* 23-62. [8] G. W. McKinney et al. (2006) *JGR, 111,* 6004-6018. [9] P. M. O'Neil (2010) *lEEE Trans. Nucl. Sci., 57(6),* 3148-3153. [10] *American National Standards Institute Tech. Rep. ISO 15390* (2004). [11] I. G. Usokin et al. (2008) *JGR, 110, A12108.* [12] M. D. Looper et al. (2013) *Space Weather, 11,* 142-152. [13] A. I. Mrigakshi et al. (2012) *JGR, 117,* A08109-A08121.

An ALSEP-like lunar surface science package in a cubesat form factor? P.E. Clark[1,3], J. Didion[2], R. Cox[3], [1]IACS, Catholic University of America, Washington, D.C. 20064, [2]NASA/GSFC, Greenbelt Road, Greenbelt, MD 20771, and [3]Flexure Engineering, 3518 Fremont Ave. N, #474, Seattle WA 98103. Contact Email: clarkp@cua.edu

Science Rationale: Although samples have been collected from the Moon, the 'dynamics' of the lunar environment itself have not been systematically studied. ALSEP packages deployed in the equatorial region during the Apollo era are no longer operational (except for passive retroreflectors), but they certainly gave indications of the nature of the fields and particle environment around the Moon. However, globally (in longitude and latitude) distributed identical instrument packages taking simultaneous measurements could provide systematic evaluation of the questions that have arisen about the dynamic nature of the lunar environment, the exosphere, dust and volatile transport, charging as a function of exposure to light, solar wind, and plasma, the nature of local and global fields. Particularly important is the capability of taking measurements for at least some portion of lunar night. These measurements should be provided before lunar landed exploration activities planned over the next decade have a significant impact on the environment. Such measurements will provide a much more comprehensive basis for understanding the protection needed for humans and robotic devices spending any length of time on the lunar surface. Because the lunar surface represents the range of conditions on most solar system objects and yet is far closer than other objects, it also represents an ideal technology testbed.

Background: In support of Project Constellation, we developed a design concept for an ALSEP-like stand-alone lunar surface instrument packages without dependence on radioisotope-based batteries [1]. An initial conventional attempt to design an environmental monitoring package with a solar/battery based power system led to a package with a unacceptably large mass (500 kg), over half of which was battery mass. We reduced the mass to 100 kg using radiation hard, cold temperature electronics and innovative thermal balance strategies using multi-layer thin reflective/insulting materials and gravity-assisted heat pipe, and were able to achieve a 10% duty cycle during lunar night.

Application: Here, we revisit this design concept with existing cubesat technology to be used in support of a fields and particles surface monitoring station. Packages based on the cubesat paradigm, standard platform and component with Class D development, acting as 'pathfinders' for environmental networks on the Moon or elsewhere, could be deployed robotically from lunar landers going to widely different latitude and longitude locations. Cubesat systems now being developed for deep space, including C&DH/ processing, communication and solar panel deployables, have components/subsystems capable of operating at colder temperatures and intrinsic radiation hardness. How scalable is the thermal design developed for the ALSEP-like LEMS (without RTGs or RHUs) concept for Project Constellation to a cubesat form factor package? Based on preliminary work, with state of the art thermal design, a 5 U payload of compact instruments could be supported in a 12 U package with cubesat deployables for power generation and communication. 3 U would be required for cubesat batteries. With alternative power storage systems under development, a larger payload might be possible.

References: [1] Clark P.E. et al. (2011) Small cold temperature instrument packages, SPESIF 2011, AIP Conference Proceedings, Physics procedia, 20, 300-307.

Deep Space Cubesat Orbiter and Compact Broadband IR Instrument to determine the systematics of Lunar Water. P.E. Clark[1,3], R. MacDowall[2], D. Reuter[2], R. Mauk[2], J. Didion[2], D. Patel[2], W. Farrell[2], R. Cox[3], [1]IACS, Catholic University of America, Washington, D.C. 20064, [2]NASA/GSFC, Greenbelt Road, Greenbelt, MD 20771, and [3]Flexure Engineering, 3518 Fremont Ave. N, #474, Seattle WA 98103. Contact Email: clarkp@cua.edu

Purpose: We have applied the CubeSat Paradigm to science requirements-driven deep space exploration mission, referred to as a LunarCube, and are developing a compact 'workhorse' instrument for a high priority science application [1]. We focus on cubesat exploration to lunar exploration because of the Moon's proximity and accessibility as a stepping stone to the rest of the solar system, combined with the great international scientific interest in the Moon and its suitability as an analog with extreme range of conditions and thus an ideal technology testbed for much of the solar system.

Science Rationale: Despite the fact that 6U deep space capable cubesat buses and deployers are now available, the development of CubeSat instruments capable of providing focused, high priority science, so critical to achieving the potential for low cost planetary exploration promised by the CubeSat paradigm, lags behind. Understanding the origin and role of volatiles is such a high priority goal. On the Moon, Mercury, Mars, and the asteroids, the source, distribution, and role of volatiles is a major question, with implications for interior, surface, and exosphere formation processes, including differentiation and structure of the bodies themselves, and for the origin of life in the early solar system. The form and distribution of water has implications for human exploration, resource exploitation, and sample curation. Recent lunar missions yielded unanticipated evidence for water from NIR instruments not optimized for finding it, without providing details of the systematics of its distribution, which could be provided by this instrument.

Cubesat Bus: Over the course of this year, we have conducted the equivalent of a pre-phase A study for a lunar orbital LWaDi (water distribution) mission, with a focus on the payload instrument capable of measuring volatiles, which is described below. Subsystems include state of the art cubesat attitude control, propulsion (for transportation from GEO, GTO or Earth escape to lunar capture), communication, power, thermal and radiation protection systems providing lunar orbital operation of a cubesat bus. Based on this work, we have concluded that a 6U bus with state of the art cubesat systems already available or now being built and tested can support a high priority science orbiter in cislunar space, providing the spacecraft is delivered to lunar orbit. We are looking at a series of progressively more challenging missions, including an impactor, and a pathfinder observatory, and considering designs using technology available now, in five years, and in ten years. Particular challenges for orbiters or impactors are communication, navigation and tracking in a volume, power, and bandwidth constrained environment. Thermal and radiation protection will be the principal challenges for landed cubesat deployables. The end result is generic design(s) for a cross-section of future high priority payloads for planetary, heliophysics, and astrophysics disciplines.

Instrument: In response to the need for 'workhorse' cubesat instruments, we are developing BIRCHES, Broadband InfraRed Compact, High-resolution Exploration Spectrometer, a miniaturized version of OVIRS on OSIRIS-REx. BIRCHES is a compact (1.5U, 2 kg, <5W) point spectrometer with a compact cryocooled HgCdTe detector for broadband (1 to 4 micron) measurements at sufficient resolution (10 nm) to characterize and distinguish important volatiles (water, H_2S, NH_3, CO_2, CH_4, OH, organics, oxides, carbonates) and mineral bands. It has built in flexibility, using an adjustable 4-sided iris, to maintain the same spot size regardless of variations in altitude (by up to a factor of 5) or to vary spot size at a given altitude, as the application requires. BIRCHES will address the high priority science goal of understanding the role of volatiles on solar system bodies by 1) enabling broadband spectral determination of the composition and distribution of volatiles in the regoliths of the Moon, asteroids, and Mars, as a function of time of day, latitude, regolith age and composition; 2) providing a geological context for those measurements through spectral determination of major and minor mineral components; and 3) expanding the understanding of the current dynamics of volatiles sources, sinks, and processes, with implications for the origin and evolution of volatiles in the solar system. In this way, we will develop a competitive instrument for future deep space CubeSat opportunities such as EM-1.

References: [1] Clark P.E. et al. (2013) LWaDi: An Overview and Application of the Cubesat Paradigm to lunar orbiter missions, LSA4 http://lunarworkshops.com.

LROC NAC PHOTOMETRY AS A TOOL FOR STUDYING PHYSICAL AND COMPOSITIONAL PROPERTIES OF THE LUNAR SURFACE. R. N. Clegg[1], B. L. Jolliff[1], A. K. Boyd[2], J. D. Stopar[2], H. Sato[2], M. S. Robinson[2], and B. W. Hapke[3], [1]Washington University in St. Louis and the McDonell Center for the Space Sciences, 1 Brookings Dr., St. Louis, MO 63130, USA, rclegg@levee.wustl.edu, [2]School of Earth and Space Exploration, Arizona State University, Tempe, AZ, [3]University of Pittsburgh, Pittsburgh, PA.

Introduction: Photometry is a powerful tool to investigate physical and compositional properties of planetary surface materials. Factors that affect how the surface of an airless silicate body reflects light include grain size, composition and mineralogy, regolith structure, surface roughness, space weathering, and glass and Fe^0 contents [1,2]. Photometric models are used to test variable parameters that depend on soil properties and composition to determine which parameters most accurately fit the reflectance characteristics.

For our studies, we use Lunar Reconnaissance Orbiter (LRO) Narrow Angle Camera (NAC) images acquired over a range of illumination conditions (incidence, emission, and phase angles) for selected sites. These data are well suited for determination of phase curves and, thus, for normalization to common viewing geometry, allowing for relative comparisons of reflectance and derived parameters among sites. Previously, NAC photometric imaging data were used to study the effects of rocket exhaust on physical changes in lunar soil ("blast zones") at the Apollo, Luna, Surveyor, and Chang'e 3 landing sites [3,4].

By coupling soil composition data with photometric techniques, we assessed compositions and variabilities in reflectance for several silicic volcanic complexes on the Moon (Compton-Belkovich Volcanic Complex, Hansteen Alpha, Gruithuisen Domes) as well as ejecta of unusually silicic composition from Aristarchus crater [5]. Here, we add data from the Lassell Massif and a reference area interpreted to be pure anorthosite (PAN) on the basis of hyperspectral data [6,7].

Methods: We selected areas of interest at each silicic and PAN region and used NAC images with a variety of illumination conditions to obtain reflectance data. We avoid areas near young craters to minimize effects of fresh, immature materials on reflectance. The NAC images were radiometrically calibrated and photometric angles were determined for each image pixel from topography (using NAC DTMs) and viewing geometry. The DN values of the calibrated images represent *I/F* (*IoF*) [8], the "radiance factor" as defined by [1].

We obtain reduced reflectance by fitting NAC data using the Hapke simplified bidirectional reflectance function, which describes the ratio of the radiance, *I*, received at the detector viewing the surface from angle, *e*, to the irradiance, πF, from the source at angle, *i*, and then normalized to the Lommel-Seeliger Function (LS) to mask the effects of viewing geometry [1-3]. Reduced reflectance (*IoF/LS*) is defined as:

$$\frac{IoF}{LS} = \frac{w}{4}[p(g) + H(\mu_0, w)H(\mu, w) - 1][1 + B_{C0}B_C(g, h_c)]S(i, e, \theta)$$

$$LS = {}^{\mu_0}/_{(\mu_0 + \mu)}$$

The single scattering albedo, *w*, is the probability that a photon will be scattered by a particle and depends on composition and grain size. The quantities *w* and *p(g)* describe the scattering by a single particle, $[H(\mu_0, w)H(\mu, w) - 1]$ describes multiple scattering, and $B_{co}B_c(g,h_c)$, the opposition effect. This approximation is reasonably valid away from the limb and terminator. The term *S(i,e,θ)* is the shadowing function and depends on the roughness of the surface and mean slope angle *θ*. In both equations, $\mu = \cos(e)$ and $\mu_o = \cos(i)$. For details, see [1-3]. The use of repeat-coverage NAC images of each site permits determination of the photometric parameters *w* and *θ*, and allows us to determine *IoF/LS* at a common phase angle of 45° [3]. We optimized this parameter determination using the landing site studies and then applied the same method to silicic volcanic areas.

Finally, we compared the landing site photometric analysis with known soil compositions [9] and found a strong correlation between *IoF/LS*, *w*, and key parameters such as FeO and Al_2O_3 contents [5]. Both *w* and *IoF/LS* increase with increasing feldspar content and decrease with increasing FeO-bearing minerals [5,10]. We then used this correlation to interpret NAC reflectance at sites of silicic volcanism and PAN.

Silicic Materials: We extracted *IoF/LS* (and *w*) for relatively flat, smooth regions at the Compton-Belkovich Volcanic Complex (CBVC), Hansteen Alpha (HA), the Gruithuisen Domes, ejecta from Aristarchus Crater, and the Lassell Massif.

The reduced reflectance for a 45° phase angle ranges from 0.23 – 0.34 at the CBVC, from 0.16 – 0.30 at HA, from 0.109 – 0.113 at Gruithuisen Delta, from 0.10 – 0.15 for the Lassell Massif, and averages 0.13 for the Gruithuisen Gamma dome and 0.16 for Aristarchus ejecta. These values are most comparable to those of the feldspathic Apollo 16 landing site, which has the highest reduced reflectance values of the studied landing zones (see [3] for detailed results), with an *IoF/LS* value of 0.16 at 45° phase (Fig. 1).

We extracted modeled *w* values of 0.38 for the Gruithuisen Gamma dome and 0.53 for Aristarchus ejecta. Modeled *w* values range from 0.40 – 0.62 for HA, 0.35 – 0.46 for the Lassell Massif, and the CBVC has the highest values for the silicic regions studied, ranging from 0.53–0.66.

PAN Materials: We also extracted *IoF/LS* and *w* values from a region of pure anorthosite (PAN) exposed along the Inner Rook Ring of Orientale. This area has essentially no detectable mafic minerals and is of interest as a highland endmember composition [6,7]. The PAN study area has the highest measured reduced reflectance for a 45° phase angle with values ranging from 0.32 – 0.37 (Fig. 1). The PAN area at Orientale also has relatively high modeled *w* values, ranging from 0.62 – 0.72.

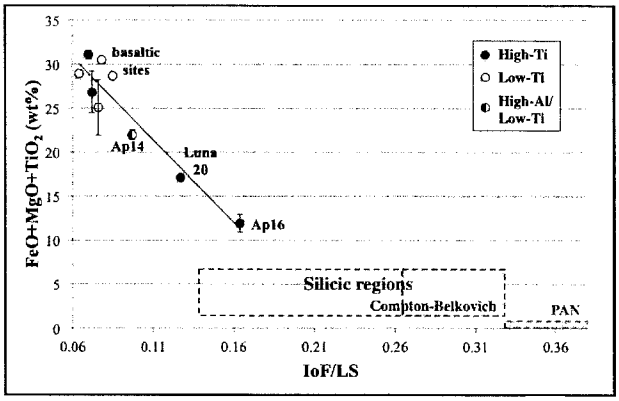

Figure 1: Relationship between reduced reflectance at 45° phase angle and mafic content for Apollo and Luna samples. Silicic volcanic regions and PAN extrapolate to the dashed regions.

Discussion: Applying the Hapke model used for our reflectance studies of spacecraft landing sites to areas of silicic composition on the Moon, we determined *IoF/LS* values at 45° phase angle and used these values to compare with compositional parameters. The Lunar Prospector Gamma Ray Spectrometer detected high Th and low FeO content at these areas, suggesting an alkali-suite rock type [11]. NAC images of these regions reveal unique morphologic and reflectance characteristics that suggest a volcanic origin and mineralogy that differs from mare basalts [12-15]. LRO Diviner spectral data also show evidence for silicic compositions at these sites [16,17]. It is also possible that pyroclastics contribute to the increased reflectance seen at CBVC [11]. Photometry provides another line of evidence for highly reflective minerals such as alkali feldspars and quartz at these areas.

The silicic volcanic regions are all, on average, more reflective than the spacecraft landing sites. The Compton Belkovich Volcanic Complex has the highest reduced reflectance of the silicic sites studied, and the exposure of PAN has the highest reduced reflectance for any of the sites we have studied thus far. Using the relationship for *IoF/LS* and mafic content of Apollo and Luna samples, we find a strong anticorrelation between reduced reflectance and the mafic content of lunar soils. Extrapolating to higher *IoF/LS* values for the silicic regions is consistent with very low $FeO+MgO+TiO_2$ contents and with interpretations of felsic rock types (Fig. 1). We also find that PAN values fall well beyond this extrapolation, which is also consistent with the interpretation that there is very little, or no, mafic mineral exposure in PAN areas such as the example at Orientale. Further work such as analysis of Mini-RF radar data and surface morphologies, as well as reflectance studies of silicic pyroclastic materials in the laboratory, is needed to verify if pyroclastics also contribute to the high reflectance seen at silicic regions.

Conclusions: We have shown, using LROC NAC images, that photometric models can be used to investigate physical changes in lunar soil and to infer compositional properties at areas of unusal composition on the Moon. The silicic volcanic regions have high reflectance that is consistent with different proportions of highly reflective minerals and low concentrations of mafic minerals. On the basis of Diviner data, we know that these areas have silicic compositions and therefore we infer that their mineralogy is dominated by SiO_2 and alkali feldspar and low contents of Fe- and Ti-bearing minerals. Areas thought to be exposures of pure anorthosite have even higher reflectance values, consistent with the interpretation that these areas contain little to no mafic mineral components. Our future work includes acquiring reflectance measurements of Apollo samples of different compositions and surface textures (roughness, compaction, porosity, etc.) to use as "ground truth" with remote sensing reflectance measurements of the sample sites.

References: [1] Hapke B. W. (2012), *Theory of Reflectance and Emittance Spectroscopy* (2nd Ed.). [2] Hapke B. W. et al. (2012), *JGR, 117.* [3] Clegg, R. N. et al. (2014), *Icarus, 227,* 176-194. [4] Kaydash V. et al. (2011), *Icarus, 211,* 89-96. [5] Clegg, R. N. et al. (2014), *45th LPSC,* Abstract #1256. [6] Ohtake M. et al. (2009), *Science, 461,* 236-240. [7] Donaldson Hanna K. L. et al. (2014), *JGR, 119,* 1805-1820. [8] Robinson M. S. et al. (2010), *Space Sci. Rev., 150,* 81-124. [9] Morris R. V. et al. (1983), *Handbook of Lunar Soils.* [10] Helfenstein P. and Veverka J. (1987), *Icarus, 72,* 342-357. [11] Jolliff B. L. et al. (2011), *Nat. Geosci., 4,* 566-571. [12] Ashley J. W. et al. (2013), *44th LPSC,* Abstract #2504. [13] Glotch T. et al. (2011), *GRL, 38.* [14] Hawke, B. R. et al. (2003), *JGR Planet, 108,* 5069. [15] Lawrence S. J. et al. (2014), *45th LPSC,* Abstract #2279. [16] Glotch T. et al. (2010), *Science, 329,* 1510. [17] Greenhagen B. et al. (2010), *Science, 329,* 1507.

LUNAR FLASHLIGHT: MAPPING LUNAR SURFACE VOLATILES USING A CUBESAT. B. A. Cohen[1], P. O. Hayne[2], D. A. Paige[3], B. T. Greenhagen[2]; [1]NASA Marshall Space Flight Center, Huntsville AL 35812 (Barbara.A.Cohen@nasa.gov), [2]Jet Propulsion Laboratory, Pasadena CA 91109, [3]UCLA, Los Angeles, CA 90095

Introduction: The Diviner instrument on the Lunar Reconnaissance Orbiter (LRO) spacecraft measured temperatures in permantly-shadowed regions (PSRs) of the lunar poles as cold as 25K [1]. Over time, significant amounts of volatile molecules are likely have accumulated in lunar PSRs [2,3]. The Lunar Prospector Neutron Spectrometer (LP-NS) experiment indicated enhanced H abundances in both lunar polar regions [4, 5]. The resolution of the LP-NS is too coarse to determine directly if the H enhancements are associated specifically with permanently shadowed craters and not the polar regions in general. Updated hydrogen maps by collimated neutron spectroscopy show that some areas of enhanced hydrogen do not seem to correlate with either permanent shadow or temperature, an observation that has caused significant scientific controversy [6-9].

The LCROSS mission measured ~3-9 wt.% water in material ejected from the interior of Cabeus crater, along with other volatiles [10]. The LCROSS impact site exhibits no radar signatures indicative of ice, suggesting that such an amount of water ice may not be detectable by orbital monostatic radar, and thus polar ice may be present even in the absence of specific radar evidence for it. In fact, recent narrow-band reflectivity data from LRO's LOLA and LAMP instruments suggest volatiles may be present on the surface, though surface roughness or porosity effects cannot yet be ruled out [11, 12].

Surface water ice and other volatiles, if they exist in sufficient quantities, would be extremely useful for in situ extraction and utilization by future human and robotic missions. Understanding the composition, quantity, distribution, and form of water/H species and other volatiles associated with lunar cold traps is identified as a NASA Strategic Knowledge Gap (SKG) for Human Exploration. These polar volatile deposits could also reveal important information about the delivery of water to the Earth-Moon system. The scientific exploration of the lunar polar regions was one of the key recommendations of the Planetary Science Decadal Survey.

Mission: NASA's Advanced Exploration Systems (AES) program selected three low-cost 6-U CubeSat missions for pre-formulation as secondary payloads on the first test flight (EM1) of the Space Launch System (SLS) scheduled for 2017. The Lunar Flashlight mission was selected as one of these missions, specifically to address the SKG associated with lunar volatiles. Development of the Lunar Flashlight CubeSat concept leverages JPL's Interplanetary Nano-Spacecraft Pathfinder In Relevant Environment (INSPIRE) mission, MSFC's intimate knowledge of the SLS and EM-1 mission and experience with development of the NanoSail-D solar sail, and JPL experience with specialized miniature sensors.

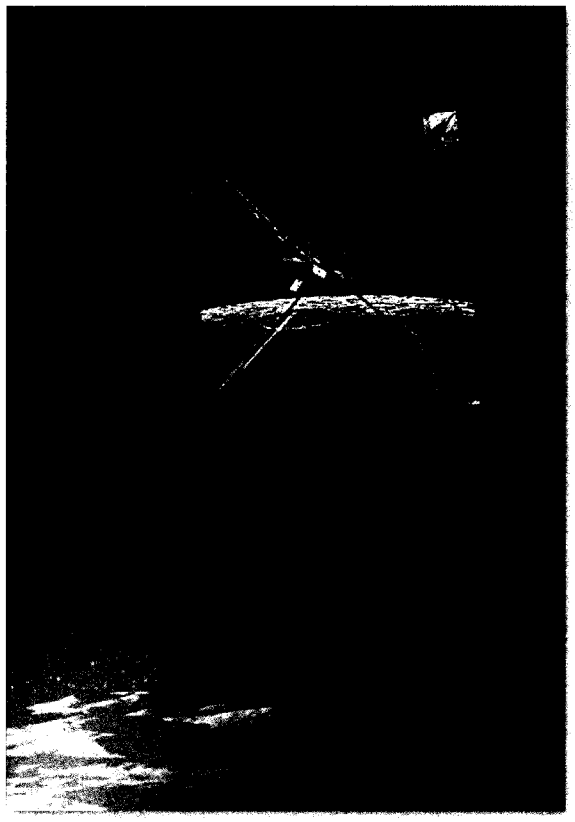

Fig. 1: Artist's concept of the Lunar Flashlight mission over the lunar surface.

The goal of Lunar Flashlight is to determine the presence or absence of exposed water ice and its physical state, and map its concentration at the 1-2 kilometer scale within the permanently shadowed regions of the lunar south pole. After being ejected in cis-lunar space by SLS, Lunar Flashlight deploys its solar panels and solar sail and maneuvers into a low-energy transfer to lunar orbit. The solar sail and attitude control system work to bring the satellite into an elliptical polar orbit spiraling down to a perilune of 30-10 km above the south pole for data collection. Lunar Flashlight uses its solar sail to shine reflected sunlight into PSRs and non-PSRs on the lunar night side, measuring surface albedo with a four-filter point

spectrometer at 1.1, 1.5 1.9, and 2.0 μm. Water ice will be distinguished from dry regolith from these measurements in two ways: 1) spatial variations in absolute reflectance (water ice is more reflective in the continuum channels), and 2) reflectance ratios between absorption and continuum channels. Derived reflectance and reflectance ratios will be mapped onto the lunar surface in order to distinguish the composition of the PSRs from that of the sunlit terrain.

Status: The Lunar Flashlight mission goals underwent a non-advocate peer review in June 2014 and the project will have presented its Mission Concept Review in August 2014. We will report on the current mission status and plans at the meeting.

References: [1] Paige, D. A., et al. (2010) Science, 330, DOI: 10.1126/science.1187726. [2] Vasavada, A. R., et al. (1999) Icarus, 141, 179-193. [3] Zhang, J. A. and D. A. Paige (2009) GRL, 36, 16203. [4] Feldman, W. C., et al. (2001) JGR, 106, 23231-23252. [5] Feldman, W. C., et al. (2000) JGR, 105, 4175-4196. [6] Lawrence, D. J., et al. (2011) Science, 334, 1058-. [7] Eke, V. R., et al. (2012) ApJ, 747, 6. [8] Mitrofanov, I. G., et al. (2010) Science, 330, 483-. [9] Sanin, A. B., et al. (2012) JGR, 117, [10] Colaprete, A., et al. (2010) Science, 330, DOI: 10.1126/science.1186986. [11] Gladstone, G. R., et al. (2012) JGR 117, CiteID E00H04. [12] Zuber, M. T., et al. (2012) Nature, 486, 378-381.

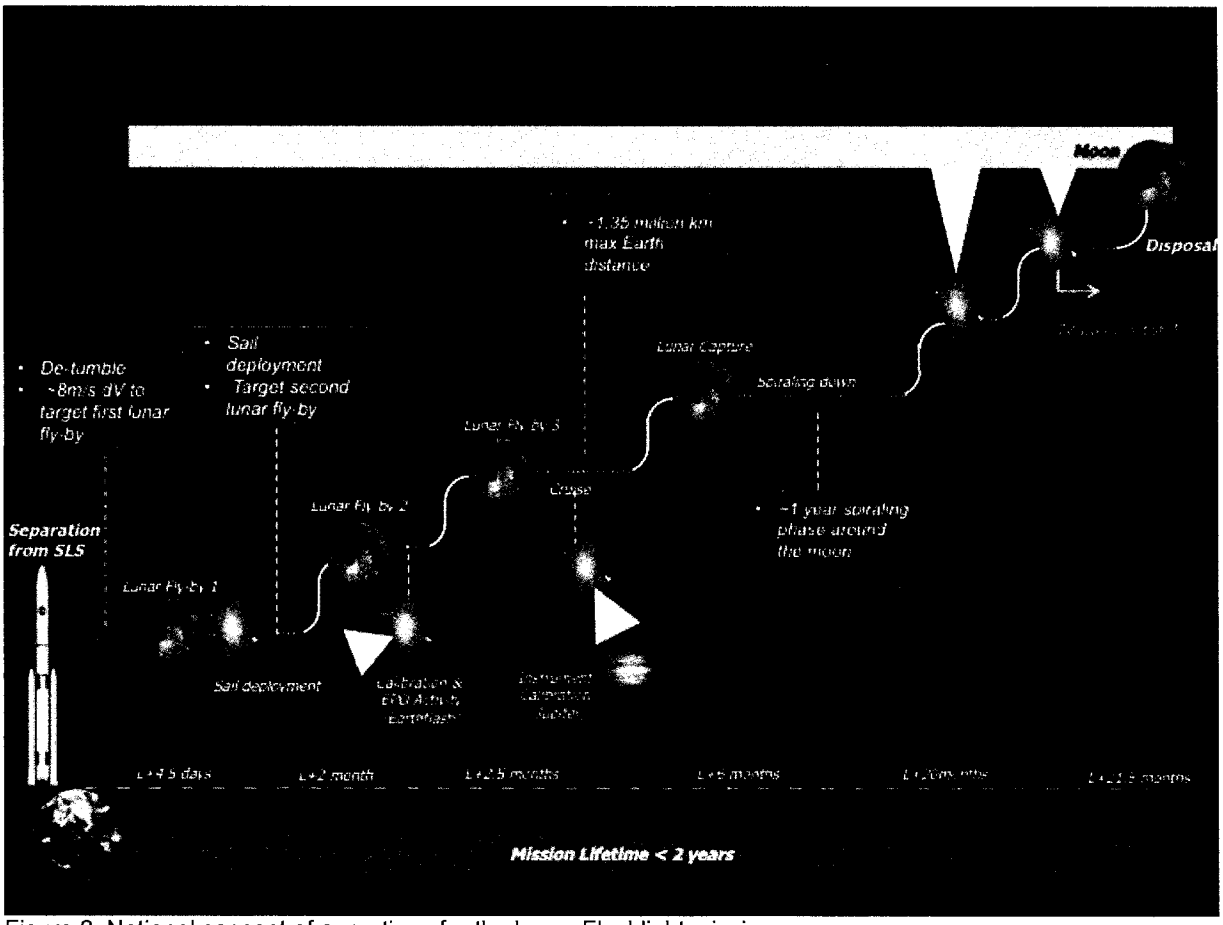

Figure 2: Notional concept of operations for the Lunar Flashlight mission.

COPERNICUS CRATER: COMPELLING SCIENCE EXPLORATION TARGET WAITING FOR FUTURE MISSIONS. Deepak Dhingra, Carle M. Pieters and James W. Head, Department of Earth, Environmental and Planetary Sciences, Brown University, Providence, RI 02906 (deepdpes@gmail.com)

Introduction: Copernicus crater (9.62° 339.92°; 96 km), located on the lunar near side, is a geologically young crater [1,2] with a cluster of towering peaks on the floor, an array of melt ponds and flow features, and an extensive ray system [3]. It was the proposed Apollo 18 landing site as well as the alternative site for Apollo 20 mission [4] before the cancellation of the lunar program after Apollo 17. Significant findings at Copernicus crater have been made since that time, starting with the discovery of olivine in the central peaks [5] and later in the northern crater wall [e.g. 6]. We highlight several new insights resulting from recent missions and suggest science/technology exploration targets that merit consideration by future lunar landers and rovers, including those being developed for Google Lunar X-prize.

New Discoveries with Modern Sensors at Copernicus: Modern imaging sensors onboard recent remote sensing missions [e.g.7,8,9,10] have provided high spatial imaging (1-10 m) and high spectral resolution near-IR data enabling a much closer look at the Moon than was previously possible. There have been at least 5 new findings made at Copernicus crater alone:

i) Impact melt origin of olivine exposed on the northern wall: The occurrence of olivine in the northern wall has been assumed to be of the same origin as olivine exposures in the central peaks [e.g. 6]. However, our high resolution integrated mineralogical and morphological analysis indicates that the northern wall exposure is associated with impact melt [11]. It is important to note the secondary nature of this material which may not be directly associated with olivine in the peaks. Similar secondary vs primary relationships for olivine may be common elsewhere on the Moon.

ii) Olivine exposures on the crater floor: Apart from previously known olivine exposures in the central peaks and the wall, several additional exposures have been identified on the crater floor (and some on the walls) [11]. These olivine occurrences represent a new geologic setting and have implications for the source region and formation mechanism of olivine since the sampling depths of the various crater units (viz. floor, wall and the peaks) are different.

iii) Mg-spinel exposure: Copernicus crater hosts a small exposure of the recently discovered Mg-Spinel lithology on the Moon [12,13,14]. The exposure is associated with a small mound on the crater floor and is in close proximity with a mafic lithology that may or may not be directly associated [15]. If true, the Copernicus Mg-spinel exposure would be unique in being associated with a mafic mineralogy.

iv) Heterogeneous mineralogy of impact melt ponds: Detailed analysis of morphologically identifiable impact melt ponds (few kilometers across) located at Copernicus crater on the walls and the rim region indicate an azimuthal variation in the mineralogy of impact melt [16]. Impact melt ponds in the NW part of the crater are mafic-poor in contrast to the mafic-rich nature of the ponds in the SE part of the crater. This mineralogical heterogeneity at small spatial scales indicates that melt could be locally derived and undergo minimal lateral mixing.

v) Mineralogically distinct impact melt feature: Apart from the pond mineralogy, Copernicus hosts a ~30 km long sinuous impact melt deposit which has a distinctly different mineralogy than impact melt in the immediate vicinity [17]. The sinuous feature is dominated by low calcium-pyroxene mineralogy while two fresh craters in nearby impact melt have a high calcium-pyroxene mineralogy. In addition, the sinuous melt-feature does not have any distinct morphological or topographic signature associated with it. As a consequence, it cannot be easily detected on imaging data unless accompanied by mineralogical information. This is so far the only documented feature of its kind on the Moon (or elsewhere) and has implications for our understanding of the large scale melt mixing and emplacement during the cratering process.

Such an impressive diversity in mineralogy and the corresponding geological context together with the young age of Copernicus makes it an extremely interesting target for further exploration in the near future.

Achievable Science/Technological Objectives: The detailed studies carried out at this crater have helped in outlining the scientific and technological objectives that could be achieved should a mission be planned to Copernicus crater:

i) *Characterizing olivine diversity at Copernicus*: The suggested primary and secondary origin of olivine lithology at Copernicus would benefit immensely from a ground-level close examination in terms of composition, surface texture (grain size, porosity), geological association and spatial distribution.

ii) *Obtaining ground truth for Mg-Spinel lithology*: Mg-Spinel lithology has so far only been detected remotely and no direct sample from any of the identified locations is yet available. Ground truth measurements in terms of Mg-spinel abundance, associated mineralogy and local geological context would be cru-

cial in refining the character and possible origin of this new rock type on the Moon.

iii) *Characterizing the mineralogical heterogeneity of impact melt at various spatial scales*: The mineralogical character of the large sinuous melt feature on the floor and the small impact melt ponds needs to be assessed on the ground in terms of surface expression, local variability, extent and geological association.

Testing of technological capabilities on scientifically relevant targets would provide practical experience on the challenges and scope for improvements. We provide two examples of technological objectives that could be fulfilled with exploration at Copernicus:

iv) *Rover mobility on the olivine-bearing central peaks and Mg-Spinel bearing mound*: Certain parts on the easternmost peaks on Copernicus crater floor would likely provide slopes amenable for a rover traverse. The slopes on the Mg-Spinel bearing mound would especially be favorable for a rover traverse. Apart from demonstrating capabilities related to traverses on variable slopes and navigation enabled by hazard avoidance, such an exercise would give an opportunity for mapping the local geological context of olivine/Mg-spinel and the characterization of any impact melt cover.

v) *3D reconstruction of small-scale and large scale scientific features of interest:* Numerous small-scale structures on the floor of Copernicus are at the limit of resolution for the currently available remote sensing datasets. Technology enabling 3D reconstruction of these features could be very useful and be demonstrated at Copernicus. Some of these features include collapse pits and fractures which could potentially support human habitats in the future.

We have utilized the available information to identify potential target locations which would be scientifically productive and time efficient from an exploration standpoint. We describe here our most preferred location which is the *crater center, in the vicinity of the central peaks*. This region has probably the maximum scientific return in view of the rich diversity of targets (Figure 1). It includes several high quality exposures of olivine lithology in the peak representing material that originated from the greatest depth. There is also a likely pseudo-tachylite exposure on the centre-most peak which could help in dating the Copernicus event. The exposure of Mg-spinel could be sampled along with the low Ca-pyroxene bearing sinuous melt feature. Several collapse pits in the area could be explored for human habitation potential, for obtaining a vertical profile of impact melt pile at that location as well as studying possible subsurface drainage pathways of impact melt. The region has a megablock, comparable in size to the central peaks that could be a morphologically subdued part of the central peak cluster. Its analysis could shed light about its provenance. All the exploration targets are situated in close proximity.

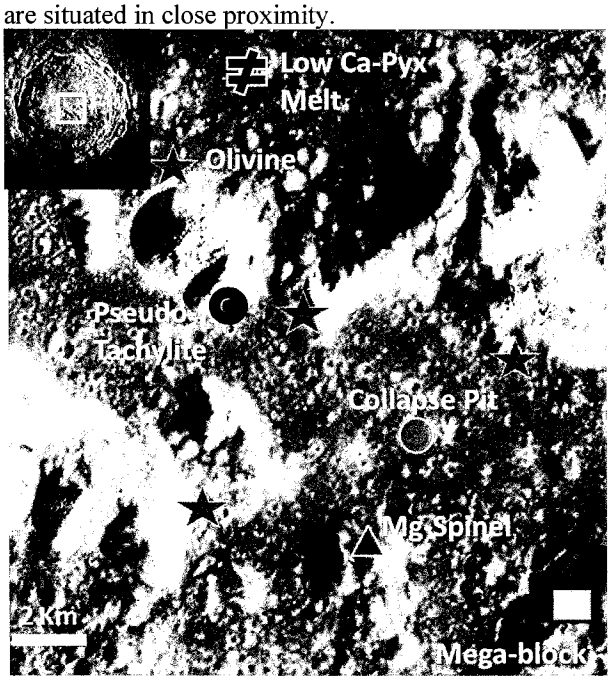

Figure 1 Exploration target diversity at the crater center.

The floor topography is relatively flat. However, the close proximity to the central peaks may provide some challenges for spacecraft landing around this location owing to the small landing ellipse requirement.

We recognize that selection of landing sites involves critical assessment of numerous engineering and scientific aspects. In this study, we are not strictly suggesting a landing site but wish to provide relevant scientific target information along with their relative proximity that could feed into landing site selection process. Copernicus crater remains a compelling target as we plan to return to the Moon.

Acknowledgements: SSERVI Grant no. NNA14AB01A

References: [1] Eberhardt et al. (1973) *Moon*, **8**, 104–114, doi:10.1007/BF00562752. [2] Hiesinger et al. (2012) *JGR*, **117**, E00H10, doi:10.1029/2011JE003935 [3] Pieters et al. (1985) **90**, 12,393-12,413 [4] http://www.hq.nasa.gov/pao/History/SP-4214/ch12-5.html [5] Pieters C.M. (1982) *Science*, **215**, 59-61[6] Lucey et al. (1991) *GRL*, **18** (11), 2133-2136 [7] Haruyama et al., (2008) *Earth, Planets Space*, **60**, 243–256 [8] Goswami & Annadurai (2009) *Curr. Sci.*, **6**(4), 486–491 [9] Pieters et al. (2009) *Curr. Sci.*, **96**, 500-505 [10] Robinson et al. (2010) *Space Sci. Rev.*, **150**, 81–124 [11] Dhingra et al., 2014 *EPSL, Submitted* [12] Pieters et al. (2011) *JGR*, **116**, E00G08, doi:10.1029/2010JE003727 [13] Dhingra & Pieters (2011) *LEAG Meeting*, #2024 [14] Pieters et al., (2014) *Am. Min.* http://dx.doi.org/10.2138/am-2014-4776 [15] Dhingra D. (2014) *Ph.D. Thesis, Brown University*, 494p. [16] Dhingra & Pieters (2013) *LMIPE-V Conference, Sudbury*, #3036 [17] Dhingra et al. (2013) *GRL*, **10**, 1–6

SOLAR WIND IMPLANTATION INTO LUNAR REGOLITH: HYDROGEN RETENTION IN A SURFACE WITH DEFECTS. W. M. Farrell [1,3], D. M. Hurley [2,3], M. I. Zimmerman [2,3], [1.] NASA/Goddard Space Flight Center, Greenbelt, MD, [2.] Johns Hopkins University/Applied Physics Laboratory, Laurel, MD, [3.] NASA's Solar System Exploration Research Virtual Institute, NASA/Ames Research Center, Moffett Field, CA

Abstract. Solar wind protons are implanted directly into the top 100 nanometers of the lunar near-surface region, but can either quickly diffuse out of the surface or be retained, depending upon surface temperature and the activation energy, U, associated with the specific implantation site. In this work, we explore the distribution of activation energies upon implantation and the associated hydrogen-retention times; this for comparison with recent observation of OH on the lunar surface.

We apply a Monte Carlo approach: for simulated solar wind protons at a given local time, we assume a distribution of U values with a central peak, U_c and width, U_w, and derive the fraction retained for long periods in the near-surface.

We find that surfaces characterized by a distribution with predominantly large values of U (> 1 eV, like that expected for vacancies) will retain implanted Hs. Surfaces with the distribution predominantly at small values of U (< 0.2 eV) will quickly diffuse away implanted Hs. However, surfaces with a large portion of activation energies between 0.3 eV < U < 0.9 eV will tend to be H-retentive in cool conditions but transform into H-emissive surfaces when warmed. These mid-range activation energies give rise to a diurnal effect with diffusive loss of H at noontime.

Lunar Surface Models in Raised Relief

Howard Fink, New York University (howard.fink@nyu.edu)

Lunar Surface Models are fully three-dimensional scale representations of selected areas of the Moon. Vacuum-formed for low cost, they are shaded to enhance the relief and include a labeled map colored by height. Regions selected to be modeled include Constellation areas of interest. The complete collection is available for sale at http://www.lunarsurfacemodels.com.

De Gerlache, Shackleton and Sverdlup; close-up of South Pole in 3D and shaded relief.

THE GEOLOGY OF INFERNO CHASM, IDAHO: A TERRESTRIAL ANALOG FOR LUNAR RILLES?

W. Brent Garry[1], Scott S. Hughes[2], Shannon E. Kobs Nawotniak[2], Catherine D. Neish[3], Christopher W. Haberle[4], Jennifer L. Heldmann[5], Darlene S. S. Lim[5], and the FINESSE Team [1]Planetary Geodynamics Laboratory, Code 698, NASA Goddard Space Flight Center, Greenbelt, MD, 20771, [2]Dept. of Geosciences, Stop 8072, Idaho State University, Pocatello, ID, 83209, [3]Florida Institute of Technology, Melbourne, FL, 32901, [4]School of Earth and Space Exploration, Arizona State University, Tempe, AZ, 85287, [5]NASA Ames Research Center, Moffett Field, CA, 94035.

Introduction: Lunar sinuous rilles are thought to have formed by thermal erosion, mechanical erosion, construction, or a combination of these processes via emplacement by lava tubes or lava channels **[e.g., 1-4]**. The investigation of Hadley Rille by Apollo 15 provided the first field observations of a rille **[5]**, but remote sensing observations remain our primary method for studying these features **[6,7]**. Terrestrial volcanic features with similar morphologies to lunar rilles can provide insight into their formation on the Moon. While the scale of lunar rilles are much larger than terrestrial analogs, there may be some morphologic comparisons and inferences we can make between the two planetary bodies through field work. Here we compare field observations at a rille-like channel in Idaho (Inferno Chasm) to a rille in Marius Hills on the Moon.

Background: The SSERVI FINESSE team (Field Investigations to Enable Solar System Science and Exploration) **[8]** conducted field studies at Craters of the Moon National Monument and Preserve (COTM) in Idaho **(Fig. 1A)** from July 28 – Aug. 8, 2014 to investigate terrestrial analogs for lunar volcanic and impact features. In addition to Inferno Chasm, field sites included Kings Bowl and North Crater Flow – each site exhibiting different volcanic attributes. Kings Bowl erupted along a N-S trending fissure system and formed a series of spatter cones, perched lava ponds, and phreatic blowouts **(Fig. 1B)**. North Crater Flow is a complex pahoehoe flow with a variety of textures that resemble an impact melt flow on Tycho crater **[9]**.

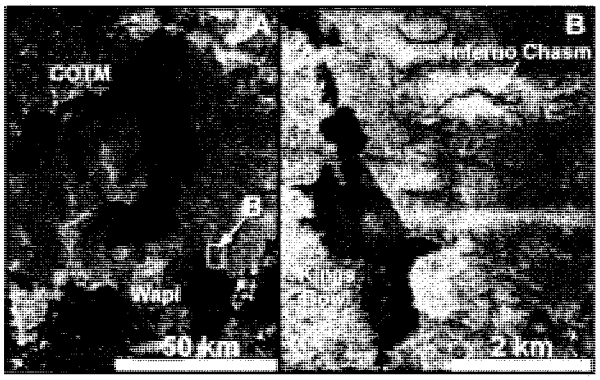

Figure 1. (A) Craters of the Moon (COTM), Idaho. (B) Location of Inferno Chasm and Kings Bowl [Google Earth].

Inferno Chasm (42°58'00"N, 113°11'25"W) is a basaltic low-shield with a vent and sinuous channel **(Figs. 1B, 2)**. The area is overgrown with sage and desert grasses, but it appears that the margins of the low shield have been embayed or buried by subsequent lava flows or loess making it difficult to define the true extent of this volcanic feature.

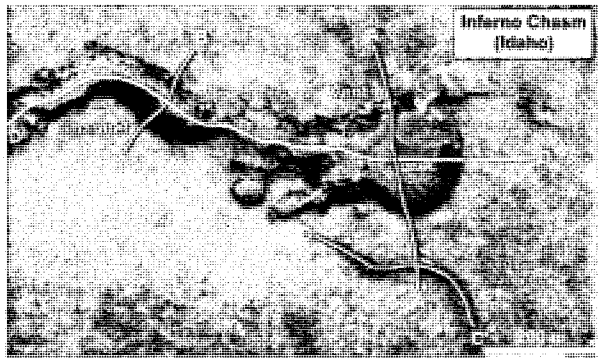

Figure 2. Location of Differential GPS and LiDAR surveys at Inferno Chasm in Idaho [GoogleEarth].

Data Collection. We documented the geology and morphology of Inferno Chasm using Trimble R8 and TopCon Hiper II Differential Global Positioning Systems (DGPS) **(Fig. 2)**, LiDAR, Unmanned Aerial Vehicles (UAV), and sampling.

Field Observations. Inferno Chasm is ~20 m high and 2 km in diameter. The main vent crater is roughly circular with a sinuous channel extending to the west. DGPS survey A-A' shows the vent is ~200 m wide, ~20 m deep and has a small 2.5 m-high mound in the center **(Fig. 3)**. DGPS profile D-D' indicates a channel length of ~1.6 km and a slope of <1° along the channel floor **(Fig. 2)**. Several outflow channels are also visible in the remote sensing images, but are much more subtle in the field (DGPS profile C-C'). Outcrops of the vent walls expose prominent massive layers (2-3 m thick) **(Fig. 4)** overlain by a 1-2 m thick sequence of thinner layers (10s cm thick). Field observations and samples collected for analysis indicate low-shield development typical of the eastern Snake River Plain **[10]**.

Lunar Rille: A rille in Marius Hills **(Fig. 5)** has a similar morphology to Inferno Chasm. The vent region is ~3 km wide and up to 225 m deep. The channel is 15 km long, 0.9-1 km wide, and ~30-100 m deep. The path of the rille diverts around the base of a mound within Marius Hills and the distal end of the rille may have been buried by subsequent lava flows obscuring

the true extent of the rille. The walls of the rille and vent region reveal layers of lava possibly related to this eruption and boulders.

Discussion: Preliminary observations at Inferno Chasm provide insight into how rille-like channels can form almost entirely via construction. The vent region at Inferno Chasm was apparently constructed by a combination of thick and thin lava layers. Evidence of thermal erosion and/or lava tube collapse along the channel were not identified, but have not been ruled out. Distinct levees were not identified along the channel margin. More field work is planned at COTM in 2015 to study the channel in more detail. Lunar rilles form through a combination of thermal and mechanical erosion **[1-7]**, plus construction **[4]**. Layers exposed in rille walls could represent sequences of lava layers related to the eruption that formed the rille and not substrate layers that have been thermally eroded by the lava flow. Determining which component of a rille was formed via construction versus thermal erosion is important for modeling eruption parameters.

References: **[1]** Greeley R. (1971) *Science* 172, 722-725. **[2]** Gornitz V. (1973) *The Moon, 6,* 337–356. **[3]** Hulme G. (1973) *Modern Geo., 4,* 107-117. **[4]** Spudis P. *et al.* (1988) *LPSC, 18,* 243-254. **[5]** Swann G.A. *et al.* (1972) *Apollo 15 Prelim. Sci. Rep., 289,* 5-1 – 5-112. **[6]** Hurwitz D.M. *et al.* (2012) *JGR Planets, 117,* E00H14,doi:10.1029/2011JE0040 00. **[7]** Hurwitz D.M. *et al.* (2013) *Planet. & Space Sci., 79-80,* 1-38. **[8]** Heldmann J. L. *et al.* (2013) AGU Fall Mtg. Abstract #P54B-01. **[9]** Carter L.M. *et al.* (2012) JGR-Planets, *117, E00H09,* doi:10.1029/ 2011JE00391. **[10]** Greeley R. (1982) *JGR-SE, 87*(B4), 2705-2712.

Acknowledgements: This research is supported by a NASA SSERVI research grant provided to NASA Ames Research Center and collaborating institutions.

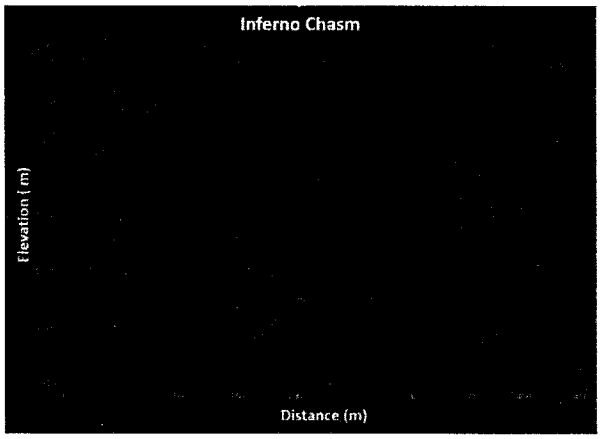

Figure 3. Differntial GPS profile A-A' across the vent at Inferno Chasm (see Fig. 2). The vent is ~200 m wide, ~15-20 m deep, and has a 2.5 m high mound near the center.

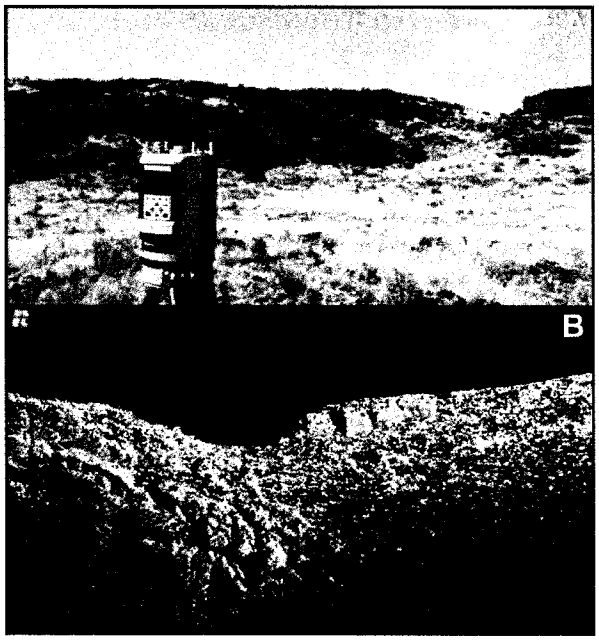

Figure 4. (A) Riegl Vz-400 LiDAR setup within the Inferno Chasm vent (See Fig. 2 for location). (B) LiDAR scan looking to the east along the northern vent wall.

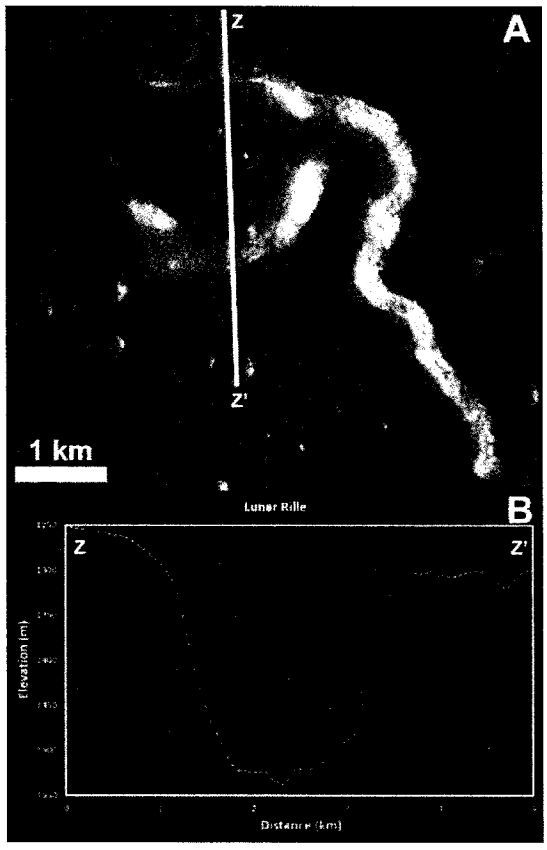

Figure 5. (A) Sinuous rille located within Marius Hills (13.95° N, 49.55° W) LROC NAC image M1096815341LE [NASA/GSFC/ASU]. Resolution (1.25 m/px). Incidence angle (66°). (B) LOLA profile across vent (1024 ppd DEM).

SPECTRAL AND THERMOPHYSICAL PROPERTIES OF LUNAR SWIRLS FROM THE DIVINER LUNAR RADIOMETER. T. D. Glotch[1] and J. L. Bandfield[2], P. G. Lucey[3], P. O. Hayne[4], B. T. Greenhagen[4], J. A. Arnold[1], R. R. Ghent[5], and D. A. Paige[6] [1]Department of Geosciences, Stony Brook University, timothy.glotch@stonybrook.edu, [2]Space Science Institute, [3]Hawaii Institute of Geophysics and Planetology, University of Hawaii at Manoa, [4]Jet Propulsion Laboratory, [5]Department of Earth Sciences, University of Toronto, [6]Department of Earth, Planetary and Space Sciences, University of California Los Angeles.

Introduction: Lunar swirls are high-albedo markings on the Moon that occur in both mare and highlands terrains in the presence of local crustal magnetic fields[1-2]. Data from the Lunar Reconnaissance Orbiter Diviner Lunar Radiometer support the hypothesis that the swirls formed as a result of deflection of the solar wind by local magnetic fields [3]. Diviner data show a shift to shorter wavelengths of the wavelength-dependent Christiansen Feature, consistent with retarded or abnormal space weathering at the swirls. Daytime temperature measurements show that the cm-scale surface roughness of the Reiner Gamma swirl is indistinguishable from the surrounding terrain, contrary to the dust-lofting [4] or micrometeorid/comet swarm impact formation mechanisms [5-7] for the swirls, which would be expected to alter the swirl regolith structure. Night-time temperature data and a thermal model indicate that the < 1K temperature difference between the Reiner Gamma swirl and the surrounding terrain can be completely accounted for by their differing albedoes. Taken together, these data support the solar wind standoff model for swirl formation.

Christiansen Feature Position: We have measured the CF positions of 12 lunar swirls and compared them to the CF positions of immediately surrounding terrain. For swirls that have anomalously low albedo dark lanes, we have also determined the dark lane CF positions. Swirl CF's are shifted to shorter wavelengths by an average of 0.06 μm, with the largest shifts of 0.09 μm found for the Van de Graaf crater and Descartes swirls and the lowest shift of 0.02 μm found for the Rima Sirsalis swirl. In every case measured, swirl dark lane CF values were within 0.01 μm of the off-swirl terrain. Figure 1 shows the CF distributions for the Reiner Gamma swirl.

Surface Roughness: In addition to CF measurements, Diviner's ability to determine the physical characteristics of the lunar surface help to constrain swirl formation mechanisms. We have determined the surface roughness, defined as root mean square (RMS) slope on the Reiner Gamma swirl and the local terrain just off the swirl. To do this, we determined the mean temperature difference on and off the swirl between Channel 3 and Channel 6 for every hour between 6 am and 6 pm local time. We then compared the results to modeled [8] temperature differences for cm-scale surface roughnesses ranging between 5 and 40° RMS. Our resuls show that surface roughnesses on and off the Reiner Gamma swirl are nearly identical, with values between 25° and 30° RMS (Figure 2). These roughnesses are in line with previously estimated sub-mm to cm-scale surface roughnesses for typical lunar surfaces of 16-25° [9].

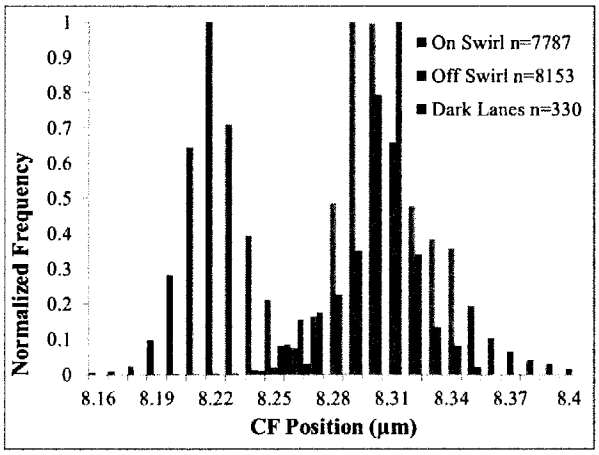

Figure 1. CF position distributions measured on the Reiner Gamma Swirl (blue), in typical off-swirl terrain (green), and within the anomalously low albedo dark lane (red).

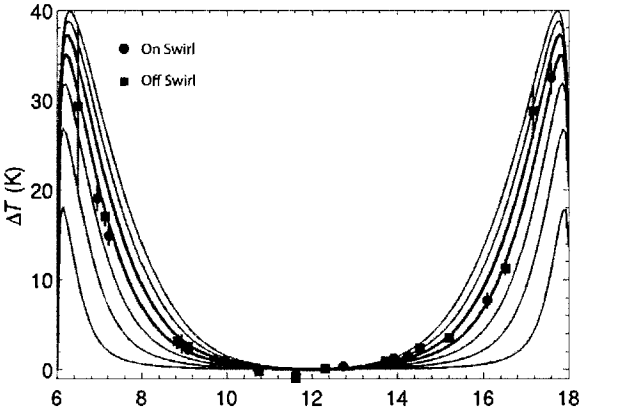

Figure 2. Channel 3-Channel 6 temperature difference plotted against local time for regions on the Reiner Gamma Swirl and Surrounding terrain. Curves are from the roughness model of [8]. Diviner data best match a cm-scale surface roughness of 25-30° both on and off the swirl.

Thermophysical Characteristics. We also use Diviner night-time temperature data and a sophisticated thermal model [10-11] to determine the surface thermophysical characteristics on and off the Reiner Gamma swirl, including vertical structure and particle size of regolith fines. We constructed 128 ppd night-time temperature maps using Diviner Channel 8 (50-100 μm) brightness temperatures acquired between local times of 19:30 and 05:30. These values are positive or negative deviations from the scene average normalized for local time variations. The average normalized temperature on the Reiner Gamma swirl is -0.8 ± 1.5 K as opposed to the average off-swirl temperature of -0.3 ± 1.8 K (1-σ standard deviations). The swirl, on average, is only ~0.5 K colder than the off-swirl surface. The measured temperature difference, though small, can be tied directly to the physical properties of the swirl surface. To do this, we use a thermal model to constrain the differences in regolith properties between the swirl and non-swirl surfaces. This standard lunar regolith model [10-11] uses Diviner night-time temperature data to constrain the upper regolith density profile. Figure 3 shows that the temperature difference between the on-and off-swirl surfaces can be accounted for completely by the albedo difference between the swirls. Additionally, we added a 2 mm low thermal inertia (~30 J m^{-2} K^{-1} $s^{-1/2}$, ~50% of the standard model) layer on top of the standard swirl model. Such a low thermal inertia layer would be expected from the admixture of additional fine particulates with typical lunar regolith, as would be predicted by the dust transport model of swirl formation [4]. Our results show that even this 2 mm thick layer would produce night-time temperatures much lower than those that are observed. Put another way, the swirls are surficial features that, thermophysically, are nearly indistinguishable from the surrounding terrain.

Discussion and Conclusions. Each of three separate analyses based on Diviner data support the solar wind stand-off model of swirl formation [3] and contradict the dust lofting [4] and impact swarm [5-7] hypotheses. Measurements of the Diviner CF positions on and off the swirls are consistent with retarded or abnormal space weathering at the swirls. They are inconsistent with a dust-lofting mechanism that would enrich the swirl surfaces in feldspar-bearing fines [4]. Diviner daytime temperature measurements compared to a roughness model show that the surface structure of the Reiner Gamma swirl is nearly indistinguishable from that of the surrounding terrain. The dust lofting mechanism would likely lead to a smoother surface, while recent impact swarms would lead to a rougher surface. Finally, night time temperature measurements, in conjunction with a standard regolith thermal model show

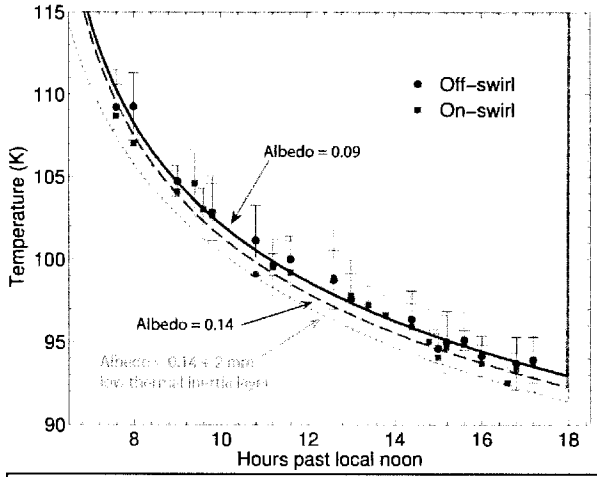

Figure 3. Diviner night-time temperature observations on (blue dots) and off (black dots) the Reiner Gamma swirl. The black solid line and blue dashed line show predicted temperatures. Predicted temperatures for a 2 mm thick low thermal inertia layer on top of the standard swirl thermal model (green dotted line) are too low to explain Diviner observations.

that the temperature difference between the Reiner Gamma swirl and the off-swirl surface can be completely explained by the albedo difference between the two. Adding even a 2 mm thick low thermal inertia layer, as might be caused by an enrichment of fine lofted dust produces temperatures that are much to low to match Diviner's observations.

Taken together, Diviner data and models complement VNIR measurements from M^3 [12-13] and radar measurements from Mini-RF [14], which support the surficial nature of the lunar swirls and their formation through the solar wind standoff mechanism.

References: [1] Blewett, D. T., B. R. Hawke, and N. C. Richmond (2007) *Geophys. Res. Lett., 34,* L24206. [2] Blewett, D. T. et al. (2011) *J. Geophys. Res., 116,* E02002. [3] Hood, L. L. and G. Schubert (1980) *Science, 208,* 49-51. [4] Garrick-Bethell, I., J. W. Head III, and C. M. Pieters (2011) *Icarus, 212,* 480-492. [5] Schultz, P. H., and J. L. Srnka (1980), *Nature, 284,* 22-26. [6] Pinet, P. C. et al. (2000), *J. Geophys. Res., 105,* 9457-9476. [7] Starukhina, L. V. and Y. G. Shkuratov (2004) *Icarus, 167,* 136-147. [8] Hayne, P. O. et al. (2013) *EGU Gen. Assembly,* abstract EGU2013-10871-1. [9] Helfenstein, P. and M. K. Shepard (1999), *Icarus, 72,* 342-357. [10] Hayne, P. O. et al. (2010), *Science, 330,* 477-479. [11] Vasavada, A. R. et al. (2012), *J. Geophys. Res., 117,* E00H18. [12] Kramer, G. Y. et al. (2011a), *J. Geophys. Res., 116,* E00G18. [13] Kramer G. Y. et al. (2011b), *J. Geophys. Res., 116,* E04008. [14] Neish, C. D. et al. (2011) *Icarus, 215,* 186-196.

THE BENEFITS OF SAMPLE RETURN: CONNECTING APOLLO SOILS AND DIVINER LUNAR RADIOMETER REMOTE SENSING DATA. B.T. Greenhagen[1], K.L. Donaldson Hanna[2], I.R. Thomas[2], N.E. Bowles[2], C.C. Allen[3], C.M. Pieters[4] and D.A. Paige[5]; [1]Jet Propulsion Laboratory, California Institute of Technology, Pasadena, [2]University of Oxford, [3]Johnson Space Center, [4]Brown University, [5]University of California, Los Angeles. Email: Benjamin.T.Greenhagen@jpl.nasa.gov

Introduction: The Diviner Lunar Radiometer, onboard NASA's Lunar Reconnaissance Orbiter, has produced the first global, high resolution, thermal infrared observations of an airless body. The Moon, which is the most accessible member of this most abundant class of solar system objects, is also the only body for which we have extraterrestrial samples with known spatial context. Here we present the results of a comprehensive study to reproduce an accurate simulated lunar environment, evaluate the most appropriate sample and measurement conditions, collect thermal infrared spectra of a representative suite of Apollo soils, and correlate them with Diviner observations of the lunar surface.

Laboratory Studies: It has been established that thermal infrared spectra measured in a simulated lunar environment (SLE) are significantly altered from spectra measured under terrestrial conditions [e.g. 1, 2]. The data presented here were collected at the University of Oxford Simulated Lunar Environment Chamber (SLEC). In SLEC, the lunar environment is simulated by: (1) pumping the chamber to vacuum pressures (<10-4 mbar) sufficient to simulate lunar heat transport processes within the sample, (2) cooling the chamber with liquid nitrogen to simulate radiation to the cold space environment, and (3) heating the samples with heaters and lamp to set-up thermal gradients similar to those experienced in the upper hundreds of microns of the lunar surface [3]. A comprehensive suite of experiments were conducted using different sample preparation and heating conditions on Apollo soils 15071 (maria) and 67701 (highland) and compared the results to Diviner noontime data to select the optimal experimental conditions. Thermal infrared measurements (Figure 1) in optimized SLE were made of 10084, 12001, 14259, 15071, 15601, 61141, 66031, 67701, and 70181. Table 1 lists soils available to this study.

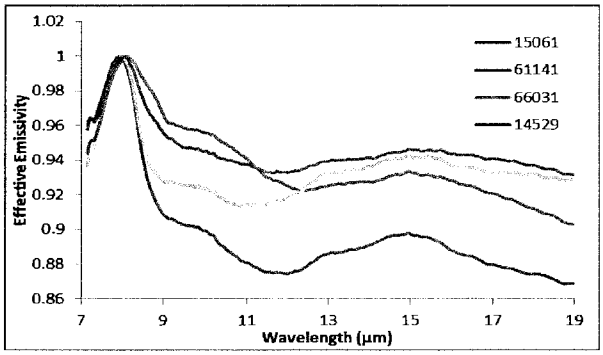

Figure 1: Subset **of thermal infrared emission spectra measured in SLE as part of this study.**

Diviner Data: The Diviner Lunar Radiometer is a nine-channel, pushbroom mapping radiometer. Diviner measures broadband reflected solar radiation with two channels, and emitted thermal infrared radiation with seven infrared channels [4]. The three shortest wavelength thermal infrared channels near 8 μm were specifically designed to characterize the mid-infrared "Christiansen Feature" emissivity maximum, which is sensitive to silicate composition [5]. The Diviner dataset includes all six Apollo sites at approximately 200 m spatial resolution.

Table 2: Apollo Soils currently available to SLEC.

Apollo Site	Station	Soil	Mass	Is/FeO
Apollo 11	LM	10084	5 g	78
Apollo 12	LM	12001	5 g	56
Apollo 14	LM	14259	3.5 g	85
Apollo 15	LM	15021	3.5 g	70
Apollo 15	Sta. 1	15071	5 g	52
Apollo 15	Sta. 7	15411	3.5 g	43
Apollo 15	Sta. 9a	15601	3.5 g	29
Apollo 16	Sta. 1	61141	5 g	56
Apollo 16	Sta. 6	66031	3.5 g	102
Apollo 16	Sta. 11	67701	3.5 g	39
Apollo 17	LM	70181	5 g	47
Apollo 17	Sta. 2	72501	3.5 g	81
Apollo 17	Sta. 9	79221	3.5 g	81

Results: We find that analyses of Diviner observations of individual sampling stations and SLE measurements of returned Apollo soils show good agreement, while comparisons to thermal infrared reflectance under terrestrial conditions do not agree well, which underscores the need for SLE measurements and validates the Diviner compositional dataset. Future work includes measurement of additional soils in SLE and cross comparisons with measurements in JPL Simulated Airless Body Emission Laboratory (SABEL).

References: [1] Logan L.M. *et al.* (1973) *JGR*, *78*, 4983. [2] Salisbury J.W. and Walter L.S. (1989) *JGR*, *94*, 9192. [3] Thomas I.R. et al. (2012) Rev.Sci.Inst., 83 (12), 124502. [4] Paige D.A. *et al.* (2010) *SSR*, *150*. [5] Greenhagen B.T. *et al.* (2010) *Science*, *329*, 1507.

International Strategy for the Exploration of Lunar Polar Volatiles. J. E. Gruener[1] and N. H. Suzuki[2], [1]NASA Johnson Space Center (Mail Code KX111, 2101 NASA Parkway, Houston, Texas, 77058, john.e.gruener@nasa.gov) [2]NASA Headquarters (Mail Code CQ000, 300 E Street Southwest, Washington, DC, 20546, nantel.h.suzuki@nasa.gov).

Introduction: The National Aeronautics and Space Administration (NASA) is participating in the International Space Exploration Coordination Group (ISECG), working together with 13 other space agencies to advance a long-range human space exploration strategy. The ISECG is a voluntary, non-binding international coordination mechanism through which individual agencies may exchange information regarding interests, objectives, and plans in space exploration with the goal of strengthening both individual exploration programs as well as the collective effort.

The ISECG has developed a Global Exploration Roadmap (GER) that reflects the coordinated international dialog and continued preparation for exploration beyond low-Earth orbit – beginning with the International Space Station (ISS) and continuing to the Moon, near-Earth asteroids, and Mars [1]. Space agencies agree that human space exploration will be most successful as an international endeavor, given the challenges of these missions. The roadmap demonstrates how initial capabilities can enable a variety of missions in the lunar vicinity, responding to individual and common goals and objectives, while contributing to building partnerships required for sustainable human space exploration that delivers value to the public.

Use of Local Resources: The initial capabilities and missions on the Moon will likely consist of small robotic missions limited in scale and mission duration, with everything needed for those missions delivered from Earth. However, when it comes to maintaining a longer-term human presence beyond low-Earth orbit, space agencies agree that the use of local resources would significantly benefit operations in the lunar vicinity, and limit the cost and complexity of bringing all the needed supplies from Earth. The most promising uses for local resource utilization are in life support systems or as propellants.

For many years, the lunar regolith was seen as the primary source for both oxygen (chemically bound in lunar minerals and glasses) and hydrogen (implanted into the regolith by the solar wind). However, recent discoveries of water on the Moon [2], particularly in polar regions, may lead to less complex methods to create life support consumables and propellants. To gain an understanding of whether lunar polar volatiles, such as water ice, could be used in a cost effective and safe manner, it is necessary to understand more about the nature and distribution of the volatiles and whether they could be processed cost effectively.

International Strategy: The ISECG has begun an effort to develop a coordinated international lunar polar volatile strategy that is technically feasible, yet programmatically implementable. The strategy would follow an incremental phased approach, beginning with robotic prospecting to understand the nature and distribution of the polar volatiles through measurements on the lunar surface, and followed by robotic in situ resource utilization demonstrations (ISRU) to understand whether potential resources could be extracted and processed economically and safely.

Core Elements: Currently, there are three initial core elements to this strategy. 1.) Common Lunar Region - build a consensus among the international community for a common "Region" on the lunar surface to be collectively explored by a variety of sequential, coordinated missions. The region would be larger than a landing site for a single mission, perhaps areas as large as several tens of kilometers in extent, and possibly including highly illuminated peaks and permanently shadowed areas. 2.) Low Entrance Barriers - facilitate participation by space agencies, commercial entities, and universities by deployment of surface or orbital infrastructure assets that provide productivity-enhancing utility services within the specified region (i.e., power generation, thermal protection, communication) to allow for simpler, lower cost rovers or other surface systems; and collaborative development of instrument or surface system capabilities between participants. 3.) Common Standards – utilize standard interfaces (mechanical, electrical, communication) and standard propellants to optimize use of surface utility services, permit interchangeability of vehicle payload complements, and maximize interoperability.

References: [1] ISECG (2013) *http://www.nasa.gov/sites/default/files/files/GER-2013_Small.pdf.* [2] Robinson K. L. and Taylor G. J. (2014) *Nature Geoscience, 7,* 401-408.

Why Do We Need the Moon: Next Steps Forward for Moon Exploration

Ugur Guven, UPES (drguven@live.com)

Perhaps one of the greatest accomplishments of mankind is when Neil Armstrong was able to step on the moon with his famous words. It was a giant step for the mankind and it signaled the me that man was able to start pu ng his dominion over the universe star ng with the moon. However, fervor of space travel of those days has not been matched by any other ac vity to this day. A er 6 manned missions to the Moon, these missions were shelved due to budgetary reasons and it has not been possible to go back since. However, the need for space travel and space explora on has remained ac ve in the collec ve consciousness of the world popula on and there are signs that it can become viable again. Especially with the advent of the private sector for space tourism, the concept for moon travel may become possible again. It is essen al that the moon is used as a stepping stones as it has been proven that the energy cost for manned missions to any planet including Mars is quite high. However, having a habitable presence on the moon would make manned missions to other planets a more probable possibility and furthermore support to these missions would also increase signi cantly. Especially with the ndings of the Chandrayaan mission, it seems more feasible to create a presence on the moon. Of course, the rst step may come through private space companies under the ag of space tourism as passengers may be given a chance to y an orbit around the moon and come back to Earth. Furthermore, more and more universi es and research ins tu ons are planning mini-moon missions with nanosatellites or with microsatellites. In addi on, with the possibility of space mining for rare materials such as Helium 3, the prospects for the moon seems to be quite posi ve. This paper outlines the various possibili es for the future of the moon and it details how it can be bene cial for future space technology endeavors.

Keywords: Moon Mission, Nanosatellites for Moon, Helium 3 Mining, Moon Base, Future Moon Missions, Private Sector Moon Missions

Space Mission To The Moon With A Low Cost Moon Probe Nanosatellite: University Project Feasibility Analysis And Design Concepts

One of the most fascinating prospects for the future is the possibility of exploring the moon with a small science mission. Ever since mankind has been to the moon since 1969, several missions by other countries have also been launched to the moon by countries such as China and India. However, the cost of such missions is unusually high and the global recession in the world has affected finance of countries in the EU as well as countries such as USA and Russia. As a result, many moon exploration programs have been put on hold or they have been downsized. Even today, the best space programs in the world are feeling the effects of this downsizing.

This paper discusses the possibility of launching a10 kg nanosatellite moon probe with a joint university effort along with industrial partners for a low cost mission to the moon. It will use low cost propulsion techniques and orbital transfers to reach the moon and it will be equipped with some fundamental, but lightweight sensors for remote sensing observation. Furthermore, it will also allow for university-student-industry cooperation for some experimental setups to be included in this low cost moon probe. At the end of its mission, it will be crashed to the moon for relevant data retrieval. The paper will discuss the basic mission design as well as cost and feasibility analysis of this project which has been planned. Furthermore, the difficulties and challenges of this project will also be discussed and a sample mission parameters will be given for a possible future work. Several universities have shown interest to be part of this moon probe project as both research as well as learning opportunities is diverse.

ARTEMIS OBSERVATIONS OF THE SPACE ENVIRONMENT AROUND THE MOON AND ITS INTERACTION WITH THE ATMOSPHERE AND SURFACE. J. S. Halekas[1] and the ARTEMIS Team, [1]Department of Physics and Astronomy, University of Iowa, jasper-halekas@uiowa.edu.

Introduction: The two ARTEMIS probes continue their successful extended mission around the Moon, studying the interaction of terrestrial and solar plasma with the lunar environment. ARTEMIS provides continuous monitoring of the incoming plasma, including protons and doubly ionized helium in the solar wind, and magnetospheric plasma during the Moon's passage through the geomagnetic tail.

The Moon is a heavily driven system, almost completely exposed to the influence of the space environment. As a result, the lunar atmosphere and surface respond to plasma inputs. In turn, the secondary particles produced from the surface and atmosphere affect the plasma environment around the Moon. ARTEMIS observes both the plasma drivers of the lunar system, and the perturbations that the Moon induces in the interplanetary environment.

ARTEMIS and LADEE: ARTEMIS observations are critical to developing a complete understanding of the dynamics of the complex neutral exosphere revealed by LADEE. ARTEMIS provides key observations of both sources and sinks of the neutral exosphere observed by LADEE. The highly variable plasma influx directly supplies some species to the lunar exosphere, most notably helium. The flowing plasma also liberates other exospheric species from the surface through charged particle sputtering. Finally, the plasma acts as the final sink for a large proportion of the exosphere, by picking up ionized constituents and sweeping them away from the Moon. ARTEMIS observes both the influx of protons and helium to the Moon. In addition, it observes the convection electric field of the plasma, which determines whether newly born pickup ions escape, or re-impact the surface. And, finally, when properly situated, ARTEMIS observes the escaping pickup ions themselves.

ARTEMIS Low-Altitude Measurements: The incoming plasma measured by ARTEMIS also contributes to space weathering of the surface. Lunar magnetic fields, though small in scale and comparatively weak, have surprisingly significant effects on the incoming plasma, and a number of observations suggest that their presence may locally alter the space weathering of the surface. Recent data from Kaguya and Chandrayaan have shown that lunar magnetic anomalies efficiently reflect incoming solar wind protons, providing substantial shielding of portions of the crust, with potential implications for both space weathering and surface sputtering.

The two ARTEMIS probes have made a number of low-altitude (tens of kilometers) passes over regions with moderately strong crustal magnetic fields, at local times both near the sub-solar point and at the terminator. Several such passes occurred over a region of the surface containing unusual albedo markings - or "swirls" - that could indicate a local reduction in space weathering. Fig. 2 shows observations from one such pass, demonstrating the highly distorted magnetic fields encountered near periapsis, and reflected protons emanating from a strong crustal magnetic field region. During this observation, >30% of the solar wind reflected before reaching the surface, with possibly much

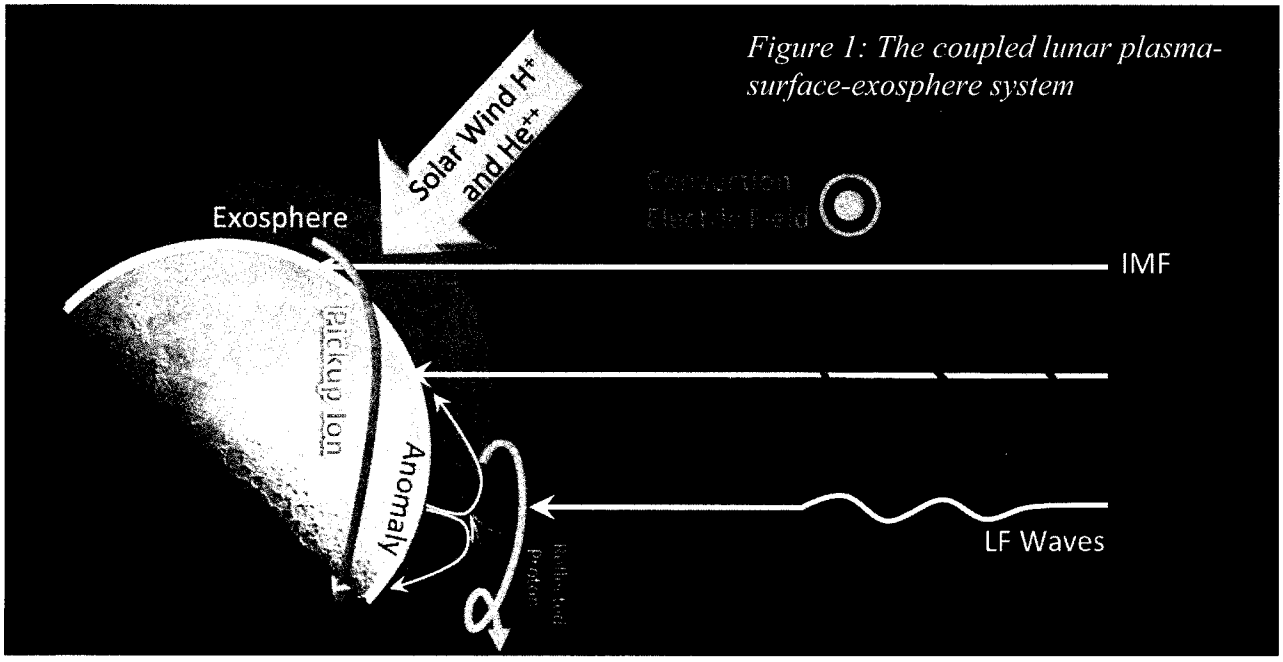

Figure 1: The coupled lunar plasma-surface-exosphere system

higher reflection percentages in localized regions.

We investigate the ARTEMIS low-altitude passes in detail, focusing on how the observed reflected protons and other local modifications of charged particle distributions and electromagnetic fields relate to the properties of the surface. ARTEMIS observations cast new light on the physics of the plasma-magnetic field interaction, with implications for both the surface and the exosphere.

Figure 2: Magnetic field vectors (top) and reflected proton velocities (bottom) observed by ARTEMIS near periapsis.

ARTEMIS Observations of Moon-Related Perturbations to the Ambient Environment: As the ambient plasma affects the Moon, it in turn affects the plasma environment. Recent observations from ARTEMIS demonstrate the numerous ways in which this can occur. Not surprisingly, the Moon blocks the plasma flow, resulting in a downstream wake which can extend to tens or even hundreds of thousands of kilometers. However, the presence of the Moon also generates perturbations that can extend thousands and sometimes even tens of thousands of kilometers upstream from the dayside surface. Reflected protons from the surface and crustal magnetic field regions can travel well upstream from the Moon for some magnetic field geometries, generating large-scale perturbations to the interplanetary environment. Electrons, meanwhile, can travel upstream even more easily, and generate more subtle perturbations. Finally, in some situations, even the pickup ions from the lunar atmosphere represent a significant enough impulse to drive observable perturbations in the ambient plasma.

Conclusions: The present day represents a golden age for the study of Moon-plasma interactions. With measurements from a flotilla of international probes, and the recent collaborative efforts between LADEE, LRO, and the ARTEMIS probes, we are learning more than ever before about the coupled lunar plasma-surface-exosphere system.

EVIDENCE FOR EXPOSED WATER FROST IN THE MOON'S SOUTH POLAR REGIONS FROM LRO ULTRAVIOLET ALBEDO AND TEMPERATURE MEASUREMENTS. P. O. Hayne[1] and A. Hendrix[2], E. Sefton-Nash[3], P. G. Lucey[4], K. D. Retherford[5], J-P. Williams[3], M. A. Siegler[1], B. T. Greenhagen[1], D. A. Paige[3], [1]Jet Propulsion Laboratory, California Institute of Technology (Paul.O.Hayne@jpl.nasa.gov), [2]Planetary Science Institute, [3]University of California, Los Angeles, CA, [4]University of Hawii, [5]Southwest Research Institute

Introduction: We investigated the relationship between lunar surface and subsurface temperatures and UV albedo spectra, using data from LRO's Diviner [*1*] and Lyman-Alpha Mapping Project (LAMP) [*2*]. Temperature data from Diviner, along with thermal models, constrain the locations where water ice would be thermodynamically stable, and the LAMP albedo data constrain the presence and abundance of water frost at the optical surface [*3*]. Diviner data present an opportunity to test the hypothesis that temperature controls the distribution of water frost in the Moon's polar regions. If water frost is present at the surface, this could represent a valuable resource for future *in situ* extraction and scientific analysis or resource utilization. Therefore, improved knowledge of the distribution of surface frost on the Moon would enable future missions to study and utilize lunar volatiles.

Data: Both the Diviner and LAMP datasets used here have high quality measurements for the lunar south polar region. LAMP uses stellar illumination sources to measure the UV reflectance of the lunar night side and polar regions. Due to the prevalence of UV-bright stars in the Moon's southern hemisphere, LAMP acquires data with much better signal-to-noise ratio (SNR) near the south pole.

Diviner. Diviner is a nine-channel filter radiometer, with spectral channels spanning wavelengths from ~0.3 to >100 μm [*4*]. We calculate and map bolometric brightness temperature, the wavelength-integrated radiance in all seven thermal Diviner channels expressed as the temperature of an equivalent blackbody [*1*]. To produce gridded map products from many observations, each observation is modeled as a Monte Carlo distribution of 100 points, each representing $1/100^{th}$ of the original observation [*5*]. Bolometric brightness temperature are gridded to produce annual maximum and average bolometric brightness temperature maps (Fig. 1).

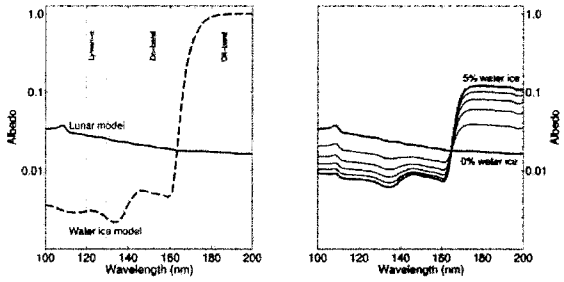

Figure 2: The effect of water ice concentration on measured LAMP spectra, based on the model described in the text. Ice and regolith are modeled as an intimate mixture.

LAMP. LAMP measures ultraviolet radiation reflected from the lunar surface, where the illumination source is a combination of starlight and emission from interplanetary hydrogen. We used publicly available gridded polar LAMP data products from NASA's Planetary Data System (PDS), dated 6 March, 2011. These gridded data records (GDR) consist of average albedo and statistical uncertainties in 250 meter-per-pixel bins, within four spectral bands: Lyman-α (119.57–125.57 nm), full stellar (129.57–189.57 nm), "on-band" (129.57–155.57 nm), and "off band" (155.57–189.57 nm). The off-band and on-band wavelengths refer to the position of a strong water absorp-

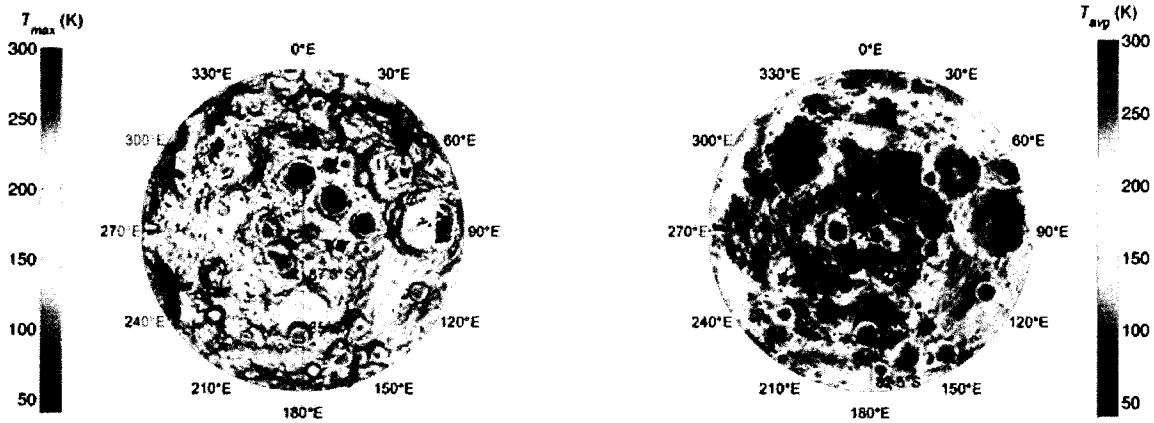

Fig. 1: Annual maximum (left) and average (right) surface temperatures from Diviner south polar measurements

tion feature, such that water frost has near-zero albedo in the on-band region, and albedo near-unity in the off-band region [*6*]. Therefore, the off-band/on-band ratio is expected to be high where any water frost is present on the surface [*3*]. To derive H_2O abundances from the measurements, we employed the albedo model of [*7*], with optical constants for water ice from [*8*] and dry regolith from [*6*]. Fig. 2 shows the effect of increasing water ice content on the expected UV reflectance spectrum.

Results: For locations with annual maximum temperatures T_{max} greater than the H_2O sublimation temperature of ~110 K, we find no evidence for exposed water frost, based on the LAMP UV spectra. For T_{max} < ~110 K, we find a strong correlation between decreasing T_{max} and apparent surface H_2O abundance (Fig. 3). Evidence for water frost comes from the following spectral features: a) decreasing Lyman-a albedo, b) decreasing "on-band" (129.57 – 155.57 nm) albedo, c) increasing "off-band" (155.57 – 189.57 nm) albedo, and d) increasing off-band/on-band ratio. All of these features are consistent with the UV spectrum of water ice, and are expected for water ice layers > ~100 nm in thickness. High regolith porosity, which would darken the surface at all wavelengths, cannot explain the observed spectral variations with temperature.

Given the observed LAMP off-band/on-band albedo ratios at a spatial scale of 250 m, the range of water ice concentrations within the cold traps with T_{max} < 110 K is ~0.1–2.0% by mass, if the ice is intimately mixed with dry regolith. If pure water ice is exposed instead, then up to ~10% of the surface area on the 250-m scale of the measurements may be ice-covered. The observed distribution of exposed water ice is highly heterogeneous, with some cold traps < 110 K having little to no apparent water frost, and others with a significant amount of water frost (Fig. 4). As noted by [*3*], this heterogeneity may be a consequence of the fact that the supply rate of H_2O molecules to the lunar poles is very similar to the destruction rate within the cold traps. However, an observed increase in apparent H_2O abundance with decreasing temperature from ~110 K to 65 K suggests that sublimation is the dominant loss process, and the rate of desorption of OH by UV photolysis may have been overestimated. We find a bimodal distribution of apparent ice concentrations with temperature, possibly due to the increasing importance of impact gardening for T_{max} < ~90 K. Finally, we cannot rule out the possibility that the colder population of ice deposits is in fact primarily carbon dioxide ice, although peak temperatures of ~65 K are slightly higher than the usual CO_2 sublimation temperature of ~60 K.

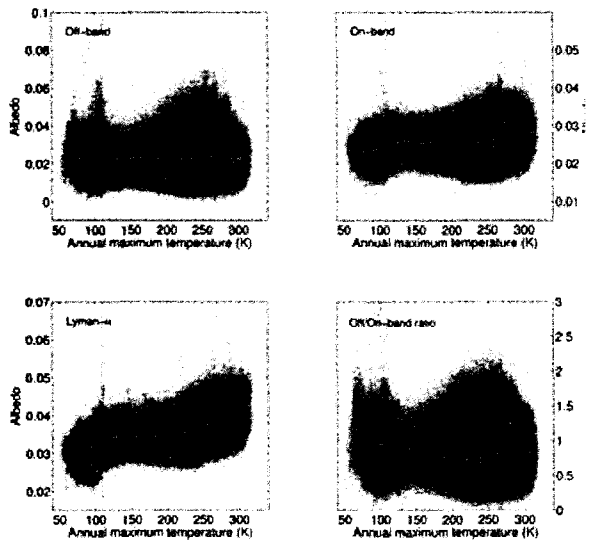

Figure 3: Ultraviolet spectral variations with temperature, for the three LAMP wavelength bands affected by the presence of

References: [1] Paige et al., *Space Sci. Rev., 150*, 2010. [2] Gladstone et al., *Space Sci. Rev., 150*, 2010. [3] Gladstone et al., *JGR, 117*, 2012. [4] Paige et al., *Science, 330*, 2010. [5] Sefton-Nash et al., *LPSC, 45*, 2014. [6] Hendrix et al., *JGR, 117*, 2012. [7] Warren and Wiscombe, *J. Atmos. Sci., 37*, 1980. [8] Warren and Brandt, *JGR, 113*, 2008.

Acknowledgment: *Part of this work was performed at the Jet Propulsion Laboratory, California Institute of Technology, under contract with the National Aeronautics and Space Administration*

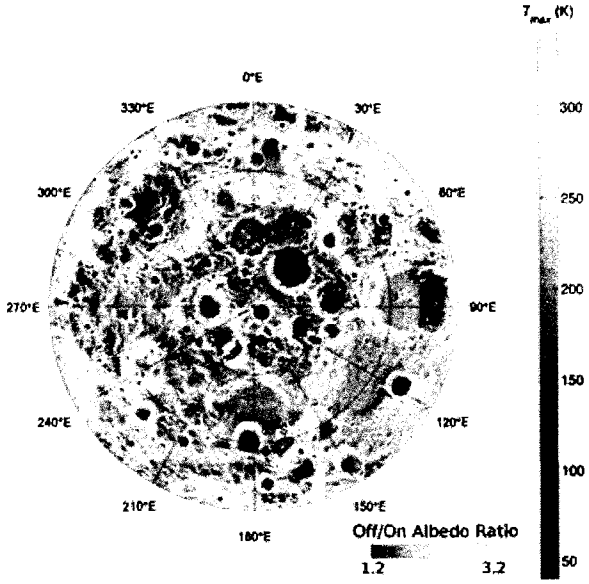

Figure 4: Distribution of exposed water frost, based on LAMP UV spectra having: a) Lyman-a albedo < 0.03, and b) off/on albedo ratio > 1.2. Note the strong correlation with the lowest temperature cold traps (grayscale indicates annual maximum temperature).

ASTROBOTIC TECHNOLOGY: PLANETARY PITS AND CAVES FOR SCIENCE AND EXPLORATION. S. A. Huber[1a], D.B. Hendrickson[2a], H.L. Jones[3b], J. P. Thornton[4a], W.L. Whittaker[5a,b], U.Y. Wong[6b], [1a]Steven.Huber@astrobotic.com, [2a]Dan.Hendrickson@astrobotic.com, [3b]hjones2@gmail.com, [4a]John.Thornton@astrobotic.com, [5a,b]red@cmu.edu, [6b]uland.wong@gmail.com. [a]Astrobotic Technology, Inc. 2515 Liberty Ave, Pittsburgh, PA 15222. [b]Robotics Institute, Carnegie Mellon University (5000 Forbes Ave, Pittsburgh, PA 15213).

Introduction: This paper describes lunar pits and caves as a potential destination for future science and exploration missions and crewed lunar outposts.

Pit and Cave Science: Pits and caves on bodies throughout the solar system are opportunistic targets to study planetary origins, geology, climate, and potentially even biology. Pit crater chains have been identified on Venus [1]; Earth [2] the Moon [3][4]; Mars [5] [6]; Eros [7]; and Europa [8].

Caves, pits, and lava tubes present unique opportunities to investigate planetary volatiles, mineralogy, origins, morphology, geologic history, and exposed surfaces without regolith cover. Because high-latitude environments are cryogenic and tube walls are regolith-free, volatiles accrete on clean cave walls and floors. As tubes cool for weeks, secondary minerals appear on the surfaces, entrapping pristine evidence of formation processes. Pit descent enables access to tens of meters of geologic column otherwise impossible to view. Thermal imaging reveals temperature transience of regolith and bedrock as solar illumination transits on pit walls. Despite the discovery of planetary pits and caves, they were not identified or adopted as a subject of study in the most recent decadal survey.

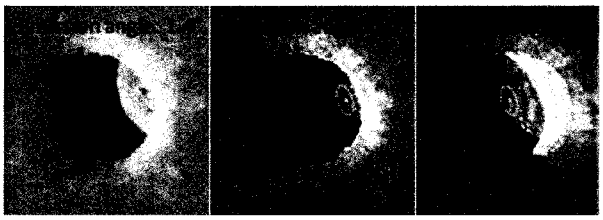

Three views of the Mare Tranquillitatis skylight on the Moon. Void space under an overhanging ceiling can be observed [3]

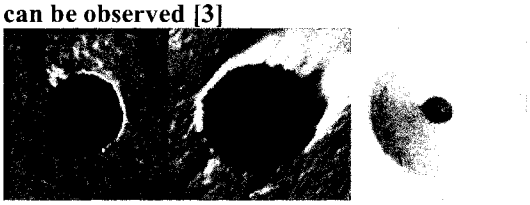

Possible skylights on Mars [5]

Pit and Cave Exploration: In addition to their rich scientific potential, planetary pits and caves could benefit future human exploration missions. Planetary caves could provide a safe haven from a number of hazardous conditions that are inherent to planetary environments. For instance, human habitats in lunar caves would protect crews from the extreme temperature variations, radiation bombardments, and micrometeorite hazards inherent in living and working on the lunar surface. By utilizing in situ cave conditions to protect human habitats, the cost of human exploration of destinations like the Moon and Mars could be significantly lowered through mass savings and reduced mission complexity. Although the utilization of caves for human exploration could yield great benefits, the potential for risk to human explorers demands robotic precursors as the first step to cave exploration and scientific study.

Robotic explorers can approach, enter, and model these features at thousand-fold increased resolution relative to orbital means, and perform physical sampling and analysis to achieve unique science not otherwise possible. Skylights, formed by partial cave ceiling collapse, provide access to subsurface voids. While robotic exploration of skylights and caves can seek out life, investigate geology and origins, and open the subsurface of other worlds to humankind, it is a daunting venture. Planetary voids present perilous terrain that requires innovative technologies for access, exploration, and modeling. The robots that venture into caves must leap, fly, or rappel into voids, traverse rubble and high grade slopes, navigate safely in the dark, self-power, and explore auton-

Robotic flyover, apron viewing, floor-traverse and caving enable a new class of missions for scientific exploration of subsurface features

omously with little or no communication to Earth. Exploiting these features necessitates a leap in technology from current planetary missions, which land with large error ellipses in statistically safe terrain, rove slowly and cautiously across the surface, depend on the Sun for power and light, and rely heavily on human commands.

Missions: Planetary pit and cave exploration demands bold new technology for flyover, apron viewing, pit descent, rock crawling, and robotic caving [9]. Modeling, visualizing, and compressing the multiphysical data associated with scientific investigation of this kind will require new techniques and data representation that must be prototyped and integrated with science, and evaluated in analog experimentation. Some pits are amenable to drive-in via trafficable ramps. A mission to pits and caves would conceive, plan, and evaluate mission concepts in a collaborative, interdisciplinary manner that draws from the needs of science interrogation.

Analog Field Experiments: Pit and cave analogs on Earth would serve as an invaluable first step to future planetary pit and cave exploration. Science investigations at analog sites can illuminate possible morphologies and formation mechanisms for pits on the Moon, Martian moons, and asteroids. Additionally, analog experiments serve as a test case for integrating scientific concept of operations, including sensor types and measurement locations. Analogs also enable field-testing that evaluates technologies for exploring these pits and caves. The first step to such a mission would identify sites on Earth where relevant analogs exist, classify these sites with regard to their applicability as analogs, and conduct field experiments at these sites.

Prior field experiments by Astrobotic have investigated options for robotic access and modeling of pits and caves at strip mines, lava tube caves, and skylights.

Analog field-testing provides invaluable test opportunities for developing technologies for exploration and modeling and scientific approaches

References: [1] Bleamaster, L., & Hansen, V. (2004). *Journal of Geophysical Research*. [2] Ferrill, D. A., Wyrick, D. Y., & Smart, K. J. (2008) *American Geophysical Union* [3] Robinson, M., Ashley, J., Boyd, A., Wagner, R., Speyerer, E., Hawke, B. R., et al. (2012). *Planetary and Space Science* [4] Head, J., & Wilson, L. (1993). *Planet. Space Sci.* [5] Cushing, G. E. (2012) *Journal of Cave and Karst Studies* [6] Wyrick, D., Ferrill, D., Morris, A., Colton, S., & Simms, D. (2004). *Journal of Geophysical Research: Planets* [7] Buczkowski, D. L., Barnouin-Jha, O. S., & Prockter, L. M. (2008). *Icarus* [8] Greenberg, R., Leake, M. A., Hoppa, G. V., & Tufts, B. (2003) *Icarus* [9] H. L. Jones, K. M. Peterson, W. L. Whittaker, and U. Y. Wong. (2013). *44th Lunar and Planetary Science Conference*.

ASTROBOTIC TECHNOLOGY: COMMERCIAL LUNAR PAYLOAD DELIVERY SERVICE. S. A. Huber[1], J. P. Thornton[2], D. B. Hendrickson[3], [1]Steven.Huber@astrobotic.com, [2]John.Thornton@astrobotic.com, [3]Dan.Hendrickson@astrobotic.com. Astrobotic Technology, Inc. 2515 Liberty Ave, Pittsburgh, PA 15222. contact@astrobotic.com.

Introduction: This paper describes Astrobotic Technology's financial and technical model for delivery of commercial lunar landing capabilities through government partnership. Topics addressed include the public-private partnership, Astrobotic's model for payload services, and *Griffin*, the lunar lander that is core to the model.

Public-Private Partnership: Astrobotic Technology is partnering with NASA to develop a commercial robotic lunar landing capability through the Lunar Cargo Transportation and Landing by Soft Touchdown (Lunar CATALYST) initiative. By partnering with Astrobotic, NASA is leveraging its half-century of exploration experience to foster a commercial ecosystem for routine lunar payload delivery. Like the successful Commercial Orbital Transportation Services program that ushered in routine, private resupply missions to the International Space Station, Lunar CATALYST brings together legacy achievements, industry resourcefulness, and disruptive innovation in a public-private partnership that is creating a remarkable new era of enterprise on the Moon.

Payload Services Model: Astrobotic Technology is a space robotics company that makes high-capability space missions possible for a broad spectrum of business, scientific, and social applications. The company is developing a robotic lunar lander to deliver and operate cargo on the surface of the Moon.

Astrobotic offers "Space Missions as a Service" by integrating multiple customer payloads into a single spacecraft with shared commodities such as power and communication. While this model exists for routine space missions (i.e., missions to low Earth orbit), Astrobotic is the first to offer it for high-capability lunar missions. Astrobotic carries customer payloads to a choice of three mission destinations. The fee is driven primarily by mass: trans-lunar injection (TLI) ($99K/kg); lunar orbit ($198K/kg); and lunar surface ($1.2M/kg for lander mount, or $2M/kg for rover mount). Customers can also purchase entire missions. Griffin's cargo mounts can accommodate a wide variety of payloads for lunar missions, including volatile prospecting, sample return, geophysical network deployment, skylight exploration, regional prospecting, lunar satellite deployment, mining, technology demonstrations, and advertising and media. Capability will be demonstrated in a first mission to deliver commercial cargo that wins the $30M Google Lunar XPRIZE, and demonstrates performance that satisfies commercial and government customer objectives for safe precision landing as well as payload delivery and support. Signed and prospective customers for this mission include NASA, international space programs, commercial ventures, and other Google Lunar XPRIZE teams.

Griffin: Griffin flies on a US commercial launch vehicle (initially the SpaceX Falcon 9) to TLI. Astrobotic's Griffin lunar lander then separates from the rocket, corrects course en-route to the Moon, enters into lunar orbit, and safely touches down on the surface.

Figure 1: Griffin's first mission will fly over and land near a lunar pit

Griffin's first lunar mission will fly over and land near a lunar pit that is suspected to be an entrance to a lava tube cave. Prevalent on the Moon and Mars, pits and caves are opportunistic destinations to study origins and geology, and are potential sites for future lunar outposts. [1][2]

The mission will carry an exploration rover developed by partner Carnegie Mellon University to explore the surface and win the $30M Google Lunar XPRIZE. Carnegie Mellon brings its world-leading robotics expertise to the partnership.

Structure: Griffin's aluminum frame is stout, stiff, and simple for ease of payload integration. The main isogrid deck accommodates flexible payload mounting on a regular bolt pattern. Thermal control is available through cruise and on the surface. Four legs absorb shock and stabilize Griffin on touchdown. Rover missions can use deck-mounted ramps for rover egress. Protoflight lander structure has been qualified for launch loads through vibration testing.

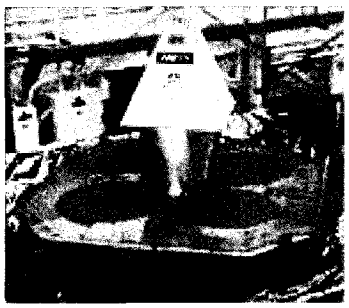

Figure 2: Griffin's primary structure vibration testing

Guidance, Navigation, and Control: During orbit and landing, cameras register Griffin to lunar terrain for precise landing,

while LIDAR constructs 3-D surface models of intended landing zone to detect slopes, rocks, and other hazards. This technology enables Griffin to safely land within 100m of any targeted landing site, even in complex and hazardous terrain.

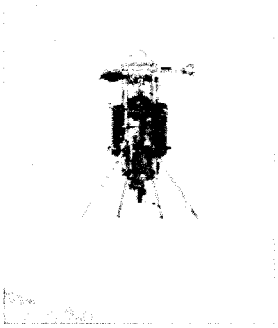

Figure 3: Griffin's precision landing and hazard avoidance system in a test flight on Masten's Xombie

Avionics: Griffin's computing platform is a combination of a radiation hardened general-purpose processor for baseline operations and a mil-spec high-speed processor. Computationally expensive operations like feature detection and hazard analysis that are required for a short period of time during landing occur on the high-speed processor. This system enables high performance and the efficiency necessary for the real-time data processing during landing.

Night Survival: Astrobotic's testing campaign has identified unique battery chemistry, power systems, avionics, and electronic components that will enable Griffin to hibernate during the lunar night, then revive the following lunar day. Nominally, primary mission operations are completed in the first lunar day and additional days support secondary and tertiary goals, until night survival is verified on the first mission.

Rover Deployment: A Griffin design option provides deployable ramps for rover egress. Once on the surface, deployable ramps enable egress of large rovers mounted to the top of the frustum ring. Ramps stow for launch and are spring-deployed upon release, accommodating both third-party rovers and Astrobotic surface rovers for payload delivery. Astrobotic rovers can support missions for any latitude – equatorial to polar. Griffin can support medium-class rovers up to 500kg.

Payload Accommodations: Griffin supports payload operation with thermal control, power, and data transmission. Deck mounting locations are thermally regulated during all mission phases. Thermal regulation is by radiation dissipation from the topside of the deck and heaters. An average of 150W of power is available to payloads during cruise and on the surface. The lander downlink can support an average of 200kbps of payload data when on the surface. A Griffin design option provides wireless surface radio to act as a communication relay for mobile rovers.

References: [1] M. Robinson, J. Ashley, A. Boyd, R. Wagner, E. Speyerer, B. R. Hawke, H. Hiesinger and C. v. d. Bogert, "Confirmation of sublunarean voids and thin layering in mare deposits," *Planetary and Space Science,* vol. 69, no. 1, 2012.

[2] G. E. Cushing, "Candidate cave entrances on Mars," *Journal of Cave and Karst Studies,* pp. 33-47, 2012.

WATER INTERACTIONS WITH LUNAR REGOLITH FROM LADEE OBSERVATIONS. D. M. Hurley[1], M. Benna[2], P. Mahaffy[2], R. Elphic[3], D. Goldstein[4], [1]Johns Hopkins University Applied Physics Laboratory (11100 Johns Hopkins Rd., Laurel MD 20723 USA; dana.hurley@jhuapl.edu), [2]NASA Goddard Space Flight Center (Greenbelt MD 20771 USA), [3]NASA Ames Research Center (Moffett Field CA 94035 USA), [3]University of Texas-Austin.

Introduction: When a spacecraft burns hydrazine, it releases vapor into the environment. The primary vapor constituents are N_2, H_2O, CO, and CO_2. Although exhaust velocities are greater than the escape speed on the Moon, with an initial component of velocity downward, some fraction of the exhaust will intersect the surface of the Moon. The details of the interaction are poorly known. Do the molecules adsorb to the surface? Do they thermalize to the local surface temperature, or do they bounce elastically? Therefore, we use data taken after engine burns to determine these surface interactions.

Events: We examine LADEE data during two engine burn events: the landing of Chang'e 3 on the surface of the Moon and LADEE's Orbital Maintenance Manuever (OMM) 21. LADEE, equipped with a neutral mass spectrometer, was able to detect water above background levels after the Chang'e 3 landing, indicating that the water does not completely adsorb to the surface. However, data from OMM-21, which occurred over the nightside of the Moon does not rule out adsorption of water to colder surfaces.

Model: We present model runs using our Monte Carlo model of the migration of water through the lunar exosphere. We bin the model results in terms of what is in the field of view of the LADEE NMS.

Conclusion: We are able to constrain the range of possible values for the adsorption fraction on pristine lunar regolith and on the thermalization factor for water with lunar regolith.

THE SPACE LAUNCH SYSTEM AND THE PROVING GROUND: PATHWAYS TO MARS. K. Klaus[1], [1]The Boeing Company, 13100 Space Center Blvd, MC HB4-20, Houston TX 77059, kurt.k.klaus@boeing.com.

Introduction: The Space Launch System (SLS) Program is making progress toward delivering a new capability for Beyond Earth Orbit (BEO) exploration. Developed with the goals of safety, affordability and sustainability in mind, SLS will start with 10% more thrust than the Saturn V that launched astronauts to the Moon 40 years ago. From there it will evolve into the most powerful launch vehicle ever flown, via an upgrade approach that will provide building blocks for future space exploration. The SLS provides a critical heavy-lift launch capability enabling diverse deep space missions. Enhanced capabilities enable missions including human exploration, planetary science, astrophysics, heliophysics, planetary defense and commercial space exploration. We will focus on mission concepts relevant to NASA's Cislunar Proving Ground and the Global Exploration Roadmap (GER).

Pathways to Mars: Cislunar space provides an excellent 'proving ground' for readying systems, operations concepts and risk mitigation strategies for missions further into space, including missions to Mars. [1] The GER demonstrates how cislunar missions are a meaningful step to Mars and a stepping stone to the lunar surface. NASA's Evolvable Mars Campaign (EMC) adds missions to cislunar space that were missing from the earlier capability driven architecture, chiefly the Exploration Augmentation Module (EAM), robotic lunar surface missions and missions to the lunar surface with international participation. We have been exploring how these missisons could fit into the current planning through EM-2 through EM-6.

EM-2 – Orion and the Asteroid Retrieval Vehicle (EAV): Bill Gerstenmaier at the NASA Lunar Science Institute (NLSI) meeting in July 2013 referred to the ARM in part as a mission to the lunar vicinity. The ARM mission requirements result in system design based on a modified version of our 702 spacecraft product line. Including a NASA Docking System (NDS) on the Asteroid Redirect Vehicle allows for easier crewed exploration mission integration and execution. The SEP ARV could be used as a cislunar tug in the event that the ARM is cancelled or deferred.

EM-3 - Orion and the EAM: Crew operations at a redirected asteroid could be significantly enhanced by providing additional systems and EVA capabilities beyond those available from Orion only missions. An Exploration Augmentation Module (EAM) located with the asteroid would improve the science and technical return of the asteroid mission while also increasing Orion capability through resource provision and providing an abort location and safe haven for vehicle contingencies.

Cislunar Exploration Platform: The EAM could be repurposed as a cislunar exploration platform that advances scientific research, enables lunar surface exploration and provides a deep space vehicle assembly and servicing site. The Exploration Platform provides a flexible basis for future exploration, since it reduces cost through reuse of expensive vehicles and reduces the number of launches needed to accomplish missions. International Space Station (ISS) industry partners have been working for the past several years on concepts for using ISS development methods and residual assets to support a broad range of exploration missions. These concepts have matured along with planning details for NASA's SLS and Multi-Purpose Crew Vehicle (MPCV) to allow serious consideration for a platform located in the Earth-Moon Libration (EML) system or a Distant Retrograde Orbit (DRO). [2]

EM-4 – Orion with a Robotic Lander – We envision EM-4 as a human tended sample return mission to the lunar farside. We chose Schrödinger Crater as the target for our study but we fully realize that the target for this mission would be chosen by the science community. While this mission could be Moonrise with samples returned by the crew and Orion, the SLS has enough mass margin that this could be re-imagined as a mission with a more capable rover telerobotically operated by the crew in the EAM. After the initial mission, the long lived rover could continue to rove and be operated from the earth while the crew is absent using the EAM as a communication relay from the lunar farside. It could be possible for a rover of this nature to contine on to Shackleton and/or Amundsen after finishing Schrödinger traverses.

EM-5 – Orion with Commercial Resupply to EAM – With assets in place, it is now possible to provide resupply to the EAM. This could be commercial resupply launched on the SLS along with the Orion and crew. The concept we studied used a cargo module based on The Orbital Sciences Cygnus. The resupply could be used to extend the mission to 80 days, prepare for EM-6, and/or extend operations at the asteroid if warranted.

EM-6 – Humans to the Lunar Surface: In the current environment, it's likely that the lander will initially be provided by one of our international partners. The mission objectives are to provide lunar surface access for crew and cargo and to provide as much system reuse as possible. Subsequent missions to the

surface can reuse the same lander and Lunar Transfer Vehicle. [3] We envision refueling initially with propellant brought from earth and stored near the EAM. Eventually the propellant will be produced from ISRU plants on the lunar surface.

Beyond the proving ground – missions to Mars Vicinity: The International space community has declared that our unified long term goal is for a human mission to Mars but major work remains to define how it will be done. Translunar infrastructure and heavy lift capability are key to this approach. Recent analysis has suggested that a habitat-based gateway in translunar space would be helpful as an assembly node for Mars and for many other missions. The moons of Mars would provide an excellent stepping stone to the surface. As a "shake-down" cruise before landing, a mission to Deimos or Phobos would test all of the systems except those needed to get to the surface and back. This test would provide confidence for the in-space transportations and crew habitat systems.

Conclusions - The ISS has established a firm basis for a vibrant exploration program with a proven management model and proven existing designs. A Deep Space capability based on ISS technology provides flexibility and is an enabling capability for key cost-reducing strategies:

- Mobility within the libration system
- Reuse of expensive spaceflight hardware
- Base for assembly of complex, deep space mission systems

International collaboration has been proven effective on ISS and could be improved and expanded for exploration. It appears that the US may embrace the International Space Exploration Coordination Group (ISECG) Global Exploration Roadmap (GER). We need to apply the lessons learned from the International Space Station program and the experiences of the current partnership

- Strong coordinated support from the associated transportation programs (Shuttle, Soyuz, Arianne, H2B)
- International partnership with strong political support
- Adequate funding to accomplish the objective
- Agreements on hardware/software interface and construction standards

References: [1] Laurini K. (2014) Science Enabled by Crew and Infrastructure in the Lunar Vicinity, GER Workshop [2] Klaus K., Post, K.E. and Lawrence S. (2013) AIAA 2013-0436. [3] Raftery M and Derechin A. (2012) IAC-12- B3.1.

Inversion Algorithms to Determine Likely 3D Solids from a Population of Particles. J. Knicely[1] and D. Rickman[2], [1]Texas A&M University (knicely_joshua@yahoo.com), [2]Marshall Space Flight Center (doug.rickman@nasa.gov).

Introduction: Shape is a fundamental property of particles, with engineering and scientific significance. While there is a need to know the 3D geometry of the particles composing the lunar regolith, the only available shape measurements are taken in two dimensions. It has been accepted wisdom in stereology, that with very few exceptions, unique relationships between measurements in 2D and solids do not exist. However, Rickman et al. (unpublished) found a probabilistic relationship between 3D solids and the 2D measures aspect ratio (AR) and Heywood factor (HF). A forward, probabilistic model can be created wherein the likelihood of all possible AR and HF measures for a given solid can be obtained. The probability distributions for a given solid are apparently unique. An inverse model, therefore, attempts to determine the solids given an observed probability distribution of AR and HF. Two inversion algorithms were developed to determine sets and proportions of 3D solids which approximate the 2D measurements of a population of particles. These sets of solids can be used to quantitatively predict the physical characteristics of the lunar regolith and lunar simulant.

Method: The lunar regolith and lunar simulant are poorly characterized. The lunar regolith experiences weathering unlike anything on Earth. This requires a large variety of 3D solids to be considered in the inversion. Forward models of the AR and HF values for sets of 3D solids are calculated and saved into text files. The inversion algorithms read from these precalculated forward models to avoid lengthy forward model calculations. The inversion algorithms use only those forward models whose most populated areas in AR/HF space are shared by the input set of data. Nonlinear, global inversion methods are used. These type of inversions are time-consuming, but necessary due to the poor constraints of the problem. The methods used are Monte Carlo, simulated annealing, genetic algorithm, particle swarm optimization, and differential evolution. In addition, a finite number of 3D solids are needed to approximate the lunar regolith and lunar simulant. The inversion algorithms include a function to modify the model complexity by allowing only a finite number of forward models to be considered during each iteration.

Results: Two inversion algorithms, TRADEOFF_MCSA and TRADEOFF_GOD, were developed in MATLAB. TRADEOFF_MCSA uses Monte Carlo and simulated annealing methods. This algorithm has the ability to re-anneal to escape locally optimal models found late in the annealing process. TRADEOFF_GOD uses simulated annealing, genetic algorithm, particle swarm optimization, and differential evolution. This algorithm coordinates the different optimization methods. If any method reaches a stopping criterion, its best found set of forward models is introduced to another method. The introduced set of forward models will be used by the new method if it results in a better fit to the data, or it will be eliminated if it results in a poorer fit to the data. Preliminary testing versus fabricated data sets show TRADEOFF_GOD to be more efficient. It finds similar sets of forward models that produce equivalent or better fits to the test case in significantly less time than TRADEOFF_MCSA. This is attributed to its coordination between the different optimization methods.

These inversion algorithms can be used with the forward models (once fully developed) to approximate the lunar regolith and lunar simulant (or any population of particles) with sets of 3D solids. These sets of 3D solids allow for a quantitative prediction of the bulk physical properties of the population of particles.

References: [1] Rickman, D., Lohn-Wiley, B., Knicely, J. "Probabilistic Particle Shape Measuremen," Unpublished. [2] Everett, M. (2013) *Near-Surface Applied Geophysics*. Cambridge University Press, New York.

PRODUCTION OF VOLATILES AT LUNAR PYROCLASTIC VOLCANIC VENTS. David A. Kring[1,2], [1]Center for Lunar Science and Exploration, USRA-Lunar and Planetary Institute, 3600 Bay Area Blvd., Houston TX 77058 (kring@lpi.usra.edu), [2]NASA Solar System Exploration Research Virtual Institute.

Introduction: More than 100 pyroclastic deposits have been identified on the lunar surface [1]. These volatile-rich eruptions were principally driven by C-O gas phases (*e.g.*, [2]), although new analyses of Apollo 15 and 17 glasses [3-4] suggest H-O species are also involved. Once liberated at the lunar surface, these volatiles would have augmented solar wind volatiles implanted in the regolith ([5] and references therein). To assess that volcanic contribution, the compositions of pyroclastic glasses collected at the Apollo 15 and 17 landing sites are used to calculate the production of volatiles degassed in lunar pyroclastic eruptions of different sizes on the Moon.

Degassed Volatile Abundances: The abundances of CO_2, H_2O, F, S, and Cl were determined in very-low-Ti and low-Ti glasses from Apollo 15 (15427,41) and high-Ti glasses from Apollo 17 (74220,864) [3]. Diffusive degassing models were then used to infer original magmatic volatile abundances. In a complementary study, the abundances of H_2O, F, S, and Cl were measured in melt inclusions trapped in olivine within pyroclastic glass spherules from the same Apollo 17 sample [4]. The goal was to measure directly the volatile abundances that existed in the magma prior to any degassing. In addition, models of the fire-fountain eruptive process that produced the Apollo 17 glass provide an independent estimate of the CO and CO_2 that was liberated [2]. In the calculations that follow, the CO and CO_2 abundances of [2] are used. The H_2O, F, S, and Cl abundances determined by [4] are generally lower than those of [3] and are used here to be conservative in estimates of degassed volatile mass.

The degassing of the volatile components is not equal – a larger fraction of the CO and CO_2 (100%) and H_2O (98%) species were lost compared to that of F (45%), S (19%), and Cl (57%) [2-4]. The corresponding minimum to maximum abundances liberated per erupted mass are 105 to 1050 ppm for CO, 18 to 183 ppm for CO_2, 77 to 401 ppm for H_2O, 3 to12 ppm for F, 36 to 67 ppm for S, and 0 to 0.6 ppm for Cl. The bulk density of a primary pyroclastic unit is taken to be 2.04 g/cm^3, which is the measured value in a portion of sample 74002 [6]. This sample is the upper part of a drive tube through orange soil that is adjacent to the soil clod sample 74220 used in the analyses of [2-4]. Sample 74220 is 92.3 to 95.9% glass [7], while the top of 74002 is 91.2% glass and the 90 to 150 μm fraction is 99.9% glass [8].

Multiplying the bulk density times the volume of a pyroclastic deposit produces the mass of spherules. Using the volatile abundances and degassing fractions described above, one then derives the mass of volatiles degassed as shown in Figure 1. These volumes are substantial, but also represent lower limits of the contribution of volcanically-produced gases to the lunar exosphere and regolith. Other types of lunar basalt eruptions released volatiles, as indicated by the 3.4 Ga vesicular mare basalt 15016 and other samples (15529 and 15556) from the Apollo 15 site, and need to be evaluated with a similar set of calculations.

Conclusions: Water and $CO+CO_2$ masses produced at the lunar surface are on the order of 10^{12} to 10^{15} g for pyroclastic volumes of 10 to 500 km^3. These substantial masses are presented with the caveat that they are based on data inferred mostly from Apollo 15 and 17 materials. Samples of additional vent material, like that at the Schrödinger basin (*e.g.*, [9-10]), are needed to determine if those values are valid for other lunar pyroclastic vents.

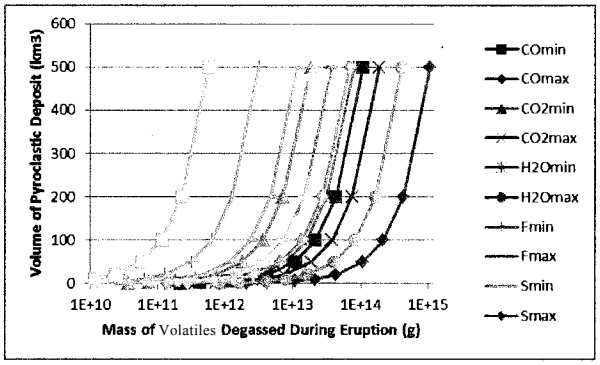

Fig. 1. Mass of volatiles degassed during eruptions producing pyroclastic deposits with volumes up to 500 km^3.

References: [1] Gaddis L. R. et al. (2003) Icarus, 161, 262-280. [2] Rutherford M. J. & Papale P. (2009) *Geology, 37*, 219-222. [3] Saal A. E. et al. (2008) *Nature, 454*, 192-195. [4] Hauri E. H. et al. (2011) *Science, 333*, 213-215. [5] Haskin L. A. & Warren P. (1991) *Lunar Sourcebook*, 357-474. [6] Mitchell J.K. et al. (1973) *Apollo 17 Preliminary Science Report*, Chapter 8. [7] Heiken G. & McKay D. S. (1974) *Proc. LSC 5th*, 843-860. [8] McKay D. S. et al. (1978) *Proc. LPSC 9th*, 1913-1932. [9] O'Sullivan K. M. et al. (2011) *GSA Sp. Pap. 477*, 117-128. [10] Bunte M. K. et al. (2011) *GSA Sp. Pap. 483*, 533-546.

PROMINENT VOLCANIC SOURCE OF VOLATILES IN THE SOUTH POLAR REGION OF THE MOON. David A. Kring[1,2], Georgiana Y. Kramer[1], D. Benjamin J. Bussey[2,3], and Dana M. Hurley[2,3], [1]Center for Lunar Science and Exploration, USRA-Lunar and Planetary Institute, 3600 Bay Area Blvd., Houston, TX 77058 (kring@lpi.usra.edu), [2]NASA Solar System Exploration Research Virtual Institute, [3]Johns Hopkins University Applied Physics Laboratory, Laurel, MD.

Introduction: Pyroclastic glasses have surfaces that are enriched in volatiles like S, Ag, Cd, Zn, and Br (*e.g.*, [1-3]) by factors of 3 to 400 compared to their interiors. That suggests modest chemical etching or abrasion may remove them for *in situ* resource utilization (ISRU) (*e.g.*, [4]). Some of the pyroclastic deposits are enriched in ilmenite (*e.g.*, [5]), which can be reduced to produce oxygen (*e.g.*, [6]), providing another ISRU opportunity. Because pyroclastic deposits are fine-grained, easily excavated, transported, and processed, they are an attractive target for sustainable exploration.

Pyroclastic Vent in Schrödinger Basin: Because of that ISRU potential, an immense ~400 m-tall pyroclastic deposit in the Schrödinger basin was among the Tier I and II targets during the Exploration Systems Mission Directorate (ESMD)-phase of the Lunar Reconnaissance Orbiter (LRO) mission. Models of those types of eruptions indicate C-O gas phases were involved (*e.g.*, [7]), although new analyses of Apollo 15 and 17 glasses [8-9] suggest that H-O species are involved too, augmenting solar wind volatiles that are implanted in the regolith ([10] and references therein).

We calculated H-O volatiles produced by the young volcanic vent, which has a Lunar Orbiter Laser Altimeter (LOLA)-derived volume of ~190 km^3. These calculations are based on pyroclastic volatile abundances inferred from green and orange glasses [8-9] and models of eruption [7]. In addition to H_2O, we calculated the abundances of CO, CO_2, F, Cl, and S. The degassed minimum to maximum masses are: $H_2O = 3.0 \times 10^{13}$ to 1.6×10^{14} g; $CO = 4.1 \times 10^{13}$ to 4.1×10^{14} g; $CO_2 = 7.0 \times 10^{12}$ to 7.1×10^{13} g; $F = 1.2 \times 10^{12}$ to 4.6×10^{12} g; $S = 1.4 \times 10^{13}$ to 2.6×10^{13} g; and Cl = 0 to 2.2×10^{11} g. These values are substantial. The mass of water, for example, is 12,000 to 62,000 times larger than that in an Olympic-size pool. There are a couple of approximations one has to make in the calculations, but those might change the values by factors of only a few. The volatile abundances are so large that any variation in those approximations is not very significant.

Cold Traps within Schrödinger Basin: Some of the volatiles may be trapped within cavities in Schrödinger (*e.g.*, lava tubes, crevices in the impact units, and the interior of the vent itself) that are emerging from extensive geologic analyses of the Schrödinger basin [11-13]. In addition, illumination analyses indicate portions of a nearby crater floor fracture and two simple craters are in permanent shadow where volatiles can be incorporated into regolith. Thus, there may be ice-rich deposits within Schrödinger that could be analyzed and utilized by future lunar surface missions.

Transport of Volatiles to the Lunar South Pole: The Schrödinger vent is one of the largest on the farside and occurs ~500 km from the lunar South Pole. There will be a strong tendency for the volatiles to migrate towards the pole (*e.g.*, [14-15]). The vent may be less than 2 billion years old [16] when the Moon was in its current orbital/spin configuration, so any volatiles released could be en route to the South Pole. Recent mapping suggests the vent may be older [17]. In either case, we suggest the transport of those volatiles be modeled and predictions made for abundances en route, so that future measurements can be used to test transport mechanisms.

Conclusions: These results indicate a mission to the Schrödinger basin, initially designed to evaluate the lunar magma ocean and lunar cataclysm hypotheses [11, 18], may simultaneously be able to address some of the exploration (ISRU) issues relevant to the Human Exploration and Operations Mission Directorate (HEOMD). Indeed, the immense pyroclastic deposit in Schrödinger, coupled with potential volatile deposits, further enhances Schrödinger as an exploration target.

References: [1] Baedeker P. A. et al. (1974) *Proc. LSC, 5th*, 1625-1643. [2] Chou C.-L. et al. (1975) *Proc. LSC 6th*, 1701-1727. [3] Wasson J. T. et al. (1976) *Proc. LSC 7th*, 1583-1595. [4] Duke M. B. et al. (2006) *Rev. Mineral. & Geochem., 60*, 597-656. [5] Hawke B. R. et al. (1990) *Proc. LPSC 20th*, 249-258. [6] Allen C. C. et al. (1996) *JGR, 101*, 26085-26096. [7] Rutherford M. J. & Papale P. (2009) *Geology, 37*, 219-222. [8] Saal A. E. et al. (2008) *Nature, 454*, 192-195. [9] Hauri E. H. et al. (2011) *Science, 333*, 213-215. [10] Haskin L. A. & Warren P. (1991) *Lunar Sourcebook*, 357-474. [11] O'Sullivan K. M. et al. (2011) *GSA Sp. Pap. 477*, 117-128. [12] Kramer G. Y. et al. (2013) *Icarus, 223*, 131-148. [13] Kumar P. S. et al. (2013) *JGR, 118*, 206-223. [14] Watson K. et al. (1961) *JGR, 66*, 3033-3045. [15] Arnold J.T. (1979) *JGR, 84*, 5659-5668. [16] Shoemaker E.M. et al. (1994) *Science, 266*, 1851-1854. [17] Mest, S.C. (2011) *GSA Sp. Pap., 477*, 95-115. [18] Burns J. O. et al. (2013) *Adv. Space Res., 52*, 306-320.

Lunar PLANE: Lunar Polar Low-Altitude Neutron Experiment for High-Spatial Resolution Hydrogen Concentration and Depth Measurements. David J. Lawrence[1], Richard S. Miller[2], Patrick N. Peplowski[1], Martin Ozimek[1], Christopher Scott[1], [1]Johns Hopkins University Applied Physics Laboratory, Laurel, MD, USA (David.J.Lawrence@jhuapl.edu); [2]University of Alabama in Huntsville, Huntsville, AL, USA.

Introduction: Permanently shaded regions (PSRs) are fascinating solar system environments. The type locations for PSRs are craters located at both poles of the Moon and Mercury. The interiors of these craters are not illuminated by sunlight and consequently their temperatures are very cold (T<100K) for geologically long periods of time. One of the most important aspects of PSRs is that they serve as cold traps for volatiles (e.g., water). Predictions dating back to the 1960s and 1970s proposed that lunar PSRs would have enhanced water concentrations [1,2]. Subsequent spacecraft and Earth-based measurements using various techniques (radar, neutron spectroscopy, spectral reflectance) have provided abundant evidence to support these predictions at both the Moon and Mercury [e.g., 3-7]. The characteristics of these regions and the processes that take place in PSRs have implications for a variety of topics such as the origin and history of solar system volatiles [8], synthesis of organic materials [9], and in-situ resources for human exploration.

Despite the fact that initial measurements of PSRs have been made, many aspects of PSRs are not known or understood. In particular, our knowledge of the spatial distribution and depth dependence of hydrogen concentrations at the lunar poles is tantalizingly incomplete. The topic of this study is to investigate the extent to which a low-cost, low-resource orbital mission can achieve significant improvements in our knowledge of the lunar polar hydrogen distribution. A better knowledge of the polar hydrogen spatial and depth distribution will have multiple benefits as it can provide key input to studies of PSR volatile processes by isolating individual craters that host enhanced hydrogen. In addition, data from such a mission will be valuable for future landed missions that seek to target landing sites with volatile enhancements [10].

Hydrogen Measurements of Planetary Surfaces: Planetary neutron spectroscopy is the standard technique for quantifying hydrogen concentrations on planetary surfaces [11]. Neutrons are created by nuclear spallation reactions when high-energy cosmic rays strike the surface of an airless or nearly airless planetary body. The energies (E_n) of the resulting neutrons are typically divided into three ranges of fast (E_n > 0.5 MeV), epithermal (0.5 eV < E_n < 0.5 MeV) and thermal (E_n < 0.5 eV) neutrons. Hydrogen has a unique ability to moderate neutrons because hydrogen atoms and neutrons have the same mass, which allows a highly efficient momentum transfer between the two. This causes the number of epithermal neutrons to be strongly depressed where hydrogen is present so that epithermal neutrons can provide a highly sensitive measure of a soil's hydrogen content. Fast neutrons are also sensitive to the hydrogen content in a planetary soil, but because their effective penetration depth differs from that of epithermal neutrons, fast neutrons also provide information about the burial depth of hydrogen enhancements [7,12].

Polar hydrogen enhancements were first measured on the Moon using the Lunar Prospector Neutron Spectrometer (LP-NS)[3]. The LP-NS was an omnidirectional detector and as a consequence its spatial resolution was sufficiently broad that individual hydrogen enhancements were generally not tied to specific PSRs. Nevertheless, combined measurements of epithermal and fast neutrons have been used to show that bulk hydrogen enhancements in Shackleton crater at the Moon's south pole reach to the surface [12], in contrast to other polar regions where the hydrogen enhancements are likely buried by tens of cm of dry soil [13].

To obtain higher spatial resolution measurements, the Lunar Reconnaissance Orbiter spacecraft carried a collimated neutron detector known as the Lunar Exploration Neutron Detector (LEND)[14], which was planned to quantify hydrogen concentrations at a spatial resolution of 10 km near both lunar poles. Despite reports that claim the LEND instrument has met its spatial resolution requirements [15-17], multiple studies have shown that the collimated neutron data have not successfully made hydrogen concentration measurements with 10 km spatial resolution [18-22]. In contrast to collimating neutrons, if a mission can be designed where the altitude over one of the poles is significantly lower than that of the LP-NS measurements, then omnidirectional neutron measurements should improve the spatial resolution roughly by the ratio of the respective altitudes.

Lunar PLANE Mission: The Lunar Polar Low-Altitude Neutron Experiment (PLANE) can be accomplished with simple neutron sensors on a small spacecraft. The most easily accomplished mission obtains high-spatial-resolution hydrogen concentrations with a single ^{3}He neutron sensor on a CubeSat-like spacecraft. To obtain spatially-resolved depth-dependent hydrogen concentrations, a fast neutron sensor needs to be included in the mission payload. High heritage fast neutron sensors are available for a few kg mass [23].

The nominal mission scenario provides for low-altitude (<25 km) passes over the lunar south pole with higher-altitude apoapsis (~200 km) values to provide orbital stability. To calculate the mission orbit, an order 50x50 lunar gravity model was used and Earth and Sun perturbations were included. Figure 1 shows histograms of the south-pole altitudes for the Lunar PLANE and LP missions. The LP mission shows a wide spread of higher altitudes, which results in a relatively broad spatial resolution. In contrast, the Lunar PLANE mission has both lower altitudes and a narrower altitude spread, which will result in improved neutron spatial resolution.

To assess the utility of the Lunar PLANE mission to obtain spatially resolved hydrogen measurements, we used the spatially-reconstructed neutron count rate map of Teodoro et al. [22] as an assumed ground truth (Figure 2). To simulate the neutron measurements for the Lunar PLANE mission scenario, we use neutron transport simulations that have been validated for prior planetary missions [7]. Figure 3 shows the simulated count rate map when the distribution of Figure 2 is used as an assumed count rate distribution. As seen, all of the largest PSRs are spatially resolved. This is in contrast to the measured LP-NS data that show a much broader spatial resolution (Figure 4).

The next step to assess the mission viability is to assign variable burial depths for different PSRs and investigate how well a Lunar PLANE mission could measure such burial depths. This analysis will be accomplished using the known response properties for a standard fast neutron detector [7].

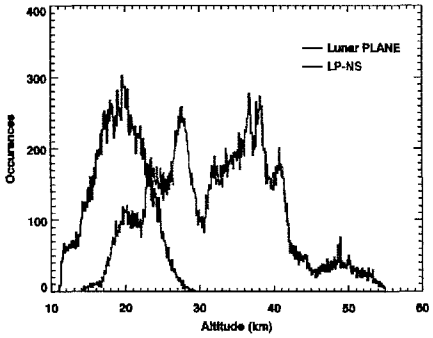

Fig. 1. Altitude histograms for the Lunar PLANE and Lunar Prospector missions for latitudes poleward of 70°S.

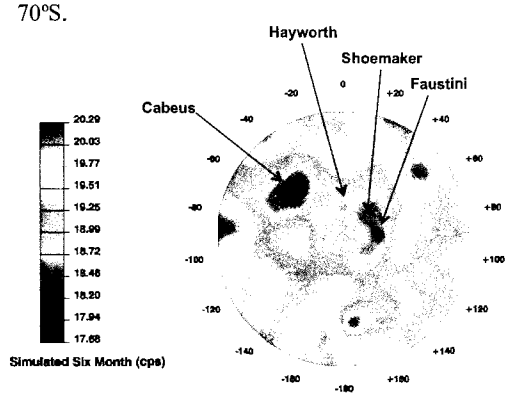

Fig. 3. Simulated epithermal neutron count rate map at the lunar South Pole for the Lunar PLANE mission.

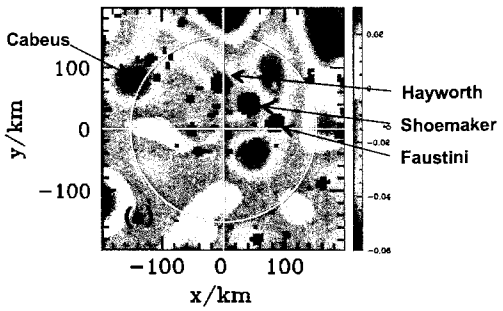

Fig. 2. Spatially-reconstructed epithermal neutron count rates for the lunar South Pole based on analysis of [22]. Prominent PSRs are labeled.

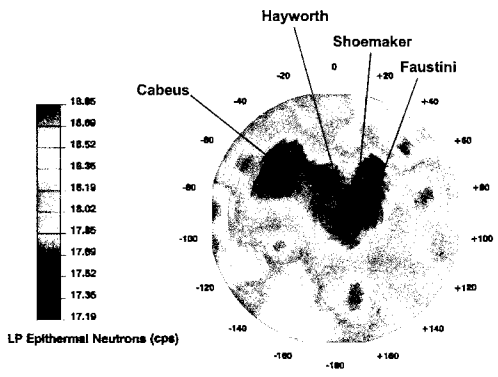

Fig. 4. Measured LP-NS epithermal neutron count rate map for the same projection as Fig. 3.

References: [1] Watson, K. et al. (1961) *JGR* 66, 3033; [2] Arnold, J. R. (1979) *JGR* 84, 5659; [3] Feldman, W. C. et al. (1998) *Science*, 281, 1496; [4] Colaprete, A. et al. (2010) *Science*, 330, 463; [5] Spudis, P. D. et al. (2010) *GRL*, 37, 10.1029/ 2009GL042259; [6] Harmon et al. (2011) *Icarus*, 211, 37; [7] Lawrence, D. J. et al. (2013) *Science*, 339, 292; [8] Lucey, P. G. et al. (2009) *Elements*, 5, 41; [9] Crites, S. T. et al. (2013) *Icarus*, 226, 1192; [10] Carpenter, J. D. et al. (2012) *Pl. Sp. Sci.*, 74, 208; [11] Feldman, W. C. et al. (1993), *Remote Geo. Ana.*, pp. 213 – 234. [12] Miller, R. et al. (2014), *Icarus*, 233, 229. [13] Lawrence, D. J., et al. (2006), JGR, 111, 10.1029/ 2005JE002637; [14] Mitrofanov, I. G. et al. (2010) *Sp. Sci. Rev.*, 10.1007/s/11214-009-9608-4; [15] Mitrofanov, I. G. et al. (2010) *Science*, 330, 483; [16] Boynton, W. V. et al. (2012) *JGR*, 117, 10.1029/2011JE003979; [17] Sanin, A. B. et al. (2012) *JGR*, 117, 10.1029/ 2011JE003971; [18] Lawrence, D.J. et al. (2010) *Astrobio.*, 10, 183; [19] Lawrence, D.J. et al. (2011) *Science*, 334, 1058; [20] Eke, V.R. (2012) *Ap. J.*, 747, 6; [21] Miller, R.S. et al. (2012) *JGR*, 117, 10.1029/2012JE004112; [22] Teodoro, L.F.A. et al. (2014) *JGR*, 10.1002/2013JE004421; [23] Goldsten, J. O. et al. (2007), *Sp. Sci. Rev.*, 10.1007/s11214-007-9262-7. [25] Eke, V.R. (2009) *Icarus*, 200, 12; [26] Teodoro, L.F.A. (2010) *GRL*, 37, 10.1029/2010GL042889.

Lunar Highlands Bulk Hydrogen Concentrations. David J. Lawrence[1], Patrick N. Peplowski[1], Jeffrey B. Plescia[1], Benjamin T. Greenhagen[2], Sylvestre Maurice[3], Thomas H. Prettyman[4], [1]The Johns Hopkins University Applied Physics Laboratory, Laurel, MD, USA (David.J.Lawrence@jhuapl.edu); [2]Jet Propulsion Laboratory, Pasadena, CA; [3]IRAP, Toulouse, France; [4]Planetary Science Institute, Tucson, AZ, USA.

Introduction: In recent years, our understanding of hydrogen (H), water, and other volatile materials on the Moon has changed dramatically [1]. This new understanding has resulted from: 1) new measurements and analyses of enhanced H concentrations at the lunar poles [e.g., 2,3,4]; 2) new orbital measurements showing exogenic and endogenic enhancements of H_2O/OH in non-polar lunar regions [5,6]; and 3) new sample measurements revealing unexpectedly high amounts of water in lunar samples [7]. Despite these advances, there does not yet exist a large-area, non-polar map of bulk lunar H abundances across the lunar surface. Such a map would be important and useful as a tie point to lunar sample studies as well as for understanding processes that relate to all aspects of global lunar volatiles. Previous ambiguities of the interpretation of Lunar Prospector Neutron Spetrometer (LP-NS) data with respect to non-polar hydrogen concentrations have been resolved by comparing the LP-NS data with maps of the 750 nm albedo reflectance, optical maturity, and the wavelength position of the thermal infrared Christiansen Feature (CF).

Global Epithermal Neutron Data: Cosmic ray-generated epithermal neutrons provide a strong measure of planetary H concentrations [8]. The global lunar map of epithermal neutrons derived from LP-NS data [9,10] can be divided into three primary regions: 1) polar regions; 2) Procellarum KREEP Terrane (PKT); and 3) Feldspathic Highlands Terrane (FHT). The polar regions show decreases in epithermal neutron count rates that are indicative of enhanced H concentrations. These polar data have been extensively studied and maps of H concentrations have been derived [10,11]. The PKT shows a strong epithermal neutron decrease that is spatially-correlated with Th, Fe, and Ti concentrations. Lawrence et al. [10] argued that these count-rate decreases are not primarily related to H concentrations but to neutron absorbers that modify thw low-encrgy epithermal neutron flux. However, the magnitude of these decreases is not fully understood, a signature indicative of H is also present in the PKT [12].

The behavior of epithermal neutrons in the FHT are also not fully understood. There is an expectation that epithermal neutrons in this region should be related to the concentrations of solar wind-implanted H. If this is the case, then young craters, which have relatively little exposure to solar wind, should be depleted in H and enhanced in epithermal neutrons. However, highlands variations in Fe concentrations can also cause variations in epithermal neutrons, thus complicating the interpretation of the FHT epithermal neutrons. Nevertheless, in this study we focus on the epithermal neutron data in the FHT, as these data have the fewest ambiguities with respect to count rate decreases from non-H neutron absorbers.

Epithermal Neutron vs. Reflectance and CF data: Three datasets can provide new understanding for epithermal neutrons in the FHT: the 750 nm albedo [14], optical maturity (OMAT)[14], and a thermal infrared emissivity maximum known as the Christiansen Feature (CF)[15]. Each of these datasets are compared with LP-NS epithermal neutron data in the FHT. The goal in carrying out this comparison is to assess the level of correlation and try to isolate the dominant factor that causes the count-rate variation of epithermal neutrons across the FHT.

Figures 1, 2 and 3 show a direct comparision between albedo, OMAT, and CF wavelength and epithermal neutrons. To equalize the spatial footprint of and achieve good statistical precision, all data were resampled to pixles with a size of 5°x5° at the equator (or 150 km x 150 km). The CF data have the most restrictive latitude coverage (±60° latitude), so a latitude cutoff of ±58° is used to reduce edge effects near 60° latitude. Within this latitude band, unrestricted (whole Moon) data are shown as black points; FHT-restricted data (gray points) are selected by identifying locations with thorium concentrations [Th] less than 1 ppm [16].

A comparison of each of the three datasets with epithermal neutrons shows clear trends in almost all cases. For unrestricted data, both the 750 nm albedo and CF wavelength data are clearly correlated. However, the comparison of unrestricted OMAT versus epithermal neutron data shows little-to-no correlation. In all cases, the FHT-restricted data show a good correlation. Various statistical analyses (correlation coefficients; scatter about the correlation lines) show that in the FHT, all four measurements – albedo, OMAT, CF, and epithermal neutrons – are linked by a single, common factor in the FHT. In the case of albedo and CF, both are sensitive to variations in both maturity and iron. However, for FHT, OMAT was derived to be sensitive only to maturity. Because maturity is related to surface exposure and solar wind hydrogen implantation, we conclude that hydrogen is the dominant factor that controls epithermal neutron count rate variations within the FHT.

We can test the consistency of this conclusion with lunar sample data by calculating the implied dynamic range of hydrogen concentrations if the FHT-restricted epithermal neutron count rate variations are due only to hydrogen. The FHT epithermal neutron count rate change within the FHT, where epithermal neutrons correlate with albedo, OMAT, and CF data, is 18.8 – 17.7 = 1.1 cps. Based on equation 2 of [10], this count rate change corresponds to a hydrogen concentration variation of 113 ppm, which is consistent with the range measured in lunar samples [17].

FHT Map of H Concentrations: After correcting the epithermal neutrons for small, residual Fe variations, a map of H concentrations is derived using the calibration procedure of [10]. Regions having thorium concentrations greater than 1 ppm are shown in black.

Summary: The average hydrogen concentration across the lunar highlands and away from the lunar poles is 65 ppm. The highest hydrogen saturation values range from 120 ppm to just over 150 ppm. These values are consistent with hydrogen concentrations from soils and regolith breccias at the Apollo 16 highlands landing site. Based on the correlation of epithermal neutrons and orbit-measured optical maturity parameters, the new highlands hydrogen concentration represents a new global maturity index that can be used for studies of the lunar soil maturation process. Due to the interpretation that these hydrogen maps represent a bulk soil property related to the long-term impact of the space environment on the lunar surface, these hydrogen concentrations are not likely related to the surficial enhancements (top tens to hundreds of microns) or local time variations of OH/H_2O measured with spectral reflectance data.

References: [1] Lawrence, D.J., *Nat. Geo.*, #4, 585 (2011); [2] Colaprete, A. et al., *Science*, 330, 463 (2010); [3] Spudis, P.D. et al., *Geophys. Res. Lett.*, 37, 10.1029 / 2009GL042259 (2010); [4] Miller, R.S. et al., *J. Geophys. Res.*, 117, 10.1029/2012JE004112 (2012); [5] Pieters, C.M., *Science*, 326, 5952 (2010); [6] Klima, R. et al., *Nat. Geo.*, 10.1038/ngeo1909 (2013); [7] Saal, A.E., et al., *Nature*, 44, 10.1038 /nature07047 (2008); [8] Feldman, W.C. et al., *Science*, 281, 1496 (1998); [9] Maurice S. et al., *J. Geophys. Res.*, 109, 10.1029/2003JE002208 (2004); [10] Lawrence, D.J., *J. Geophys. Res.*, 111, 10.1029/ 2005JE002050 (2006); [11] Teodoro, L.F.A. et al., *Geophys. Res. Lett.*, 37, 10.1029/2010GL042889 (2010); [12] Prettyman, T. H., 45th LPSC, #2451 (2014); [14] Lucey, P.G., *J. Geophys. Res.*, 205, 20377 (2000); [15] Greenhagen, B T. et al., *Science*, 329, 1507 (2010); [16] Lawrence, D.J., et al., J. Geophys. Res., 108, 10.1029/2003JE002050 (2003); [17] Haskin, L.A., Warren, P., Lunar Sourcebook, 357–474 (1991);

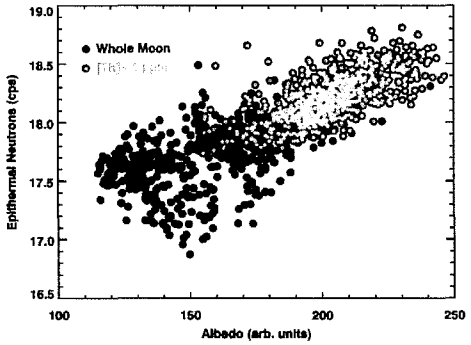

Fig. 1. Scatter plot of 750 nm albedo [14] versus epithermal neutrons. Black data points show unrestricted data, and the gray data points show values from the FHT that have thorium concentrations less than 1 ppm.

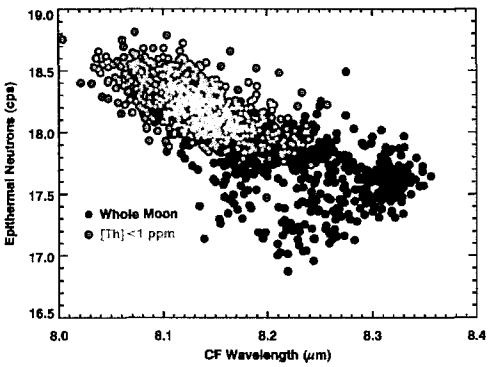

Fig. 3. Scatter plot of CF wavelength [15] versus epithermal neutrons. Data labels are the same as in Fig. 1.

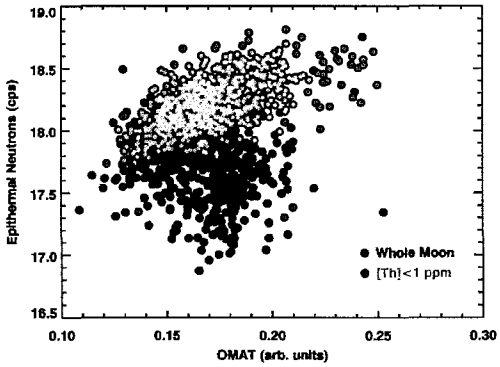

Fig. 2. Scatter plot of OMAT [14] versus epithermal neutrons. Data labels are the same as in Fig. 1.

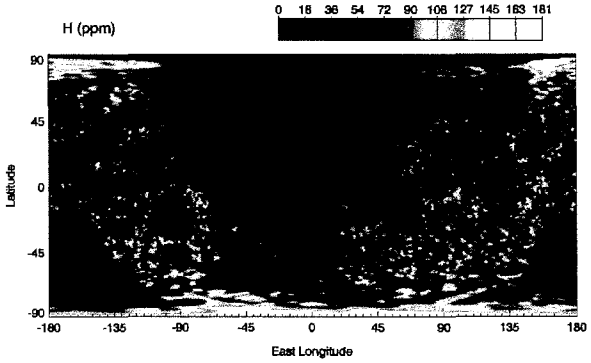

Fig. 4. Map of bulk hydrogen concentrations in the FHT. The black regions indicate locations where Th concentrations are greater than 1 ppm and therefore excluded from this analysis.

ROBOTIC SAMPLE RETURN II: ADDRESSING FUNDMENTAL EXPLORATION THEMES. S. J. Lawrence[1], B. L. Jolliff[2], C. Shearer[3], M. S. Robinson[1], J. D. Stopar[1], S. E. Braden[1], E. J. Speyerer[1], J. T. Hagerty[4], B. W. Denevi,[5] C. R. Neal[6], D. S. Draper[7] [1]School of Earth and Space Exploration, Arizona State University (samuel.lawrence@asu.edu) [2]Department of Earth and Planetary Sciences, Washington University in St. Louis [3]Institute of Meteoritics, University of New Mexico [4]United States Geological Survey, Astrogeology Science Center [5]Applied Physics Laboratory, the Johns Hopkins University [6]University of Notre Dame [7]NASA Lyndon B. Johnson Space Center

Introduction: Lunar sample return is a critical aspect of an integrated lunar exploration strategy that includes sample return [1] and rovers [2] designed to address fundamental Solar System science goals and objectives expressed in the Planetary Decadal Survey [3] and the Lunar Exploration Roadmap (LER) [4]. Automated sampling of key locations will address fundamental questions about the Moon (with implications for all of the terrestrial planets), and prepare for future human exploration and resource utilization.

Background: The Moon preserves a record of time erased on other terrestrial planets [5]. The Moon is the only other planet from which we have contextualized samples, yet critical issues need to be addressed: we lack important details of the Moon's early and recent geologic history, the full compositional and age ranges of its crust, and the bulk composition of the crust, mantle, and whole Moon.

The ongoing Lunar Reconnaissance Orbiter (LRO) mission continues to produce data sets that are essential for lunar science and exploration, particularly exploration planning [6-10]. LRO data enables the preliminary identification of key sites for in-situ exploration, an activity useful for defining hardware and mission design choices [11-15]. While the importance of a sample return from South Pole-Aitken basin is well-established [16], there are numerous additional locations on the Moon where targeted sample return is also required to address Solar System research priorities with relatively low risk. A companion abstract by C. Shearer discusses the role of lunar sample return for advancing our knowledge of the early differentiation of the Moon and other planetary bodies. Here, we outline how themes outlined in the LER can be readily addressed through sample return missions to specific locations.

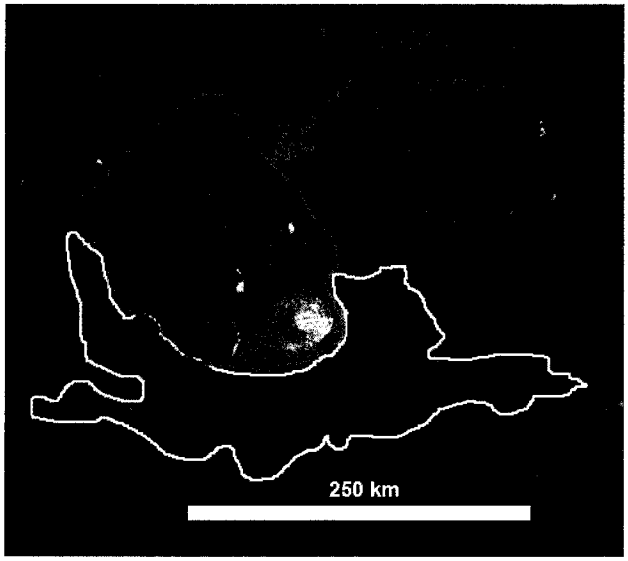

Figure 1: *LROC WAC base map highlighting the P60 area of [26] (white line), along with the crater counting region used to derive the model basalt age (in blue). The Aristarchus Plateau is highlighted in red for reference.*

Understand the Evolution of the Lunar Interior: Science results from the LRO mission confirmed the presence of nonmare, silicic volcanic constructs on the lunar surface [17-21]. Significant questions exist regarding the origin and emplacement of these evolved lithologies. Sample collection at Hansteen Alpha, the Lassell Massif, the Gruithuisen Domes, and Mairan T will dramatically expand our knowledge the compositional diversity, age, and differences in emplacement style of nonmare lunar volcanism.

Understand Lunar Volcanic Processes: In-situ investigations of lunar maria are needed to fill out our understanding of the Moon's volcanic history. For example, what processes produced low shield volcanoes within the lunar mare? Although morphologically distinct, many mare low shields cannot be distinguished on a compositional basis from surrounding mare plains. Low shields are ideal locations for targeted sample return to determine compositional or other differences between low shields and mare basalts that form plains [22-24]. Excellent candidate locations include the Marius Hills, Mons Rümker, Hortensius Domes, and the Isis and Osiris cones.

Understanding Lunar Time-Stratigraphy: Determining the chronology of geologically recent (i.e., Copernican and Eratosthenian) lunar events requires sample return [1] and is required not just for lunar exploration, but for calibrating the cratering statistics used to age-date surfaces on other terrestrial planets [e.g., 25]. Sample return locations with high-priorty, geologically recent materials for age-dating include: the youngest (~1 Ga) Procellarum basalts defined by [26]; Lichtenberg Crater; the Ina-like Irregular Mare Patches [27]; Copernicus (the defined division between the Eratosthenian and Copernican epochs); and Tycho, Aristarchus, and Giordano Bruno craters.

The Youngest Basalt Example: Some mare basalt flows dated by crater counting methods provide significantly younger model ages than any Apollo basalt [28]. Hiesinger et al. [26] mapped 60 spectrally homogenous basalt units in Oceanus Procellarum. Crater counting methods determined that 5 of these units have model ages ranging from ~1.5-2.0 Ga. Unit P60 (**Fig. 1**) directly south of the Aristarchus Plateau has the youngest model age (1.2 Ga; uncertainty +0.32/-0.35 b. y.).

The analysis of returned samples from the P60 region would provide knowledge about isotopic and trace-element variations in lunar basalts, distinguish differences in basalt source regions/reservoirs and eruption rates over time, and redefine knowledge of the Moon's absolute chronology.

Understanding Lunar Resource Potential: Regional lunar dark mantling deposits are not only primitive materials that yield insights into the lunar mantle, but are some of the most common and accessible lunar ores and can be processed to produce key lunar resources, particularly oxygen [29,30]. The Aristarchus-1, Aristarchus-2, and Sulpicius Gallus Constellation Regions of Interest offer excellent locations to assess the physical properties and compositional variability of these resources [31]. Sample return from these deposits will greatly facilitate design and flight qualification of in-situ resource utilization hardware to expand the capability and reduce the cost of Solar System exploration.

Notional Mission Strategy: An automated sample return mission functionally similar to the Soviet Luna 24 mission and the recently proposed MoonRise mission [32] can meet the return requirements. The advanced scouting capabilities provided by LRO enable precisely targeted landings. The required spacecraft would consist of a single landed element with sampling capabilities, an ascent vehicle, and a sample return system. After landing, a robotic arm collects and stores a scoop of bulk regolith, then collects a kilogram of 3-20 mm rocklets by raking or sieving. Following collection, the samples are returned to Earth. The mission duration is less than a lunar day; no-long-duration survival for the landed element is required, and any nearside location would not require a communications relay.

Sample Return is Required: The Apollo experience demonstrates the importance of returning planetary samples to Earth [33]. The science objectives discussed here require detailed analysis of compositions, mineralogy, rock textures, and physical properties in addition to laboratory-determined radiometric ages. In-situ measurements can provide important data points, but terrestrial laboratories offer more capability for the foreseeable future, and to date, the only method with sufficient precision to adequately answer the question of the age of the youngest lunar materials. Furthermore, samples become resources, so new measurements can be made as analytical techniques improve, as indicated by recent reanalysis of lunar water in Apollo materials [e.g. 34]. Sample return missions will also play an important complementary role towards human lunar return by providing experience to the next generation of lunar scientists prior to the seventh human lunar landing.

References: [1] B. L. Jolliff et al. LEAG 2013 Abs. #7050 [2] Robinson et al. 2014, this conference [3] Comm. Plan. Sci. Decadal Survey; NRC 2011 [4] Lunar Exploration Roadmap [5] G. J. Taylor and P. D. Spudis (1990) NASA Conf. Pub. 3070 [6] S. J. Lawrence et al. (2014) LEAG 2013, Abs #7048. [7] J. Gruener et al. (2009 AGU Fall Meet. Vol. 31, p. 0010. [8] M. S. Robinson et al. (2010) Space Sci. Rev., 150, 1–4, pp. 81–124. [9] R. Vondrak et al. (2010) Space Sci. Rev., doi:10.1007/s11214-010-9631-5. [10] G. Chin et al. (2007) Space Sci. Rev., vol. 129, no. 4, pp. 391–419, Apr. 2007. [11] E. J. Speyerer and M. S. Robinson (2013) Icarus, 222, 1, pp. 122–136. [12] J. Gruener and B. Joosten (2009) LPI Contrib. 1483 pp. 50–51. [13] E. J. Speyerer et al. (2013) LPSC 44, Abs. 1745. [14] Stopar J. D. et al. (2013) LEAG 2013, Abs. 7058 [15] Lawrence S. J. (2014) LPSC 45, Abs.#2785 [16] NRC (2007) Scientific Context for the Exploration of the Moon [17] T. D. Glotch et al. (2010) Science, vol. 329, no. 5998, pp. 1510–1513. [18] B. T. Greenhagen et al. (2010) Science, vol. 329, no. 5998, pp. 1507–1509. [19] B. L. Jolliff et al. (2011) Nat. Geosci, vol. 4, no. 8, pp. 566–571. [20] B. R. Hawke et al. (2003) JGR, 108, 8. [21] J. W. Ashley et al. (2013), LPSC 44, Abs. 2504. [22] S. J. Lawrence et al. (2013) JGR, doi:10.1002/jgre.20060. [23] J. B. Plescia, (2013) "Small Volcanic Shields of Mare Tranquillitatis," 2013 NASA Lunar Science Forum. [24] P. D. Spudis et al. (2013) JGR, doi:10.1002/jgre.20059 [25] D. Stöffler and G. Ryder (2001) Space Sci. Rev., 96, 9–54. [26] H. Hiesinger et al. (2011) GSA Spec. Pap., vol. 477, pp. 1–51. [27] Braden S. E. et al (2014) "Irregular Mare Patches as Lunar Exploration Targets", NESF2014. [28] P. H. Schultz and P. D. Spudis, Nature, 302, 5905, 233-236, 1983. [29] B. R. Hawke et al. (1990) Proc. LPSC 20, pp. 249–258. [30] B. R. Hawke et al. (1991) Proc. LPSC 21, pp. 377–389. [31] S. J. Lawrence and B. R. Hawke (2008) LPSC 38, Abstract 1804. [32] B. Jolliff et al. "MoonRise: A US Robotic Sample-Return Mission to Address Solar System Wide Processes," in DPS Abstracts, 42, 2010. [33] G. J. Taylor et al. Lunar Sourcebook, Cambridge, 1991, 183-284. [34] K. Robinson and G. J. Taylor (2014) Nat. Geosci., 7: 401-408.

LUNAR SURFACE TRAVERSE AND EXPLORATION PLANNING: FARSIDE LOCATIONS.

S. J. Lawrence[1], M. S. Robinson[1], J. D. Stopar[1], E. J. Speyerer[1], B. L. Jolliff[2]. [1]School of Earth and Space Exploration, Arizona State University, Tempe, AZ, USA (samuel.lawrence@asu.edu) [2]Department of Earth and Planetary Sciences, Washington University in St. Louis, St. Louis, MO, USA

Introduction: We are systematically assessing (from both scientific and operational perspectives) locations on the Moon [1] considered to be likely locations for near-term robotic precursor missions. In order to maximize the practical utility of the research, our goals are directly traceable to three generalized examples of robotic missions (short-duration rover, long-duration rover, and automated sample return) that have been recommended as desirable precursor missions [2]. However, the results of this study will also be applicable to future human lunar exploration.

Our previous efforts have focused on nearside sites of high-near term exploration potential, but an optimized lunar exploration program will include farside locations of high scientific interest, where exploration will provide important new information about the composition of the lunar crust and the temporal evolution of lunar volcanic processes. One prime example of a geologically complex far side exploration site is the Dewar geochemical anomaly.

Background: Dewar (Fig 1.) is an Imbrian-age crater with a diameter of approximately 50 km, located north of the South Pole-Aitken (SPA) basin [3]. An anomalous area exhibiting low albedo materials can be discerned northeast of the crater. This low albedo area correlates with an area of enhanced FeO, TiO_2, and thorium abundance, which [3] concluded were ancient buried mare basalts, also referred to as "cryptomare". The mode of emplacement for a small mare basalt deposit in this farside location remains poorly understood, and for this region, Dewar was a Constellation Region of Interest [4]

Dewar is an example of a geologically complex field location where sample return, possibly enhanced by a limited-duration rover, will provide new science and exploration results (Fig 1). Dewar is also a relatively representative area in the central far side highlands, rendering the systematic assessment methodology here generically relevant to a variety of far side exploration tasks.

Methods: We are fusing LROC (NAC, WAC, and DTMs), Diviner, and LOLA datasets with Moon Mineralogy Mapper (Chandrayaan-1), Kaguya Terrain Mapping Camera, Clementine, and Apollo Metric Camera frames. The integrated datasets are being used to determine important lithologies and geologic units, identify productive exploration locations and resources such as pyroclastic deposits, and then identify candidate landing sites. LROC DTM datasets are being used to assess the accessibility of each site in terms of the Terrain Ruggedness Index [5] and slopes. Finally, we have developed a preliminary path planning algo-

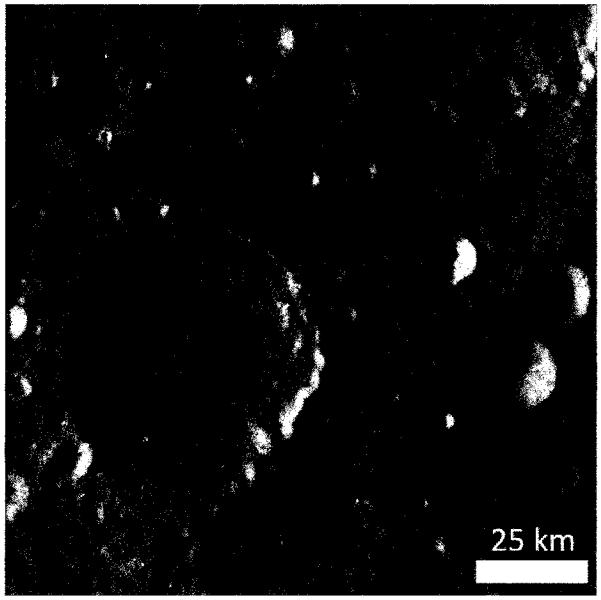

Figure 1: Wide Angle Camera (WAC) of Dewar crater and environs.

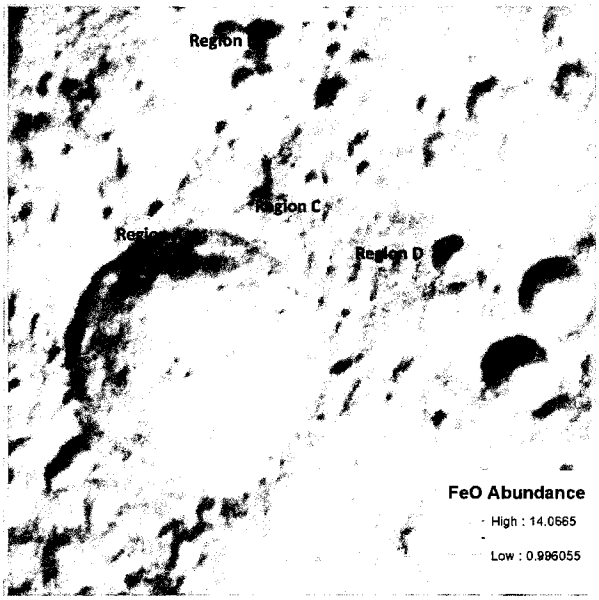

Figure 2: Clementine-derived FeO Abundance Map overlaid upon a GLDJOO synthetic hillshade data product.

rithm [6] based on a generalized least-energy model for planetary rovers, altered for the lunar use case [7]. This algorithm identifies least energy traverse paths and allows us to determine capabilities (rolling resistance, turning capability, maximum slopes) that are required to reach specific targets.

Results: The key science goal of exploring the Dewar region is determining the composition of the cryptomaria exposed by the Dewar satellite impact craters, making this an ideal candidate location for automated sample return. Cryptomaria exposures can be straightforwardly distinguished through the Clementine FeO abundances. Accordingly, through our data fusion process, we selected four candidate regions of interest (Figure 2) for automated sample return based on the accessibility of the basalt exposures (Table 1). Accessibility analysis of the morphometric properties of the four candidate regions of interest indicated that, in general, Site D offered the most accessible locality for the exposed cryptomaria. Site D is also partially includes a Constellation Region of Interest, so the full range of Constellation data products can therefore be leveraged for a rigorous science operations assessment.

Analysis of the LROC Narrow Angle Camera DTMs identified three sites within Region D (Figure 3) where automated sample return could be reasonably executed. Sample return from these locations will require autonomous landing technology capable of executing a landing within a well-defined 2-km diameter region of interest. Additionally, while near-side locations are more feasible short-term destinations for surface exploration, the importance of far side targets like Dewar means that technologies required to enable far-side communication must remain part of the exploration roadmap moving forward.

References: [1] S. J. Lawrence et al. (2014) LPSC 45, Abstract 2785. [2] LEAG (2011) "Lunar Exploration Roadmap". [3] S. J. Lawrence et al. (2008) doi:10.1029/2007JE002904 [4] Gruener and Joosten (2009) LPI Contrib. 1483, p. 50-51. [5] M. F. J. Wilson et al. (2007) Mar. Geod., 30, 1–2, 3–35. [6] E. J. Speyerer et al. (2013) LPSC 44 1745. [7] G. Ishigami et al. (2007) 2007 IEEE International Conference on Robotics and Automation, pp. 2361–2366.

Figure 3: NAC DTM with recommended candidate automatic sample return locations highlighted.

Table 1. Physical Parameters of Notional Dewar Region Scientific Regions of Interest

Location	Mean FeO (wt %)	Max FeO (wt %)	Mean DRA	Mean TRI	Mean WAC Slope	Max WAC Slope
Region A	8.785	14.067	3.745	14.164	10.34	26.66
Region B	11.067	12.474	3.519	10.743	7.91	18.7
Region C	10.665	13.631	4.199	11.064	8.05	25.87
Region D	11.283	13.482	3.216	5.9	4.35	17.82

Small Payloads and Advanced Concepts for Exploration (SPACE) Early Mission Design Tool. R. Leiter[1,2], Z. Himwich[1], A. Natarajan[1], J. Rosenthall[1], P.E. Clark[1,3], [3]IACS, Catholic University of America, Washington, D.C. 20064, [1]NASA/GSFC Summer Student Interns Program, NASA/GSFC, Greenbelt Road, Greenbelt, MD 20771, and [3]University of Virginia, 472-4 Lambeth Field, Carlottesville, VA 22904. Contact Emails: rml3yb@virginia.edu and clarkp@cua.edu

Rationale: As interest in the development of cubesats for deep space applications grows, and as the first opportunities for lunar cubesat missions are becoming available, more commercial off-the-shelf components for CubeSats, nanosatellites with standard bus, components, and interfaces, are becoming available.

Tool: Our project at NASA Goddard was to create a program and user interface that facilitates the design of deep space CubeSat missions, based on the nature of the science investigation, in the early stages of mission design. The SPACE tool separates the design process of a CubeSat mission into selection of an instrument or payload and selection of various subsystems. In addition to the SPACE program, we created a database of commercially available satellite components designed for CubeSats, which the SPACE tool is able to search and select from. After subsystems are selected, the tool allows the user to tweak their mission concept or subsystem selections. Ultimately, the user will be able to access 3D models of the CubeSat parts and bus that can be printed individually or as a complete CubeSat layout assembled in a CAD program.

Result: This tool allows scientists and engineers in early phases of mission development to select an compact instrument for a science application, to determine the state-of-the-art technological capability of CubeSats for that application, and find initial estimates mass, power, volume, and bandwidth for a specific nanosatellite mission. Our hope for the future of this tool is that it will be made available online for public use, and as more scientists, engineers, and manufacturers use the tool, they will contribute to the CubeSat database, increasing the functionality of our tool.

DIURNALLY VARIABLE HYDROGEN-BEARING VOLATILES AT THE MOON'S EQUATOR: EVIDENCE, CONCENTRATION, TRANSPORT, IMPLICATIONS. T. A. Livengood[1,2,3], G. Chin[2], R. Z. Sagdeev[3], I. G. Mitrofanov[4], W. V. Boynton[5], L. G. Evans[2,6], M. L. Litvak[4], T. P. McClanahan[2], A. B. Sanin[4], R. D. Starr[2,7] and J. J. Su[3], [1]CRESST, Code 693, NASA Goddard Space Flight Center, Greenbelt, MD 20771, timothy.a.livengood@nasa.gov, [2]NASA Goddard Space Flight Center, Greenbelt, MD, [3]University of Maryland, College Park, MD, [4]Institute for Space Research, Moscow, Russia, [5]Lunar and Planetary Laboratory, University of Arizona, Tucson, AZ, [6]Computer Sciences Corporation, Lanham-Seabrook, MD, [7]Catholic University of America, Washington, DC.

The Lunar Exploration Neutron Detector (LEND) detects the presence of hydrogen on the night side of the Moon near the equator, peaking in concentration on the dayside of the dawn terminator and diminishing through the dawn-to-noon sector with minimum hydrogen in the mid-afternoon to post-dusk sector. The chemical form of detected hydrogen is not determinable from these measurements, but is expected to be in the form of water molecules or hydroxyl ions. LEND, on the polar-orbiting Lunar Reconnaissance Orbiter (LRO) spacecraft [1,2], detects hydrogen in the regolith through the localized suppression of epithermal neutron flux from the Moon's surface. The greatest flux suppression is at dawn, with the least suppression and least hydrogenation in the lunar afternoon to post-dusk sector. The minimum-to-maximum contrast is greater than 5σ. The peak concentration within the upper ~1 m of regolith is estimated to be 0.0125±0.0022 weight-percent water-equivalent hydrogen (wt% WEH), yielding about 187±33 ml recoverable water per cubic meter of regolith at dawn. The non-uniform distribution of hydrogen with respect to local time implies active volatile transport on the Moon at low latitudes. Volatiles are deduced to collect in or on the cold night-time surface, then distill out of the regolith after dawn as rotation exposes the surface to sunlight, achieving maximum dehydration in the afternoon. The liberated volatiles migrate away from the warm subsolar region toward the cold night-time surface beyond the terminator, resulting in maximum concentration at the dawn terminator. Since the water is naturally distilled from the regolith by sunlight every lunar day and restored to the cold regolith by adsorption every lunar night, a cold metal plate on the surface could intercept and collect up to the full peak concentration of 187 ml water per square meter of surface through every lunar night for *in situ* resource utilization (ISRU), with no expenditure of energy for distillation from mined regolith.

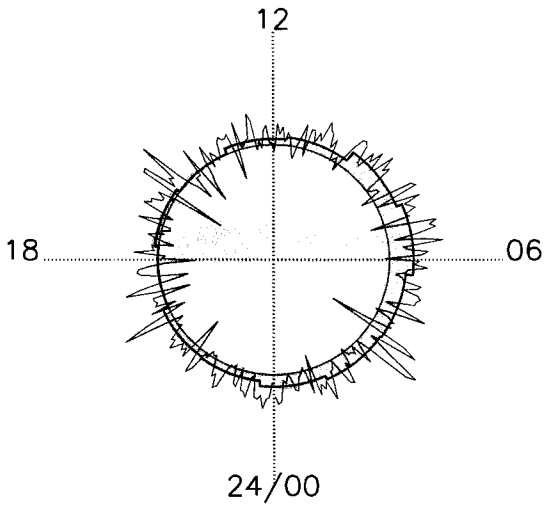

Fig. 1. Variable H distribution as a function of local time, deduced from LEND uncollimated epithermal neutron detector SETN. Volatiles that move east to the dusk terminator condense or adsorb in the surface overnight, then remobilize after dawn and migrate west to the cold dawn terminator, building up a local maximum of volatiles near dawn.

The implied concentration of volatiles is nontrivial. Previous detections of equatorial volatiles as hydroxyl or water in mineral hydration [3,4,5] could be accommodated by a skin layer only microns thick, but the volatiles detected by neutron remote-sensing are about four to five orders of magnitude greater in areal density. This is not a discrepancy between the measurements, as the observed mineral hydration can establish only a lower limit due to the uncertain depth of hydration. If the mineral hydration were estimated to extend even as much as millimeters deep, that would diminish the ratio between the measurements by about three orders of magnitude. Measurements of mineral hydration also have provided evidence for diurnally variable concentrations of adsorbed volatiles that maintain a local maximum at the dawn terminator [4]. Maintaining a region of maximum density in hydration that is fixed to the local time as the Moon rotates requires desorption from the surface and transport to the nightside cold trap faster than the Moon rotates, at

4.3 m/s, necessitating that volatile transport be accomplished by thermal desorption into free space above the surface, as a gas. Conservation of mass at the terminator between adsorbed volatiles in slow prograde rotation and desorbed volatiles in rapid retrograde transport across the terminator implies that less than 1% of volatiles present at the terminator are gaseous while more than 99% of the volatiles remain adsorbed within the regolith at that local time. This fractionation reconciles the lower limit quantity of observed variability in mineral hydration with the 10^7 mol/cm^3 density of evanescent atmosphere estimated from lunar dawn measurements by the Apollo 17 LACE instrument [6], assuming the hydrated layer thickness were only 1-10 μm.

Volatile concentrations detected by neutron remote-sensing remain about four orders of magnitude greater than the Apollo 17 estimate, even assuming that only 1% of volatiles at the terminator contribute to the detectable above-ground atmosphere. Solar ultraviolet photolysis lifetimes of molecules at Earth-Moon orbit are about 10^5 seconds [7]. Assuming that photolysis acts only on the fraction of volatiles that are above-ground at any given moment, effectively increasing the lifetime by two orders of magnitude, the required supply rate of new molecules to replace photolysed molecules and maintain equilibrium is about 5 orders of magnitude greater than the total solar wind delivery rate of about 2×10^8 p$^+$/cm^2/s at the Moon [8]. The estimated quantity of volatiles delivered by micrometeoroids is lesser, creating an even greater discrepancy. Although solar wind implantation and micrometeoroid impact processes will contribute to lunar volatiles, the only remaining delivery mechanism that has the potential to account for contemporary volatile equilibrium is outgassing from the Moon itself.

References: [1] Vondrak, R., *et al.* (2010). *SpaSciRev* **150**, 7–22, doi: 10.1007/s11214-010-9631-5. [2] Mitrofanov, I. G., *et al.* (2010). *SpaSciRev* **150**, 183–207, doi: 10.1007/s11214-009-9608-4. [3] Pieters, C. M., *et al.* (2009). *Science* **326**, 568–582, doi: 10.1126/science.1178658. [4] Sunshine, J. M., *et al.* (2009). *Science* **326**, 565–568, doi: 10.1126/science.1179788. [5] Clark, R. N. (2009). *Science* **326**, 562–564, doi: 10.1126/science.1178105. [6] Hoffman, J. H., and R. R. Hodges, Jr. (1975). *The Moon* **14**, 159–167, doi: 10.1007/BF00562981. [7] Budzien, S. A., and P. D. Feldman (1991). *Icarus* **90**, 308–318, doi: 10.1016/0019-1035(91)90109-7. [8] Crider, D. H., and R. R. Vondrak (2002). *AdvSpRes* **30**, 1869–1874, doi: 10.1016/S0273-1177(02)00493-3.

A laser spectrometer for global mapping of the abundance, distribution and variability of water on the moon.

P. G. Lucey[1], J. B. Abshire[2], X. Sun[2], G.A. Neumann[2], E. M. Mazarico[2,3], Hawaii Institute of Geophysics and Planetology, University of Hawaii, Manoa, 1680 East-West Rd., Honolulu, HI 96822, lucey@higp.hawaii.edu, [2]NASA Goddard Space Flight Center, Code 698, Greenbelt, MD 20771, [3]Department of Earth, Atmospheric and Planetary Sciences, Massachusetts Institute of Technology, Cambridge, MA 02139.

Introduction: It is an understatement to describe the recent flood of data on the poles of the Moon and Mercury as revolutionary. MESSENGER and LRO reveal two planets nominally similar in surface state, yet drastically different in volatile character. The north pole of the planet Mercury appears to convey a straightforward story of a distribution of volatiles controlled entirely by the vapor pressure of water and the arrangement of temperatures on the planet [1]. Bright radar anomalies indicating buried ice are found everywhere model temperatures allow buried ice to be stable against sublimation for geologic time. Where model surface temperatures are low enough to preserve surface ice, the surface of the radar anomalies are bright in reflectance at 1064 nm as revealed by laser reflectance. Where model surface temperatures of the bright radar anomalies are too high for long-term preservation of exposed ice, the surfaces of the radar anomalies exhibit very low reflectance. These low reflectance anomalies are interpreted to be due to lag deposits of more refractory material either emplaced with the ice, or formed in situ from complex ices by interaction with radiation. Apparently the lags accumulated until the underlying ice was protected from further sublimation. Similar dark deposits are found away from the radar anomalies, but are found where subsurface temperatures are low, but not quite low enough to preserve ice for geologic time. These dark surfaces speak to the presence of former ice, where a lag also accumulated, but was not sufficient to protect ice in these warmer areas from sublimation over time.

These characteristics suggest that Mercury experienced a massive influx of volatiles that filled both long and short-term cold traps, and this massive influx has retreated to the thermal equilibrium we observe today. In stark contrast, the Moon exhibits none of the clear evidence that suggests the Mercury story. Cold surfaces that enable preservation of buried ice do not exhibit clear and obvious radar anomalies; there is no evidence for the dark lag deposits ubiquitous in polar Mercury. There are many indications of volatile-rich locations on the Moon, but indicators are frequently contradictory, and the distributions are certainly not well understood. If the Moon did experience a massive volatile influx as suggested for Mercury, it occurred so long ago that the thermally controlled dark lag deposits, and even thick ice deposits have succumbed to regolith turnover and space weathering.

To understand the distribution of volatiles on the Moon, we must understand the less catastrophic processes that govern the slow input, transport, sequester and loss of volatiles. We must quantify the steady drip of water originating from the solar wind and degassing meteors; the occasional squall from the impact of a small comet or wet asteroid; the meandering march of water to the poles, attritted by ionization and sweeping; the temporary capture into the cold traps and sequester by weak thermal pumping, chemical reactions and regolith overturn; and finally loss to sublimation, sputtering and ultraviolet.

Active laser measurements of the reflectance of the Moon in key water absorption features offer key pieces of evidence to fill in this picture. First, laser reflectance is free of thermal contamination that plagues determination of abundance variation using passive IR spectroscopy [2]. Global, day/night measurements of the strength of the 3um feature, made famous by [3,4,5], would 1) quantify the global abundance and distribution of adsorbed water on the Moon; 2) Detect and quantify diurnal variation in the abundance of surface water that would constrain the supply of water to the poles; 3) Quantify the abundance of water, and water ice, in regions of permanent shadow, at cold locations on the lunar night side, and regions seasonally shadowed; 4) Detect ice in the ejecta of any small craters that expose shallow buried ice in areas that can preserve buried ice for geologic time, and surface ice for shorter periods; and 5) Detect and quantify all exposures of igneous water present in lunar rocks.

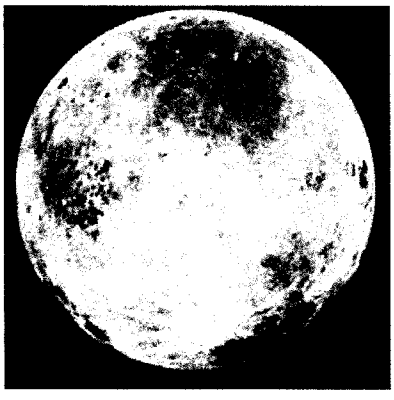

Figure 1. View of the Moon's South Pole from LOLA

These measurements, with spatial resolution as fine as tens of meters, would provide definitive answers to many questions: Is surface ice present in the polar regions and what is its geologic setting? Are there extensive regions of shallow buried surface ice suitable for sampling and exploitation? What proportion of surface water is mobile and hence ultimately available for polar cold trapping? Is transient surface frost present in areas only temporarily cold, for example on seasonal timescales? Do meteor showers emplace frost temporarily into the poles? What is the distribution of igneous water revealed Moonwide?

Instrument: The instrument is based on two developments at Goddard Space Flight Center. The first is an existing airborne lidar system operating in the near-IR near 1.5 microns that can be used to map the ice overtone bands for relatively abundant (>1 wt.%) surface frost [5]. The second, described here, is a laser system operating in the 3um region for extremely sensitive water detection. Both wavelength regions will be solar blind, and capable of obtaining high quality data during the lunar day and lunar night, and of course the permanently shadowed regions.

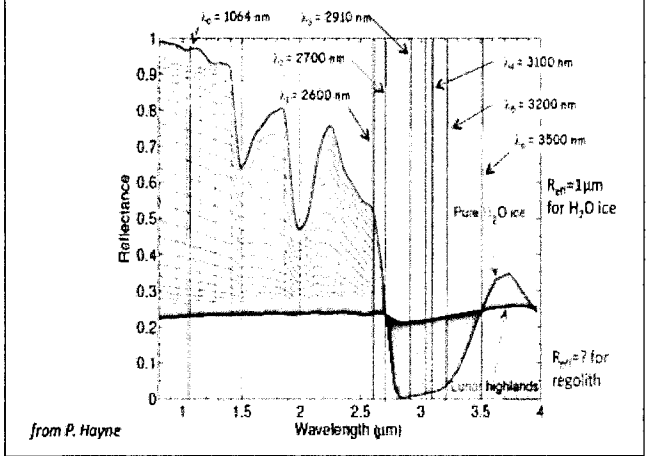

Figure 2. Locations of nominal 3um region bands for the laser system. The shorter wavelength system would cover the 1.4 micron ice band in two addition wavelengths.

The lidar (Figure 3) will measure the range along with reflectance of the surface in the same spot simultaneously at 7 wavelengths. The spectral distribution of example laser wavelengths is shown in Figure 2 plotted against the spectral signature of a surface with varying surface densities of water ice frost. The 1064 nm wavelength of the pump laser was chosen to match that of LOLA to allow intercomparisons with LOLA measurements. Six additional wavelengths were chosen distributed from 2600 to 3500 nm and are also transmitted to sample the continuum (2600 nm) and absorption signatures (2910, 3100, 3200 nm) of the O-H stretch of water ice. These bands shown are examples: for the flight mission a final band set might differ somewhat based on addition analysis.

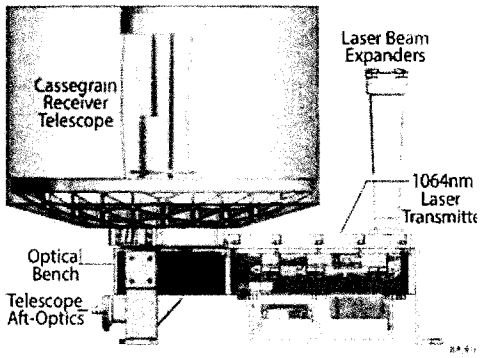

Figure 3. Rendering of the laser transmit and receive system.

All components have been shown to work in the laboratory, and the infrared detection system has had extensive field-testing. The laser subsystem is currently being used to collect ice reflectance data in the laboratory. The aggregate TRL of the system is 4.6 and ongoing efforts continue to raise the TRL.

References: [1] Paige, D.A., Siegler, M.A., Harmon, J.K., Neumann, G.A., Mazarico, E.M., Smith, D.E., Zuber, M.T., Harju, E., Delitsky, M.L., and Solomon, S.C., 2013, Science, v. 339, p. 300–303. [2] Combe, J.-P., T. B. McCord, P. O. Hayne, and D. A. Paige (2011), EPSC-DPS Joint Meeting 2011, Nantes, France, October 2-7, 2011, abstract #1644. [3] Clark, R.N., (2009), Science 326, 562–564. [4] Pieters, C. M., et al. (2009), Science, 326, 568–572. [5] Sunshine, J. M., et al. (2009), Science, 326, 565–568. [6] Abshire, J. B., H. Riris, C. Weaver, J. Mao, G. Allan, W. Hasselbrack, and E. Browell, Appl. Opt. 52, 4446-4461 (2013).

LUNAR POLAR SURFACE FROST: THE VIEW FROM LOLA. P. G. Lucey[1], G.A. Neumann[2], D.E. Smith[2], M.T. Zuber[3], D.B. J. Bussey[4], J. T. S. Cahill[4], E. M. Mazarico[2], D. A. Paige[5], Hawaii Institute of Geophysics and Planetology, University of Hawaii, Manoa, 1680 East-West Rd., Honolulu, HI 96822, lucey@higp.hawaii.edu, [2]NASA Goddard Space Flight Center, Code 698, Greenbelt, MD 20771, [3]Department of Earth, Atmospheric and Planetary Sciences, Massachusetts Institute of Technology, Cambridge, MA 02139, [4]Applied Physics Laboratory, Laurel, MD 20723, USA, [5]Department of Earth and Space Sciences, University of California, Los Angeles, CA 90095-1567, USA

Introduction: In addition to its function as a laser altimeter, the Lunar Orbiter Laser Altimeter (LOLA) on LRO also measures the reflectance of the lunar surface by comparing the strength of the returning altimetric pulse to the transmitted laser energy, compensating for the dependence of the signal upon range. Exploiting this capability, one of the goals of the experiment was to measure the reflectance of the Moon within regions of permanent shadow at the poles in a search for possible surface frosts [1]. LOLA measurements of reflectance at the laser wavelength of 1064 nm have demonstrated that regions in permanent shadow (PSR) consistently exhibit higher reflectance than nearby surfaces that sometimes receive illumination [2,3]. Whether this increased reflectance is due to surface frost is the subject of on-going investigation.

The many processes that affect the albedo of the lunar surface challenge establishing the presence of surface frost from reflectance measurements. Outside the polar regions, and at visible and near-IR wavelengths, composition and space weathering dominate albedo variations. Space weathering darkens the lunar regolith by producing both dark glass and nanophase iron, while fresh impacts and mass wasting act to renew the surface locally. Composition also has a strong effect on reflectance; more iron rich materials are darker than feldspathic rock, and also contribute more iron to the space weathering process to enhance its effects. To attribute a reflectance anomaly to the presence of frost, these sources of "geologic noise" must be mitigated.

The nature of polar regions helps to some extent. There is no evidence for strong polar compositional variations in Lunar Prospector gamma ray data, and LOLA's reflectance maps do not reveal evidence of any significant mare or pyroclastic deposits. Dark albedo anomalies are rare and highly localized. Therefor, interpreting LOLA reflectance data is a matter of separating geologic processes that enhance space weathering variations from exposures that may indicate the presence of frost.

Zuber et al. 2012 [2] grappled with these issues in the first study using LOLA reflectance data. They showed that the south polar crater Shackleton was locally strongly anomalous, with its floor exhibiting higher reflectance than the surroundings. While they cautioned that mass wasting within the crater revealing immature lunar regolith could account for this local reflectance enhancement, they ventured that several percent water frost could also account for the anomaly. They also suggested that the sheltering effect of the deep crater could partly shield the floor of Shackleton from the solar wind and micrometeorites that are the engine of space weathering.

So, Zuber et al. 2012 offer three hypotheses for polar brightening: surface frost, routine mass wasting, or an environmental influence upon space weathering. With the availability of quantitative reflectance data within the PRSs we can begin to test these hypotheses.

Controlling for mass wasting and sky visibility:

Because PSRs must be in local topographic lows, it was plausible that they might systematically feature steeper slopes and hence exhibit generally higher reflectance because of generally steeper slopes. To control for this we examined the reflectance of PSR and nearby surfaces that sometimes receive illumination and constrained the slopes to less than 10 degrees where mass wasting cannot operate. We find that even on these flat surfaces PSRs are strongly brighter than areas that receive illumination. Interestingly, controlling slopes to greater than 25 degrees where mass wasting is active also reveals systematically brighter surfaces in permanent shadow.

To control for exposure to space, we calculated the solid angle of sky subtended as viewed from every pixel in the polar regions. Like the ease for slopes, PSRs with large sky access (mountains and large flat surfaces) are brighter than illuminated regions with the same access. Similarly, the reflectance of surfaces with very restricted sky access (crater bottoms, cliff bases) are more reflective in PSRs than illuminated surfaces.

Discussion: The reflectance of polar surfaces in permanent shadow is systematically different than that of areas that sometimes receive illumination. But are they frosty? While we appear to have eliminated topographic shielding as a systematic effect, Gladstone et al. 2012 [5] suggested that the porosity of polar surface in shadow may be systematically higher than other areas due to unique charging properties of the cold

polar soil. The albedo of the polar regions shows strikingly the uniqueness of the permanently shadowed regions at the Lyman alpha wavelength (122 nm). At this wavelength space weathering has a relatively weak effect on reflectance, so the polar images collected by the LAMP spectrometer show vividly that the PSRs have lower albedo than their surroundings. Increased porosity does have a strong darkening effect on regoliths, however theory [5] suggests this effect is not wavelength dependent and so porosity alone cannot account for the LOLA reflectance anomalies.

Another alternative is that the low temperatures within the PSRs inhibit the production of either nanophase iron, or dark impact glass. This possibility is subject to experimental verification. However, as noted, space weathering is relatively ineffective at altering reflectance at LAMP wavelengths.

Combinations of porosity and decreased space weathering, or porosity and surface frost can both account for the LOLA 1064 nm and LAMP 122 nm reflectance. We use methods developed by [5] to arrive at these conclusions for "typical" PSR surfaces. In summary, porosity and surface frost require 9% frost by area, or 14% ice by weight to account for the two albedoes. In contrast, the space weathering model requires that polar soil contain only half the nanophase iron of similar mature surfaces that are illuminated.

The ice abundances result in strong predictions regarding the spectral properties of the permanently shadowed regions. Even small amounts of ice mixed with the regolith would have a powerful effect on absorption at 3um, and patchy exposures of ice at the few percent level will produce strong ice overtone bands at 1.4 and 1.9 microns. It is possible that some PSRs can be observed at these wavelengths using groundbased telescopes, but the ideal experiment would be a LOLA-like experiment operated at a few near-IR wavelengths. Such an experiment would definitively detect and map the presence of surface ice at abundances above ~ 1wt %.

References: [1] Smith, D. E. et al. (2010b), Space Sci. Rev., 150(1-4), 209–241, doi:10.1007/s11214-009-9512-y. [2] Zuber, M. T. et al. (2012), Nature, 486(7403), 378–81, doi:10.1038/nature11216. [3] Lucey et al. 2014, JGR, in press. [4] Gladstone, G. R. et al. (2012), JGR 117, E00H04, doi:10.1029/2011JE003913. [5] Hapke, B. (1993), Theory of reflectance and emittance spectroscopy, 1st ed., Cambridge University Press, Cambridge, UK.; Hapke, B. (2001), JGR, 106(E5), 10039, doi:10.1029/2000JE001338; Hapke, B. (2008), Icarus, 195(2), 918–926, doi:10.1016/j.icarus.2008.01.003.

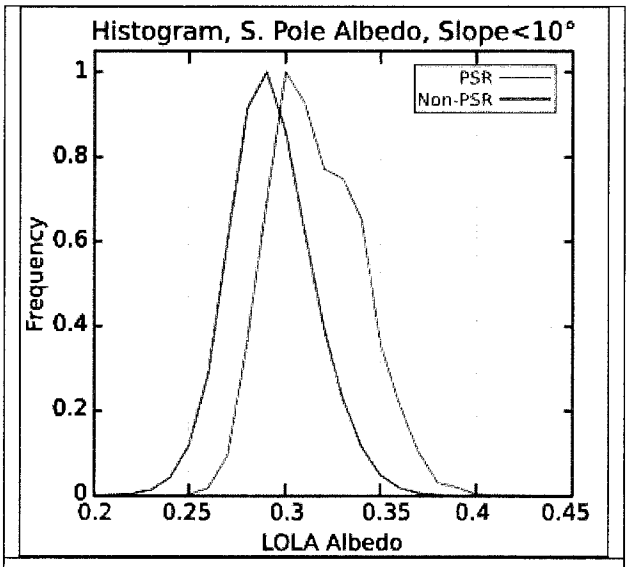

Figure 1. Distribution of reflectances for south polar PSR and illuminated areas showing that PSR are systematically more reflective than illuminated surfaces.

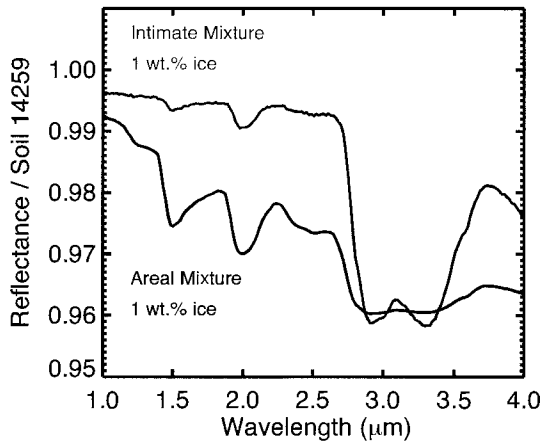

Figure 2. Spectra of intimate (well mixed) and areal (patchy) mixtures of ice, divided by dry lunar regolith. Intimate mixtures are best revealed by measurements near 3um, while patchy ice exposures are better detected near the overtone bands near 1.4 and 1.9 microns.

COMMUNICATION AND ILLUMINATION CONDITIONS AT INA D: AN INFORMATION FUSION APPROACH FOR LUNAR EXPLORATION PLANNING. P. Mahanti, M. S. Robinson, S. J. Lawrence, R. Stelling and A. Boyd (School of Earth and Space Exploration, Arizona State University, Tempe, AZ; pmahanti.lroc@gmail.com)

Introduction: Knowledge of line-of-sight and local solar illumination conditions (LoSSIC) drive science and exploration mission planning for lunar surface operations. Accurate knowledge of LoSSIC (derived from high resolution digital terrain models, or DTMs) greatly enhances communication and traverse planning. The use of viewsheds and solar illumination maps for selecting potential lunar landing sites can be found in earlier work [**1,2**]. However, lunar LoSSIC map products or tools for generating combined LoSSIC knowledge maps were not widely available since DTMs for LoSSIC evaluation have existed only recently at a scale relevant to surface landers and rovers. New high-resolution (2-m postings) Lunar Reconnaissance Orbiter Camera (LROC) Narrow Angle Camera (NAC) based DTMs [**3**] are now available for key sites on the Moon.

In this work a LoSSIC analysis is presented for the feature known as Ina D (18.634°N, 5.308°E); an enigmatic depression exhibiting both smooth mounds surrounded by a relatively rough floor [**4**], and is likely volcanic in origin is one of the youngest endogenic forms on the Moon [**5,6**]. Since Ina D is a high priority central nearside science target we choose it to demonstrate the utility of LoSSIC analysis for mission planning.

Methods: We first generated three basic (level 1) LoSSIC components from the NAC DTM and positional knowledge of the Earth, the Sun and the Moon in a fixed reference frame. All three components have a pixel sampling of 5 m.

The first component is the viewshed, a location (geographic/cell/pixel) specific visible area from one asset to another (traced out by scanning the LOS). The second LoSSIC component is an Earth visibility map that represents LoS availability between each surface location and Earth at a particular time (indicating the feasibility of direct-to-Earth (DTE) communication). The third LoSSIC component is a time dependent solar illumination map for the site (indicating the availability of solar power). In this study solar illumination maps and Earth visibility maps were generated over an analysis period of ~ 29.53 days sampled at 15 minute intervals. The basic LoSSIC components are stacked and then used to make the level 2 map products which represent information accumulated over time or possibilities (position of observer in case of viewsheds). In the case of viewsheds, the information accumulated over multiple observer positions is obtained by merging all

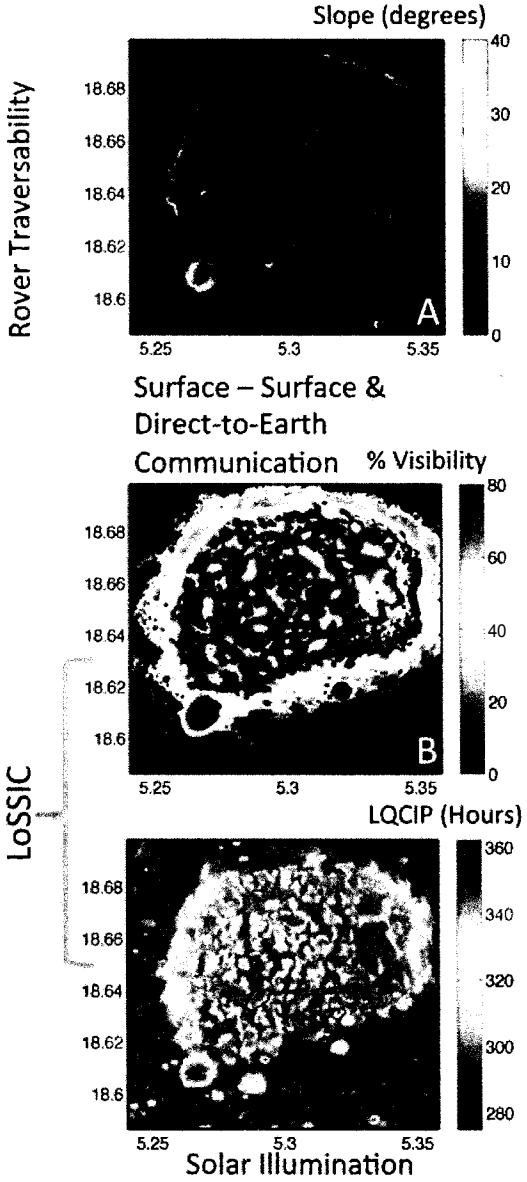

Figure 1: (A) Slope map for estimating rover traversability conditions. (B) Visibility index map for Ina D showing what percentage (area) of the entire site is visible from a location. (C) Continuous solar illumination availability in hours.

possible viewsheds to form a visibility index map (**Fig. 1B**). For Earth visibility, the probability of the Earth being visible for the entire analysis period is evaluated. For the Ina D site every location always visible from Earth (a nearside exploration was assumed to minimize complexity). Information is accumulated from the stack of illumination maps by computing at each location the duration of the longest quasi-continuous illu-

mination period (LQCIP [1]) (**Fig. 1C**) and also the probability of a continuous illumination for an hour. In addition to LoSSIC, surface slope (15 m baseline) was generated (**Fig. 1A**) from the DTM for use as a roughness parameter indicating rover traversability conditions. The LoSSIC information aggregates and the rover traversability information were combined in an information fusion framework. Fusion methods can be a simple weighted average (used for this example) or Bayesian networks which would take into account the uncertainty present at each location.

Discussion: The aspect of resolution is vital if viewsheds, illumination maps and other similar products are used for predictive analysis in the planning phase for a lunar mission. At lower resolutions, uncertainty magnitudes related to LoS computations are higher [7] making their use inefficient and possibly misleading. Changes in illumination with time (direction and magnitude) can be used to define the required velocity of a rover for a traverse segment and can also affect the traverse path selection (to maintain a particular speed between waypoints under specific illumination conditions). However, effectiveness of such computations improves as the map sample spacing approaches the physical dimensions of a rover (2 m or smaller). Moreover minimum elevation uncertainty is also important (NAC DTM products at 5 m/pixel have an elevation uncertainty less than 0.5 m).

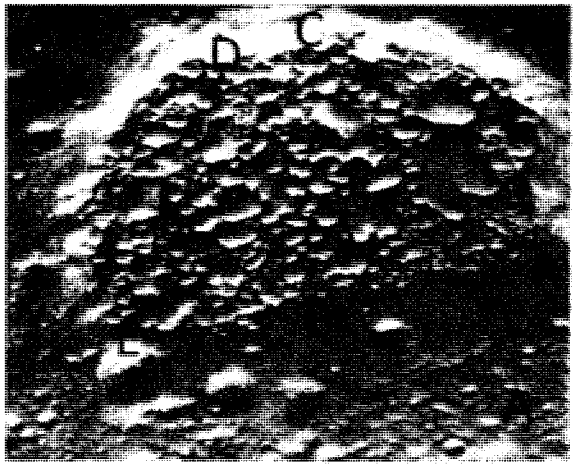

Figure 2: LoSSIC and traversability for Ina D; colors are formed as Solar illumination availability (R,) Slope (G) and Percent visibility (B).

Structured information accumulation improves efficiency during the exploration planning process and this is the focus of this work. While viewsheds are useful by themselves, N^2 viewsheds are possible for a DTM raster of side N cells making individual viewshed assessment inefficient while evaluating the condition for the entire site. Visibility indices enable a hierarchical scheme for statistically assessing the feasibility of a location for surface communication purposes. Higher values indicate better locations for setting up antennas. For Ina D, a region of high visibility in the north (**Fig. 1B**) also indicates an efficient traverse route for scouting. The associated local slopes are less than 25°. The Earth visibility map was not analyzed separately for Ina D because at every location on the visibility index map a DTE link exists.

The spatio-temporally accumulated LoSSIC information can be used directly for making decisions during the planning phase and in defining the mission conops. Visualization based methods are a powerful tool for reducing multiple layers of information to a sensible map. In this work, LoSSIC and slope information are displayed together (**Fig. 2**) by using a pseudo RGB colormap (R-solar illumination availability, G-slope, B-percent visibility index). The resulting colors display the conditions of all the variables aid decision making (**Table 1**) in an easily interpretable form.

Table 1: Color based exploration planning

Region	Color explanation from component state	Remarks
A	High solar illumination, Low slope, low visibility index	Landing/ touchdown location
B	High solar illumination, Low slope, high visibility index	Waypoint to the interior caldera
C	High solar illumination, low slope, high visibility index	Scouting without risk
D	High solar illumination, high slope, high visibility index	Scouting with risk
E	High solar illumination, High slope, low visibility index	Illuminated crater

Conclusion: High quality LoSSIC information integrated over time and spatial extents simplify future lunar exploration planning. An example of Ina-D was chosen in this work to illustrate the proposed method of extracting information for 3 key pertinent variables (LoS between surface assets, LoS between a surface asset and Earth, and solar illumination availability). Regions near the poles have more complicated Earth viewing and solar illumination conditions that are easily delimited and integrated with LoSSIC products for cognizant mission planning.

References: [1] Diego De Rosa et al., Planetary & Space Sci.,74(1), 224-246 (2012) [2] Mahanti et al. *Proc.* Annual Meeting of the Lunar Exploration Analysis Group *No. 1748* (7014). [3] Tran, T., et al. *Proc. ASPRS/CaGIS Fall Specialty Conference.* (2010). [4] Strain, P. L. and El-Baz, F. *Proc. Lunar Sci. Conf.* 11, 2437–2446 (1980). [5] Braden et al., *Nat. Geo.*, in review. [6] Schultz et al.. *Nature* 444, 184-186 (2006). [7] Mahanti et al. *Proc. Lunar Sci. Conf. 44*, 1739 (2013).

LUNAR POLAR ILLUMINATION MODELING TO SUPPORT DATA ANALYSIS. Erwan Mazarico[1], Joseph B. Nicholas[2], Timothy P. McClanahan[1], Gregory A. Neumann[1]. [1] Planetary Geodynamics Laboratory, NASA Goddard Space Flight Center, Greenbelt, MD 20771, USA (erwan.m.mazarico@nasa.gov); [2] Emergent Space Technologies, Greenbelt, MD 20770, USA.

Introduction: Regions of extreme insolation environments exist in the polar regions of the Moon because of its low obliquity and lack of an atmosphere. Altimetric data from the Lunar Orbiter Laser Altimeter (LOLA) [1] yield precise high-resolution topographic maps of the poles, which enable the computational modeling of the solar illumination and thermal environment [2,3]. In addition to the determination of the permanently shadowed regions (PSRs) and their relationship to remote sensing data such as neutron flux observations [4] and surface albedo [5], we show that the modeling of the illumination conditions can be helpful for data calibration and data analysis of scientific datasets, such as the LEND data [4].

Method: As outlined in [2], our approach is to precompute the angular elevation of the horizon from each point in the region of interest. This expensive but one-time computation has been parallelized to achieve larger study areas and higher resolution. The resulting horizon data allow rapid direct comparison to the elevation of a source at any time. While we previously computed solar illumination for large polar regions at every time step to obtain average illumination maps, we can readily perform calculations on small patches of the surfaces. This can prove useful to reproduce the geometry of specific spacecraft observations, as the illumination modeling only needs to be done over a given field of view at any given time. Therefore, for data calibration and analysis, the increased number of temporal steps (e.g., one measurement per second, instead of the more typical hourly timesteps, e.g. [2]) can be compensated by the limited spatial extent to be modeled. Figure 1 illustrates the application to LEND.

Analysis: Algorithm improvements have allowed us to update our past results [2] over both poles (65-90°) with improved resolution. The information in each field-of-view can be condensed statistically, to create time series of average illumination (Figure 2), illumination texture, etc., to be compared with the measurements. The study of insolation-driven variability of the LEND-measured neutron counts [6] can potentially benefit from the modeling of actual illumination conditions over the instrument footprint, as the local solar time is not necessarily an accurate proxy for actual insolation in the polar regions.

References: [1] Smith D. E. et al. (2010) *GRL*, 37, L18204. [2] Mazarico E. et al. (2011), *Icarus*, 211, 1066. [3] Paige D. et al. (2010), *Science*, 330, p479-482. [4] Mitrofanov I. G. et al. (2010) *Science*, 330, 483-486. [5] Gladstone G. R. et al. (2011), JGR, 117, E00H04. [6] Livengood T. A. et al., AGU 2013, P51B-1733.

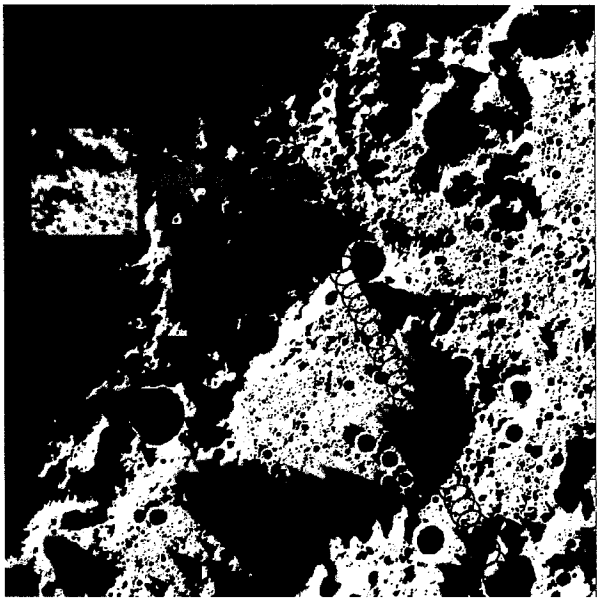

Figure 1. The illumination conditions of all the pixels within each LEND footprint (red circles) are calculated with the exact solar, lunar and spacecraft positions. The red insert shows the obtained sun visibility for each pixel in one LEND footprint.

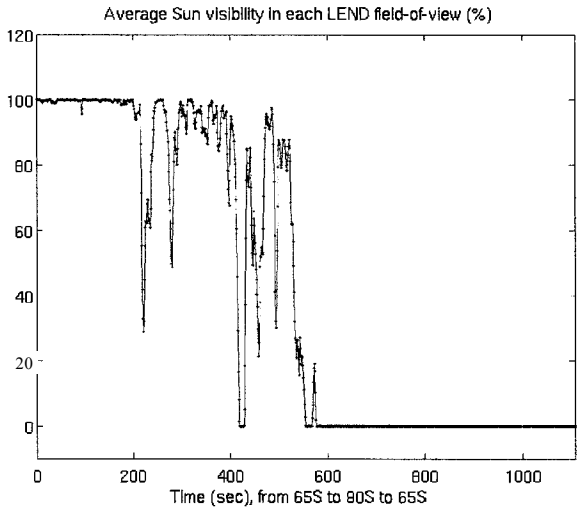

Figure 2. Average sun visibility in the LEND field-of-view over the north polar region during one LRO orbit.

Epithermal Neutrons, Illumination, Spatial Scale and Topography: An Correlative Analysis of Factors Influencing the Detection of Slope Hydration using LRO's Lunar Exploration Neutron Detector. T.P. McClanahan[1], I.G. Mitrofanov[2], W.V Boynton[3], G. Chin[1], R.D. Starr[4], L.G. Evans[5], A. Sanin[2], T. Livengood[1,6], A. Parsons[1], E. Mazarico[1], R. Sagdeev[6], J. Bodnarik[3], K. Harshman[3], D. Hamara[3], J. Su[6], J. Murray[6], M. Litvak[2], Astrochemistry Laboratory, NASA Goddard Space Flight Center, Greenbelt, MD 20771, (timothy.p.mcclanahan@nasa.gov), [2]Institute for Space Research, RAS, Moscow 117997, Russia, [3]Lunar and Planetary Laboratory, Univ. of Arizona, Tucson AZ, [4]Catholic Univ. of America, Washington DC, [5]Computer Sciences Corporation, Lanham MD 20706, [6]Univ. of Maryland, College Park.

Introduction: In this research we correlate the Moon's south polar epithermal neutron flux, topography and a visible illumination model to illustrate evidence that there is a widespread hydration of polward-facing (PF) slopes that is occurring at a continuum of spatial scales. By limiting our analysis to large PF slopes we show that there is a broad decrease in the lunar epithermal neutron flux derived over the large PF slopes relative to the average lunar induced epithermal flux derived over all PF slope conditions. The additional ~1% decrease in epithermal neutron flux over large PF slopes raises the EF vs PF rate contrast to ~2% near the south pole. Results also indicate that an identical scale-dependent comparison of epithermal rates derived over equator-facing (EF) slopes do not contrast, inferring that hydrogen concentrations on those slopes are in equilibrium with local levels. Fully registered south polar maps derived from the Lunar Reconnaissance Orbiter's Lunar Exploration Neutron Detector (LEND) as well as topography and an illumination model derived from the Lunar Observing Laser Altimeter (LOLA) are correlated to characterize slope conditions [1-3]. Regolith temperature does not appear to be an influence in the slope epithermal rates. Lunar Prospector Neutron Spectrometer (LPNS) and LEND's Sensor for Epithermal Neutrons (SETN) corroborate these results but to a lesser extent [4].

Background: Strong evidence for hydrogen concentrations at the lunar poles has been observed by both LPNS, and more recently LEND as indicated by a broad ~4% suppression in the epithermal neutron flux. For decades the prevailing hypothesis had been that cryogenic conditions in permanently shadowed regions were necessary for near surface concentrations of hydrogen [5]. LPNS and LEND results show the suppression of epithermal neutron flux begins near ±70° latitude. Yet only ~1% of this latitude band lies in permanent shadow. Also, evidence from LEND's Collimated Sensor for Epithermal Neutrons, (CSETN) indicate that only a few of the permanently shadowed regions (PSR)'s contain significantly enhanced concentrations of hydrogen [6]. So, what explains the polar epithermal flux suppression?

A possible explanation lies in evidence derived from near infra-red observations. Results from Chandraayan-1's Moon Mineralogy Mapper M^3, suggested enhanced concentrations of hydrogen are diurnally associated with the darkened slopes of mid-latitude craters [7]. Deep Impact suggested a global scale production process where solar wind interactions with regolith oxygen-bearing minerals yield hydroxyl and water [8]. Further, recent re-analysis of M^3 data suggest surface hydrogen concentrations begin near ±40° latitude and increase to ~1000's of ppm hydrogen diurnally present at latitudes above ±60° [9].

Our hypothesis unifies the epithermal and infrared results by suggesting that the broad polar-suppression of epithermal neutrons is primarily due to the localized trapping of hydrogen on PF slopes where locally minimum temperatures and illumination conditions may provide trapping conditions in a continuum of spatial scales perhaps down to a meter. Also, that the nccessary PF trapping conditions for hydrogen increase towards the poles.

If our hydrogen trapping hypothesis is correct, then considerations derived from convolution theory provide two predictions regarding the detection of hydrogen in slope conditions. **H1**) The suppression of epithermal count rates should increase in large PF slope conditions as compared to all slope conditions. In these locations hydrogen concentrations are expected to be maximized. Plus, the large slopes subtend a greater fraction of the CSETN field-of-view than small slopes. **H2**) EF slopes are postulated to be anhydrous. If so, there should be no epithermal rate contrast due to those slopes spatial scale.

Methods: To study slopes as a function of spatial scale we decompose the LOLA topography as a function of slope aspect to isolate PF and EF slopes. Fully registered epithermal neutron count rates derived over PF and EF slopes are averaged by convolving a 10° latitude-band analysis window from west to east longitudes between -45° to -90° latitude, using 0.5° latitude steps. At each center position of the window the average epithermal count rates are calculated for PF and EF pixels. A parallel analysis of a LOLA visible illumination model [10] is included to quantify the contrasting average illumination conditions on

PF and EF slopes. Average visible illumination is also used as a proxy for slope temperatures.

Large scale slopes are classified and segmented from the topography as a function of their local variation in slope aspect and its first derivative properties of slopes in craters. PF and EF pixels are aggregated by a region growing process. Small scale slopes whose pixel aggregate areas fall below 15-km^2 area are eliminated, thus isolating large scale slopes.

Results: *Figures-1a,b* illustrate corresponding visible illumination and epithermal neutron % rates derived over LOLA topography as a function of slope aspect and latitude. (*Fig-1a: left*) Baseline visible illumination results illustrate the lower levels of average illumination modeled for PF slopes (*light blue*) relative to equivalent illumination rates modeled for EF slopes (*green*) vs. latitude. Rates derived for large scale slope conditions show the average illumination goes up by 0 to 3% for EF conditions (*red*) and down 2 to 7% for PF (*dark blue*) conditions. Relative rates derived for large scale slopes suggest the isolation of spatially larger and deeper features.

(*Fig-1b: right*) Corresponding baseline epithermal neutron count rates on poleward (*light blue*) and EF (*green*) slopes as a function of latitude. **H1**) Results show the relatively decreased rates on PF slopes between -50° W and -60° E that are consistent with expected illumination trends. At the pole the rate difference is ~1% of the lunar induced epithermal count rate. In large scale slope conditions the suppression of epithermal neutron rates on PF slopes (*dark blue*) is enhanced by an additional ~1%, yielding a ~2% contrast at the poles. The contrast decreases towards mid-latitudes. Importantly, the rates derived from large-scale EF conditions (*red*) are equivalent to the rate of the baseline measurements (*green*). This result is consistent with **H2**) Non-contrasting epithermal rates derived over EF slopes suggest anhydrous conditions that are in equilibrium with local near surface hydration conditions.

Conclusions: Our results indicate that there is a widespread hydration of PF slopes occurring in a continuum of spatial-scales, possibly down to the level of a meter-scale in latitudes >±60°. Evidence for the hydrogen concentration bias towards PF conditions is that epithermal neutron rates from PF slopes are scale dependent and EF slopes are not. This result importantly suggests EF slopes are hydrated to local equilibrium levels.

If slope temperature was the sole contributor to the observed epithermal-rate contrasts we should expect: 1) In EF conditions epithermal rates should go up with the observed illumination rates, they don't. 2) Temperature should provide a uniform contribution to the rate contrasts as slope scale distributions are assumed similar in low to high latitudes. Instead the rate contrasts are maximized at the poles and diminish towards mid-latitudes.

References: [1] Vondrak et al. (2010) *Sp. Sci. Rev., 150(7-22)* [2] Mitrofanov et al.(2010) *Sp. Sci. Rev., 150(183-207)* [3] Smith et al.(2010) *Sp. Sci. Rev., 150(1-4)* [4] Feldman et al. (1998) *Science*, 281(5382) [5] Arnold (1979) *JGR 84-B10* [6] Sanin et al., (2012) JGR-Planets 117-E12 [7] Pieters et al., (2009) *Science*, (23) 568-572 [8] Sunshine et al., (2009) *Science* (326) 595 [10] Li et al. *Proc. of the 44th Lun. and Plan. Sci. Conf.* #1337

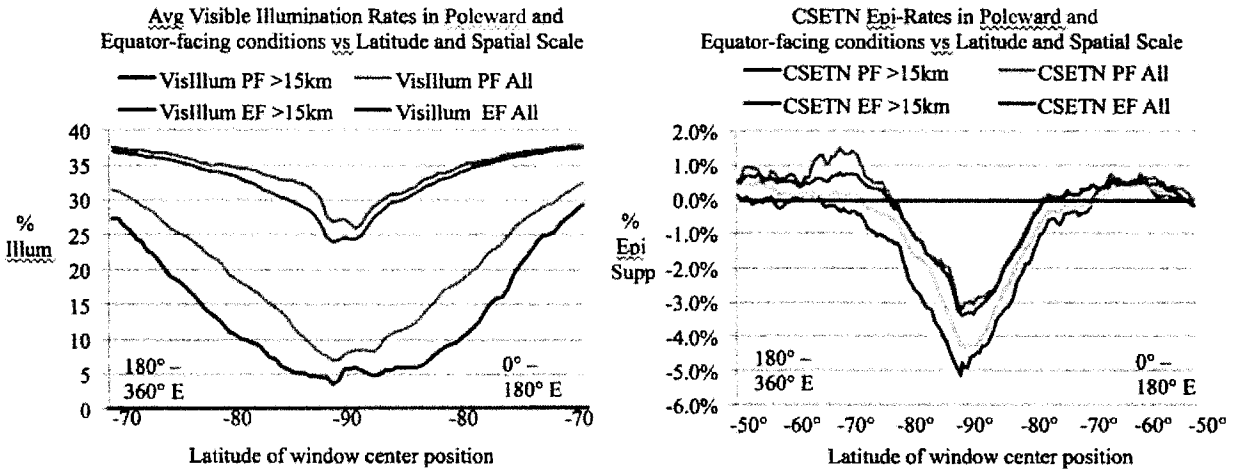

Figure 1: (*left*) Plots of Visible Illumination rates on poleward and EF conditions vs latitude and slope spatial scale. By limiting the slope analysis to slopes of larger spatial scale (>15km) compared to the baseline rates (All) illumination rates increase (*red*) in equator-facing conditions and decrease (*dark blue*) for poleward-facng conditions. (*right*) Plots of corresponding epithermal rates vs latitude and slope spatial scale. The suppression of epithermal rates is enhanced by ~2% of the lunar induced epithermal rate at the pole for large-scale slopes in PF conditions as compared to the baseline evaluation for both EF scale conditions. In EF conditions the rates for both large and All cases are equivalent suggesting hydration on EF slopes is in equilibrium with local surroundings.

VOLATILES (H, C, N, F, S, CL) IN THE LUNAR MANTLE, CRUST, AND REGOLITH: WHAT QUESTIONS REMAIN AND WHERE DO WE GO NEXT? F. M. McCubbin[1] and C. K. Shearer[1] [1]Institute of Meteoritics, University of New Mexico, Albuquerque, NM 87131. fmccubbi@unm.edu

Introduction: Magmatic volatiles (H_2O, H_2, CO_2, CO, CH_4, HCl, HF, H_2S, SO_3, N_2, NH_3, noble gases, etc.) affect a wide range of important physical properties of geologic materials from the stability of minerals and melts to the structural and rheological characteristics of various rocks and minerals. On the Moon, magmatic volatiles are poorly understood, and the magmatic volatile inventory of the lunar mantle, crust, and surface, aside from being very low, is largely unconstrained. Although the Moon is volatile-depleted [e.g., 1], there is evidence indicating that magmatic volatiles have played a role in a number of geologic processes within and on the Moon.

In recent years, there has been a focused effort to determine the abundances and distributions of magmatic volatiles in lunar materials both through laboratory studies and through orbital spacecraft-based investigations. These modern efforts were largely sparked by substantial advances in detection sensitivity for a number of analytical/remote observation techniques, which led to a renaissance in the study of lunar volatiles that largely started in 2007 when two groups independently began reassessing the hydrogen inventory of lunar samples [2-3]. In addition to all of these recent analyses of volatiles, there were substantial efforts in the 1970's and to a lesser extent the 1980's and 90's to understand the abundances, distribution, and origin of volatiles in lunar materials. Little effort has been made to bridge the initial studies of lunar volatiles to more recent ones. Furthermore, many of the results from sample analysis and remote sensing are highly complementary in nature, and little has been done to merge these data sets into a clear picture of volatiles in and on the Moon. A recent review paper forthcoming in The Lunar Highlands Special Issue in American Mineralogist [4] has compiled information and data on the elements H, C, N, F, S, and Cl in lunar materials and from lunar remote sensing to determine what we know about volatiles and their respective isotopes on the Moon.

Findings and Progress in lunar volatiles: In the review [4], the authors provide the first complete inventory of volatile-bearing minerals that have been reported to occur in lunar samples, along with an estimated likelihood of existence. Analyses of volatiles from lunar glass beads as well as the phase assemblages present in coatings on those beads were used to determine that H_2 is likely the primary gas phase most responsible for propelling the eruptions that produced the pyroclastic glass beads as opposed to CO with an H_2/H_2O molar ratio in the vapor species of about 10:1 at 1 log unit below the IW buffer at 1300 °C. Mineral-melt partitioning data and analyses of volatiles in lunar soils, glasses, and apatites were used to estimate the relative and absolute abundances of some volatile elements within the bulk Moon, urKREEP, lunar mantle, and crust. Sample studies on lunar soil and remote sensing data are combined to better understand the distribution, origin, and abundances of volatiles on the lunar surface. Isotopic data on volatile elements is used to determine possible sources and reservoirs in and on the Moon. Finally, a compilation of unanswered questions and future avenues of research are presented along with a critical analysis of approaches for answering these questions, which we include in the next section below.

Outstanding questions and future avenues: *1) What volatile-bearing minerals are indigenous to lunar samples?* Many of the volatile-bearing minerals that have been reported in lunar rocks remain "unverified" and a modern effort to re-examine some of these samples with modern techniques could yield additional important mineral systems through which one can try to understand lunar volatiles. A substantial effort has been put forth to understand the mineral apatite and what secrets it holds regarding volatiles in the lunar environment, but apatite is a complicated mineral to use for determining volatile abundances [i.e., 5-6], and we still have a lot to learn from it. Including additional volatile-bearing mineralogical systems, if present, would greatly enhance the wealth of information about volatile abundances and isotopic compositions of the Moon, which could potentially move the field forward much further than with apatite alone.

2) Concentrations and distribution of volatiles in the lunar interior. Estimates of the relative abundances of H_2O, F, and Cl in the lunar mantle differ substantially from the estimated relative abundances of H_2O, F, and Cl in urKREEP (i.e., mantle has $H_2O > F > Cl$, urKREEP has $Cl > H_2O \approx F$). Either the estimates for volatile abundances in urKREEP and lunar mantle are inaccurate, or a process that forces the lunar mantle to preferentially store H_2O and F and exclude Cl during LMO crystallization must be at work. The partitioning behavior of H_2O, F, and Cl between pyroxene and silicate melt could operate to include F, and OH in the

mantle while excluding Cl, or there is another phase in the LMO cumulate pile in which F and H_2O are compatible and Cl is incompatible (Fe-Ti oxides?). Experimental work on mineral-melt partitioning of H_2O, F, and Cl between LMO minerals (olivine, pyroxene, Fe-Ti oxides, and anorthitic plagioclase) and silicate melt under reducing conditions relevant to lunar magmatism could help shed light on this issue. Furthermore, the continued analysis of volcanic glasses, including the A-14 KREEP-rich glasses [7] will help constrain the volatile abundances in the lunar mantle and in urKREEP. Lastly, the continued analysis of apatite in mare basalts (including the KREEP basalts), with a specific focus on variations among petrologic types, will help one to understand the range in volatile compositions of the various lunar mare source regions.

3) What are the sources and/or reservoirs of volatiles on the Moon? It is still very unclear whether or not the isotopic variations in H and Cl in volcanic lunar samples are being primarily driven by fractionation processes or mixing of various reservoirs. Given that almost the entire spread of $\delta^{37}Cl$ values observed in lunar samples is thus far observed only on the Moon, it is highly likely that Cl has been fractionated by some process on the Moon, but the process responsible has yet to be proven. Sharp et al. [8] provided evidence for Cl-isotope fractionation occurring as a result of degassing or vaporization of metal chlorides, but this process has yet to be demonstrated experimentally. In fact, experimental work on Cl-degassing from H-poor silicate melts under reducing conditions relevant to lunar magmatism is highlighted here as an important avenue of future research. Determining the fractionation process is a prerequisite to solving the question of the origin of the seemingly heavy Cl isotopic signature in urKREEP. Importantly, this process does not seem to have pervasively affected the lunar mantle in the same way it has affected the lunar crust.

H isotopes were likely affected by secondary processes and mixing of multiple reservoirs, which preclude straightforward interpretations of the existing data. From the plethora of data on lunar soils, it is clear that there is a very light (~-1000 ‰) reservoir of solar wind and a fairly heavy reservoir of spallogenic D at the lunar surface available for assimilation into erupted lava flows and impact melts. Furthermore, there has been substantial meteoritic and cometary infall to the Moon over the last ~4.35 Ga that could have produced distinct pockets of unique hydrogen isotopic reservoirs in and on the Moon. On account of low oxygen fugacity prevalent in the Moon, H_2 would dominate over H_2O in any degassing vapor, which would cause substantially higher isotopic fractionation of H compared to H_2O-dominated systems. Additional challenges involve identification of any terrestrial contamination in lunar samples and thin sections (e.g., thin section epoxy or terrestrial water in cracks). All of these possible sources could affect our ability to determine the indigenous H isotopic composition of the Moon, which many have recently argued is essentially the same as Earth and chondrites [9-12]. This tantalizing possibility of a common source for water in the Earth-Moon system is gaining traction, but further support for this idea will require placing the isotopic data in the context of Petrographic textures and timing of crystallization. For example, Tartèse et al. [12] report SIMS data for apatites in KREEP basalt 15386, for which apatite H_2O contents increase with decreasing δD values. Petrographic observations show that while most of the apatite grains in 15386 occur closely associated with late stage mesostasis areas, one apatite analyzed is included within a pyroxene, suggesting it crystallized relatively early. Interestingly, this apatite grain is characterized by the lowest δD (~ 90 ± 100 ‰) and highest OH content (~ 780 ppm H_2O), which is precisely what one would expect if the observed OH/δD relationship in apatites in 15386 resulted from crystallization during progressive magmatic degassing of H_2.

References: [1] Taylor et al., (2006) *GCA*, 70, 5904-5918. [2] McCubbin, F.M., Nekvasil, H., and Lindsley, D.H. (2007) *Proc 38th LPSC*. #1354. [3] Saal, A. E., Hauri, H., Rutherford, M.J., and Cooper, R.F. (2007) *Proc 38th LPSC*. #2148. [4] McCubbin, F.M. et al., (In Review) *Am. Min.* [5] Boyce et al., (2014) *Science*, 344, 400-402. [6] McCubbin et al., (In Review) *EPSL*. [7] Shearer C. K. et al., (1991) *EPSL*, 102, 134-147. [8] Sharp, Z.D. et al., (2010) *Science*, 329, 1050-1053. [9] Barnes, J.J. et al., (2014) *EPSL*, 390, 244-252. [10] Saal, A.E. et al., (2013) *Science*, 340, 1317-1320. [11] Tartese et al., (2013) GCA, 122, 58-74. [12] Tartese et al., (2014) Geology, 42, 363-366.

Acknowledgements: I would like to acknowledge all of the coauthors and contributors to the submitted review paper on lunar volatiles that is currently in review in American Mineralogist, including Kathleen E. Vander Kaaden, Romain Tartèse, Rachel L. Klima, Yang Liu, James Mortimer, Jessica J. Barnes, Allan H. Treiman, David J. Lawrence, Stephen M. Elardo, Dana M. Hurley, Jeremy W. Boyce, and Mahesh Anand.

Cross Calibration of Omnidirectional Orbital Neutron Detectors LPNS of Lunar Prospector and SETN/LEND of Lunar Reconnaissance Orbiter. J. Murray[1], J.J. Su[1] (jjsu@umd.edu), R. Sagdeev[1], G. Chin[2], T. McClanahan[2], T. Livengood[3] , R.D. Starr[4], L.G. Evans[5] [1]University of Maryland College Park, Physics, College Park, MD, United States, [2]NASA Goddard Space Flight Center, Greenbelt, MD, United States, [3]CRESST/UMD/GSFC, Greenbelt, MD, United States, [4]Catholic Univ. of America, Washington DC, [5]Computer Sciences Corporation, Lanham MD

Introduction: The lunar neutron spectrum is sensitive to hydrogen-bearing volatiles such as water or hydroxyl in the Moon's regolith. Monte Carlo (MC) simulations have been used to investigate neutron production and leakage from the lunar surface to assess lunar surface compositions [1-2]. Orbital neutron spectroscopy has become a standard technique for access of planetary chemical composition from orbit. The Lunar Prospector Neutron Spectrometer (LPNS)[3] of the Lunar Prospector mission and the Lunar Exploration Neutron Detector (LEND)[4] of the Lunar Reconnaissance Orbiter mission were the most recent orbital measurements with similar omnidirectional helium-3 neutron proportional counters. These two instruments have different angular sensitivities and neutron detection efficiencies because of the geometries and helium 3 pressures. In addition, the Lunar Prospector's spin-stabilized design makes its detection efficiency latitude-dependent, while the SETN instrument faces permanently downward toward the lunar surface.

We use the GEANT4 Monte Carlo simulation code[5] to investigate the leakage lunar neutron energy spectrum, which follows a power law of the form $E^{-0.9}$ in the epithermal energy range, and the signals detected by LPNS and SETN in the LP and LRO mission epochs respectively. Using the lunar neutron flux reconstructed for LPNS epoch, we calculate the signal that would have been observed by SETN at that time. The subsequent deviation from the actual signal observed during the LEND epoch is due to the significantly higher intensity of Galactic Cosmic Rays during the anomalous Solar Minimum of 2009-2010.

[1] W. C. Feldman, et al., (1998) Science Vol. 281 no. 5382 pp. 1496-1500. [2] Little, R. C., et al. (2003), J. Geophys. Res., 108(E5), 5046. [3] W. C. Feldman, et al., (1998) Science Vol. 281 no. 5382 pp. 1496-1500. [4] I.G. Mitrofanov et al., Space Sci Rev (2010) 150: 183–207. [5] J. Allison, et al, (2006) IEEE Trans. on Nucl Sci, Vol 53, No 1.

MODULAR HEAT FLOW PROBE FOR SMALL LUNAR LANDERS. S. Nagihara[1], K. Zacny[2], M. Hedlund[2], and P. T. Taylor[3], [1]Department of Geosciences, Texas Tech University, Lubbock, TX 79409 (seiichi.nagihara@ttu.edu), [2]Honeybee Robotics, Pasadena, CA 91103, [3]Goddard Space Flight Center, Greenbelt, MD 20711.

Introduction: Heat flow measurement is considered a top priority for future lunar-landing missions by the latest Decadal Survey by the National Research Council [1]. The Survey recommends a *New Frontiers*-class, *Lunar Geophysical Network* (LGN) mission, which would deploy a 'global, long-lived network of geophysical instruments on the surface of the Moon' and that heat flow measurement would be a part of it. Besides LGN, a number of robotic and human lunar-landing missions are proposed by government agencies and private organizations such as *Resource Prospector*, *SELENE-2*, *Luna-Glob*, *Golden Spike*, and the missions competing for the Google Lunar X Prize.

Heat flow is obtained as a product of two separate measurements: the thermal gradient and the thermal conductivity of the depth interval of the regolith penetrated by a probe. A panel of scientists [2] recommend that a heat flow probe on a future lunar mission should penetrate to a minimum of 3 m into the lunar regolith, ~0.7 m deeper than the depth reached by the Apollo 17 heat flow experiments [3].

The enhancement in excavation capability is necessary for high-quality data, while a light-weight, compact system is desired for relatively small landers considered for the aforementioned missions. Here we report our progress in designing and testing prototypes of such low-mass, low-power lunar heat flow probes for possible use in future lunar robotic missions.

System Description: Our heat flow probe utilizes a pneumatic excavation system in deploying thermal sensors into the subsurface. The deployment mechanism (~28-cm tall, Fig. 1) of the probe spools out a glass fiber composite stem downward. The stem then forms a hollow cylinder of ~1.5-cm diameter (Fig. 2). It pushes the penetrating cone into the regolith, while gas jets, emitted from the cone tip, blow away loosened material. Removing material from the bottom of the excavated hole allows the stem to advance deeper with minimal thrust. A short (~1.5 cm), thin (~2-mm diameter) thermal probe attached to the cone tip measures temperatures and thermal conductivities of the regolith by stopping for 30 minutes at different depths on the way down. During each stop, to measure the thermal conductivity of undisturbed regolith, the probe shuts off the gas jet and pushes the needle probe into the bottom-hole regolith. After the stem reaches the targeted, 3-m depth, the temperature sensors embedded on the fully extended stem monitor long-term stability of the thermal gradient.

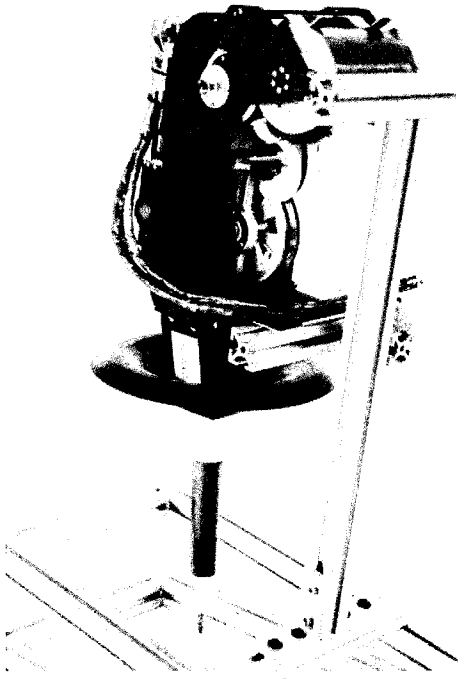

Figure 1. The latest prototype of the lunar heat flow probe with the stem stowed.

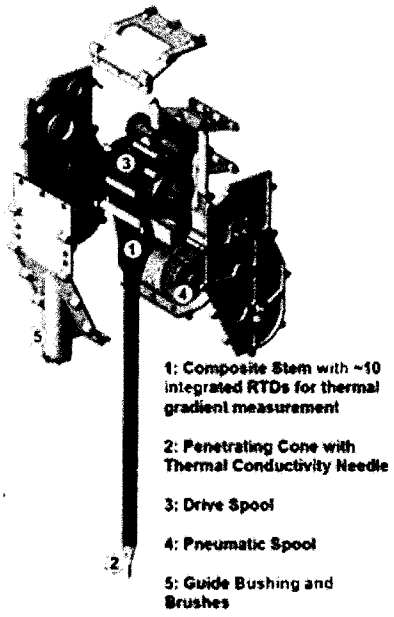

Figure 2. Schematics of the major components of the heat flow probe.

In its current design, the probe weighs 1.2 kg and can operate with a minimal power (< 10 W). The compressed gas required for excavation can be provided from a dedicated gas tank or from a pressurant tank which is part of the propulsion system (and in turn comes "free"). The gas excavation efficiency can reach 1:6000 (1 g of gas can loft 6000 grams of soil) in vacuum [4]. The use of the pneumatic excavation system enables more than 10 kg of saving in total mass, compared to a rotary-percussive drill such as the one used in the Apollo heat flow experiments [3].

Our heat flow probe is a modular system, and it can be accommodated into a variety of lander configurations. It only requires a stable platform for deployment on the lunar surface. It is also an ideal science payload for a human lunar-landing mission, because it is a set-it-and-forget-it system from the astronaut's point of view. All the astronauts need to do is to find a suitable location and set up the probe. Then, it can be remotely deployed from the earth [5].

Lab Tests: We have presented elsewhere the results from our thermal conductivity probe measurements on JSC-1A lunar regolith simulant in a vacuum chamber [6]. Here, we focus on our recent excavation tests using the latest prototype of the heat flow system (Fig. 1).

In our first test, the probe was deployed into well compacted JSC-1A lunar simulant filling a 1-m deep bin placed in a vacuum chamber set at 4 Torr. The penetrating cone reached the bottom of the bin in less than one minute, using 5 grams of nitrogen gas pressurized at 400 kPa, while weight on bit (WOB) was kept under 30 N most of the time (Fig. 3).

Next, we deployed the probe into NU-LHT-2M lunar highlands simulant filling a 3-m tall bin placed in a vacuum chamber. Using gas pressures and thrusting forces similar to our earlier penetration tests, we were able to advance the probe down 1.9-m depth into the simulant in ~2 minutes. The penetration stopped at that depth even at increased gas flow rates. Inspection after the test revealed that simulant particles were blown inside the hollow cylinder of the stem instead of being lofted between the stem and the borehole.

Finally, we carried out a stop-and-go operation test into NU-LHT-2M simulant in a vacuum chamber. The probe excavated down to 0.5-m depth, stopped for 30 minutes for a heating experiment for thermal conductivity measurement, resumed excavation down to 1-m depth, and carried out another heating experiment successfully. This demonstrated that it is possible to stop and re-start penetration, and in turn conduct thermal conductivity tests at various depths.

Discussion and Future Work: Our excavation test fell short of reaching the 3-m target depth because some regolith particles found their way into the interior of the hollow, cylindrical glass-fiber stem. The regolith particles inside the stem also made their way into the deployment mechanism and caused it to jam. We are now designing a new stem that can prevent regolith particles from entering its interior. We believe that would enable us to reach the targeted 3-m depth. On a separate test, we have already confirmed that a 3.5-m long, hollow aluminum tube can penetrate to 3-m depth into NU-LHT-2M just by blowing gas down the tube and its nose cone. The 3-m depth was reached in 3 minutes.

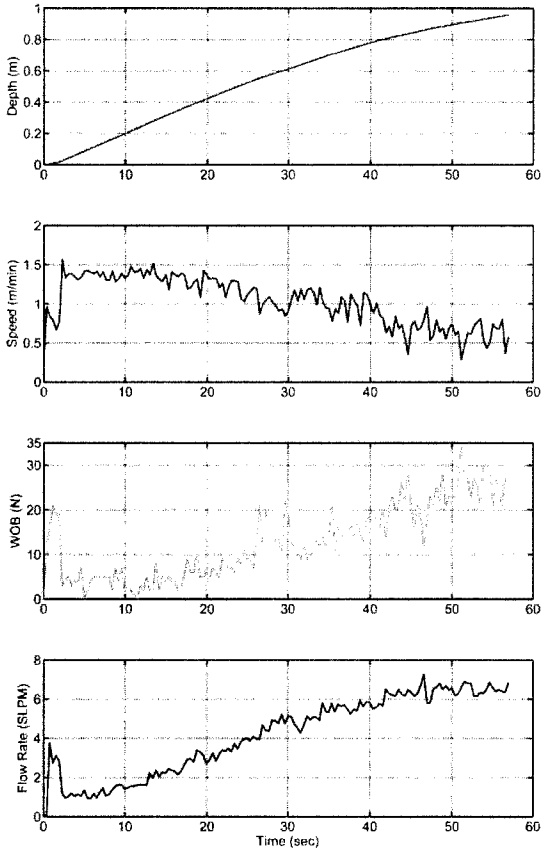

Figure 3. Instrument readouts from the 1-m excavation test on JSC-1A lunar regolith simulant in vacuum chamber.

Acknowledgments: This work is supported by NASA under 10-PIDDP10-0028.

References: [1] National Research Council (2011) pub# 13117. [2] Cohen, B. A. et al. (2009) *ILN Final Report*. [3] Langseth et al. (1976) *LPSC VII* 3143-3171. [4] Zacny, K. et al. (2011) *LEAG* 2028. [5] Nagihara, S. et al. (2013) *Workshop on Golden Spike Human Lunar Expedition*, 6003. [6] Nagihara, S. et al., (2012) *International Workshop on Instrumentation for Planetary Missions*, 1014.

Developing The Global Exploration Roadmap. C. R. Neal[1], G. Schmidt[2], I. A. Crawford[3], P. Ehrenfreund[4], J. Carpenter[5]. [1]Dept. Civil & Env. Eng. & Earth Sciences, University of Notre Dame, Notre Dame, IN 46556 USA (neal.1@nd.edu), [2]SSERVI, NASA Ames Research Center, Moffett Field, CA (gregory.k.schmidt@nasa.gov), [3]Department of Earth and Planetary Science, Birkbeck College, University of London, UK (i.crawford@ucl.ac.uk), [4]Elliott School of International Affairs, George Washington University, Washington DC 20052 USA (pehren@gwu.edu). [5]ESA-ESTEC, 2201 AZ, Noordwijk, The Netherlands (James.Carpenter@esa.int)

Introduction: The Global Exploration Roadmap (GER, [1]) has been developed by the International Space Exploration Coordination Group (ISECG – comprised of 14 space agencies) to define a pathway to get humans beyond low Earth orbit and eventually to Mars. This document has been written at a high level and many details are still to be determined. However, a number of documents regarding international space exploration can inform this document (e.g. [2,3]).

In this presentation, we focus on developing the "Humans to the Lunar Surface" theme of the current GER [3] by adding detail via mapping a number of recent reports/documents to it. Precedence for this scenario is given by Szajnfarber et al. [4] who stated after the initial GER [2] "We find that when international partners are considered endogenously, the argument for a "flexible path" approach is weakened substantially. This is because international contributions can make "Moon first" economically feasible".

The documents highlighted here are in no way meant to be all encompassing and other documents can and should be added, (e.g., the JAXA Space Exploration Roadmap). This exercise is intended to demonstrate that existing documents can be mapped into the GER despite the major differences in granularity, and that this mapping is a way to promote broader national and international buy-in to the Lunar Vicinity scenario.

The documents used here are: the Committee on Space Research (COSPAR) Panel on Exploration report on developing a global space exploration program [5], the Strategic Knowledge Gaps (SKGs) report from the Lunar Exploration Analysis Group (LEAG) [6], the Lunar Exploration Roadmap developed by LEAG [7], the National Research Council report Scientific Context for the Exploration of the Moon (SCEM) [8], the scientific rationale for resuming lunar surface exploration (SR [9]), the astrobiological benefits of human space exploration [9,10].

A Summary of the Global Exploration Roadmap [1]: The common goals are as follows:

- Develop Exploration Technologies & Capabilities.
- Engage the Public in Exploration.
- Enhance Earth Safety.
- Extend Human Presence.
- Perform Science to Enable Human Exploration.
- Perform Space, Earth, and Applied Science.
- Search for Life.
- Stimulate Economic Expansion.

Three paths are articulated to get to Mars - Exploration of a near-Earth asteroid; Extended duration crew missions; Humans to the lunar surface. The GER gives 5 goals for the Lunar Surface scenario:

- Technology test bed (surface power systems, long distance mobility concepts, human-robotic partnerships, precision landing).
- Advance knowledge base related to use of lunar resources.
- Characterize human health/performance in a reduced gravity environment beyond Earth's magnetosphere.
- Conducting high priority science benefiting from human presence, (inc. human-assisted sample return).
- Explore landing sites for extended durations.

The Mapping Process: Unlike our previous mapping efforts (Schmidt et al., 2014; Neal et al., 2014), mapping directly to the GER is employed. Two examples are reported here (and more will be presented at the workshop): Polar Volatiles and Technology Test Bed/Human Health.

1. Advance knowledge base related to use of lunar resources: It has been known since the Apollo that the Moon is home to resources that could be used to facilitate human space exploration. Since that time, lunar volatiles have become an intensive topic of lunar research and could form the basis of an important natural lunar resource.

COSPAR [5]. Support the development of evolutionary concepts for making use of local resources to enable sustainable human presence and fruitful operations on the surface of Moon and Mars.

LEAG-SKGs [6]. Composition/quantity/distribution/form of water/H species and other volatiles associated with lunar cold traps (13 SKGs), for example:

- Map & characterize broad features of polar cold traps;
- Determine lateral & vertical extent of polar volatiles;
- Processes and history of water and other polar volatiles.

LEAG-LER [7]. Obj. Sci-A-3: Characterize the environment and processes in lunar polar regions & the lunar exosphere. Also in the Feed Forward theme.

SCEM [8]. Priority 4 - The lunar poles are special environments that may bear witness to the volatile flux over the latter part of solar system history.

SR [9]. The Moon is the type locality to study volatile loss, transport, and retention on airless bodies; the polar deposits represent targets for in situ resource applications;

ASTROBIO [9,10]. It is possible that some infor-

mation concerning the importance of comets in "seeding" the terrestrial planets with volatiles and prebiotic organic materials can be found. Lunar polar ice deposits will have been continuously subject to irradiation by cosmic rays and may have played host to organic synthesis reactions of the kind thought to occur in the outer Solar System and on interstellar dust grains.

2. Human Health: The major research platform for studying the effects that space exploration can have on human health is currently the International Space Station (ISS). The ISS is not ideal for examining the effects of space radiation (it is within the Earth's magnetic field) or the effects of reduced gravity on human physiology. We have a knowledge base on how the human body reacts to Earth's gravity and at microgravity (from the ISS, etc.), but is there a linear degradation between the two extremes? Long duration human missions to the lunar surface should be able to inform us about this. In addition to the test documents, a recent study highlight the Moon as an ideal place to study the effects of long-duration space exploration [11]. The test documents map to these in the following ways.

COSPAR [5]. The ISS is highlighted as the place where current research is being conducted on the impact the space environment has on human health. highlighted the US NRC Report 2012 [12], where both physical and psychological affects of space exploration are discussed. Finally, this document notes that space radiation is a major barrier to human exploration of the Solar System and concluded that environmental characterization, as well as materials testing should be conducted by robotic precursor missions, and that a focus on space weather prediction should be made.

LEAG-SKGs [6]. Five SKGs were identified that relate to this topic and these are: Solar event prediction; Radiation at the lunar surface; Biological impact of dust; Maintaining peak human health; Radiation shielding.

LEAG-LER [7]. Human health is a theme that pervades through the LER:

Objective Sci-D-14: Study the fundamental biological & physiological effects of the lunar environment on human health and the fundamental biological processes and subsystems upon which health depends.

Objective Sci-D-15: Study the key physiological effects of the lunar environment on living systems & the effect of pharmacological and other countermeasures.

Objective Sci-D-16: Evaluate consequences of long-duration exposure to lunar gravity on the human musculo-skeletal system.

Objective FF-A-2 and FF-C-8: Develop Crew Health Systems That Enable Safe, Long, Surface Stays.

SCEM [8]. While this report focused on lunar science, understanding the pristine lunar environment is important for designing mitigation technologies in order to provide safe living and working conditions. Therefore the SCEM maps into this through "Priority 8 - *Processes involved with the atmosphere & dust environment of the Moon are accessible for scientific study while the environment is in a pristine state.*"

SR [9]. This document emphasizes the importance of using the Moon to understand the effects of the space environment on human health: 1) Monitoring human adaptation to prolonged exposure to partial gravity may offer significant insights into vestibular disorders and a range of processes beyond associated in aging, disusepathology and lifestyle conditions such as the metabolic syndrome and cardiovascular disease; and 2) There would be much to learn about life support (e.g., bio-regenerative food, breathable air, and water closed-loops), and medical support provision, from human operations in a lunar base beyond research into partial gravity effects.

ASTROBIO [9,10]. Use of the Moon to understand the long-term effects of the space environment (e.g., the radiation, microgravity, psychological aspects) is required because our knowledge is not sufficient. Several areas of investigation are highlighted: Study of the adaptation of terrestrial life to the lunar environment; Use of the lunar environment: for *panspermia* experiments and as a test bed for planetary protection protocols; as a test-bed for the development of bioregenerative life-support systems, for long-term use on the Moon and future long-duration deep space exploration missions (see also [11]).

Conclusions: Our major conclusion is that while the GER has broad goals that define a framework for international cooperation in human space exploration, detail from existing, international & community developed documents can be mapped to these goals. By broadening the scope of this effort to include other internationally developed documents and space agency roadmaps the GER can become an important long-range planning document for human space exploration.

References: [1] Global Exploration Roadmap (2013) http://www.globalspaceexploration.org; [2] Logsdon (2008) *Space Pol. 24*, 3-5; [3] Schaffer (2008) *Space Pol. 24*, 95-103; [4] Szajnfarber et al. (2011) *Space Pol. 27*, 131-145; [5] Ehrenfreund et al. (2012) *Adv. Space Res. 49*, 2-48. [6] Strategic Knowledge Gaps for the Moon First Human Exploration Scenario (2012) http://www.lpi.usra.edu/leag/GAP_SAT_03_09_12.pdf [7] Lunar Exploration Roadmap (2013) http://www.lpi.usra.edu/leag/ler_draft.shtml [8] NRC (2007) http://www.nap.edu/catalog/11954.html; [9] Crawford et al. (2012) *Planet. Space Sci. 74*, 3-14. [10] Crawford (2010) *Astrobiology 10*, 577-587. [11] Goswami et al. (2012) *Planet. Space Sci. 74*, 111-120. [12] NRC Report. Research for a Future in Space: The Role of Life and Physical Sciences, 2012 http://www.nap.edu/catalog.php?record_id=13450.

High-Spectral Resolution, May 2013 Ground-Based Observations of the Lunar Sodium and Potassium Exosphere. R. J. Oliversen[1], E. J. Mierkiewicz[2], D. C. P. Kuruppuaratchi[2], N. J. Derr[3], D. D. Gardner[3], O. L. Lupie[1], F. L. Roesler[3]. [1]NASA Goddard Space Flight Center, Greenbelt, MD (ronald.j.oliversen@nasa.gov), [2]Embry-Riddle Aeronautical University, Physical Sciences Department, Daytona Beach, FL (mierkee@erau.edu), [3]University of Wisconsin, Physics Department, Madison, WI (roesler@physics.wisc.edu).

We apply high resolution spectroscopy to investigate the lunar exosphere by measuring sodium and potassium spectral line profiles to determine the variations in exospheric effective temperatures and velocities as a function of time, solar conditions and geometries. Observations are made with a dual-etalon Fabry-Perot spectrometer from the National Solar Observatory McMath-Pierce Telescope. The spectrometer has a Field of View (FOV) of 3 arcmin (~336 km at semi-major axis = 384,400 km) and a resolving power of 180,000 and 150,000 to measure the line widths and radial velocity Doppler shifts of the sodium D2 (5889.951 Å) and potassium D1 (7698.965 Å) emission lines, respectively. We first measured the sodium profile in March 2009 [1] followed by the first potassium line profile measurements in June 2012 (Fig. 1) during the moon's waning gibbous phase. As previously reported [2], [3] potassium has a smaller scale height than sodium (Fig. 1). We only detected the potassium emission within ~0.25 R_{moon} of the lunar limb while we measure sodium out to ~1 R_{moon}. A lunar scattered light gradient underlying the Fabry-Perot circular interference fringes is the dominant continuum source and limiting factor in the precision of these measurements.

During the May 2013 full moon period, we obtained our first data set that covered both pre- and post-full moon phases. For these observations, we developed a scattered light removal algorithm that was an iterative fit of a two-dimensional 5th degree polynomial and radial Gaussian distributions. The subtraction eased the fitting process by significantly flattening the image before the annular ring summing which creates the spectra, thereby increasing the accuracy and sensitivity. The instrument's 3 arcmin FOV was positioned at several locations, centered 1.5 arcmin off the limb. Observations near 1st and 3rd quarter (phase angles 70° - 110°) have temperatures of 1100° K and 2100° K for sodium and potassium, respectively. As the phase angle decreased for both the waxing and waning phases the measured line width and corresponding temperature increased (Fig. 2). However, the relative increase is more pronounced for sodium when compared to potassium. While the sodium in the Earth's magnetotail region (phase angle < 30°) has followed the familiar pattern of being fainter and hotter [6]. It is about 30%

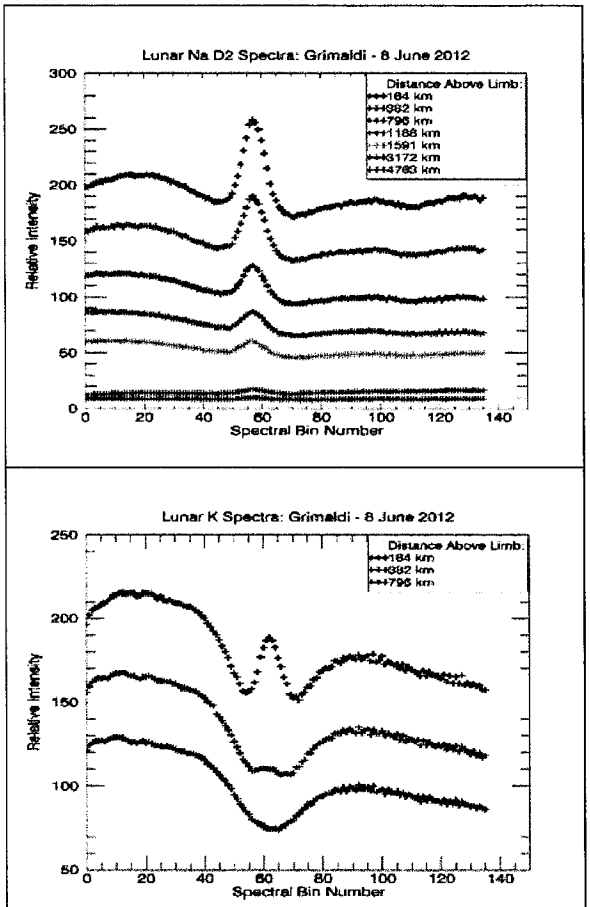

*Figure 1. Lunar Na D2 and K D1 emissions measured with a 327 km FOV (moon range = 375,000 km) off the limb near Grimaldi crater (68.3° W, 5.5° S). The Na spectra are comprised of the solar Na Fraunhofer line (5889.9509 Å), the lunar s-resolved Na emission doublet (5889.9386, 5889.9584 Å) and 3 terrestrial H_2O absorption features (*5889.637, 5890.090, 5890.227 *Å)[4]. The K spectra contains the solar K absorption line (7698.9646 Å) and the lunar s-resolved emission doublet (7698.9586, 7698.9681 Å) [5]. The dip on the left side of the spectra is an image artifact due to not being flat field corrected. Wavelength scale decreases to the right (red → blue) with a spectral bin = 0.3097 km/s. Integration times were 300 sec per exposure. Lunar phase angle = 52° (illumination 81%).*

fainter than when compared to the 1st and 3rd quarter phase intensities with temperatures just inside the magnetometer of order 3000° K increasing to over on 6000° K at full moon (Fig. 3). Although potassium emission was not detected in the magnetotail, there are indications that it was hotter pre-magnetotail passage as compared to post-magnetotail passage. Additionally, the potassium intensities were 1/3 brighter following the post-magnetotail passage. Figure 3 shows examples of sodium line width as a function of distance off the limb. The moon was deep within the magnetotial on May 24 and 25 while observations taken on May 28 are after the moon had exited the magnetotail.

This work was partially supported by the NASA Planetary Astronomy programs, NNX11AE38G and NNX13AL30G.

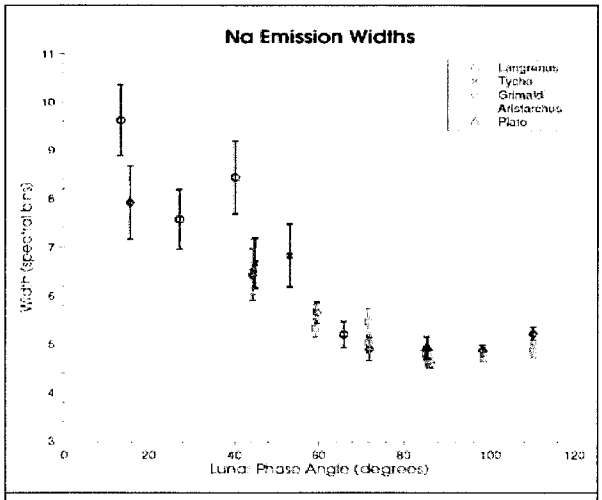

Figure 2. Na (K) spectral fits include the 6 (3) components listed in Figure 1. The Na and K s-resolved doublet wavelength spacing and intensity ratios are fixed [4], [5]. Observations off the Langrenus (Grimaldi, Aristarchus) limb(s) are taken during the waxing (waning) phase. A spectral bin = 0.3097 km s^{-1}. The line width is the deconvolved line width (FWHM) where a thorium line is used to measure the instrument profile. The errors correspond to the model fit errors. Temperature ($T_{eff}(K)$) is calculated from the Doppler width ($\delta V_{FWHM}(km/s)$) by $T_{eff} = C(m) \times \delta V^2$ where C(Na) = 501 and C(K) = 850.

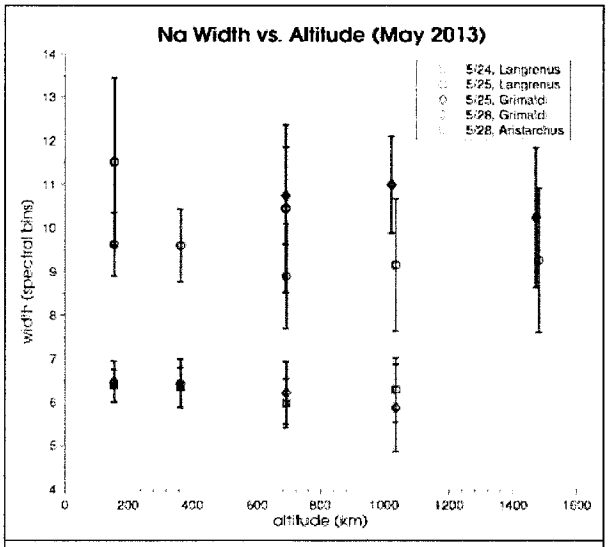

Figure 3. The Na widths (FWHM) are plotted vs the distance to the center of a 3' FOV (312 km). The FOV was moved from the limb due East of the Langrenus crater (61.1° E, 8.9°) and due West of the Grimaldi crater (68.3° W, 5.5° S) and the Aristarchus crater (47.4° W, 23.7° N). The full moon was May 25 at a distance of 356,000 km. The lunar phase angles were 13°, 2° and 44° for May 24, 25 and 28, respectively.

References:

[1] Mierkiewicz, E. J. et al. (2014), JGR-SP, 119, 4950 - 4956. [2] Porter, A. E. and Morgan, T. H. (1988), Science, 241, 675 - 680. [3] Sprague, A. L. (1992), Icarus, 96, 27 - 42. [4] McNutt, D. P. and Mack, J. E. (1963), JGR, 68, 3419 -3429. [5] Von Zahn, U. and Hoffner, J. (1996), GRL, 23, 141 - 144. [6] Potter, A. E. et al. (2000), JGR, 105, 15073 - 15084.

MINI-RF BISTATIC OBSERVATIONS OF CABEUS CRATER. G. W. Patterson[1], D. B. J. Bussey[1], A. M. Stickle[1], J. T. S. Cahill[1], P. Spudis[2], and the Mini-RF Team. [1]Johns Hopkins University Applied Physics Laboratory, Laurel, MD (Wes.Patterson@jhuapl.edu), [2]Lunar and Planetary Institute, Houston, TX.

Introduction: Observations of the south polar crater Cabeus indicate anomalous scattering behavior associated with crater floor materials (behavior not observed with monostatic data). We interpret this behavior as consistent with the presence of water ice. It is probable that the incidence angle at which the data was acquired plays a role in the differences observed between bistatic images and with the monostatic data.

Background: Radar observations of planetary surfaces provide important information on the structure (i.e., roughness) and dielectric properties of surface and buried materials [1-4]. These data can be acquired using a monostatic architecture, where a single antenna serves as the signal transmitter and receiver, or they can be acquired using a bistatic architecture, where a signal is transmitted from one location and received at another. The former provides information on the scattering properties of a target surface at zero phase. The latter provides the same information but over a variety of phase angles. NASA's Mini-RF instrument on the Lunar Reconnaissance Orbiter and the Arecibo Observatory in Puerto Rico are currently operating in a bistatic architecture (the Arecibo Observatory serves as the transmitter and Mini-RF serves as the receiver) in an effort to understand the scattering properties of lunar terrains as a function of bistatic (phase) angle. This architecture maintains the hybrid dual-polarimetric nature of the Mini-RF instrument [5] and, therefore, allows for the calculation of the Stokes parameters (S_1, S_2, S_3, S_4) that characterize the backscattered signal (and the products derived from those parameters).

Previous work, at optical wavelengths, has demonstrated that the material properties of lunar regolith can be sensitive to variations in phase angle [6-8]. This sensitivity gives rise to the lunar opposition effect and likely involves contributions from shadow hiding at low phase angles and coherent backscatter near zero phase [1]. Mini-RF bistatic data of lunar materials indicate that such behavior can also be observed for lunar materials at the wavelength scale of an S-band radar (12.6 cm). Among the terrains observed thus far, we have found the response of materials associated with the floor of the crater Cabeus to be particularly interesting.

Observations: A common product derived from the Stokes parameters is the Circular Polarization Ratio (CPR),

$$\mu_C = \frac{(S_1 - S_4)}{(S_1 + S_4)} \quad (1).$$

CPR information is commonly used in analyses of planetary radar data [1-4], and is a representation of surface roughness at the wavelength scale of the radar (i.e., surfaces that are smoother at the wavelength scale will have lower CPR values and surfaces that are rougher will have higher CPR values). High CPR values can also serve as an indicator of the presence of water ice [9].

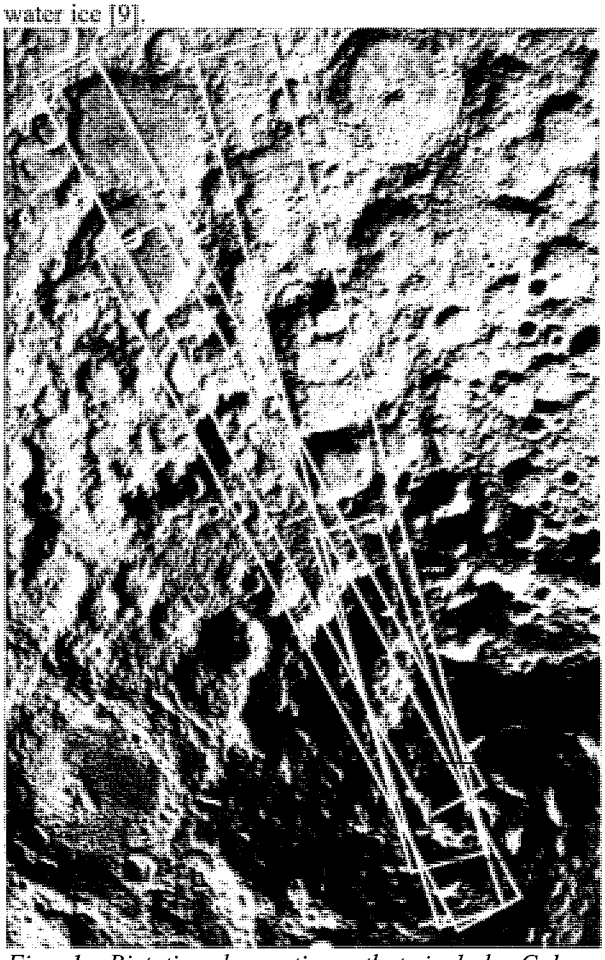

Fig. 1. Bistatic observations that include Cabeus crater (outlined in white).

Data for the south polar crater Cabeus has been acquired on four occasions (Fig. 1) and these data cover a phase angle range of 0° to 18°. When viewed at near zero phase (Fig. 2), the floor of Cabeus crater shows an enhancement in CPR with respect to surrounding materials. This is not apparent in data acquired of Cabeus crater when Mini-RF operated in a monostatic mode

[10]. Further, when viewed at phase angles of several degrees (Fig. 2), the floor of Cabeus crater shows a suppression of CPR with respect to surrounding materials.

Summary: The scattering behaviour of the floor of Cabeus crater indicates a clear opposition effect at low phase angles that is consistent with the presence of water ice [11-13]. We suspect that the difference in the scattering behaviour observed with a monostatic architecture is related to the grazing incidence (~85°) at which the region is viewed by Mini-RF when operating in a bistatic mode. This would suggest that the water ice observed would need to be confined to a relatively thin layer, near the surface.

References: [1] Campbell et al. (2010), *Icarus*, 208, 565-573; [2] Raney et al. (2012), *JGR*, 117, E00H21; [3] Carter et al. (2012), *JGR*, 117, E00H09; [4] Campbell (2012), *JGR*, 117, E06008; [5] Raney, R. K. et al. (2011), *Proc. of the IEEE*, 99, 808-823; [6] Hapke et al. (1998), *Icarus*, 133, 89-97; [7] Nelson et al. (2000), *Icarus*, 147, 545-558; [8] Piatek et al. (2004), *Icarus*, 171, 531-545. [9] Black et al. (2001), *Icarus*, 151, 167-180; [10] Neish et al. (2011), *JGR*, 116, E0100; [11] Hapke and Blewett (1991), Nature, 352, 46-47; [12] Mishchenko (1992), Astrophysics and Space Science, 194, 327-333; [13] Mishchenko (1992), Earth, Moon, and Planets, 58, 127-144.

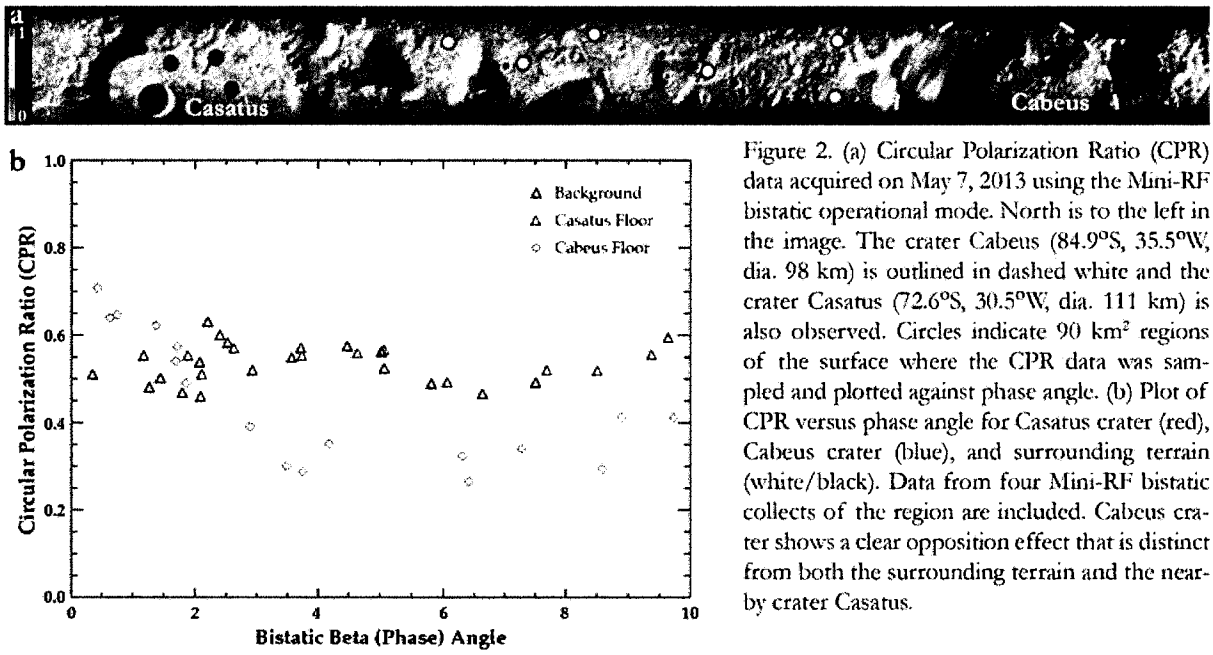

Figure 2. (a) Circular Polarization Ratio (CPR) data acquired on May 7, 2013 using the Mini-RF bistatic operational mode. North is to the left in the image. The crater Cabeus (84.9°S, 35.5°W, dia. 98 km) is outlined in dashed white and the crater Casatus (72.6°S, 30.5°W, dia. 111 km) is also observed. Circles indicate 90 km^2 regions of the surface where the CPR data was sampled and plotted against phase angle. (b) Plot of CPR versus phase angle for Casatus crater (red), Cabeus crater (blue), and surrounding terrain (white/black). Data from four Mini-RF bistatic collects of the region are included. Cabeus crater shows a clear opposition effect that is distinct from both the surrounding terrain and the nearby crater Casatus.

ASSOCIATION BETWEEN SMALL THORIUM ENHANCEMENTS, SILICIC VOLCANISM, AND ENHANCED OH/H_2O AS MEASURED BY THE MOON MINERALOGY MAPPER. N. E. Petro NASA Goddard Space Flight Center, Planetary Geodynamics Lab, Code 698, Greenbelt, MD 20771 (Noah.E.Petro@nasa.gov).

Introduction: The discoveries of OH/H_2O at the Moon in numerous locales/settings have been one of the biggest surprises in lunar science in the last 10 years. The identification of OH/H_2O in lunar samples, buried below the surface, and on the surface raises questions about the abundance and variability of volatiles on the Moon. Potentially related to both the presence of OH/H_2O from inside the Moon and on the surface is the finding of hydroxyls associated with the central peak of the crater Bullialdus [1] and the Compton-Belkovich volcanic complex [2-4].

Here we a preliminary evaluation of the association of other small-scale Thorium hotspots [5] with the 3.0 μm absorption feature measured in Moon Mineralogy Mapper (M^3) data [6, 7]. The association between Thorium (and presumably KREEP) and endogenic OH/H_2O may indicate variations in formation processes and/or magma/crustal evolution.

Small-area Thorium Features: Lawrence et al. [5] identified 42 small Thorium features across the lunar surface (Figure 1). These features are mostly associated with the Procellarum KREEP Terrane [8] but several are found in the FHT and SPAT. Of particular interest to this study are the 34 features that are associated with Thorium enhancements, relative to their surroundings. Although not included in the Lawrence et al. list of Thorium enhancements, we also consider the two Thorium enhancements within northwestern SPA [9, 10], as they represent larger-scale anomalies, relative to the rest of SPA.

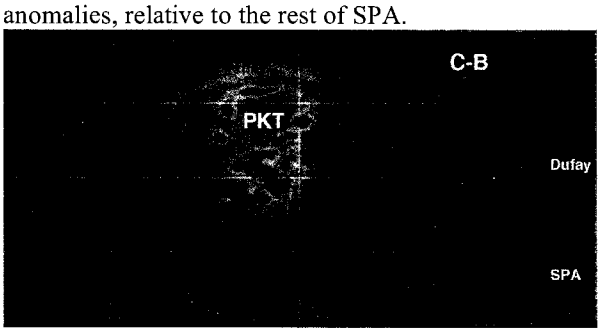

Figure 1. Map of lunar Thorium with several enhancements identified.

The small-area Thorium anomalies are commonly associated with areas of silicic volcanism [11-13] or with exposures of KREEP-bearing material, such as is observed across the broad enhancement in the PKT [8].

Other Small-scale Thorium Enhancements Associated with OH/H_2O: In addition to the OH/H_2O associated with Compton-Belkovich and Bullialdus, several other small-scale OH/H_2O enhancements have been observed in association with Thorium anomalies. Here we evaluate two of these cases.

Dufay Anomaly: North of the main Dufay Thorium anomaly [5] there is a diffuse, bright albedo pattern associated with a enhancement in Thorium and, based on the strength of the 3.0μm a localized enhancement in OH/H_2O (Figure 2). It is apparent in both the M^3 data as well as in high-resolution LROC NAC images of the albedo anomaly that the albedo marking is a thin layer with non-OH/H_2O bearing material beneath.

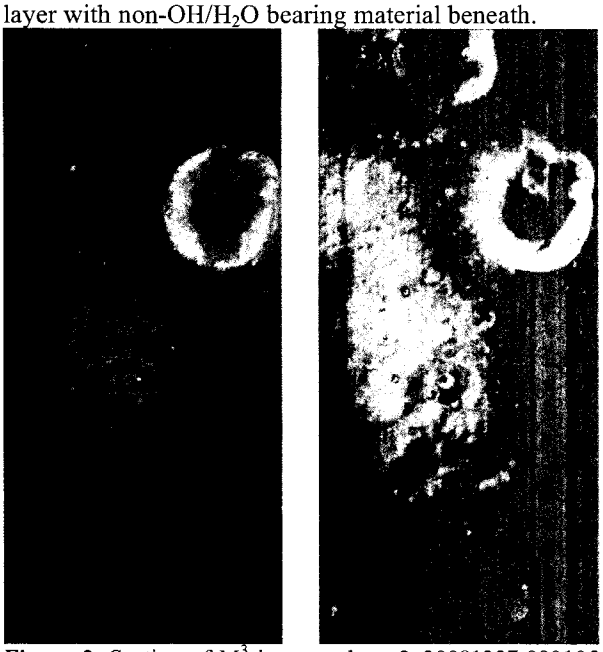

Figure 2. Section of M^3 image cube m3g20081227t090105 showing small area albedo enhancement and associated 3.0μm enhancement. Image at left is 750nm band; image at right is the Integrated 3.0μm Band Strength Map. Small crater at top right is 20km in diameter.

Hansteen Alpha: The Hansteen Alpha volcanic construct is a site of silicic volcanism in southern Oceanus Procellarum [12, 14]. The M^3 data for Hansteen Alpha show that the entire volcanic construct is enhanced in OH/H_2O [4] relative to the surrounding mare basalts and, more importantly, the northern rim of Billy Crater (Figure 3).

Thorium Enhancements Not Associated with OH/H_2O: While the two cases described here illustrate a potential relationship between enhanced Thorium and OH/H_2O, there are a number of other locations that do not demonstrate the same relationship. Namely the Marian Domes [11] lack any 3.0μm feature and the Thorium enhancements in SPA (the two in north-

eastern SPA and south of Fizeau crater [5]) are similarly lacking in a 3.0μm absorption.

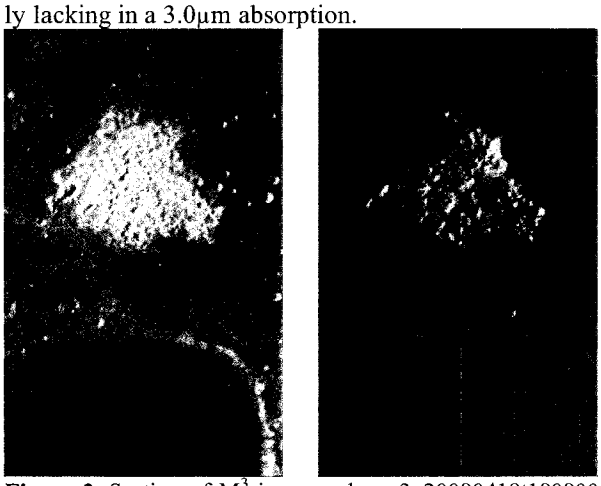

Figure 3. Section of M^3 image cube m3g20090418t190900 showing small area albedo enhancement associated with Hansteen Alpha and associated 3.0μm enhancement. Image at left is 750nm band; image at right is the Integrated 3.0μm Band Strength Map.

References:

[1] Klima, R., et al., (2013) *Nature Geosci*, 6, 737-741.

[2] Bhattacharya, S., et al., (2013) Study of 2800-nm OH/H_2O Feature at Compton-Belkovich Thorium Anomaly (CBTA) in the Far Side of the Moon Using Chandrayaan-1 Moon Mineralogy Mapper (M^3) data, 44, 1382.

[3] Petro, N. E., et al., (2013) Presence of OH/H_20 Associated ith the Lunar Compton-Belkovich Volcanic Complex Identified by the Moon Mineralogy Mapper (M^3), 44, 2688.

[4] Standart, D. L. and J. M. Hurtado, (2012) *AGU Fall Meeting Abstracts*, 53, 2058.

[5] Lawrence, D. J., et al., (2003) *Journal of Geophysical Research*, 108(E9), 5102, doi:1029/2003JE002050.

[6] McCord, T. B., et al., (2011) *Journal of Geophysical Research*, 116,

[7] Pieters, C. M., et al., (2009) *Science*, 326, 568-572.

[8] Jolliff, B., et al., (2000) *JGR*, 105, 4197-4216.

[9] Garrick-Bethell, I. and M. T. Zuber, (2005) *GRL*, 32, L13203, doi:13210.11029/12005GL023142.

[10] Wieczorek, M. A. and M. T. Zuber, (2001) *JGR*, 106, 27,853-827,864.

[11] Glotch, T. D., et al., (2011) *GRL*, 38, 21204.

[12] Glotch, T. D., et al., (2010) *Science*, 329, 1510-.

[13] Jolliff, B. L., et al., (2011) *Nature Geoscience*, 4, 566-571.

[14] Hawke, B. R., et al., (2003) *Journal of Geophysical Research*, 108, 5069.

Conclusions: A combination of Lunar Prospector Thorium data, M^3 Spectra, and Diviner Christiansen Feature data suggests that there may be an association between silicic volcanism and the abundance of OH/H_2O at the lunar surface. Previous work on the Compton-Belkovich volcanic complex [3] suggests that there is a pyroclastic deposit there which may be the source of the endogenic hydroxyl signature.

It is clear that not all silicic volcanic sites contain endogenic hydroxyls (i.e., the Marian Domes), however, the presence of a 3.0μm band in M^3 data may help determine the source of such volcanic features.

Further investigation using Mini-RF radar data for Hansteen Alpha, Lassell Crater, the Gruithuisen Domes [4], and other silicic volcanic sites [5, 12] may shed some light on the apparent relationship between endogenic hydroxyls and silicic volcanism and whether only silicic pyroclastic volcanism contains endogenic hydroxyls.

FIVE YEARS AT THE MOON WITH THE LUNAR RECONNAISSANCE ORBITER (LRO): NEW VIEWS OF THE LUNAR SURFACE AND ENVIRONMENT. N. E. Petro and J. W. Keller, NASA Goddard Space Flight Center, Greenbelt, MD 20771. (Noah.E.Petro@nasa.gov)

LRO Overview: The Lunar Reconnaissance Orbiter (LRO) has been orbiting the Moon for over five years. In that time, data from the seven instruments onboard the spacecraft have made significant advances in our understanding of the Moon and its environment. In September 2014 LRO completed its first Extended Science Mission (ESM) and began a second ESM (pending NASA approval). During the ESM and the second ESM, LRO has been in a quasi-stable, eccentric orbit of ~30 x 180 km with a periapse near the South Pole. This orbit enabled high-resolution measurements around the South Pole. LRO's seven instruments are operating nominally, and have experienced no significant degradation since beginning the ESM. The spacecraft has performed exceptionally well, with 98.4% uptime during the mission. LRO retains sufficient fuel so that its current orbit can be maintained for at least 8 years.

LRO's science teams have been extremely productive, focusing on the distribution of volatiles, evidence for early differentiation, measuring the lunar impact record, and the Moon's interactions with its external environment. Three of the most exciting findings by LRO have been the identification of LRO-era impacts, global tectonic features, and the transient nature of some volatiles at the surface. These findings will areas of focus for future LRO measurements.

LRO Data: LRO's data is released to the PDS every 3 months, as of August 2014 over 528.75 TB of data have been delivered by LRO. Many of the teams have delivered higher-level data products as part of their routine PDS deliveries (e.g., mosaics, maps, derived products). These products are intended to act as useful resources for the science and explorations communities (Figure 1).

Additionally higher-level LRO data products are of interest for future lunar landers. These products include illumination maps (Figure 2), meter-scale digital elevation models, roughness maps, and sub-meter per pixel images of possible landing sites. All of these products are available either from the PDS [1] or individual team websites [e.g., 2].

Tracking Lunar Volatiles: The LRO mission was initially conceived to identify the presence and abundance of volatiles in the lunar polar regions, specifically in permanently shadowed regions (PSRs), among other science questions related to lunar exploration [3]. In the five years of measurements from LRO, the paradigm for the distribution of lunar volatiles has significantly changed. Not only is there widespread evidence for volatiles both in and outside of PSR's, there is increasing evidence for temporal variability in the abundance of volatiles at and near the surface.

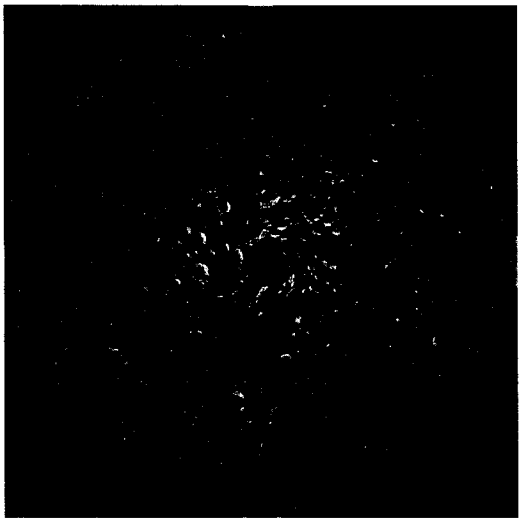

Figure 1. The LROC Northern Polar Mosaic (http://lroc.sese.asu.edu/images/gigapan), a 2-meter per pixel mosaic from 60° North to the pole.

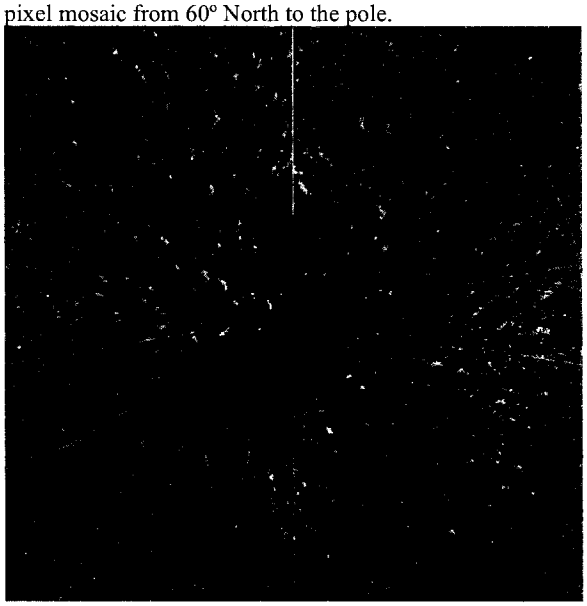

Figure 2. LOLA derived map of areas of permanent shadow at 240-meters per pixel (in red) for areas poleward of 65° North.

During LRO's second ESM there will be a focus on new measurements of the mobility and abundance of volatiles in the southern hemisphere. Taking advantage of not only 2 additional years of measurements to im-

prove statistics as well as the drifting of LROs periapse away from 90° South, additional measurements will:

- Identify the presence of transient surface frost in areas that are shadowed for a significant portion of the lunar day.
- Image the interior of PSR's to identify variations in regolith properties.
- Measure the temperature of the polar regions over a wider range of lunar time of day in order to improve models for subsurface ice stability.
- Constrain the role of small-scale cold traps (meter sized) in harboring volatiles.
- Make improved measurements of the distribution of volatiles outside of PSRs using multiple instruments.
- Make new targeted bistatic radar measurements of locations near the South Pole that may have buried ice deposits.

Data from LRO continues to refine our understanding of the unique environment at and near the lunar poles. Continued data from the mission will aid in measuring the scales (both temporal and spatial) that volatiles are found at and near the surface.

References:

[1]http://pds-geosciences.wustl.edu/missions/lro/default.htm

[2] http://imbrium.mit.edu/, http://diviner.ucla.edu/, http://lroc.sese.asu.edu/ , www.boulder.swri.edu/lamp/, http://lro.gsfc.nasa.gov/

[3] Vondrak, R., J. Keller, G. Chin, and J. Garvin (2010), Lunar Reconnaissance Orbiter (LRO): Observations for Lunar Exploration and Science, *Space Science Reviews, 150*, 7-22.

IMPORTANT SKGs FOR LUNAR WATER RESOURCES: TIME/SPACE VARIATIONS OF SURFICIAL OH/H2O. C. M. Pieters and R. E. Milliken[1], [1]Brown University, DEEPS, Providence, RI 02912 (Carle_Pieters@brown.edu)

Introduction: An important potential resource on the Moon is its pervasive layer of surficial OH/H_2O. The presence of this form of OH/H_2O was found to occur over widespread portions of the illuminated surface of the Moon (Pieters et al., 2009, Sunshine et al., 2009, Clark et al., 2009). It is believed this form of OH/H_2O is tied to the oxygen-rich nature of surface materials and the hydrogen-rich nature of the solar wind (e.g. Dyar et al., 2010; McCord et al. 2011; and refs. therein). Although most attention has been given to understanding possible buried volatiles in permantly shadowed regions of the lunar poles, the pervasive nature of surficial OH/H_2O makes it an attractive potential resource.

There are several Strategic Knowledge Gaps (SKGs) that need to be addressed to evaluate surficial OH/H_2O as a resource. They can be formulated as the following questions:

1. What is the distribution and abundance of OH/H_2O across the lunar surface?
2. What are the processes responsible for formation of surficial OH/H_2O on the Moon?
3. At what rate does surficial OH/H_2O form and what role, if any, does composition play in this rate?
4. How mobile is surficial OH/H_2O?
5. What is the resource potential of the surficial OH/H_2O and is it renewable?

Near-infrared reflectance spectra from the Moon Mineralogy Mapper (M^3) onboard Chandrayaan-1 acquired in 2008/2009 has provided a first assessment of global surficial OH/H_2O on the Moon (Pieters et al., 2009; McCord et al., 2010), although with non-ideal spectral, spatial and temporal characteristics (Boardman et al., 2011). Such spectroscopic measurements rely on fundamental absorptions of OH and H_2O between 2800 and 3000 nm. At these wavelengths, most radiation measured from the Moon is reflected solar radiation. However, thermal emission from warm lunar surfaces can also contribute a significant component to measured radiation. Identifying and removal of the thermal component (e.g. Clark et al., 2011) is essential for evaluating the character of the OH/H_2O absorption.

The basic calibration of M^3 data (Green et al., 2011) and ongoing approaches for improving the thermal removal have resulted in not only refining estimates of surficial OH/H_2O at the cool high latitudes (Li and Milliken, 2013), but also in identifying several local concentrations of OH/H_2O, linked to the inherent geologic character of deposits at Buldialdus (Klima et al. 2013), Compton-Belkovich (Bhattacharya et al., 2013; Petro et al. 2013) and several regional pyroclastic deposits (Li and Milliken, 2014).

Although progress has been made, in order to evaluate the character of the pervasive OH/H_2O associated with surface materials of the Moon and to assess the potential of surficial OH/H_2O as a *renewable* resource, focused new data are needed to close key SKGs.

Accurate measurements of the time variability of surface hydration in a geologic context is the first essential step for understanding the physics of OH/H_2O production and loss on the Moon. Data must be acquired over multiple lunar days at different local times in a clear spatial context. Distinguishing OH from H_2O requires high spectral resolution across the entire absorption feature. Although local analyses can be obtained from the surface, the critical global assessment is best accomplished from orbit.

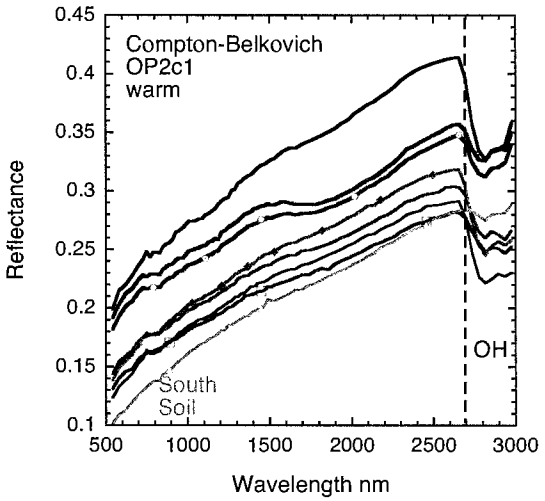

M^3 spectra of the Compton-Belkovich region of the Moon exhibit prominent 2800+ nm absorptions due to the presence of OH/H_2O. Surrounding soil (orange spectrum) exhibits a less prominent absorption. [A few instrumental artifacts occur at shorter wavelengths.]

References:

Bhattacharya et al., 2013, *Current Science* 105, No.5.
Boardman et al., 2011, *JGR* 116, E00G14.
Clark, RN, 2009, *Science* 326, 562.
Clark et al., 2011, *JGR* 116, E00G16.
Dyar et al., 2010, *Icarus* 208, 425–437.
Green et al., 2011, *JGR*, 116, E00G19.
Klima et al., 2013, *Nature Geoscience* DOI: 10.1038/NGEO1909
Li and Milliken, 2013, LPSC44 #1337.
Li and Milliken, 2014, LPSC45 #2012
McCord et al., 2011, *JGR*, 116, E00G05.
Petro et al., 2013, LPSC44 #2688.
Pieters et al., 2009, *Science* 326, 568.
Sunshine et al., 2009, *Science* 326, 565.

VARIABLE ABUNDANCE AND ISOTOPIC COMPOSITION OF HYDROGEN INSIDE THE MOON.
K. L. Robinson[1,2,3] and G. J. Taylor[1,2,3], [1]Hawaii Institute of Geophysics and Planetology, 1680 East-West Rd., Honolulu, HI 96822. [2]UHNAI [3]CLSE. krobinson@higp.hawaii.edu

Introduction: Water has been detected in samples from the lunar interior ([1], recently reviewed in [2]) and on the surface, remotely (e.g. [3]), in permanently shadowed regions [4], and in glass agglutinate samples [5]. Surface water, particularly ice trapped in permanently shadowed regions near the lunar poles, is a prime target for in situ resource utilization on the Moon, but could the water in the lunar interior or in rocks from the interior be useful as a resource?

Lunar interior water, which accreted with the Moon or was added very early after lunar formation, has now been measured in pyroclastic glasses [1], olivine-hosted melt inclusions [6,7], ferroan anorthosite plagioclase [8], and apatite grains from all major lunar rock types [2, 9-16,18]). The brunt of the analytical effort has focused on lunar glasses/melt inclusions, and apatite.

The overarching goal of these measurements is twofold: to try to constrain the water content of the bulk Moon, and to determine the source(s) of the Moon's water via hydrogen isotopic ratios. Estimating the pre-eruptive water content of a parental magma from glasses and melt inclusions is relatively straightforward, and it was initially thought that similar estimates could be made using OH abundances in apatite [9]. Recent work showing the complexities of volatile partitioning into apatite invalidates the estimates of parental melt water content from apatite [17]. However, apatite data is still a useful recorder of D/H ratios and relative water contents might be discernible among different rock types [2]. This data from lunar apatite (and glasses) indicates there may be multiple reservoirs in the lunar interior.

Water in the interior: Fig. 1 summarizes all currently published apatite data, averaged by individual sample and plotted by lithologic type. Several trends are evident. The water content of apatite in the major rock suites varies by 10-50x and seems to be related to rock type. KREEP-rich lithologies have the driest apatite, while mare basalt apatite is much richer in water (Fig.1). Though we cannot estimate the water content of the parental magmas for any of these samples based on the OH abundance measured in the apatite [17], it seems reasonable that samples with drier apatite likely came from drier magmas, and vice versa, if F and Cl contents were roughly similar.

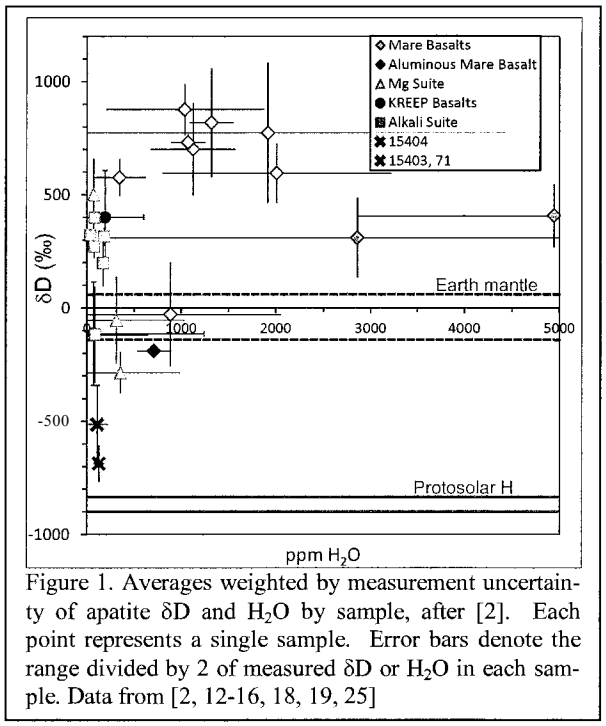

Figure 1. Averages weighted by measurement uncertainty of apatite δD and H_2O by sample, after [2]. Each point represents a single sample. Error bars denote the range divided by 2 of measured δD or H_2O in each sample. Data from [2, 12-16, 18, 19, 25]

The δD values of apatite also vary widely. The elevated δD in mare basalts is almost certainly caused by degassing upon eruption from lava flows, when lighter H is lost and heavier D is left in the melt. [13]. The mare basalts likely had an initial δD closer to ~100‰ [13]. Some evolved, intrusive rocks also appear enriched in D (+200 to +500‰), but are not thought to have lost H through degassing as they formed at depth and pressure [2, 14]. There is another cluster of samples that fall in the range of the terrestrial upper mantle (-140 to +60‰ D, [19]), but due to analytical uncertainties, they might not be completely resolvable from the moderately elevated reservoir.

Our measurements of apatite in quartz monzogabbro 15404, 51 and -,55 and 15403, 71 have the lowest δD (down to -750‰) values reported from the Moon so far, indicating a third, low D source inside the Moon (this work,). Though the range of δD measured in 15404 and 15403 is very similar to the δD observed in agglutinate glasses [5], we do not believe that the low apatite δD reflects solar wind contamination. Soil sample 15400 was taken from on top of impact melt breccia 15405, which has a low exposure age of 11 m.y. [20]. The impact melt breccia itself has no detectable solar wind in it [20, 24]. Addition of solar wind when the clasts were exposed on the lunar sur-

face atop the 15405 boulder is impossible. Solar wind gases do not diffuse in from the outer surface (less than a micron penetration) when a rock sits on the lunar surface. Even if H were to migrate along cracks and came in contact with apatite, the apatite diffusion rate is simply too low at lunar surface temperature. For example, using data from and the interdiffusion coefficient for OH, F, and Cl [26], the total diffusion distance is only ~10^{-5} microns at 100 C (typical lunar surface temperature at noon) in 11 My, the exposure age of 15405 [20]. Thus, contamination with solar wind of clasts exposed on the surface or incorporation into the 15405 impact melt is unlikely. The low δD value may represent a mantle source that contains a primitive component in the lunar interior, similar to low δD melt inclusions in primitive Baffin Island basalts [21].

Analysis of lunar glasses and melt inclusions also provides evidence for multiple water reservoirs in the lunar interior. The picritic glass beads and melt inclusions originated from a magma with ~1000 ppm H_2O [1, 6, 7]. Assuming ~10% partial melting, the source region for the pyroclastic bead magma would have contained 100ppm H_2O. In contrast, our measurements of residual quenched glass in KREEP basalt fragments in 15358 contain 58-95 ppm H_2O [14]. Based on the modal abundances of the glass (15-20%) and accounting for H loss, the initial melt would have contained ~100 ppm H_2O. The KREEP source would have thus contained ~10 ppm, an order of magnitude less than the picritic magmas. These calculations are rough, but indicate that there are at least two possible water reservoirs in the lunar interior based on water content.

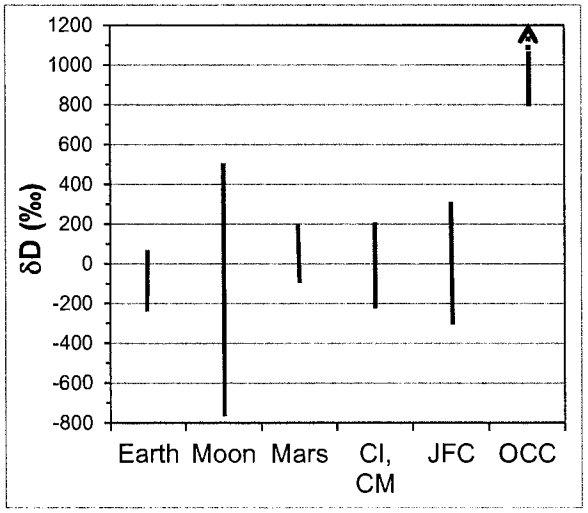

Fig. 2. δD values for solar system objects, after [2]. JFC, Jupiter Family Comets [23], OOC, Oort Cloud Comets (see [2]). Earth and Mars[19], Moon [this work, 2], CI,CM chondrites [22]

Implications: The huge range in measured δD in lunar samples makes determining a primordial lunar δD very complicated. It might thus be impossible to determine if a water-bearing deposit in a permanently-shadowed region contained water from the lunar interior or from an external source, at least by D/H ratios alone (Fig. 2). Water is distributed heterogeneously inside the Moon, as shown by δD and water content. The pyroclastic glass source seems to be the most water rich [2,6,7]. However, the Moon is still quite dry. The wettest lunar reservoir yet sampled (represented by olivine hosted melt inclusions in A17 pyroclastic glass beads [6,7]) contains about the same amount of water as depleted MORBs, which are some of the driest rocks on Earth. From a resource exploitation standpoint, it is much more efficient to search for ice, rather than trying to locate water-rich rocks. Examples of potential sites for resource exploration and utilization, such as Amundsen crater, are given by [27].

References: [1] Saal, A. E. et al. (2008) *Nature*, 454, 192-195. [2] Robinson K. L. and Taylor G. J. (2014) *Nature Geosci. 7*, 401-408. [3] Pieters C.M. et al., (2009) *Science*, 326, 568-572. [4] Colaprete A. et al. (2010) *Science*, 330, 463-467. [5] Liu Y. et al. (2012) *Nature Geosci.* 5, 779–782. [6]Hauri E. et al. *Science* 333, 213-215. [7] Saal A. E. et al. (2013) *Science*, 340, 1317-1320. [8] Hui H., et al. (2013) *Nature Geosci.* 6, 177-180. [9] McCubbin, F. M. et al. (2010) *PNAS,* 107, 11223-11228. [10] Greenwood, J. P. et al. (2011) *Nature Geosci.*, 4, 79-82. [11] Boyce J. W. et al. (2010) *Nature,* 466, 466-469. [12] Barnes, J. J. et al. (2013) *Chem. Geo.*, 337-338, 48-55 [13] Tartèse R. et al. (2013) *GCA*, 122, 58-74. [14] Robinson K. L. et al. (2013) *44th LPSC* Abst.#1327. [15] Barnes J. J. et al. (2014) *EPSL* 390, 244-252. [16]Tartèse R. et al. (2014) *Geology* 42, 363-366. [17] Boyce J.W. et al. (March 20, 2014) *Science Express*. [18] Robinson K. L. et al. (2014), *LPS XLV,* Abst. #1607. [19] Hallis L.J. et al. (2012) *EPSL, 359-360*, 84-92. [20] Drozd R. J. et al. (1976) *Proc. Lunar Sci. 7*, 599-623. [21] Hallis L.J et al. (2014) *45th LPSC* Abst.#1283. [22] Alexander C.M.O'D. et al. (2012), *Science, 337,* 721-723 [23] Hartogh P. et al. (2011) *Nature* 478, 218-220. [24] Bernatowicz T. et al. (1978), *Proc. 9th LPSC*, 905-919 [25] Geiss J. and Gloeckler G. (1998) *Space Sci. Rev.* 84, 239-250. [26] Cherniak D.J. (2010), *Rev Min. & Geochem* 72, 827-869. [27] Lemelin M. et al. (2014) *Planet. Space. Sci.* DOI: 10.1016/j.pss.2014.07.002

INTREPID: LUNAR ROVING PROSPECTOR - PROVIDING GROUND TRUTH AND ENABLING FUTURE EXPLORATION. M. S. Robinson[1], S. J. Lawrence[1], E. J. Speyerer[1], J. D. Stopar[1], School of Earth and Space Exploration, Arizona State University, Tempe, AZ (mrobinson@asu.edu).

Introduction: The Decadal Survey (DS) and the Lunar Exploration Roadmap (LER) [**1,2**] outline critical science and exploration measurements needed from the lunar surface. Orbiting spacecraft (i.e., Lunar Reconnaissance Orbiter (LRO), Clementine, Lunar Prospector, and others) and impactors like the Lunar Crater Observation and Sensing Satellite (LCROSS) were designed to provide key information about potential landing sites, identify potential resources, and characterize the lunar regolith [**3,4**]. However, ground truth is required to tie these remote sensing datasets to physical characteristics and fulfill the DS and LER objectives. Thus we propose a Lunar Roving Prospector, *Intrepid*, to collect essential measurements to address key scientific and exploration questions, and demonstrate technologies required for future robotic and human exploration of the Moon, Mars and other terrestrial bodies.

Rovers offer many operational advantages over static landers, which lack the capability to perform investigations beyond a limited distance from the original landing site. Intrepid offers the flexibility and the capability to perform wide-scale investigations that characterize the composition and properties of the lunar regolith over hundreds of square kilometers to address key science and exploration objectives. For example, with respect to studies designed to address in-situ resource utilization assessment, mobility allows assessment of *grade and tonnage* of an ore body – essential information for planning ISRU.

Science Measurement Objectives: The Intrepid rover will investigate twenty major (and hundreds of minor) scientific sites over a ~1000 km traverse during two Earth years. Extended mobility will enable Intrepid to acquire measurements over broad areas and address many key scientific objectives, including:

- Provide ground truth for all major terrain types measured by orbiting spacecraft.
- Characterize the composition of the components of the lunar regolith to provide key constraints on the lithologic diversity of the crust.
- Investigate volcanic processes and increase our understanding of the evolution of the crust and mantle.
- Examine and quantify magnetic anomalies and lunar surface swirls.
- Create a sample cache that could be retrieved by future human and robotic exploration systems.

Exploration Opportunities: In addition to providing key measurements for scientific studies, Intrepid will provide measurements essential for future robotic and human missions to the lunar surface, including:

- Detect, assay, and map potential resources (identifying and quantifying ISRU potential).
- Quantify the nature of dust, its environments, and interactions with systems.
- Measure the radiation environment (primary and secondary) present on the lunar surface.

Mission Concept: The Intrepid rover is designed to be highly mobile with a baseline traverse of over 1000 km over a two-year nominal mission. To meet this ambitious goal, Intrepid is required to drive autonomously at 1 km/hr for sustained periods (>4 hrs). The extended traverse enables measurements over a variety of geologic terrains in both mare and highlands.

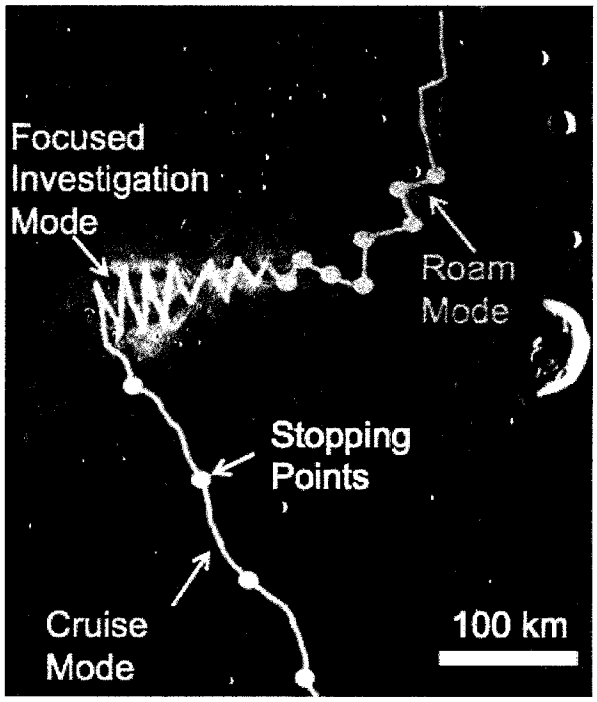

Figure 1. Traverse modes

Intrepid is designed to acquire measurements in three traverse modes: cruise, roam, and focused investigation [**Fig. 1**]. In the cruise mode, in which Intrepid will predominately be between discrete scientific sites, the rover will mainly acquire measurements while in motion (for example, passive magnetometer measurements). However, infrequent stops will be made to provide basic measurements that cannot be acquired while the rover is motion. In the roam mode, the rover will make more frequent stops during its traverse to acquire more science measurements. In the focused

investigation mode, Intrepid will acquire measurements with a higher frequency (less than every 10 meters) to enable focused analysis of the scientific sites of interest. An advanced, sliding autonomous navigation system will enable the rover to traverse in all three operating modes with little interaction with human drivers. However, operators will be able to intervene if sites of opportunities are identified in the live feeds.

Notional Instrument Suite: The proposed emphasis on mobility in the Intrepid concept makes standoff measurements critical for operations. We baselined a notional instrument suite consisting of a multispectral stereo imaging system, a narrow angle FARCAM for long-distance imaging of potential targets, a Raman spectrometer, an APXS and GRS for major element chemistry determinations, a magnetometer, and a radiation environment sensor.

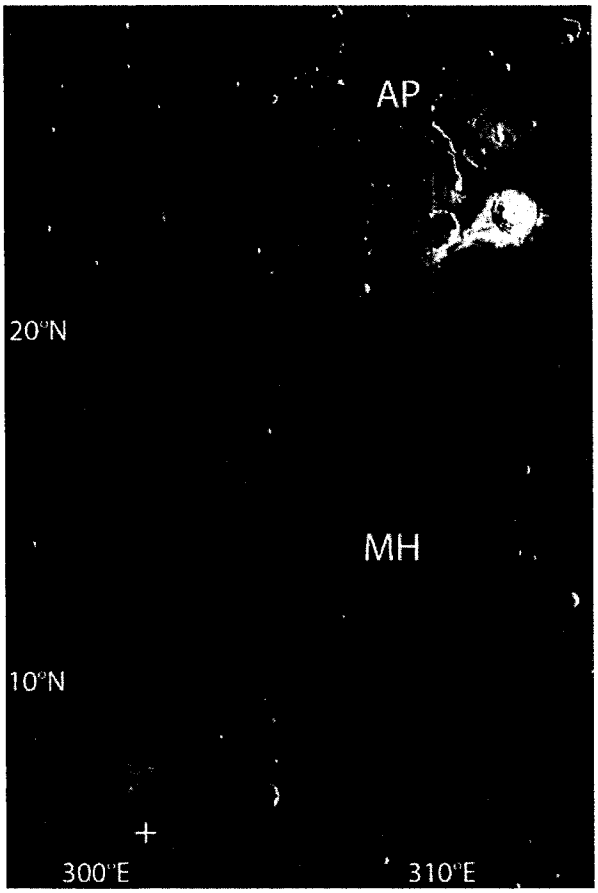

Figure 2. Current planning traverse begins 50 km south (+) of Reiner Gamma swirl, over the swirl to Marius Hills (MH) volcanic complex, north around Rima Marius and across Oc. Procellarum to the Aristarchus plateau (AP) and Aristarchus crater (east edge of AP). Ten degrees of latitude is ~300 km.

Traverse Options: With a range of 1000 km, a series of high-priority targets will answer both scientific and exploration questions in a single mission. Leveraging data returned by the LRO, we are in the process of defining several high-value scientific traverses on the lunar nearside. For example, one traverse initiates in southern Oceanus Procellarum near the Reiner Gamma Constellation Region of Interest, continues through the Marius Hills volcanic complex, proceeds northward along the youngest mare basalts as defined by crater statistics [**5**], and concludes with an in-depth exploration of the Aristarchus plateau [**Fig. 2**]. This traverse includes diverse lithologies, regions of unexplained albedo, color, and magnetic anomalies, a wide range of lunar volcanic types and ages, and includes four Constellation Regions of Interest (Reiner Gamma, Marius Hills, Aristarchus 1 and 2).

Opportunities to Develop Technologies: Future explorers (to the Moon and beyond) will require new technologies, and the Moon is the ideal location to develop and validate them. One of the highest priorities identified in the decadal survey for near-term, multi-mission technology investment is for the completion and validation of the Advanced Stirling Radioisotope Generator (ASRG). An ASRG/solar hybrid rover enables electronics to survive and operate in the extreme lunar environment. In addition, Intrepid offers other opportunities to test technologies essential for future robotic and human exploration, including precision autonomous landing and surface navigation, instrument development, and tele-operations.

Leveraging Existing Remote Datasets: A key objective of LRO is to provide datasets to enable future ground based exploration activities. The Lunar Reconnaissance Orbiter Camera (LROC) acquires high-resolution and synoptic images that provide high resolution maps, digital elevation models, and illumination maps. Datasets from other instruments onboard LRO and other satellites (Clementine, Lunar Prospector, Chandrayaan, Chang'e, SMART-1, and future orbiters) will be used in traverse planning and identifying features of scientific and exploration interest and potential hazards that could disrupt rover operations.

Participatory Exploration: The proposed Intrepid rover has outstanding opportunities for immersive public engagement with both passive (live high-definition video streams, 3-D surface panoramas, and daily views of Earth) and participatory (remote rover driving and imaging, collective data analysis, and communication via social media) participation throughout the two-year nominal mission. Intrepid operations and data analysis will also contribute to developing NASA's future workforce (undergraduates, graduates, and postdocs).

References: [**1**] Committee on the Planetary Science Decadal Survey; National Research Council, 2011 [**2**] LEAG Exploration Roadmap (2011) [**3**] Vondrak et al., *SSR*, 150, 7-22 [**4**] Schultz et al. (2010) *Science*, 330: 468-472. [**5**] Hiesenger et al. (2010), *J. Geophys. Res., 115, E03003.*

ARNE - SUBLUNAREAN EXPLORER. M.S. Robinson, J. Thanga, R.V. Wagner, V.A. Hernandez, School of Earth and Space Exploration, Arizona State University, 1100 S. Cady Mall, 85287, robinson@ser.asu.edu

Introduction: Lunar mare "pits" are key science and exploration targets. The first three pits were discovered within Selene observations [**1,2**] and were proposed to represent collapses into lava tubes. Subsequent LROC images revealed 5 new mare pits and showed that the Mare Tranquillitatis pit (MTP; 8.335°N, 33.222°E) opens into a sublunarean void at least 20-meters in extent [**3,4**]. Additionally more than 200 pits were discovered in impact melt deposits [**4**]. A key remaining task is determining pit subsurface extents, and thus fully understanding their exploration and scientific value. We propose a simple and cost effective reconnaissance of the MTP using a small lander (<130 kg) named Arne that carries three flying microbots (or pit-bots) each with mass of 3 kg [**5,6,7**]. Key measurement objectives include decimeter scale characterization of the structure of wall materials, 5-cm scale imaging of the eastern floor, determination of the extent of sublunarean void(s), and measurement of the magnetic and thermal environment.

Why Arne?: Rationale: The future of the human race lies in space. The first step in extending our current pitiful knowledge and capabilities in our transition to a space-faring species requires lunar exploration. First step - discover a sustainable architecture for lunar exploration. Need: Enable sustainable crewed lunar exploration (reduce mass, cost, risk) Goals: 1) Investigate suitability of void(s) at MTP for exploitation (radiation shield, micrometeorite shield, benign thermal conditions). 2) Technology demonstration (Autonomous precision landing and hazard avoidance, flying payload with autonomous navigation). 3) Investigate nature of mare flood volcanism (thickness of flows, nature of void. 4) Engage the public (Explore the voids! What else can we find? What lies beneath?) Objectives: Land safely and accurately, under autonomy, image pit wall during descent, fly autonomous pit-bots into void, measure extent of voids, characterize roughness of voids, high resolution mapping of pit floor for future landing planning, characterize magnetic and thermal environment of pit floor and void(s).

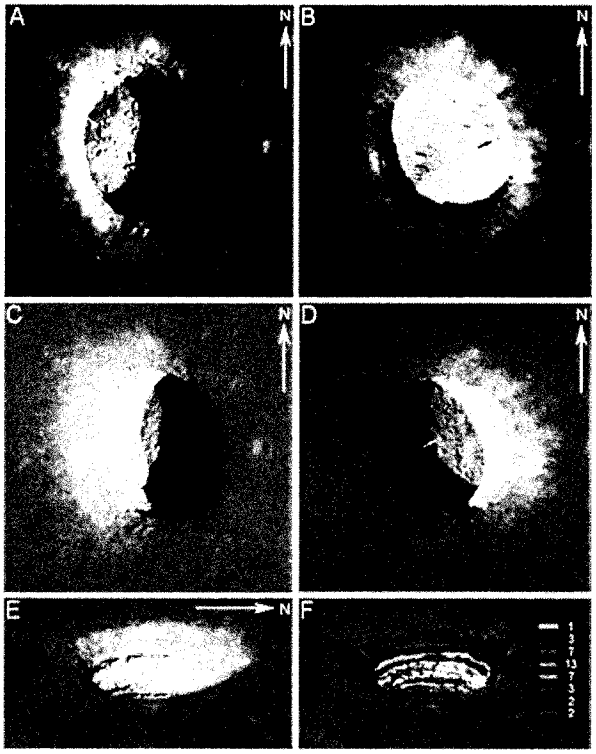

Figure 1. (A, B) MTP in two near nadir images with opposite Sun azimuth angles, both images are approximately 175 m wide. Oblique views: (C) layering in west wall and a portion of pit floor beneath overhanging mare (29° ema); (D) A significant portion of the illuminated area is beneath the eastern over hanging mare in this image (26° ema), white arrow indicates same boulder marked with black arrow in B. Detailed layering is revealed in (E) and (F). Outcropping bedrock layer thickness estimates are presented in (F) in meters, ±1m.

Arne Concept of Operations: Arne will make a noontime descent and optically lock onto the MTP rim and floor shadow, 100 meters above the surrounding mare Arne will descend vertically (~1 m/s). At the top of the

pit Arne will determine the position of boulders on the floor known from LROC images [3], and then maneuver to a relatively smooth spot in view of the Earth.

After initial surface systems check Arne will transmit full resolution descent and surface images. Within two hours the first pit-bot will launch and fly into the eastern void. Depending on results from the first pit-bot the second and third will launch and perform follow-up observations (continue exploring same void or head west, north, and/or south). The primary mission is expected to last 48-hours, before the Sun sets on the lander there should be enough time to execute ten flights with each pit-bot.

Arne will carry a magnetometer, thermometer, 2 high –res cameras, and 6 wide angle cameras. The pit-bots are 30-cm diameter spherical flying robots [**5,6,7**]. Lithium hydride [**5,6**] and water/hydrogen peroxide power three micro-thrusters and achieve a specific impulse of up to 400 s. The same fuel and oxidizer is used for a fuel cell (energy density 2,000 Wh/kg) [**5,6**]. Each pit-bot flies for 2 min at 2 m/s for 100 cycles; recharge time is 20 min. The pit-bots are equipped with a flash camera, magnetometer, thermometer and obstacle avoidance infrared sensors. Once on the ground and initial check out is complete the exploration begins!

- Launch PB-1, 120 second flight into void, 1-m/s at an altitude of <3 meters
- 75 seconds to characterize topology of unseen void, send data to lander
- 5 seconds to touch down
- 30 minute pressurize H and O reservoirs, image, temperature, magnetics measurements
- Second flight - transmit remaining data from 1st flight and data collected on surface, collect additional ranging and images
- Lander transmits PB-1 data to Earth between flight 1 and flight 2
- During PB-1 second repressurization period plus 1 hr pause while flight team evaluates returned data and plans further PB-1 activities and PB-2 first flight (**Fig. 2**)
- If void terminus not found PB-2 launches and serves as relay for PB-1
- If void terminus found PB-1 continues mapping east void and PB-2 heads west
- PB-3 launches follows up on discoveries from PB-1 and PB-2
- PB-3 explores third direction (N, S?), or…
- PB-3 relay data for PB-1 and 2, or …
- PB-3 ascends and images pit walls, or …
- PB-3 acquires detailed imaging of lander and surroundings

Due to the short ground operations time (<72 hours) the ground science support team must be nimble and plan final operations in real time.

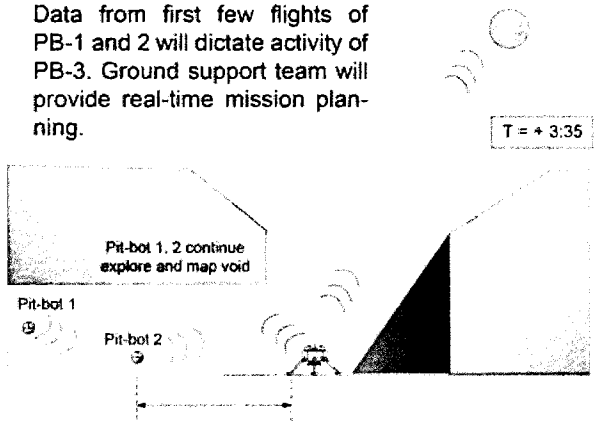

Figure 2. Basic Arne ConOps during mid-mission.

References: [**1**] Haruyama et al. (2010) *41st LPSC*, #1285 [**2**] Haruyama et al. (2010) *GRL*, 36, dx.doi.org/10.1029/2009GL0406355 [**3**] Robinson et al (2012) *PSS*, 69, dx.doi.org/10.1016/j.pss.2012.05.008 [**4**] Wagner and Robinson (2014) *Icarus*, dx.doi.org/10.1016/j.icarus.2014.04.002 [**5**] Thangavelautham et al. (2012) *IEEE ICRA* [**6**] Strawser et al. (2014) *J. Hydrogen Energy* [**7**] Dubowsky et al. (2007) *Proc. CLAWAR*.

ROBOTIC SAMPLE RETURN I: ADVANCING OUR UNDERSTANDING OF PLANETARY DIFFERENTIATION. C.K. Shearer[1], S. Lawrence[2], and B.L. Jolliff[3]. [1]Institute of Meteoritics, Department of Earth and Planetary Sciences, University of New Mexico, Albuquerque, New Mexico 87131(cshearer@unm.edu), [2]School of Earth and Space Exploration, Arizona State University, Tempe, Arizona 85287, [3]Department of Earth and Planetary Sciences, Washington University in St. Louis, St. Louis, Missouri, 63130.

Introduction. The Moon is an exceptional target for sample return (SR) because it is easily accessible, a witness plate for early Solar System events (e.g. impact history), preserves a record of early terrestrial planet processes that may be applicable to other planetary bodies (e.g. differentiation, crustal formation and evolution), exhibits an extended thermal and magmatic history of an evolving planet, and provides a near-Earth environment to demonstrate SR technologies that may feed forward to more distant destinations and complex mission architectures. Here, we examine the role of lunar SR for advancing our knowledge of the early differentiation of the Moon and other planetary bodies. A companion abstract by S. Lawrence addresses other science themes that may be fulfilled by SR.

SR and Links to LEAG Roadmap. The Lunar Exploration Analysis Group (LEAG), chartered by NASA to analyze key components, time phasing, and prioritization of lunar exploration, developed a roadmap for the robotic and human exploration of the Moon (http://www.lpi.usra.edu/leag/ler_draft.shtml). The roadmap consists of three themes - Science, Feed Forward, and Sustainability - divided into goals, objectives, and investigations. SR is intimately integrated into all three themes. For example, developing and implementing SR technologies and protocols is one of the Feed Forward objectives. Conducting a comprehensive resource and market assessment of commercial support for scientific and exploration activities is one of the sustainability objectives that require prospecting and assaying of lunar surface materials. SR is given a relatively high priority in the roadmap for fulfilling lunar science goals across various time phases. Time phasing includes various stages of exploration from simple non-mobile robotic SR to more complex robotic SR (with mobility) and human-enabled SR.

Examples of SR targets for understanding Planetary Differentiation and Crustal Evolution. Here, we provide examples of SR targets that will further our understanding of fundamental processes tied to the differentiation of the terrestrial planets. Interpretation of returned samples from the Moon within the context of recent mission results (e.g. GRAIL, LRO) will further enrich the science return from all these missions.

Example 1. South Pole-Aitken Basin (SPA) sample return: The Moon's SPA has been identified as a high-priority target for SR by numerous NRC studies and decadal surveys as well as NASA advisory committees. SPA SR will directly enable a more comprehensive understanding of the nature of the far-side crust and mantle with implications for planetary differentiation will be accomplished through a SPA SR. For example, sampling of basalts is important because they represent materials produced by melting of the lunar interior. Basalts returned from SPA Basin can be used to determine the composition of the mantle from which the basalts were derived, as well as the depth and extent of melting and chronology of mantle melting-crustal growth. These results can be used to test a variety of models relevant to the primordial differentiation of the Moon, origin and nature of lateral asymmetry in the Moon's mantle and its relationship to the well-defined crustal asymmetry, as well as test theoretical models for the effects of large basin-forming impacts. Samples of basalt, including cryptomare and volcanic glasses, are needed to determine the chemistry, petrology, and history of the sub-SPA mantle.

Example 2. Sampling of the "primordial lunar crust" from the farside highlands: A fundamental concept derived from the samples returned from the Apollo Program was that the Moon experienced large scale melting (Magma Ocean (MO)) and that primordial crust was formed during this event as a result of plagioclase flotation. This primordial crust is thought to be represented by the ferroan anorthosites (FANs). This MO concept has been extended to many of the terrestrial planets. However, more recent crystallization ages for FANs using multiple chronometers have yielded relatively younger ages than expected for most MO models. These ages (4.3 to 4.4 Ga) have been interpreted in several divergent ways: (a) a young Moon, (b) a Moon-wide thermal event, (c) FAN samples collected during Apollo do not represent primordial crust, or (d) there was no MO. Sampling FANs from farside targets is one feasible pathway to provide valuable insights concerning a fundamental planetary process and solar system chronology.

Example 3. Sampling of the deep lunar crust excavated in central peaks: Unlike the Earth, in which the deep crust and shallow mantle are accessible through tectonic and volcanic processes, the deep crust (and perhaps the shallow mantle) on the Moon are accessible in central peaks associated with large impact basins. Sampling central peaks will allow the reconstruction of the chronology of lunar crustal growth and the thermal history of both the lunar crust and mantle.

A New Moon. An initiative to integrate new lunar information into our fundamental understanding of the Moon and the next stages of lunar exploration. C.K. Shearer[1], C.R. Neal[2], B.L. Jolliff[3], M.A. Wieczorek[4], and S. Mackwell[5]. [1]Institute of Meteoritics, Department of Earth and Planetary Sciences, University of New Mexico, Albuquerque, New Mexico 87131(cshearer@unm.edu), [2]University of Notre Dame, Notre Dame, Indiana, 46556, [3]Department of Earth and Planetary Sciences, Washington University in St. Louis, St. Louis, Missouri, 63130, [4]Insitut de Physique de Globe de Paris, Saint Maur, France, [5]Lunar and Planetary Institute, Houston, Texas, 77058.

Introduction: In 1998, Curation and Analysis Planning Team for Extraterrestrial Materials sponsored a long-term initiative to improve our understanding of the Moon and its history by integrating all available types of data: in situ investigations, analyses of lunar samples, telescopic observations, and spacecraft datasets. This initiative, New Views of the Moon (NVM), was supported by NASA's Science Mission Directorate and the Lunar and Planetary Institute. The initiative was guided principally by Brad Jolliff, Charles Shearer Mark Wieczorek and Clive Neal. The goals of the initiative were (1) to summarize new insights that have been gained about the Moon as a result of recent global data sets and their integration with sample and other data; (2) to define current understanding of the Moon's geologic history, resources, and potential for scientific exploration; and (3) to communicate implications of knowledge gained from research and exploration of the Moon for planetary science and exploration beyond the Moon. This initiative involved over 100 individual scientists and engineers, consisted of numerous workshops and special sessions at national and international meetings, and cumulated in a book "New Views of the Moon" that was published in 2006 as volume 60 of Reviews in Mineralogy and Geochemistry (Fig. 1). In 2012 the book was translated into Chinese. Unfortunately, NVM went to press prior to analysis of the data from missions flown since 2000, and before the major discoveries from sample analyses made this century.

FIG 1. End products of the NVM initiative.

Our view of the Moon has dramatically changed since NVM was published, based on mission observations and new measurements made on lunar samples. We propose to start a new lunar initiative that will integrate these new observations into producing a richer understanding of our nearest neighbor in space, revealing new clues about the history of the Solar System, and providing new information for renewed exploration of the Moon with robotic and human missions.

A New Perspective from Missions: Following the publication of NVM, numerous missions to the Moon have been launched by a variety of space agencies examined the surface and interior of the Moon. These include SMART-1 (ESA), Kaguya (Japan), Chang'e 1, 2, 3 (China), Chandrayaan-1 (India), LRO, LCROSS, ARTEMIS, GRAIL, and LADEE (USA). The resulting new datasets have rewritten our view of the Moon with regards to lunar evolution, terrain formation, tectonic and geochemical processes, volatile reservoirs, and potential resources. During the duration of the proposed initiative a variety of orbiter, rover, and sample return missions are possible.

A New Perspective from Samples: Since 2006, using new or improved analytical approaches, sample studies have shed light on the nature, behavior, and role of volatile reservoirs in the lunar mantle and crust, the age and evolution of the lunar highlands, age and origin of the Moon, and dynamical processes in the early Solar System. For example, ion microprobe studies of volcanic glasses and apatite in mare basalts indicate distinct volatile reservoirs in the lunar mantle.

A New Perspective from Engineering and Resource Utilization: In addition to the vast science return from recent missions, these missions have also generated new observations that will enable future human missions to the Moon. They also provide a foundation for future human activity in the Earth-Moon system and beyond enabled by potential lunar resources. For example, new gravity and illumination maps enable future human activity by characterizing the distribution and nature of volatile and solar resources on the lunar surface, permitting optimization of future utilization of resources to sustain exploration and commerce.

Proposal for a New Lunar Initiative: The time is right to synthesize data from all of these new observations and integrate them with our understanding of the Moon prior to 2006. This new lunar initiative will build upon both NVM and the Lunar Sourcebook (a user's guide to the Moon), and produce a new science and engineering assessment of the Moon. The initiative will consist of several topical workshops, meeting special sessions, web-based resource collections, and a final book product. This abstract and presentation is the first solicitation for input from LEAG and the lunar community (both USA and internationals).

Evidence for surface volatiles on the Moon and Mercury: A Planetary Comparison

M.A. Siegler[1,2], Paul Lucey[3], Gregory Neumann[4], Paul Hayne[1], David Paige[5], Benjamin Greenhagen[1], 1-Jet Propulsion Laboratory, California Institute of Technology, 2-Planetary Science Institute, 3-University of Hawaii, Manoa, 4-Goddard Space Flight Center, 5-UC, Los Angeles (matthew.a.siegler@jpl.nasa.gov)

Introduction: The Moon and Mercury both have cold, permanently shadowed regions featuring temperatures low enough to preserve water ice and other volatiles. With data from the Lunar Reconnaissance Orbiter (LRO) and MESSENGER missions, we can now begin to make detailed comparisons between comparable data sets to look for evidence of polar volatiles on these two solar system bodies.

Background: Both LRO and MESSENGER carried 1064 nm wavelength laser altimeter instruments that provide a unique, zero-phase measurement of surface reflectance. Surfaces measured by the Mercury Laser Altimeter (MLA) showed higher than average surface albedo within some shadowed craters near the North Pole [1]. Modelling surface temperatures with MLA topography, these same areas were found to provide thermally stable environments for surface water ice to survive for geologic time (with loss rates less than 1mm per Gyr) [2].

Areas where ice was modeled to be stable only if covered by a low thermal conductivity surface material (such as Mercury regolith) showed an unusually dark MLA reflectance [2, 1]. This material is hypothesized to be one or more compounds less volatile than water ice, plausibly an organic material originating from comet impacts. Both bright and dark areas showed high circularly polarization ratio returns from earth based radar [3,4] and neutron spectrometer detections consistent with near surface concentrations of water ice [Lawrence, 2013]. Reflectance data from the the Lunar Orbiting Laser Altimeter (LOLA) show that the lunar permanently shadowed regions are anomalously bright compared to areas that receive illumination, but direct comparisons of temperature and LOLA reflectance has not been carried out [6,9]. These reflectance variations can be affected by many things, including soil composition, space weathering, geology and roughness. Comparing the data sets between these two bodies can help differentiate these processes and potentially strengthen any claims volatile presence.

This study: Here we further the MLA reflectance vs. temperature study of Paige et al. [2] and apply a similar technique to newly available data from LOLA. In the previous studies for Mercury [2,1] MLA data was unavailable at latitudes northward of 84° (due to the MESSENGER orbit). Since this time, a campaign of off-nadir measurements has extended both MLA topography and reflectance measurements to colder areas nearer to the North Pole (southern polar data is not available due to MESSENGER's elliptical orbit). Thermal model comparisons to be extended to much lower temperatures than previous work, which featured surfaces generally exceeding 100K.

These colder environments on Mercury are more comparable to those found in the permanent cold traps on the Moon. This allows for a direct comparison between the two bodies within areas whose surface maximum temperatures are roughly 50-100 K. These environments, water and other volatiles should be stable at the surface over geologic timescales.

Impact gardening should mix and bury ice, causing these surface features to slowly disappear [e.g.14]. We would like to test an hypothesis that deeply buried, thermally mobile volatiles would then rise to the ice table, outpacing loss by gardening. Conversely, at colder temperatures, gardening will again dominate, causing a surface to return to the average regolith albedo.

As some gardened material is mixed from below a thick layer should stay volatile dominated longer than a thin layer. Therefore, surface brightening found at temperatures far below the "volatility temperature, T_v", where thermal migration could outpace gardening, could imply thick ice deposits. Cold areas smaller than the resolution of the thermal models/data, so a brightening above the volatility temperature should also be expected. The presence of a surface volatiles should therefore result in characteristic "bumps" and "dips" in brightness as a function of maximum surface temperature, a *volatility spectrum*.

Results: Figures 1 and 2 show the volatility temperatures of several volatile materials plotted as dashed lines on top of a point cloud (grey) of all available MLA (Fig 1) and LOLA (Fig 2) data as a function of MLA modeled/Diviner data maximum surface temperature. Maximum surface temperature controls the abundance of surface ice perceptible to laser altimeters.

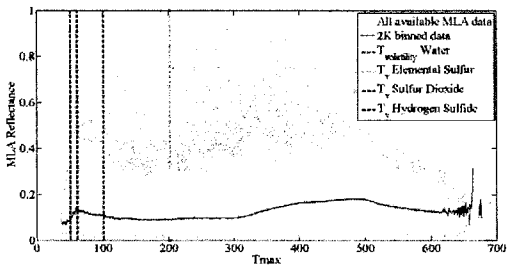

Figure 1: MLA reflectance vs maximum modeled surface temperature [updated models from Paige et al., 2013].

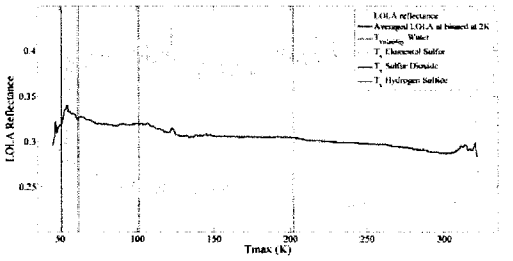

Figure 2: LOLA reflectance vs maximum Diviner measured surface temperature.

We note that both the Moon and Mercury show substantial brightening of their surfaces below roughly 120K. This could be indicative of surface water frost on both bodies. Water has a volatility temperature of about 100K (seen in figures 1-4), so one might expect a dark surface to brighten around 100K if water is present. If the water layer were thin one might expect a decreased brightness below 100K due to impact gardening. LOLA data shows a clear dip near 80K, which could imply a thin water frost layer that is being mixed into the regolith by impact gardening. In MLA, this dip is more subdued, potentially pointing to a thicker volatile layer.

Both also show a second increase in brightness at lower temperature. This lower peak could be evidence for a second bright volatile. Candidates for this peak are SO_2, with a T_v of about 62K, or CO_2 with a T_v of about 54K. Mercury appears to have brightening closer to SO_2, while the Moon favors CO_2.

Rather than being a separate volatile, this lower peak could also be indicative of either a very thick water ice layer (as might be supported by radar evidence on Mercury, but not the Moon), or a very freshly deposited layer (as theorized in [15])

Noted in Paige et al. [2], MLA data showed substantial darkening between ~150 and 350K. In Figure 3, we see enhanced darkening within this temperature range at ~200K, as might be expected from elemental Sulfur or a family of complex organics (such as linear amides or carboxylic acids), especially when processed by Mercury's high radiation environment [16,17]. This could be explainable by volcanic activity on Mercury or by delivery of organics from a comet. Such a dip is not present in the LOLA measurements, implying an absence of this dark material (which should show an even stronger contrast with higher albedo lunar regolith) is not present.

These comparisons hint that both of these planetary bodies may have evidence for surface stable volatiles, but that that these volatiles are not the same on the two planets and may have different source materials. Understanding these potential volatile materials and their sources can substantially impact our understanding of the delivery and retention of volatiles in the inner solar system.

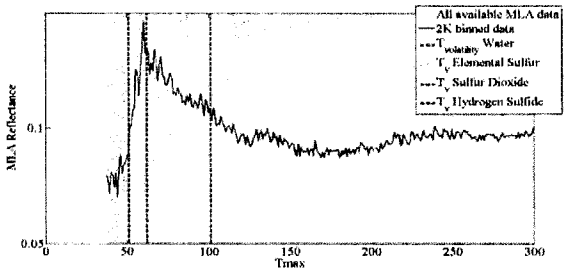

Figure 3: Close up of MLA reflectance vs maximum modeled surface temperature [updated models from Paige et al., 2013].

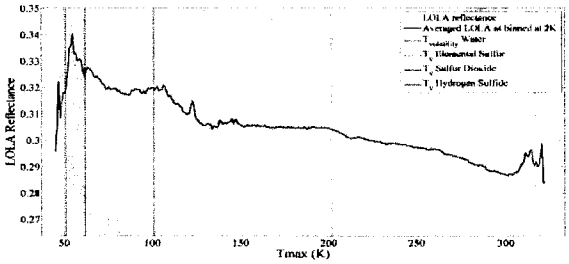

Figure 4: Close up of LOLA reflectance vs maximum Diviner measured surface temperature.

References:[1] Neumann et al. 2013, Science [2] Paige et al. 2013, Science [3] Slade et al., 1992, Science [4]Harmon et al, 2011, Icarus [5] Lawrence et al, 2013, Science [6] Lucey et al, 2013 AGU [7] Campbell et al, 2006, Nature [8] Feldman 2001, JGR[9] Lucey et al., 2014, JGR in press [10] Schorghofer 2007, JGR [11] Siegler et al. 2011, JGR [12] Siegler et al., 2014, Icarus, in press [13] Paige et al., 2010, Science [14] Crider and Killen, 2005, GRL [15] Hayne, et al. 2014, Icarus, In press [16] Zhang and Paige, 2010, GRL.[17] Delensky et al. Icarus, in review.

OPTIMIZED TRAVERSE PLANNING FOR FUTURE LUNAR POLAR PROSPECTORS. E. J. Speyerer[1], S. J. Lawrence[1] J. D. Stopar[1], M. S. Robinson[1], B. L. Jolliff[2], [1]School of Earth and Space Exploration, Arizona State University, Tempe, AZ, (espeyerer@asu.edu). [2]Department of Earth and Planetary Sciences, Washington University, St. Louis, MO.

Introduction: Recent lunar missions provide the planetary science community with vast amounts of new data enabling important insights into the geology and evolution of the Moon on a global scale. Remotely sensed observations of the polar regions reveal the location of persistently illuminated regions and evidence for volatiles captured in cold traps [1-5]. In-situ resource utilization (ISRU) of these volatiles has the potential to transform these regions into fueling stations for future lunar missions as well as create a sustainable architecture for the exploration of the Solar System [6]. However, there are still many questions regarding the chemistry and extent of these cold-trapped resources.

Ground-truth measurements are required to fully understand the resource potential of lunar volatiles. A mobile polar prospector could address many outstanding questions by sampling a series of sites to assay resources not only along the surface, but also at shallow depths. These ground measurements are key in calibrating and understanding an array of remotely sensed observations and providing first order estimates of *tonnage* and *grade* of any resource deposit. As part of the mission concept, a precise landing system will deliver a rover to the surface to traverse into several permanently shaded regions (PSRs). By accessing several PSRs, the science payload will determine how volatile contents vary from one PSR to another at the surface and at depth. To optimize the mission and maximize the science return, we propose a traverse-planning algorithm that uses regional data products to identify the least-energy traverse paths around selected landing sites and regions of resource interest.

Traverse Planning: To locate potential traverse options, a digital terrain model (DTM) of the region is required. The DTM must be high enough resolution to capture all the major topographic features (<100 m/pixel) and contain very few areas of interpolation. Therefore, for the polar regions, we use the gridded DTM product produced by the Lunar Orbiter Laser Altimeter (LOLA) team due to their dense collection of points near the poles and their ability to accurately measure elevations in shadowed areas [7].

After selecting the DTM, a grid of evenly spaced nodes (typically several meters to 10s of meters apart) is superposed. Each of the nodes is connected to up to eight neighboring nodes and each connection, or edge, is assigned a value that corresponds to the amount of energy required for the rover to traverse from the current node to the corresponding neighboring node.

Next, we use the A* ("A star") search algorithm [8] to calculate the least energy required and associated path for the model rover to traverse from an initial waypoint to a goal waypoint in the DTM. The A* algorithm is similar to the Dijkstra's graph search algorithm [9] with the exception that a heuristic estimate is used to optimize the search. By varying the order of the waypoints, an optimal mission plan can be derived.

Case Study: Shackleton is a 21 km diameter impact crater near the south pole (89.655°S, 129.2°E) with 235 km^2 of its interior in perpetual shadow [1,5,11]. The first images of the region provided by the Clementine UVVIS camera indicated that a portion of the rim was persistently illuminated [11]. With the recent images and topographic data returned by the Lunar Reconnaissance Orbiter (LRO), knowledge of these regions of persistent illumination were refined and quantified [5,12].

In order for a long-duration polar prospector to survive without the benefit of a Radioisotope Thermoelectric Generator, the rover needs to access and leverage these persistently illuminated areas throughout its mission to meet its power and thermal needs. Therefore, we first map out the traverses between three stations of persistent illumination along the rim of Shackleton crater that were identified by Speyerer and Robinson (2013) with LROC Wide Angle Camera (WAC) images. All three stations are within close proximity to one another (~2 km) enabling a mobile prospector to travel between stations to increase the overall available solar energy throughout the lunar year.

Using a 40 m/pixel LOLA-derived DTM of the south polar region and the traverse-planning tool described above, we identified the optimal path between each pair of stations along the crater rim (**Fig. 1**). The optimal (least-energy) traverse from Station 1 to Station 2 is 2.0 km long with an average absolute slope of 2.3° and a maximum slope of 10.3°. From Station 2 to Station 3, the optimal traverse is 2.5 km long with an average absolute slope of 1.7° and a maximum slope of 6.0°. These slopes are well within the range of previous rover designs and many proposed rovers designs. By leveraging several of the persistently illuminated areas, the amount solar radiation received throughout the year could be increased and the longest eclipse period could be minimized (Table 1).

In addition to looking at the rim of Shackleton, we also investigated traverse options for a pair of local topographic highs near a large flat region that is an ideal site for the lander to deliver the rover to the sur-

face. These sites (Station 4 & 5), which are each illuminated for 45.6% and 63.3% of the lunar year, respectively, collectively remain illuminated for 91.8% of the year and are eclipsed for only 104 h [5]. The optimal traverse from Station 3 to Station 4 is 11.8 km long with an average absolute slope of 4.1° and a maximum slope of 11.7°, while the optimal traverse between Station 4 and 5 is 2.7 km long and has average absolute slope of 2.1° and a maximum slope of 6.5°.

While each of these five stations is illuminated for a majority of the year, areas nearby and along the traverse are in permanent shadow. These relatively small PSRs provide access to potential cold traps that may harbor volatiles. A long duration polar prospector would be able to evaluate the resources in multiple small PSRs, examine how the quantity of volatiles change in areas that receive different percentages of sunlight, and study the mobility of volatiles over short time scales as a region falls in and out of shadow. In addition, Stations 1, 2, and 3 offer ideal views inside of a large PSR (floor of Shackleton crater). Standoff instruments, particularly those with long-integration measurements, could assess surface deposits without risking a traverse down the steep walls (~30°).

***Table 1**- Persistently illuminated regions identified in [5].*

Station	% illumination	Longest eclipse
#1 (89.685°S, 196.7°E)	69.0	147 h
#2 (89.740°S, 201.2°E)	71.6	145 h
#3 (89.808°S, 205.9°E)	63.0	155 h
Station #1 and #2	86.9	63 h
Station #2 and #3	85.5	60 h
Station #1, #2, and #3	**92.1**	**43 h**
#4 (89.500°S, 222.1°E)	45.6	281 h
#5 (89.418°S, 221.3°E)	63.3	308 h

Discussion and Future Work: The traverse-planning tool outlined here provides a means to examine and identify optimal (least-energy) traverses around the lunar poles as well as any region of interest on the Moon or other terrestrial body with accurate topographic data. From our analysis, we conclude that each of the five stations noted above are accessible without exceeding slopes of 12° (40 m scale).

Future work will focus on adding time-varying data sets to the traverse-planning tool. For example, synthetic illumination maps can be used to ensure the roving prospector is never in shadow for more than a predefined amount of time. In addition, by including time-varying thermal data, we can identify traverses where the prospector can sample potential deposits when the temperature of the regolith is at its maximum or minimum. We also plan to improve the DTM by integrating a merged NAC/LOLA product. Overall, this framework, along with the ability to model different size rovers and configurations, enables mission planners to accurately design traverses that maximize the science return while certifying the safety of the prospector.

***Fig. 1**- LROC NAC-derived illumination map (top) and LOLA slope map (bottom) overlaid with optimal traverses between persistently illuminated regions (red line; green dots) derived from a 40 m/pixel LOLA DTM. The blue lines highlight 6.8- and 4.8-km traverses inside two nearby PSRs. Stations 1, 2 and 3 are all on the rim of Shackleton crater; the map is 11.2 km across.*

References: [1] Bussey et al. (1999) *GRL*, 9, 1187–1190. [2] Feldman et al. (2001) *JGR*, 105, 4175–4195. [3] Colaprete et al. (2010) *Science*, 330, 463–468. [4] Mitrofanov et al. (2010) *Science*, 330, 483–486. [5] Speyerer and Robinson (2013) *Icarus*, 222, 122–136. [6] Spudis (2011) *Toward a Theory of Spacepower*, National Defense University Press, 241-251. [7] Smith et al. (2010) *GRL*, 37, L18204. [8] Hart et al. (1968) *IEEE Trans. Sys. Sci. and Cybernetics*, 4, 100-107. [9] Dijkstra (1959) *Numerische Mathematik*, 1, 269-271. [10] Spudis et al. (2008) *GRL*, 35, L14201. [11] Nozette et al. (1996) *Science*, 274, 1495–1498. [12] Mazarico et al. (2010) *Icarus*, 211, 1066–1081.

MINI-RF OBSERVATIONS OF MARE EJECTA EMPLACEMENT DIVERSITY. A. M. Stickle[1], G. W. Patterson[1], D. B. J. Bussey[1], J. T. S. Cahill[1], and the Mini-RF Team, [1]Johns Hopkins University Applied Physics Laboratory, Laurel, MD (angela.stickle@jhuapl.edu).

Introduction: Impact cratering is a primary weathering process of airless bodies and is the dominant method of redistributing material across the lunar surface [1]. Crater ejecta blankets are a window into the impact cratering process and can provide important information regarding the properties of subsurface materials. Radar scattering information, in particular the circular polarization ratio (CPR) [e.g., 2], provides a useful means of investigating these properties. Here, we examine the CPR characteristics of 22 craters that are relatively young and located within nearside Mare deposits (Figure 1). We observe significant diversity in average CPR profiles as a function of crater radius and propose that much of this diversity is an expression of subsurface layering excavated during the impact process.

Figure 1. LROC WAC mosaic showing the locations of the 22 young, fresh mare craters studied here. Squares show craters with visible layering structures in the craters walls as identified by Sharpton (2014) [3]. Colors represent general categories of profile shape.

Background: The Miniature Radio Frequency (Mini-RF) instrument flown on NASA's Lunar Reconnaissance Orbiter (LRO) is a Synthetic Aperture Radar (SAR) with a hybrid dual-polarimetric architecture. I.e., the radar transmits a circularly polarized signal, and receives orthogonal linear polarizations and their relative phase [4]. The returned information can be represented using the classical Stokes parameters (S_1, S_2, S_3, S_4) [5], which can be used to derive a variety of useful products to characterize the radar scattering properties of the lunar surface. CPR is commonly used in analyses of planetary radar data [6-7] and is given by: CPR = $(S_1-S_4)/(S_1+S_4)$. It is a representation of surface roughness on the order of the radar wavelength (e.g., meter scale features).

We have examined the radar scattering properties of the ejecta blankets for 22 young, fresh, mare craters with diameters ranging from 2–55 km, 15 of which have visible layering within the crater walls (Figure 1). Average profiles of the Stokes parameters (S_1 and S_4), and CPR have been calculated as a function of radius for each crater, beginning at the crater rim and extending outward for 100–200 km (approx. 7-10 crater radii). For some of the craters, radial profiles were taken as an average over a select azimuthal range. This is especially useful for examining asymmetries in ejecta blankets due to oblique impacts or anomalous signals due to topography.

Observations and Analysis: Comparing scattering properties as a function of radius reveals information about ejecta emplacement in mare craters. Some commonalities in the scattering profiles are observed for all crater diameters: higher CPR values occur near the crater rim, which decay with radial distance outward, larger craters have a higher CPR than smaller craters, and the overall shapes of the profiles are similar.

When distance from the crater rim is normalized to crater radius (Fig. 2), however, these trends are not as obvious. The overall size progression is still apparent and larger craters have higher CPR near the rim. However, the profile shapes are no longer similar across the size range, and a high CPR "shelf" near the rim is prominently observed for some craters within a region of high CPR extending out to ~0.5 R_c before the signal transitions to the lunar background value. Gambart A and Harpalus E, however, do not follow this trend. A laterally extensive region of high CPR is not observed at Gambart A, where CPR begins to decrease immediately outside the crater. These observations are contrary to what would be expected from optical images, where there is a large, optically bright ejecta blanket around the crater. In contrast, the CPR is high near the rim of Harpalus E and the surface remains rough (with moderate to high CPR values) out to several crater radii from the rim, unlike other area craters. It is possible that age may account for these differences in profile shape. Although all these craters are Copernican, perhaps crater degradation is more apparent in the roughness of the surface than in optical images.

Figure 2 also compares CPR profiles to crater size. With the exception of Petavius B, all the mare craters > 20 km have similar scattering profiles, though different in magnitude. The CPR drops rapidly near the crater rim, but then plateaus for a short distance before dropping again to the lunar background level. These plateaus neither begin nor end at the same relative radius from the crater rim and exhibit significant variations

from the expected CPR characteristics of crater ejecta. We use these data to infer the presence of subsurface layers that, when ejected onto the surface, have different scattering characteristics than surrounding material. The mechanical property differences between layers could result in more blocks on the order of the radar wavelength to be emplaced on the surface, causing a shelf in the CPR profile. This hypothesis is consistent with preliminary M^3 observations [8] that show differing compositions of material being ejected in these craters.

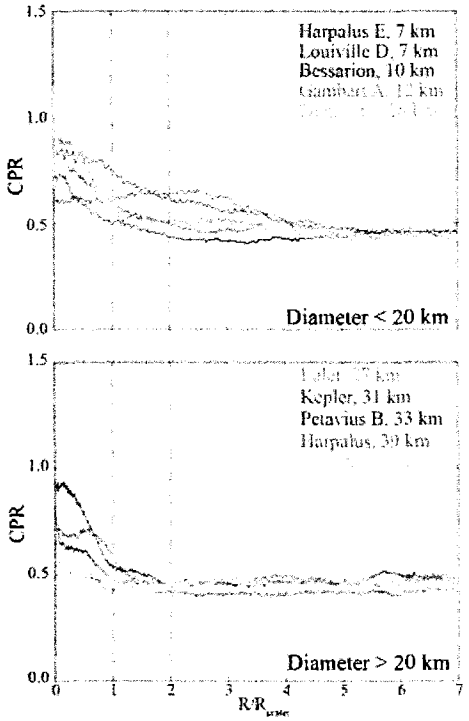

Figure 2. Profiles of average CPR as a function of normalized distance from the crater rim. (top) Mare craters with diameters less than 20 km. (bottom) Mare craters with diameters > 20 km.

These observations reveal that CPR profiles observed adjacent to craters (e.g., Kepler crater) may provide insight regarding subsurface layering in mare regions. Hörz *et al.* [9] estimate that the dominant source depth for primary ejecta within the continuous ejecta blanket is <0.01 times the crater diameter. To a first order, the depth from which material in the continuous ejecta blanket (within approximately 1 crater radius from the rim [10]) is excavated at Kepler crater would then be approximately 300 m, consistent with the approximate depth of the layering observed in LROC NAC images (Fig. 3 top). Thus the CPR profile from Kepler crater may be revealing a discrete subsurface layer that was emplaced at the surface during the impact process.

These observations are consistent for craters with visible layering in the walls studied here. For craters with capping layers (e.g., Bessarion (Fig. 3 bottom) and Dionysius, where the mechanically different layer is seen at the top of the crater wall), the CPR plateaus tend to be at the crater rim, and extend outward a short distance. These high CPR plateaus may be due to the capping layer fragmenting differently than material beneath it, or to the presence of impact melt at the crater rim [e.g., 11]; further detailed analysis will help distinguish these two processes. In contrast, if discrete layers are seen farther down the walls in NAC images (e.g., Kepler), the signal in the CPR appears outward from the crater rim. If no layering is visible in the crater walls (e.g., Gambart A), no shelf is seen in the CPR. Using layer depth estimates with CPR profiles as a function of distance, it may be possible to generate a model for excavation depth of ejecta emplaced on the surface.

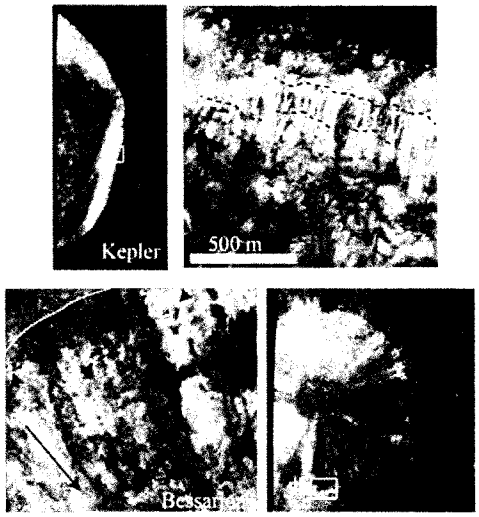

Figure 3. (top, left) LROC NAC mosaic of Kepler Crater (31 km); (top, right) NAC image of layering in the wall of Kepler crater. Dotted lines show approximate edges of subsurface layers observed behind landslides. (bottom, left) NAC image of capping layers in the wall of Bessarion crater, indicated by white box in the NAC mosaic (bottom right).

References: [1] Melosh, H. J. (1989), Oxford Univ. Press; [2] Campbell et al. (2010), *Icarus*, 208, 565-573; [3] Sharpton, V.L. (2014) *JGR-P 119*, 1-15; [4] Raney, R. K. et al. (2011), *Proc. of the IEEE*, 99, 808-823; [5] Stokes (1852), Trans. of the Cambridge Phil. Soc. 9, 399; [6] Campbell et al. (2010), *Icarus*, 208, 565-573; [7] Carter et al. (2012), JGR, 117, E00H09; [8] R. Klima, personal communication; [9] Hörz, F. et al. (1983) *Rev. Geophys. and Space. Phys.*, 21, 1667-1725; [10] Moore et al. 1974, *Proc. 5th LPSC*, 71-100; [11] Neish et al. (2014), *Icarus 239*, 10-117.

IN SEARCH OF IMPACT-INDUCED H2O-ALTERATION SIGNATURES: INITIAL THERMAL CONSTRAINTS. J. D. Stopar[1], M. S. Robinson[1], E. Asphaug[1], B. L. Jolliff[2], E. J. Speyerer[1], P. R. Christensen[1] [1]SESE, Arizona State University, Tempe, AZ (jstopar@asu.edu), [2]Department of Earth and Planetary Sciences, Washington University in St. Louis, MO.

Introduction: Reservoirs of volatiles, including water (H_2O), may persist within the lunar polar regions, where burial and cold-trapping prevent rapid loss to space [e.g., 1-9]. Water-ice, along with other volatiles, potentially exists as masses, an intimate regolith mixture, or adsorbed on grains [e.g., 3,10]. At very low temperatures (e.g., <110 K), which are typical of many polar regions, water-ice may even be geologically stable at the surface [e.g., 11].

The nature and extent of lunar polar volatiles are not yet well-constrained, and volatiles possibly exist as a variety of species or in various forms. The LCROSS impact-generated plume supports ~6 wt% water-ice within a small permanently shaded region (PSR) of Cabeus crater [5-8]. Surface temperatures suggest that as much as two-thirds of the surface pole-ward of 85°S may be an effective cold-trap, if not necessarily a PSR [12]; even small shaded regions may harbor volatiles [11]. Over time, these modest volatile resources may affect near-surface chemistry and its evolution, if conditions permit.

To further constrain the distribution of water-ice, which is a key driver of future exploration, as well as methods of its detection and determination, we investigate the probability of near-surface, water-mineral reactions that might result in detectable signatures (e.g., via in-situ and/or stand-off sensing techniques).

Background: To enable water-mineral reactions in cold polar regions, a heat source is needed. One plausible environment where reactions between water and minerals may occur is in the near-surface adjoining an impact event. Impacts generate a large amount of thermal energy, affecting a radius of target rock that scales with impactor parameters and target properties [e.g., 13-15]. Impact-generated heat can provide the energy needed to melt and vaporize target rocks, as well as water-ice. However, it is unclear if, or what quantity of, volatiles delivered, melted, and/or vaporized during impact can be retained; though a few vol% of cometary and meteoritic volatiles may be imparted to the surface [e.g., 16]. Moderate impact heating of already buried volatiles, however, could allow for localized oxidation or hydration reactions when subsurface materials are heated.

The length of time and extent of heating depend on thermal conductivity as well as rates of thermal radiation and volatile diffusion, which vary with compaction, fractures, and pore-interconnectivity [e.g., 17-18]. The duration and radius of heating directly affect the amount of chemical alteration reactions that can occur. As a point of reference, the terrain around two small terrestrial craters (4-km Kardla and 1.5-km Lonar) are thought to have cooled over several thousand years, even with enhanced convective cooling resulting from hydrothermal circulation [e.g., 19-20]. Apollo materials contain evidence for long-duration (e.g., thousands of years) and shorter-lived, high-temperature (600-1000°C) vapor-phase reactions during large (i.e., basin-forming) impact events [e.g., 21-24]. These temperatures and timescales are generally favorable for mineral alteration reactions [e.g., 25].

Methods: Heat-transfer modeling [e.g., 2,8,18,26-27] provides a straightforward approach to assessing the potential for water-mineral reactions in the lunar polar regions. For our preliminary model, we employ a simple, uniformly distributed, two-layer model of hot crater materials overlying a porous, non-mare regolith with 6 wt% pore-bound water-ice. While the bulk of impact-generated heat is expected adjacent to the crater cavity, we adopt a flat-lying model volume for ease of calculation (and refer to this model as ejecta overlying regolith), but the general principle of heat transfer also applies to the areas adjacent to the crater cavity. We allow for large thermal losses through radiation, and we employ published values of heat capacities, latent heats, and densities for the lunar regolith and H_2O [e.g., 9,18,28]. We also assume constant pressure, minimal diffusion, effective heat transport, no pore connectivity, pore-pressures can exceed the triple point of water, and H_2O and regolith warm on similar timescales. These simplifications provide an estimate of the maximum amount of water-ice that can be liberated during various impact events. Future work will refine these preliminary models.

Results: Materials ejected near the crater rim will be the thickest, and most volumetrically significant, though often the least shocked. However, ejecta materials experience a wide range of shock pressures and temperatures, and range from a few hundred degrees to more than 1450°C [e.g., 29]. A single, small 5-km crater with cool ejecta (200°C), is unlikely to melt significant ice, but a 30-km crater with warmer ejecta (600-1000°C) has enough heat to melt several hundred km^3 of ice or vaporize ~50 km^3 of ice (**Fig. 1**). However, small craters form much more frequently than larger craters, and may over time activate volumetrically significant water.

If ice is confined to a thin layer (e.g., upper meter), then, for modeled craters larger than ~1 km in diameter, there is less ice available for melting than energy to melt it. However, low thermal conductivity of the porous upper regolith [e.g., 18], may help concentrate heat in the near-surface and increase the duration of the heating event.

Initial surface and subsurface temperatures of target materials also affect the volumes of melt/vaporized ice. Target materials with an initial temperature of 200K can significantly reduce the amount of heat required to raise regolith and ice temperatures to the melting point compared to those at 40K, thereby increasing the maximum volume of ice melting by a factor of two (**Fig. 2**).

The initial assumption that radiation reduces the available impact-generated heat by 90%, strongly controls the magnitude of the maximum melt volumes. Decreasing radiation losses from 98% to 50% increases potential ice-melting by a factor of 25.

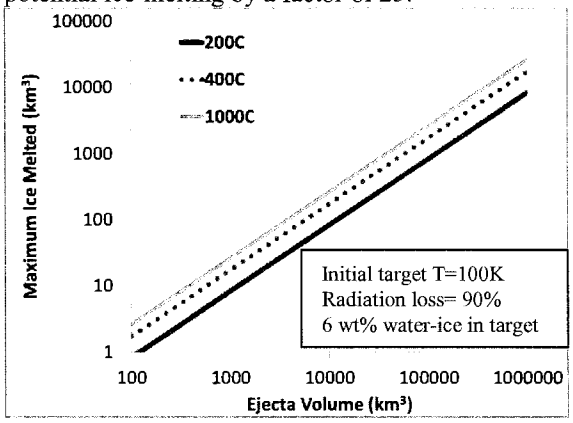

Figure 1. Maximum volume of ice melted by heating from overlying ejecta as a function of ejecta temperature. Assuming 50% of ejected materials are within two crater radii of the transient crater (TC) rim crest, and depth/diameter of the TC is 1/3, a volume of 1,000,000 km^3 equates to a ~140-km diameter crater and 100 km^3 to a ~5-km crater.

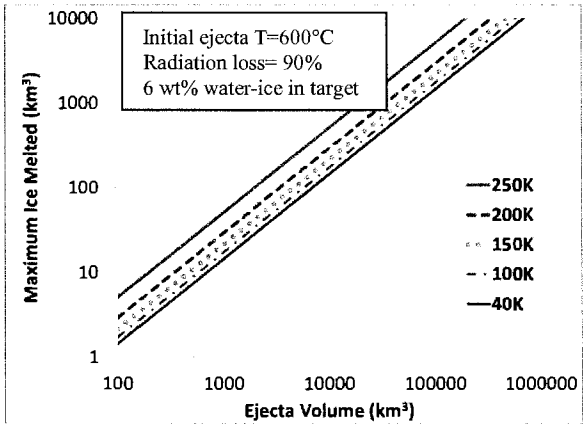

Figure 2. Maximum volume of ice melted as a function of ejecta volume and initial target temperature.

Implications: Chemical reactions are generally enhanced by surface defects such as fractures, shocking, and disordered chemical structure [e.g., 30-31], all of which should be relatively common in the battered, near-surface lunar regolith. Our initial calculations of the maximum volumes of melted and vaporized ice suggest that the formation of detectable chemical signatures during impact-events into polar, volatile-enhanced reservoirs might be possible.

Where pore-interconnectivity is minimized (as modeled), liquid-water alteration pathways are reactant-limited, and chemical reactions are strongly controlled by local mineralogy [e.g., 25]. Under these conditions, liquid solutions tend to quickly become saturated [e.g., 30]. While saturation may slow reactions, it also can also favor the formation of secondary product.

Over time, near-surface materials, including any alteration products, will tend to be churned up through impact gardening, potentially becoming exposed at the surface, where they can be detected and studied. The pervasiveness (or dearth) of alteration signatures ultimately informs the persistence, reactivity, and evolution of volatile resources on the Moon.

References: [1] Arnold (1979) JGR 84:5659-5668. [2] Vasavada et al. (1999) Icarus 141:179-193. [3] Cocks et al. (2002) Icarus 160:386-397. [4] Crider and Vondrak (2003) JGR 2002JE002030. [5] Colaprete et al. (2010) Science 330:463-468. [6] Schultz et al. (2010) Science 330:468-472. [7] Gladstone et al. (2010) Science 330:472-476. [8] Hayne et al. (2010) Science 330:477-479. [9] Schorghofer and Aharonson (2014) Astrophys. J. 788:169. [10] Poston et al. (2014) LPSC #2283. [11] Hayne et al. (2013) DPS 45 #107.03. [12] Paige et al. (2010) Science 330:479-482. [13] O'Keefe and Ahrens (1977) Proc. LPSC 8:3357-3374. [14] Wünneman et al. (2008) EPSL 269:530-539. [15] Pierazzo and Melosh (2000) Icarus 145:252-261. [16] Gibson and Moore (1973) Science 179:69-71. [17] Binder and Lange (1980) JGR 85:3194-3208. [18] Fagents et al. (2010) Icarus 207:595-604. [19] Kirsimae and Osinski (2013) in *Impact Cratering*, pp. 76-89. [20] Newsom et al. (2013) in *Impact Cratering*, pp. 271-289. [21] McKay et al. (1972) Proc. LPSC 3:739-752. [22] Treiman et al. (2013) LPSC #1567. [23] Hudgins et al. (2008) GCA 72:5781-5798. [24] Shearer et al. (2014) GCA 139:411-433. [25] Brantley (2003) in *Treatise on Geochem.*, pp. 73-117. [26] Abramov and Kring (2004) JGR 109:2156-2202. [27] Schwenzer et al. (2012) EPSL 335/336:9-17. [28] Carrier et al. (1991) in *Lunar Sourcebook*, Ch 9. [29] Simonds et al. (1976) Am. Min. 61:569-577. [30] White and Brantley (2003) Chem. Geol. 202:479-506. [31] Hamilton et al. (2000) GCA 64:2603-2615.

LUNAR GENE BANK FOR ENDANGERED SPECIES. Swain, R. K. Undergraduate,Integrated BS-MS,Indian Institute of Science Education and Research,Bhopal, India E-Mail: Rkswain28@gmail.com , ramakrushnas@iiserb.ac.in

Introduction: Before the dawn of the 22nd century, we face the huge risk of losing our genetic heritage accumulated during aeons of evolution. The losses include hundreds of vertebrates, hundreds of thousands of plants and over a million insect species. The gene pools of many human ethnic groups are also threatened. As we have observed, adequate conservation of habitat is unfeasible and active breeding programs cover only a handful of the many thousand species threatened.

Against such indispensable losses scientists are starting cryopreservation of germplasms by creation of gene banks. I propose to construct a cDNA library based gene bank for endangered species in the permanently shadowed polar lunar craters that would provide immunity from both natural disadvantages and humanitarian intrusions [4].

Rationale: In the pursuit of conservation of biodiversity, enormous money is spent all over the globe but they are unable to address the severity of the problem. Under such alarming circumstances, we turned to cryopreservation as an option but over thousands of years economic depression, sabotage, conflicts, warfare or even a brief disruption to the precise cryopreservation can hamper the storage of genetic samples.When we are considering conservation it is always preferable to go for a more secure and permanent solution. It was found out that the climatic and strategic location of the lunar polar craters are adequately hospitable, remote and free of maintenance and human observation as they provide naturally cryogenic temperature, reduced gravity and vacuum environment, non-reactive surface, safety from celestial intrusion and permanent shadow which doesn't allow the temperature to fluctuate thus providing most suitable storage facilities for the germplasms. PSRs provide steady temperature of 40-60K and immunity to earthquakes due to low seismic activity. At these sites, burial in one meter or more of the regolith will provide protection against the solar wind, solar and galactic cosmic rays and micrometeorite impact. It provides the minimum necessary barrier from human intervention and at the same time enables easy retrieval for future usage. Genetic samples of endangered species can enable restoration even after its extinction. Preserved tissues can secure the genetic heritage of species, and may allow future cloning to restore biodiversity. Furthermore, there would be no scientific extinction [4].

Biological Processes: For storage of a huge number of genetic samples, we need to follow the basic protocols of construction of a cDNA library based gene bank.cDNA library represents the genes that were being actively transcribed in that particular source under the physiological, developmental, or environmental conditions that existed when the mRNA was purified [2]. Total RNA can be extracted from plants by using LiCl method [5]. The message RNA can be isolated and purified double-strand cDNA can be synthesized using the cDNA Library Construction Kit in a PCR machine. Five microliters of PCR products can be labeled with α32PdATP)fractionated by electrophoresis in 1.0% alkaline agarose gel to check the ds-cDNA quality along with the single stranded cDNA. One microliter of the purified cDNA can be ligated into the predigested vector (1 μg) digested by EcoR I-Xho I following the protocol of overnight ligation at 16 °C in a sense orientation. The lambda library can be packaged in a high-efficiency system and plated on the E. coli cell line .After amplification of the library titre can be calculated as per the manufacturer's recommendation and it came to 1 X 107cfu. The library can be stored in 7% DMSO at -80°C until further screening of the gene of interest. The size of the insert fragments can be measured by PCR method using random selection of 10-15 clones from the SOLR infected positive clones (growing in LB ampicillin agar plates) [5].Using 0.1 gram of genetic material from about 20 individuals per species can allow the future restoration of a species. A realistic payload of 2,000 kg can save one million species. The storage medium would contain liquid nitrogen [4].

Location: After a thorough search, it has been concluded that the gene bank containing container should be buried under the regolith of the PSR of the base of Shoemaker Crater located near the Lunar South Pole, centered at 88.1 S, 45E[1]. It provides diameter of 20-51km with an immense 100m^2 of PSR [6].

The physical properties of the floor material can be modeled. This floor is known to be flat, providing simple geometry for understanding impact dynamics and the Ejecta plume in case required. In addition, about half of the crater floor is invisible from earth but access from polar lunar orbiter is good because a spacecraft would pass overhead every two hours[6]. Hence, it enables easy storage, surveillance and prolonged retention of the proposed gene bank.

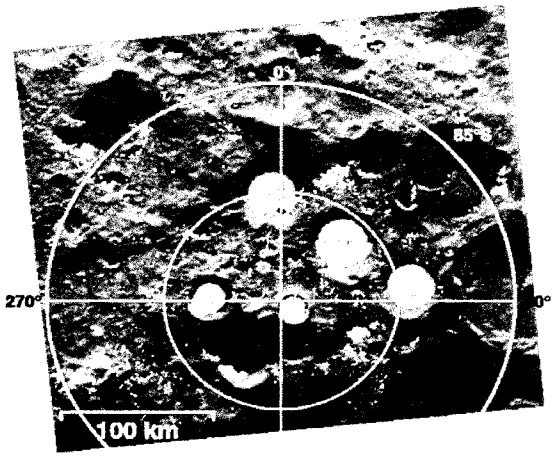

Figure 1.Radar DEM of south polar craters, Shoemaker crater indicated by arrow; white – permanent shadow (calculated), gray – no radar return; from [3]

Conclusion: Cryoconservation can add an important ethical component to the space programme and help raising public support. Conversely, the permanent safety of the genetic

material can also make cryoconservation itself more attractive and fundable. Many nations may wish to participate to secure the genetic heritage of their unique biota and ethnic groups[4]. It is highly advisable that developed countries associate with biologically rich countries and biotechnologists all over the world to collect the genetic samples as many as possible which they can include in their future lunar missions to secure the future of the living world. Until habitat losses are controlled, cryoconservation may provide the best chance to secure and eventually revive many endangered species. For this purpose, space-based depositories can provide precise conservation ,the most cost-effective and secure means for permanent storage of irreplaceable genetic materials with a single one time expenditure for ages instead of the prevalent ineffective conservation programs.

References:

[1] Allen, C. C., NASA Johnson Space Center, Mail Code KT, Houston, TX 77058 carlton.c.allen@nasa.gov. Shoemaker crater – going where we can "see" [2] Anonymous, http://en.wikipedia.org/wiki/Library_(biology) [3] Margot J. L. et al. (1999) *Science, 284,* 1658-1660 [4] Mautner, M.N. (1996) Space-based Genetic Cryoconservation of Endangered Species. *Journal of The British Interplanetary Society.* , Vol. 49, pp 319-320 [5] Sambrook J, Fritschi EF and Maniatis T (1989) Molecular cloning: a laboratorymanual, Cold Spring Harbor Laboratory Press, New York [6] Shevchenko, V.V. and E.A.Kozlova, Sternberg State Astronomical Institute, Moscow University, 13 Universitetsky pr., 119992 Moscow, Russia; e-mail: shev@sai.msu.ru Permanently shadowed areas at the lunar poles: nature and possible utilization.

The Search for a Diurnal Effect in Lunar Hydrogen Abundance

Luís F.A. Teodoro[1], David J. Lawrence[2], Richard C. Elphic[3], Vincent R. Eke[4], William C. Feldman[5], Sylvestre Maurice[6] [1] BAER, NASA Ames Research Center, Moffett Field, CA 94935-1000 USA (luis.f.teodoro@nasa.gov); [2] Johns Hopkins University Applied Physics Laboratory, 11100 Johns Hopkins Road Laurel, MD 20723, USA; [3] NASA Ames Research Center, Moffett Field, CA 94935-1000 USA; [4] Institute for Numerical Cosmology, Department of Physics, University of Durham, South Road, Durham DH1 3LE, UK; [5] Planetary Science Institute, 1700 E. Fort Lowel, Suite 106, Tucson, AZ 85719, USA; [6] Université Paul Sebatier, Centre d'Etude Spatiale des Rayonnements, 9 avenue Colonel Roche, B.P. 44346 Toulouse, France.

Mapping the abundance of hydrogen-bearing materials has led to significant advances in our understanding of the sequestration of volatiles at the poles of the Moon. Neutron spectroscopy, and especially mapping of epithermal neutron fluxes, has been central to this endeavor [e.g. 1]. In this talk we present a study of the diurnal variation of the Lunar Prospector neutron spectrometer (LPNS) measurements to search for the possible low-latitude mobility of water molecules. This study is prompted by reports of local-time-varying concentrations of H_2O/OH, based on near-infrared spectral reflectance data [e.g. 2], as well as reports of a diurnal hydrogen signature in the Lunar Exploration Neutron Detector epithermal neutron fluxes [e.g. 3]. While the spectral reflectance signatures could be due to small amounts of surficial water or hydroxyl molecules within the instrument view, the neutron result implies the diurnal mobility of volumetrically significant amounts of water and/or hydroxyl. Such an extraordinary finding, if confirmed, could have significant ramifications for our understanding of the H_2O/OH distribution and mobility at the lunar surface.

To quantify the variability of the epithermal count rate, $cr(\mathbf{x}, t)$, we introduce the random *over count rate* variable, $\delta cr(\mathbf{x}, t)/cr$:

$$\delta cr(\mathbf{x}, t)/cr = (cr(\mathbf{x}, t) - cr_f(\mathbf{x}, t))/cr_f(\mathbf{x}, t))$$

where $cr_f(\mathbf{x}, t)$ is the fiducial count rate maps at 6 pm (local time), $\mathbf{x}$ is the a location on the lunar surface and t denotes local time. To quantify $cr(\mathbf{x}, t)$ we use three sub time-series defined as follows: *i)* All the instants of the overall LPNS time-series within the latitude range $[-55°, -55°]$, *ii)* measurements with high altitude (average $\sim$ 100km) at the same latitude range as the previous data-set (hereafter High Altitude), and *iii)* measurements with low altitude (average $\sim$ 30km) at $|\text{latitude}| < 55°$ (hereafter Low altitude). In Figure 1 we show the average *over count rate* (averaged over the latitude domain) of the three sub time-series. In this talk, we will show that Lunar Prospector epithermal neutron data exhibit diurnal variations of the same magnitude (1-2% of the average lunar epithermal neutron flux) as those reported by [3], however the LPNS variations do not follow the same diurnal trend. Instead, the LPNS variations are systemically anti-correlated with instrument temperature, and are related to very small changes in instrument gain. These findings suggest that, rather than reflecting diurnal changes in hydrogen, the temporal fluctuations in the count rates are due to small residual systematic effects in the data reduction.

References

[1] W. C. Feldman, S. Maurice, A. B. Binder, B. L. Barraclough, R. C. Elphic, and D. J. Lawrence. Fluxes of Fast and Epithermal Neutrons from Lunar Prospector: Evidence for Water Ice at the Lunar Poles. *Science*, 281:1496–+, September 1998. doi: 10.1126/science.281.5382.1496.

[2] J. M. Sunshine, T. L. Farnham, L. M. Feaga, O. Groussin, F. Merlin, R. E. Milliken, and M. F. A'Hearn. Temporal and Spatial Variability of Lunar Hydration As Observed by the Deep Impact Spacecraft. *Science*, 326:565–, October 2009. doi: 10.1126/science.1179788.

[3] T. A. Livengood, G. Chin, R. Z. Sagdeev, I. G.

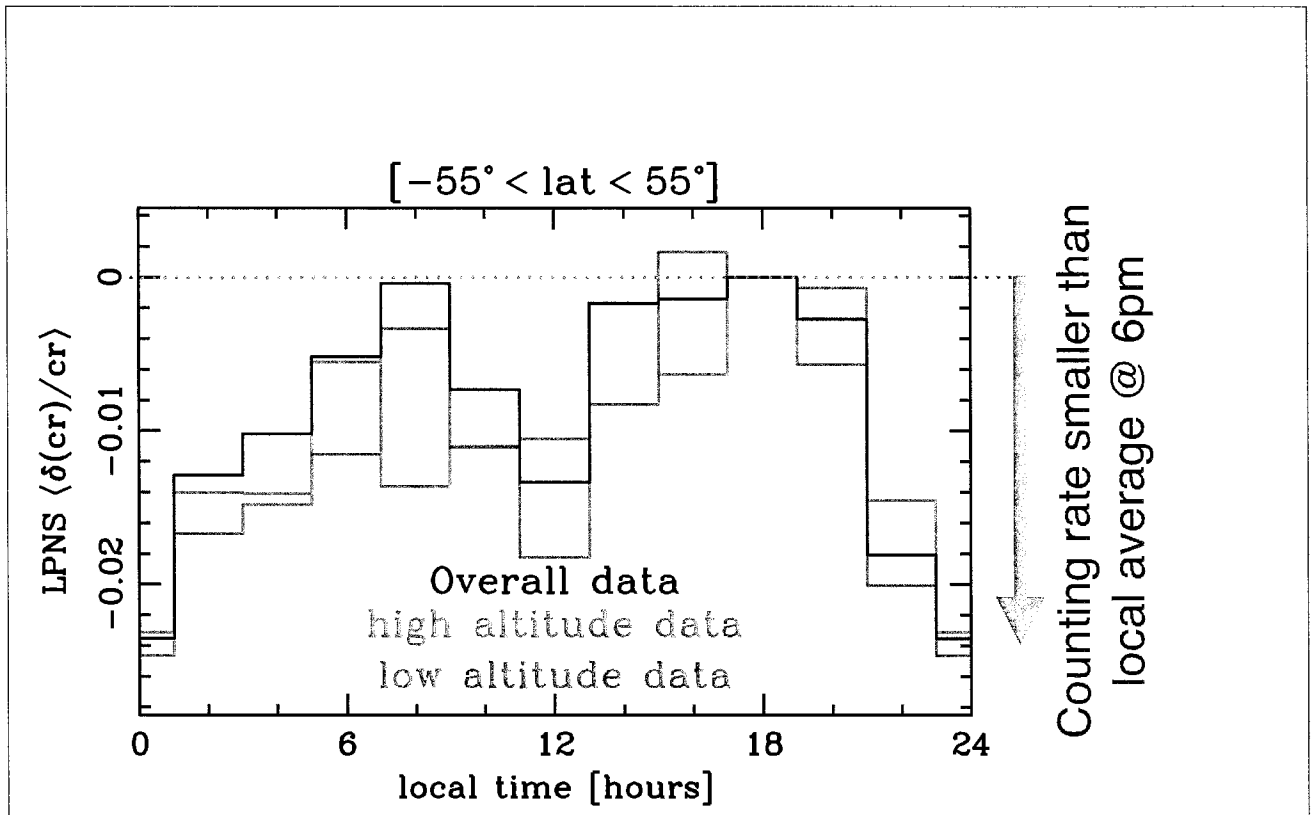

Figure 1: Average *over count rate* per *local time* bin. The *fiducial map* is the mean counting rate at a given location over a two hour local time bin centered around 6 pm local time. The random errors in the measurements are smaller than 2.1×10^{-4}, 5.2×10^{-4}, 3.5×10^{-4} for the overall (black), high altitude (green) and low altitude (violet) data, respectively. The shaded regions of the diagrams represent the night period of the day. The x-axis tickmarks coincide with the local time bin centers.

Mitrofanov, W. V. Boynton, L. G. Evans, M. L. Litvak, T. P. McClanahan, A. B. Sanin, and R. D. Starr. Evidence for Diurnally Varying Hydration at the Moon's Equator from the Lunar Exploration Neutron Detector (LEND). In *Lunar and Planetary Science Conference*, volume 45 of *Lunar and Planetary Science Conference*, page 1507, March 2014.

Lunar Proton Albedo Anomalies: Soil, Surveyors, and Statistics

J. K. Wilson, N. Schwadron, H. E. Spence, A. W. Case, M. J. Golightly, A. P. Jordan, J. Kasper, M. D. Looper, J. E. Mazur, N. E. Petro, M. S. Robinson, T. J. Stubbs, C. Zeitlin, J. B. Blake, S. S. Smith, L. W. Townsend

Since the launch of LRO in 2009, the CRaTER instrument has been mapping albedo protons (~100 MeV) from the Moon. These protons are produced by nuclear spallation, a consequence of galactic cosmic ray (GCR) bombardment of the lunar regolith. Just as spalled neutrons and gamma rays reveal elemental abundances in the lunar regolith, albedo protons may be a complimentary method for mapping compositional variations.

We presently find that the lunar maria have an average proton yield 0.9% ±0.3% higher than the average yield in the highlands; this is consistent with neutron data that is sensitive to the regolith's average atomic weight.

We also see cases where two or more adjacent pixels (15° × 15°) have significantly anomalous yields above or below the mean. These include two high-yielding regions in the maria, and three low-yielding regions in the far-side highlands. Some of the regions could be artifacts of Poisson noise, but for completeness we consider possible effects from compositional anomalies in the lunar regolith, including pyroclastic flows, antipodes of fresh craters, and so-called "red spots". We also consider man-made landers and crash sites that may have brought elements not normally found in the lunar regolith.

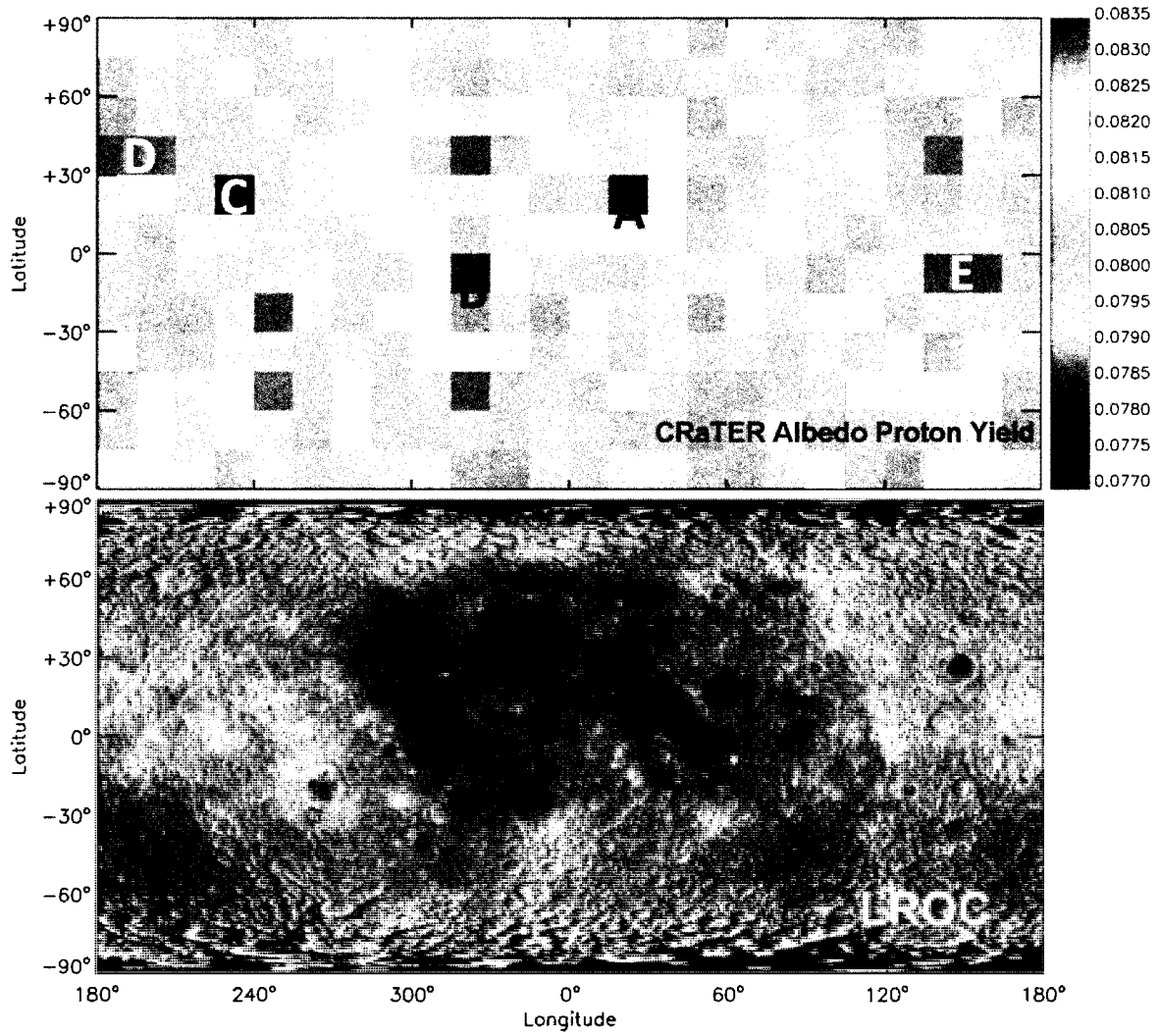

RADIOISOTOPE THERMOELECTRIC GENERATORS (RTGS) FOR LUNAR EXPLORATION.
D. F. Woerner[1], [1]Jet Propulsion Laboratory/Caltech, 4800 Oak Grove Drive, MS 321-520, Pasadena, CA 91109, david.f.woerner@jpl.nasa.gov

Introduction: RTGs have been used for deep space exploration for decades, including powering lunar surface instruments during NASA's Apollo missions. RTGs have proved to bc highly reliable. NASA and the Department Of Energy (DOE) are working on future generator designs in addition to producing the currently available Multi-Mission Radioisotope Thermoelectric Generator or MMRTG. An MMRTG is currently powering the Curiosity rover on Mars and was designed as a compact, rugged power source capable of landing on other bodies. This specific generator is now more than six years old and performing as predicted.

This presentation will provide the latest information on MMRTGs and other RTGs being engineered and studied.

Body: An MMRTG is on Mars powering the Curiosity rover[1], an enhanced or eMMRTG is being engineered with an industrial partner, and a study of an Advanced RTG, or ARTG, recently concluded with a briefing on the parametric analysis. Each of these generators relies upon several decades of RTG flight experience. The MMRTG is a derivative of the generators used for the Viking and Pioneer missions. The eMMRTG[2] uses almost the exact design of the MMRTG. The ARTG draws on the platform flown on the Cassini and Galileo missions. Similarly the enhancement to the MMRTG thermoelectric couples (unsegmented) is a stepping-stone for the couples needed for the ARTG (segmented).

The MMRTG development was started to satisfy the requirements of multiple missions including the Mars Science Laboratory (MSL) mission. The generator development began in late-2002 to support the 2009 launch of the MSL mission. The DOE completed the generator on time and fueled it; shortly thereafter the mission chose to slip the launch date. This left the MMRTG fueled and in storage for more than two years before it was launched and still following the 2011 launch, the MMRTG produced 114W, more than required. As it now operates on Mars it is providing more energy than the mission routinely requires, and power output degrades at approximately 4.8% per year, close to the degradation rate predicted months before launch and more than three years ago.

The MMRTG is a heat source for MSL[3] as well as a power source. The rover design includes heat exchangers that pick up waste heat from the MMRTG and transfer the heat to a circulating fluid. The fluid is routed throughout the rover to keep the avionics operating in a temperature band favorable to prolonging their lifetime.

The MMRTG was conceived as a multi-mission generator and as such operates in both vacuum and planetary atmospheres of Earth and Mars; it could power spacecraft in orbit around distant planets or be landed on them. It was also designed to multi-mission requirements that were not relevant to the MSL mission including the atmosphere of Titan. Further examples incude that the MMRTG was qualified to worst case Atlas V launch vehicle environments and was designed to minimize magnetic field emissions to meet the needs of science missions requiring the most powerful launch vehicles and/or measuring planetary magnetic fields.

There are two MMRTGs in NASA's inventory and both are allocated to the proposed Mars 2020 mission. In time, the mission will down select to one MMRTG and have it fueled for flight.

As part of a plan to enhance the MMRTG, JPL has begun to transfer thermoelectric couple (TEC) technology to the MMRTG TEC manufacturer that will enhance power output and reduce degradation, and JPL has begun performing systems engineering for the eMMRTG system using these new TECs.

eMMRTG engineering has identified a single, simple change to the MMRTG's design to support the new TECs; an emissivity coating added to a thin metal surface inside the generator will lower the temperatures that would be problematic if left unchanged. The new TECs and the change to the liner result in approximately a 24% enhancement to conversion efficiency. Further, the Beginning Of Life (BOL, the time of fueling) power boost is estimated to be approximately 166 W in a 4k thermal sink and under a 32V load. That is a 36% increase over the MMRTG in the same conditions. The eMMRTG is estimated to also degrade more slowly than the MMRTG. The eMMRTG is estimated to produce 109W, 101% more than the MMRTG's 54W, at EODL, or after 17 years of operation.

The eMMRTG technology transfer from JPL to industry is scheduled to be complete by the end of the 2018 fiscal year. NASA will then have the option to build and qualify an eMMRTG, if the transfer was completed successfully. The first eMMRTG could be ready for fueling as early as late 2020 or early 2021.

NASA will also have the chance to enhance the unsegmented TEC technology if the technology transfer

was successful. Power output can again be increased significantly by adding a small segment to each of the two TEC legs, thereby creating segmented TECs. Generator concepts using these segmented TECs have been named Advanced RTGs or ARTGs.

Thermoelectric couples in general, due their design, allow for a great deal of flexibility, and this enabled the ARTG trade space to be studied parametrically and focusing on three unique designs: a single-point design, a modular design, and a multi-mission design. The single-point design looks very similar to the RTGs used on the Galileo and Cassini missions. This design would likely be large relative to the MMRTG, over twice the length but capable of producing ~500W at BOL and be designed to operate in vacuum only. Had this generator been available when Cassini launched, the mission would have needed only two generators rather than the three that were launched.

The modular ARTG design is significantly different from the single-point design. This generator would consist of modules that could be stacked to produce more powerful generators. The "base" module would produce approximately 45W. Power output would reach approximately 425W by stacking eight of these modules together. The TECs for this modular design would be made of the same materials as the TECs for the other ARTGs, but rather than use standalone TECs, the TECs would be packaged in a higher-density matrix, sometimes called a close-packed array. The modular ARTG would be rated for vacuum operation only.

A multi-mission ARTG would draw heavily upon the eMMRTG and enhance it further. The generator would be longer and weigh more but would produce approximately 200W of power at BOL as compared with the eMMRTG's 166W at BOL. The multi-mission ARTG would preserve the multi-mission requirements of the eMMRTG to the maximum extent practicable.

Conclusion: RTGs to support a variety of lunar missions are available or in detailed engineering development. Some designs could be available in less than eight years and could offer significant benefits over the current generation RTG.

References:

[1] NASA/JPL, *Mars Curiosity Rover - Mars Science Laboratory MMRTG Power System 2011,* video, http://www.youtube.com/watch?v=VsYC3Yz2kZM.

[2] Woerner, D., Cairns-Gallimore, D., Zakrajsek, J., O'Malley, T. (2014) NETS 2014, *Getting to an enhanced MMRTG.* [3] Bhandari, P. et al. (June 2011) SAE International Journal of Aerospace, vol. 4 no. 1 299-310.

THE INTEGRATION OF HANDHELD TECHNOLOGIES INTO PLANETARY SURFACE EXPLORATION. K. E. Young[1,2], J. E. Bleacher[2], C. A. Evans[3], Z. Arzoumanian[1,2], K. Gendreau[2], K. V. Hodges[4]. [1]CRESST/University of Maryland, College Park, [2]NASA Goddard Space Flight Center, [3]NASA Johnson Space Center, [4]School of Earth and Space Exploration, Arizona State University. Corresponding email address: Kelsey.E.Young@nasa.gov.

Introduction: Future manned planetary surface exploration will be highlighted by a need for effective and efficient surface characterization prior to sample selection for return to Earth. This sample high-grading, while not the only necessary step in exploring a site [1], is crucial in maximizing the science return of a surface mission. Astronauts will have many constraints limiting their surface time devoted to science activities and it is therefore of paramount importance to design sample high-grading technology to be both efficient and unobtrusive to an astronaut's surface activities.

Work is underway to design a suite of instruments to both enhance astronauts' geologic and contextual awareness of a site of interest and to enable them to collect and high-grade samples real-time during surface operations. Initial investigations centered on the effectiveness of the handheld x-ray fluorescence spectrometer (hXRF) [2,3], a commercial off-the-shelf (COTS) technology designed for use in industry and mining applications. Limitations, both in the technology (which focuses only on chemical composition and not structure), the detector hardware (which is unable to accurately detect lighter elements), and the software, have led to the development of the Chromatic Mineral Identification and Surface Texture (CMIST) instrument [4]. CMIST is a contact XRD/XRF instrument currently in development at NASA Goddard Space Flight Center. Instrument testing is taking place in part through SSERVI mission (Solar System Exploration and Research Virtual Institute) activities, specifically with the RIS4E team (Remote, In Situ, and Synchrotron Studies for Science and Exploration).

Primary study goals include evaluating how these developing handheld and field-portable technologies fit into astronaut surface operations. Time available to crews for science data collection is limited, so any implemented technologies can't require extensive time or attention from each astronaut.

Handheld X-Ray Fluorescence Technology: The use of laboratory x-ray fluorescence (XRF) technology in geological applications has been extensive and well-documented [5, 6, etc.]. Recently, companies such as Innov-X, ThermoScientific, and Bruker, for use in industry and mining, have miniaturized this technology. These handheld XRF (hXRF) instruments have potential applications in conducting field geology, both on Earth and in planetary surface exploration. In order to implement this technology into scientific applications, however, we first sought to validate the accuracy of the hXRF. Through a series of analyses conducted over a period of two and a half years at NASA Johnson Space Center, we calibrated an Innov-X hXRF instrument using a suite of terrestrial basaltic sample standards (on loan from the Spectroscopy and Magnetics Lab run by Dr. Richard Morris). Chemical compositional information about these standards was collected using the Franklin and Marshall College's PANalytical 2404 X-ray fluorescence vacuum spectrometer. Calibration curves for nine major elements (Al, Ca, Fe, K, Mg, Mn, P, Si, and Ti; Na is too light to be accurately detected with the hXRF) were developed that are now used to convert raw hXRF counts into major element oxide data (ex. Figure 1).

Additional hXRF investigations have centered on the sample preparation necessary to obtain reasonably accurate hXRF data. Figure 2 shows the comparison between laboratory data and hXRF data taken on both sawed and rough sample surfaces. The data show that, while sawed surfaces give a better approximation to the laboratory standard data, data collected on rough sample surfaces also yield data that can inform astronaut sampling activities.

A small case study was conducted [3] in conjunction with the 2010 NASA Desert RATS (Research and Technology Studies) field test. Four crews (each composed of one astronaut and one field geologist) traversed the San Francisco Volcanic Field in NASA's habitat rover (the MMSEV), with the goal of unraveling the geologic history of the region through exploration and sample collection. [3] evaluated the samples collected by one of these crews with the hXRF to determine how effective the instrument would have been had it been included in the field test. The hXRF was able to differentiate between two lava flows that were indistinguishable during mission operations.

While these preliminary instrument evaluations demonstrated that the hXRF could be a valuable addition to a planetary surface mission and give the user contextual information about their sampling site, there are several limitations with using this COTS technology. Lighter elements (i.e. Na) cannot be detected with current detector technologies. Additionally, as the calibration and software/user interface programming are proprietary, there is no flexibility in data reduction and

integration with other data sets. We now turn to developing new instrumentation to satisfy the need for technology designed to maximize an astronaut's effectiveness in real-time sample high-grading.

Developing CMIST: While traditional X-ray diffraction (XRD) requires crushing and sieving for powder analysis, contact XRD technology requires minimal sample preparation. The CMIST instrument combines this contact XRD capability with XRF technology to allow for a look both at sample chemical composition as well as texture analysis of that sample's surface. In data acquisition times of as low as 10s of seconds, the CMIST instrument can give the user valuable, real-time information about composition, mineral phase identification (including ice), and size and orientation of a variety of mineral phases.

While this instrument is still in the development phase, it shows great potential to be applicable to a variety of exploration scenarios. In order to maximize its utility to an astronaut, software must be developed for this technology that will allow the user access to a) real-time data viewing with no need for data reduction; b) potential integration with other mission data streams; and c) a balance in highlighting available data while not overwhelming the crewmember with overly detailed analyses (but instead helping to inform sample collection and high-grading). This software development will be ongoing over the next several months.

RIS4E Field Activities: The development of the CMIST instrument will take place in part through the field deployments conducted by the Remote, In Situ, and Synchrotron Studies for Science and Exploration (RIS4E) team, one of nine nodes of NASA's SSERVI program (Solar System Exploration and Research Virtual Institute). Team members will travel to the December 1974 flow at Kilauea, HI, in September 2014. Overall mission goals include investigating both the subsurface structure and surface topography of the flow as well as the in situ geochemistry and mineralogy of the site. While CMIST is not yet field portable, samples will be collected in September for future analysis with the laboratory-bound instrument.

Conclusions: Developing a suite of instruments for inclusion in the next generation of planetary surface exploration is of paramount importance in maximizing mission science return. Initial investigations on one such technology, the handheld XRF spectrometer, have shown that in situ geochemical technologies increase the real-time contextual and geologic awareness of an astronaut in the field. More work is needed, however, on streamlining user interface technology to ensure that the crewmember is not overwhelmed with data quantity but instead receives condensed data summaries to assist in sample high-grading decisions.

It should also be noted that sample collection alone is not enough to fully understand a geologic field site. Crewmember observations from the field are also crucial in understanding the context of a site to allow for a complete understanding of where each collected sample fits into the larger regional history [1]. In situ field assessment of geologic context is at least as important as in situ sample analysis for sample high-grading [7], meaning that the former must complement the latter.

References: [1] Hurtado Jr., J. M. et al. (2013) *Acta Astro, 90.* [2] Young K. E. et al. (2012) *LPSC 2012,* A2628. [3] Young K. E. et al. (2012) *AGU 2012,* A V33B-286. [4] Arzoumanian Z. (2013) *LPSC 2013,* A2116. [5] Beckhoff, B. et al. (2006) *Springer,* Handbook of practical x-ray fluorescence analysis. [6] Jenkins, R. (1999), *Wiley-Interscience,* X-ray fluorescence spectrometry: second edition. [7] Hodges, K.V. and H.H. Schmitt (2011) *GSA Spec. Pub., v. 483.*

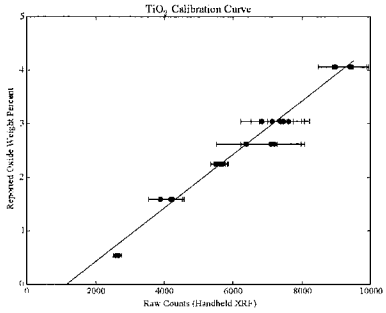

Figure 1: Handheld XRF calibration curve for TiO_2. The equation for the line is y = 0.0005x – 0.5738, R^2 = 0.97411. These curves formed the basis for the conversion from raw instrument counts to calculated weight percent oxides for the nine major elements discussed in this study. Error bars are all 2σ and errors on the reported oxide weight percent are smaller than the symbols shown.

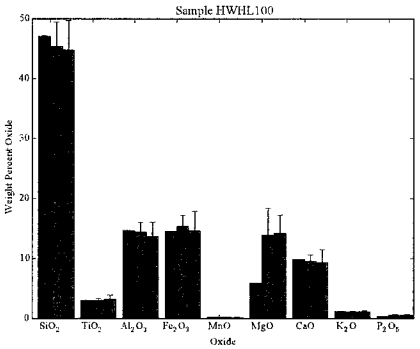

Figure 2: Plot showing comparisons for the nine major elements of interest. Data from the laboratory XRF (blue), hXRF on sawed surfaces (red), and hXRF on rough surfaces (green) are compared. Error bars represent ±2σ. If the error bars are not visible, the errors on that point are too small to be visible.

LUNAR PROSPECTING DRILL. K. Zacny[1], G. Paulsen[1], P. Chu[1], J. Kleinhenz[2], J. Smith[3], J. Trautwein[3], J. Quinn[3], [1]Honeybee Robotics, Pasadena, CA, zacny@honeybeerobotics.com, [2]NASA Glenn Research Center, Cleveland, OH, [3]NASA Kennedy Space Center, FL

Introduction: Near term exploration of the Moon will most probably focus on northern or southern cold traps. This is because these regions were found to contain large fraction of water and other volatile resources within the top meter of the regolith [1]. Water and volatiles are not only of interest for science investigations but also as source of valuable resource.

For over a decade, Honeybee Robotics has been focusing on development of a one meter class robotic drill systems, called Icebreaker, for capturing of icy samples on Mars. Although majority of work has been done having Mars polar caps as primary target, the sampling approach and hardware is applicable to the lunar drilling goals, with some modifications to account for hard vacuum and more extreme temperatures (low and high) [2-4]. The Lunar Prospecting Drill (LPD) is a 'Moon' rated copy of the TRL 5/6 Mars Icebreaker3 (IB3) drill, the third generation of rotary-percussive one meter class drills. The 'Moon' rating included changes to actuator lubrication, upgrading some hardware subsystems to account for Coefficient of Thermal Expantion (CTE), and installing heaters on critical elements. In August of 2014, the LPD has been undergoing a series of tests in a Lunar chamber (VF13) at the NASA Glenn Research Center (GRC).

This abstract describes the drill and reports on preliminary test data from the lunar chamber tests.

Subsystems of the Drill: The drill system can be divided into five major components as described below and detailed in **Figure 1**.

The Deployment Z-stage is a pulley based system (more dust tolerant than a ballscrew) that lowers the Drilling System to the ground. It can preload the Drilling Z-Stage with up to 500 N if required; although the exact preload is software limited to whatever value is achievable given rover weight. The baseline preload is 150 N.

The Drilling Z-Stage is also a pulley based system that lowers the Sampling Auger up to 1 meter into the ground. It should be noted that the pulley system was selected not only because of its dust tolerance but also to enable efficient propagation of percussive energy generated in a Drill Head hammer. Since the Drill Head is free to move up and down on the carriage connected to the pulley via set of cables, vibrations are not transferred to the drill structure and the rover as much. The Drilling Z-Stage can also apply up to 500 N of downward force (called Weight on Bit or WOB) and it can retract the drill by applying up to 500 N pull force (note that in this case the force is reacted into the ground). During drilling operation, the WOB is software limited to approx. 100 N.

The Drill Head Assembly consists of 1. 200 Watt Rotary Actuator to spin auger up to 180 rpm; 2. 200 Watt Percussive Actuator to hammer the auger at 1600 blows per minute with 2.6 Joules per blow, and 3. 4 channel slipring to enable temperature measurements at the drill bit.

The Auger is made up of three parts: 1. Transport Auger is a top 100 cm section designed for moving cuttings out of the hole in the most efficient manner; 2. Sampling Auger is a bottom 10 cm section designed for capture and retention of sample within the flutes; 3. Drill Bit is responsible for penetrating through dry and volatile rich formations in most efficient manner enabled by custom tungsten carbide cutters. It has a temperature sensor for monitoring the subsurface temperature during drilling and measuring subsurface temperature when the drill is lowered onto the hole bottom.

The Sampling Assembly consists of an Auger Tube, passive rotating Brush, and a Spout. As the Sampling Auger passes through the Auger Tube, its flutes rotate the Brush (the Auger and the Brush form worm gear configuration), and the Brush in turn scrapes the sample on the flutes into the Spout. If the sample needs to be discarded, the Spout is positioned above the ground. If the sample needs to be captured, the Spout is positioned above the sample cup.

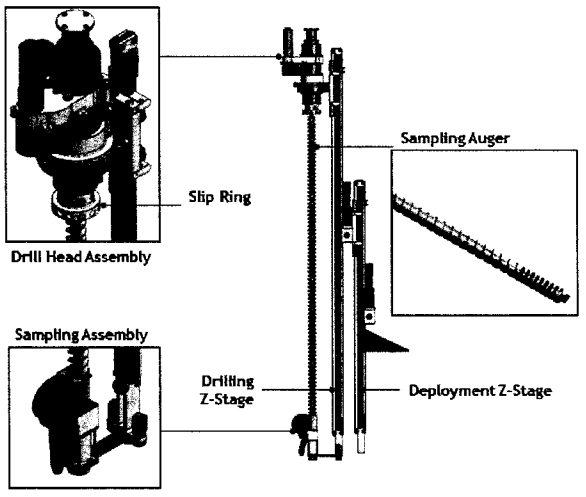

Figure 1. Lunar Prospecting Drill subsystems.

Sampling Process: The sampling routine follows 'Bite' sampling approach which is similar to peck drilling (**Figure 2**). The drill penetrates subsurface in 10 cm

depth intervals and upon capture of a 10 cm sample, it retracts back to the surface. The sample is then either discarded or transferred to an instrument cup. A Near Infrared Spectrometer could view the cuttings as they fall onto the ground to determine if the sample is volatile rich and in turn decide whether to send a sample to a GCMS. To capture next sample, the drill is lowered back into the same hole and the process repeats. This approach has many advantages. The stratigraphy is somewhat preserved because a 1 meter hole is now represented by 10 samples. Lowering the drill into a hole each time allows measuring of subsurface temperature and in turn plotting of thermal gradient. When a sample is being analyzed, the drill is above the hole and in turn in a safe position. Moving the drill out of the hole also allows the drill and the subsurface to cool down.

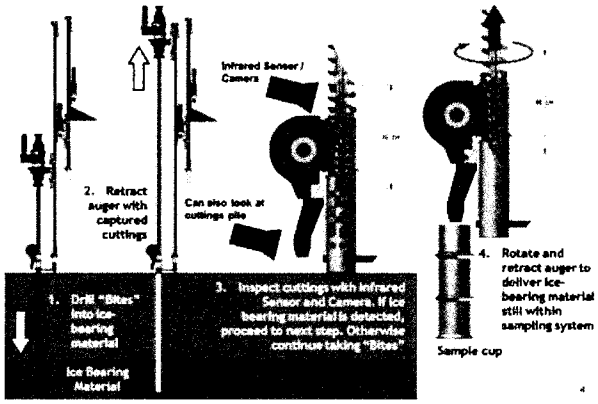

Figure 2. "Bite" Sampling approach.

Testing. A number of tests were performed inside a lunar vacuum chamber, VF13, at the NASA GRC to determine sampling efficiency as well as fraction of volatiles (water) loss during sample capture and delivery to an instrument (**Figure 3**).

The lunar chamber vacuum level was ~10^-4 torr while the LN2 shroud was kept at approx. -150 °C. The sample of NU-LHT-3M lunar regolith simulant was mixed with 5 wt% water and compacted to ~1.5 g/cc, and frozen prior to installing within VF13. During vacuum chamber tests, the sample bin was chilled to -130 °C. The Z-actuators of the RPD were kept at approx. +20° C, while the Drill Head, Auger and Percussive Actuators were kept at approx. +50 °C. The bit temperature measured ~ -70 °C while cable harness was at -60 °C.

The goal of the tests was to capture six, ~10 cc samples from 40-50 cm depth, delivering them to six crucibles, and hermetically sealing. The first test followed the 10 cm 'Bite' approach, while during tests 2-6, the drill initially penetrated to 40 cm in a single 'Bite', was retracted to clean the hole, and lowered back in the hole to capture the 40-50 cm sample. This routine was used to speed up the sampling process.

The RPD successfully delivered six samples to the six crucibles. The average drilling power was 30 Watt (including actuator losses), Weight on Bit was ~10 Watt or less, while Penetration Rate was software limited to 2 mm/sec. Percussive actuator engaged only several times during the process, while majority of drilling was done with rotary approach, only. The bit temperature while the drill was in the hole was approximately – 80 °C and no temperature increase was observed during drilling indicating the thermal changes to the sample due to the drilling process were minimal.

The end to end sampling sequence consisted of drill deployment, sample capture, sample delivery, and crucible sealing took approximately 1 hr.

The data will be analyzed over the next weeks and published at AIAA SciTech.

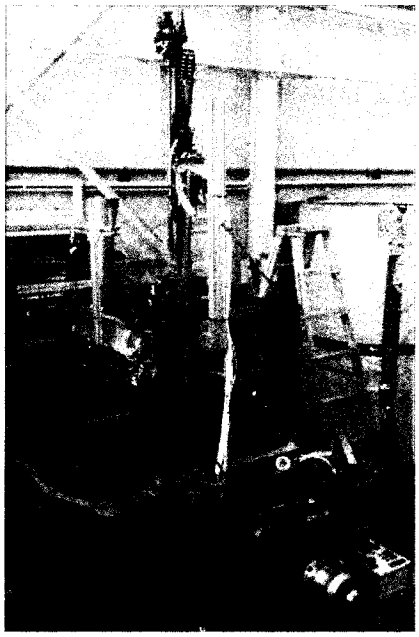

Figure 3. Lunar Prospecting Drill mounted inside VF13 lunar chamber facility at NASA Glenn Research Center.

References: [1] Colaprete et al., (2010). Detection of water in the LCROSS ejecta plume. Science. [2] Zacny et al., (2013) Reaching 1 m Deep on Mars: The Icebreaker Drill, Astrobiology. [3] Paulsen et al., (2011), Testing of a 1 meter Mars IceBreaker Drill in a 3.5 meter Vacuum Chamber and in an Antarctic Mars Analog Site, AIAA Space 2011., [4] Zacny et al., (2013) LunarVader: Development and Testing of a Lunar Drill in a Vacuum Chamber and in the Lunar Analog Site of the Antarctica. J. Aerosp. Eng.

Acknowledgements: The project has been funded by the NASA SBIR program.

Can Solar Wind Volatiles Survive the Day inside a Lunar Pit?

M. I. Zimmerman, D. B. J. Bussey, D. M. Hurley

We use a new three-dimensional illumination and heat diffusion code to characterize the daily insolation and heating cycle inside a lunar pit, as shown in Figs. 1 and 2. This allows a detailed assessment of volatile stability in adjacent shadowed regions such as prospective lava tubes. While sometimes relatively cold with respect to the exposed lunar surface, shadowed regions inside a pit can still receive significant amounts of reflected sunlight and heat re-radiated by directly illuminated surfaces nearby. Finally, the daily delivery of solar wind volatiles is characterized via a plasma particle code. Combining the heat and plasma codes enables an analysis of volatile stability as well as patterns of migration from hot, illuminated areas into colder, shadowed regions.

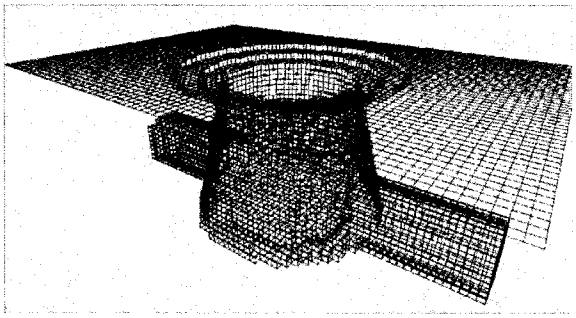

Figure 1: Mesh representation of a lunar pit, similar in geometry to the Mare Tranquilitatis pit. Prospective lava tubes with circular cross-sections have been added to either side of the pit below the surface. This geometry was used to create the voxel representation seen in Fig. 2.

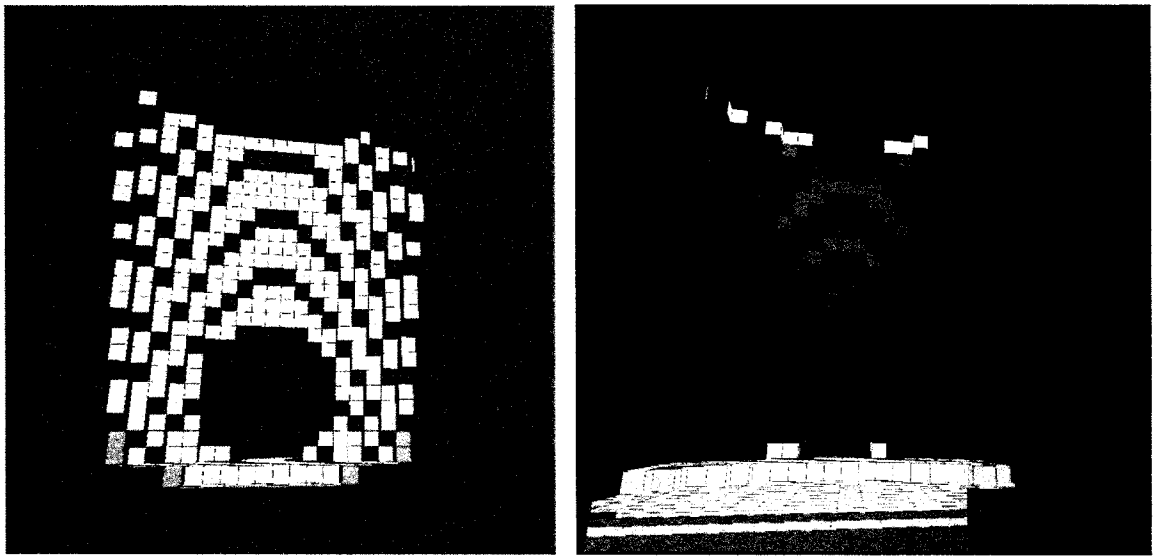

Direct Illumination at 2:30 PM

Solar + Conductive Heated Surfaces

Figure 2: (Left) View of the illuminated voxelized pit of Fig. 1 from within one of the subsurface lava tubes. (Right) Temperature profile as observed from the same vantage point. The hottest regions are in direct sunlight, and the brightest shades of yellow correspond to a temperature >400 K.

NOTES